The sedimentary dynamics in natural and human-influenced delta channel belts

De sedimentatiedynamiek van natuurlijke en
door de mens beïnvloede rivieren in delta's

(met een samenvatting in het Nederlands)

PROEFSCHRIFT

ter verkrijging van de graad van doctor aan de Universiteit Utrecht
op gezag van de rector magnificus, prof.dr. G.J. van der Zwaan,
ingevolge het besluit van het college voor promoties in het openbaar te verdedigen

op donderdag 5 november 2015 des middags te 2.30 uur

door

Noortje Hobo

geboren op 25 november 1980 te Ammerzoden

Promotor:
Prof.dr. H. Middelkoop

Copromotor:
Dr. A. Makaske

Dit proefschrift werd (mede) mogelijk gemaakt met financiële steun van Delft Cluster, het ministerie van LNV en Alterra

The sedimentary dynamics in natural and human-influenced delta channel belts

Utrecht Studies in Earth Sciences

ISSN 2211-4335

Utrecht Studies in Earth Sciences 097

The sedimentary dynamics in natural and human-influenced delta channel belts

Noortje Hobo

Utrecht 2015

Promotor
Prof.dr. H. Middelkoop

Copromotor
Dr. A. Makaske

Examination committee
Prof. dr. T.E. Törnqvist, Tulane University
Prof. dr. R.T. van Balen, Free University Amsterdam
Prof. dr. F. Klijn, Delft University of Technology
Dr. R.M. Frings, Aachen University
Prof. dr. M.G. Kleinhans, Utrecht University

ISBN 978-90-6266-410-8

Cover: High water level of the Nederrijn near Wageningen, the Netherlands. Photo by Noortje Hobo.

Printed in the Netherlands by CPI - Koninklijke Wöhrmann B.V., Zutphen.

Contents

Figures

Tables

Preface

Eight years ago I started my PhD study. Four years later, when I was almost finished, my son Mats was born, shifting my focus away from the research. I needed some time to rebalance my life. Research, however, was never far away, and neither was the urge to finish what I started. By finishing this thesis, that achievement is completed. And that wouldn't be possible without the contribution – either directly or indirectly – from many other people. So in this section I would like to acknowledge them.

In the first place I would like to thank my supervisors Bart and Hans. I am grateful for the opportunity you offered me to start this research, and for all effort you made to let this develop into a real PhD study. I am even more grateful for your patience and continuing support when I ran out of time. Bart, I learned a lot from you. You introduced me into the subject, and showed me geomorphological and sedimentary features along rivers, which I didn't notice before. Moreover, you helped me to find my way during this study, and when I did not know how to proceed, a little talk with you was always inspiring. I thank you for carefully reading all my manuscripts. Your focus on the details – not only on the content, but also on the language – so much improved this thesis. Hans, the further I got in my research, the more important you became for me. Where Bart pointed out all details, you provided me with an overview. And when I got lost in the large amount of information, your ability to separate the relevant subjects from the irrelevant details helped me to focus again. I thank you for the intensive editing work you did in the last phase of my research, and for your positive attitude over the course of my PhD study.

I also want to acknowledge my co-authors Jakob and Maarten, who contributed to the content of this thesis. Jakob, you invited me at the NCL for several weeks to let me date my own OSL samples. I learned interesting things during those weeks. Thanks to you and all the other NCL colleagues for making me feel so welcome. I met you again a few years later, when you moved to Wageningen, and I just returned from maternity leave to finish my thesis. Thank you for offering me the opportunity to do this at the SGL group. Maarten, I appreciate your infinite enthusiasm. From you I learned how to simplify reality into a model, and to be happy with the results. Whenever I was fussing over ignored details and inaccurate results, you were happily pronouncing that it was great.

In these past years, I have had many work places. Some were for just a few weeks of indispensable laboratory work. Therefore, I want to thank TNO, Deltares, NCL and WUR for the use of their laboratories, and for the assistance I got. And in particular Eef, who not only introduced me into soil analyses, but also showed much interest in my work. One on my work places was 'the field'. I have rarely been in the field alone, and thank all colleagues, family and friends for their assistance. And in particular Chris, who, with his technical skills, developed a special soil auger for my research.

Other workplaces were for a longer period. The first few years of this study I spent a lot of time at Alterra, where I shared a room with Michiel and Jetty. They were the best roommates I could wish for, because Michiel helped me a lot with GIS, and Jetty arranged all computer-related things, and was always available for social talks. I also want to thank all other Alterra colleagues. Concerning the research content we didn't have very much in common, but I

enjoyed the lunch breaks and the team excursions very much. The last few years I spent at the SGL group of Jakob. Besides him, I also want to thank all other members of this group. You provided me with a great work atmosphere. And Maricke, thank you for showing so much interest. Finally, I want to thank my DFG colleagues. Although I wasn't in Utrecht very often, I appreciate the lunch walks and the inspiring talks we had. And special thanks go to Esther, Kim, Harm Jan and Maarten for the brainstorm session we had last year, which was a great starting-point for me to write my last chapter. Furthermore, I want to thank my college friends Marjolein and Nelleke for believing in me, and for letting me believe in myself. Marjolein, you offered me a variety of diversions during my study. Nelleke, with you as a colleague, it was nice to share our complains and pleasures. Thank you both for being my paranymphs, and for reviewing the informal parts of my thesis.

Indirect heb ik ook veel steun gehad van mijn familie en vrienden. In de eerste plaats van mijn ouders Gijs en Annemiek, want wat hebben jullie veel van mij overgenomen opdat ik maar aan mijn proefschrift kon werken. Of jullie nou moesten oppassen, of klussen in huis, jullie stonden altijd klaar. Bedankt ook dat jullie mij de mogelijkheid hebben gegeven om te doen wat ik leuk vind, en dat jullie het geloof in mij nooit opgegeven hebben. Ook mijn schoonouders Jan en Els wil ik graag bedanken voor alle steun. Niet alleen Mats vond de logeerweekendjes heerlijk, maar ook ik genoot van de rust die ik had om aan mijn proefschrift te werken. Mijn broers Roel en Dirk, bedankt voor jullie interesse in mijn onderzoek, en alle gezelligheid. Roel, als ervaringsdeskundige was jij bovendien meer dan bereid om mijn proefschrift door te bladeren op foutjes, bedankt.

Mijn vrienden en familie wil ik bedanken voor alle momenten van afleiding en gezelligheid. Van reizen naar Londen, naar baantjes trekken in het zwembad, tot geocaches zoeken op grote hoogte; het is allemaal erg waardevol voor mij geweest. Ook mijn scoutingvrienden wil ik bedanken voor alle plezier die we hebben gehad. De kampen en activiteiten hebben mij soms iets teveel afgeleid, maar waren vooral ook een welkome afwisseling. En hier is dan het resultaat van vier jaar gaatjes boren in de grond. Loes, ik wil je bedanken voor je praktische hulp, want alle uurtjes dat Mats bij jou mocht spelen, kon ik aan mijn proefschrift werken. Maar ook jouw steun als ik het even niet meer zag zitten heeft me erg geholpen.

Als laatste de belangrijkste personen in mijn leven: Joost en Mats. Lieve Joost, bedankt voor jouw onvoorwaardelijke steun, en voor het aanhoren van mijn frustraties en blijdschap. Het is voor jou ook niet altijd makkelijk geweest als ik weer eens tot in de late uurtjes aan het werk was. Je hebt veel van me overgenomen, maar je deed het met zoveel liefde. Lieve Mats, jij hebt mijn leven zoveel verrijkt. Zonder het zelf te weten heb jij mij enorm gemotiveerd om dit proefschrift te kunnen afronden. En nu is eindelijk tijd voor een heleboel drietjesdagen!

1 General introduction

1.1 Background

Worldwide, densely populated deltas have increasingly become threatened by flooding due to sea-level rise, storm surges, river peak discharges and land subsidence (e.g., Syvitski et al., 2009). Recent examples of severely flooded deltas include the Mississippi delta (Törnqvist et al., 2008), the Chao Phraya River delta (Komori et al., 2011; Chan et al., 2012), and the Ganges-Brahmaputra delta (Auerbach et al., 2015). Syvitsky et al. (2009) indicated that 85% of the world's major deltas have experienced flooding, and that with persistent sediment starvation of deltas a further 50% of deltas will become vulnerable to flooding in this century.

Humans have greatly disturbed the natural morphodynamics of deltas when compared to the 'pre-Anthropocene' situation (Syvitski and Saito, 2007). These activities also have been a major cause of the increasing vulnerability of deltas to flooding: anthropogenic influence on global warming has caused a global rise in eustatic sea-level rise (IPCC, 2013), while excessive land drainage and extraction of oil, natural gas and water have caused subsidence of the deltas. Under natural conditions, the newly generated accommodation space might have become filled-in with fluvial and marine sediments. However, human activities have decreased, or even eliminated the natural mechanisms for delta aggradation, and promoted wetland loss. Upstream river damming and sediment trapping in reservoirs have dramatically reduced the amounts of sediment reaching the deltas (Syvitski, 2008; Syvitski et al., 2009). Within deltas, artificial levee building and damming of river distributaries has isolated large parts of the deltas from sediment input and deposition, preventing these areas to fill the increasing accommodation space with sedimentation.

In the coming century, it is expected that deltaic area facing flooding risk will continue to increase, both due to ongoing subsidence and sea-level rise, and increasing peak flows in the rivers (Vellinga et al., 2008; Syvitski et al., 2009). As river sediment fluxes towards deltas remain notoriously limited, prudent management of the remaining material delivered to the delta becomes increasingly important to prevent deltas from drowning (Kolker et al., 2012; Giosan et al., 2014; Manh et al., 2015).

Delta management comprises a combination of preventing further land subsidence, and protecting land from flooding. The first involves reducing drainage and subsurface reservoir depletion within the delta, as well as measures to enhance sediment accumulation, such as currently attempted in the Mississippi delta (e.g., Kim et al., 2009; Kolker et al., 2012). Reducing river flooding risk in the delta requires improving the capacity of the delta channels to discharge peak flows. This may not be simply achieved by raising dykes along the river, because this will increase floodwater levels high above the protected area, which will increase the damage in the event of dyke breach. Where feasible, management strategies are promoted that focus on creating more space along the rivers to accommodate extreme discharges and peak water levels, and to improve the ecological quality, thereby at the same time accounting for other – often competing – river services such as navigation, agriculture, and fishery. Measures for river restoration and flood protection include lowering the floodplain surface,

digging secondary channels, or adapting the main channel, as currently being implemented in the Rhine-Meuse delta (Room for the Rhine; Silva et al., 2001).

Re-establishment of delta aggradation and many flood protection measures all involve sediment dynamics in deltas. Sediment management measures such as in the Mississippi delta, and so-called 'cyclic rejuvenation' measures of floodplains – multi-decadal cycle of artificial lowering of floodplains and opening of side channels (Baptist et al., 2004) – may directly affect local to delta-wide changes in storage, throughput and trapping of sediment. On the longer term, sediment budgets may be affected as well, perhaps unintendedly: large-scale lowering of the floodplain surface not only enhances local floodplain deposition (Thonon et al., 2007), but may also affect amounts of sediment deposition in other parts of the delta. Evaluation of the potential effects of delta and river restoration measures therefore not only requires tools to predict their direct and long-term morphodynamic and ecological effects, but also raises the need to define references and benchmarks for these effects. To achieve these requirements, we need insight into and understanding of the natural sedimentary dynamics within deltas, and how these have been affected by past human activities.

1.2 Sedimentary dynamics

The sedimentary dynamics of a river comprise the way sediment moves through the system. This can be defined as the whole of processes that involve erosion, transport and deposition of sediment in a river – including its floodplain – across a range of spatial and temporal scales. Sedimentary dynamics of a delta include trapping of sediment in the delta, re-erosion of older sediments within the delta and throughput of sediment to the coast. At the delta scale, aggradation rates and avulsion of the river channels are the main components of these dynamics; within a delta, the sediment dynamics scale down to stretches of its river distributaries and adjacent floodbasins. The large number of studies on deltas and lowland rivers reported in the past decades has provided valuable insight into the different components of the sedimentary dynamics of deltas and lowland rivers, covering a wide range of spatial and temporal scales.

Reconstruction and modelling studies have demonstrated the chronological development of deltas (e.g., Törnqvist et al., 1996; Panin, 2003; Ta et al., 2005; Marriner et al., 2012), their avulsion history (e.g., Stouthamer and Berendsen, 2001), sedimentary architecture, and the controls and forcing factors of these (e.g., Gouw and Autin, 2008; Hoyal and Sheets, 2009; Geleynse et al., 2011). Modeling studies and flume experiments have provided great insight into delta channel patterns, sediment sorting, the role of upstream controls (discharge and sediment) and base level (tides, waves), and processes of avulsion, deposition and erosion (e.g., Hutton and Syvitski 2008; Geleynse et al., 2010, 2011).

Studies on sedimentary dynamics of lowland rivers and floodplains at century to decadal or event scale have addressed various components of sedimentary dynamics, including rates and patterns of overbank sedimentation (e.g., Walling and He, 1998; Middelkoop and Asselman, 1998; Hung et al., 2014a, 2014b), trapping efficiency and conveyance loss by floodplains (e.g., Walling et al., 1986; Walling and Owens, 2003), channel bank retreat rates (e.g. Kummu et al., 2008), channel-bed sediment transport (e.g., Church et al., 2012), and channel-floodplain interactions, such as the natural process of floodplain rejuvenation by

migrating channels (e.g., 'floodplain shaving'; Lauer and Parker, 2008c) and contemporary sediment budgets (Brewer and Passmore, 2002; Walling et al., 2006). In particular, contamination studies have concerned the downstream dispersal of polluted sediments through river catchments (e.g., Macklin et al., 1997, Bird et al., 2010).

Although previous studies have addressed all components of sedimentary dynamics of river systems, yet these have provided little quantitative information on how humans have disturbed the full sedimentary dynamics in deltas at timescales from centuries to decades. To address this issue, the Rhine-Meuse delta in the Netherlands may provide a unique opportunity, for two main reasons. Firstly, the delta has been massively affected by humans, with major impacts on the sediment dynamics (Van de Ven, 1993; Ten Brinke, 2005; Vos, 2015). Secondly, over the past decades a large series of studies on this delta has been reported, and an extremely detailed database of borehole descriptions, datings, maps and cross-sections of former channel belts, as well as alluvial architecture of the delta has been established (Berendsen and Stouthamer, 2001; Stouthamer, 2001; Cohen et al., 2009). Previous projects on the delta have addressed various components of the sedimentary dynamics in the delta across a range of temporal and spatial scales. Törnqvist (1993), Weerts (1996), Makaske (1998), Stouthamer (2001), Makaske and Weerts (2005), Makaske et al. (2007), Gouw (2008), and Gouw and Erkens (2007) provided a detailed reconstruction of the Holocene evolution of the delta, its channel belt chronology, avulsion history, and channel belt and floodbasin architecture. Erkens (2009) quantified storage and preservation of channel belt and floodbasin deposits in 500-year time slices within different parts of the delta during the past 9000 years. Schoor (1994), Middelkoop (1997), Hesselink (2002) and Hesselink et al. (2003) reconstructed the morphological development of the remaining active floodplains that occurred after the Rhine-Meuse branches were embanked in the late Middle Ages. Kleinhans et al. (2011) and Frings et al. (2009) investigated the dynamics of the main channels, their bifurcations, and bedload transport during the past decades, while Middelkoop (2000) and Van den Berg and Van Wijngaarden (2000) quantified floodplain deposition rates in de past century. Contemporary and event-scale overbank deposition along the Rhine branches and how these relate to discharge characteristics is known from the studies of Sorber (1997), Ten Brinke et al. (1998), Middelkoop and Asselman (1998), Middelkoop and Van der Perk (1998), Maas et al. (2003), Thonon (2006) and Middelkoop et al. (2010).

These previous studies have addressed the Rhine delta's morphology, architecture, chronology, delta scale sediment budgets, and sedimentary processes, but they have not directly addressed the within channel-belt sedimentary dynamics in the delta in terms of amounts and rates of deposition, erosion, and reworking. Yet, this rich set of data and studies comprises a tremendous number of 'building blocks' for quantifying the sedimentary dynamics of the Rhine delta across a range of scales, enabling us to assess how natural sedimentary dynamics were affected by humans, and giving clues to identify opportunities to (partly) restore natural sedimentary dynamics in the context of sustainable delta management programmes.

1.3 The Rhine-Meuse delta

Figure 1.1 shows the location of the Rhine-Meuse delta in the Netherlands. The Rhine-Meuse delta deposits form a wedge or prism, of which the thickness increases from east to west (Figure 1.2). The western boundary is formed by the North Sea, and the eastern boundary by the delta apex. The northern and southern boundaries are defined by the paleovalley morphology. The lower boundary is formed by Pleistocene subsurface, and the upper boundary is the modern land surface (Cohen, 2005). The wedge is filled with peat and with fluvial deposits from meandering rivers, deposited since ~9000 years ago (Beets and Van der Spek, 2000). Deposition in the delta started in the west, and during the Holocene the volume of the deltaic wedge increased. As a result of eustatic sea-level rise and land subsidence, accommodation space increased and aggradation occurred. Moreover, the zone of floodplain aggradation expanded in an upstream direction.

The main type of sediments present in the delta are clastic overbank deposits (Erkens, 2009). These sediments were deposited during peak discharges, and include the silty deposits of natural levees, which become finer with increasing distance to the channel, and grade into clayey floodbasin deposits. Relative sea-level rise made the delta an efficient trap for overbank sediments by creating accommodation space, and about 82% of the fine sediment supplied to the delta has been trapped (Erkens 2009). In the lower delta, sedimentation could not keep up with rapid early Holocene relative sea-level rise, and peat partly filled the accommodation space (Berendsen and Stouthamer, 2001). Peat development was less abundant in the upper deltaic plain, and declined when sea-level rise slowed down. Floodbasin clay and peat are intersected by channel belts. These were formed by avulsions (Stouthamer, 2001), and widened by meandering processes. In the process of channel-belt formation, clayey and peaty floodbasin deposits were eroded and replaced with channel sand. After another avulsion, the channel was abandoned and its sandy channel belt remained present in the floodbasin. The cross-section in Figure 1.3 shows a typical example of such a floodbasin with clay and peat, intersected by sandy channel belts of abandoned rivers.

The Rhine branches in the Netherlands have been subjected to many human activities, affecting the sediment dynamics in the channels and on the floodplains. Human influence became important around 4 - 2 ka BP, when cultivation and deforestation of the hinterland resulted in significant increase in sediment load of the river, enhancing deposition in the delta (Erkens et al., 2006). Human activities *within* the delta started with artificial drainage, land reclamation and the construction of dykes (1000 – 1350 AD) to protect the reclaimed floodbasin from inundation (Van de Ven, 1993). Consequently, fluvial processes of channel erosion and overbank deposition became restricted to a 500–1000-m wide embanked floodplain, in which little room was left for meandering. After completion of the embankments many other activities took place to improve water management: meander cut–offs, closure of smaller branches, stabilization of bifurcations, and construction of minor levees (Van de Ven, 1993). Furthermore, groynes were constructed to support sedimentation and floodplain accretion

Figure 1.1 (next page). Geological–geomorphological map of the Rhine-Meuse delta, the Netherlands (Berendsen and Stouthamer, 2001). The black line indicates the location of the cross-section in Figure 1.3.

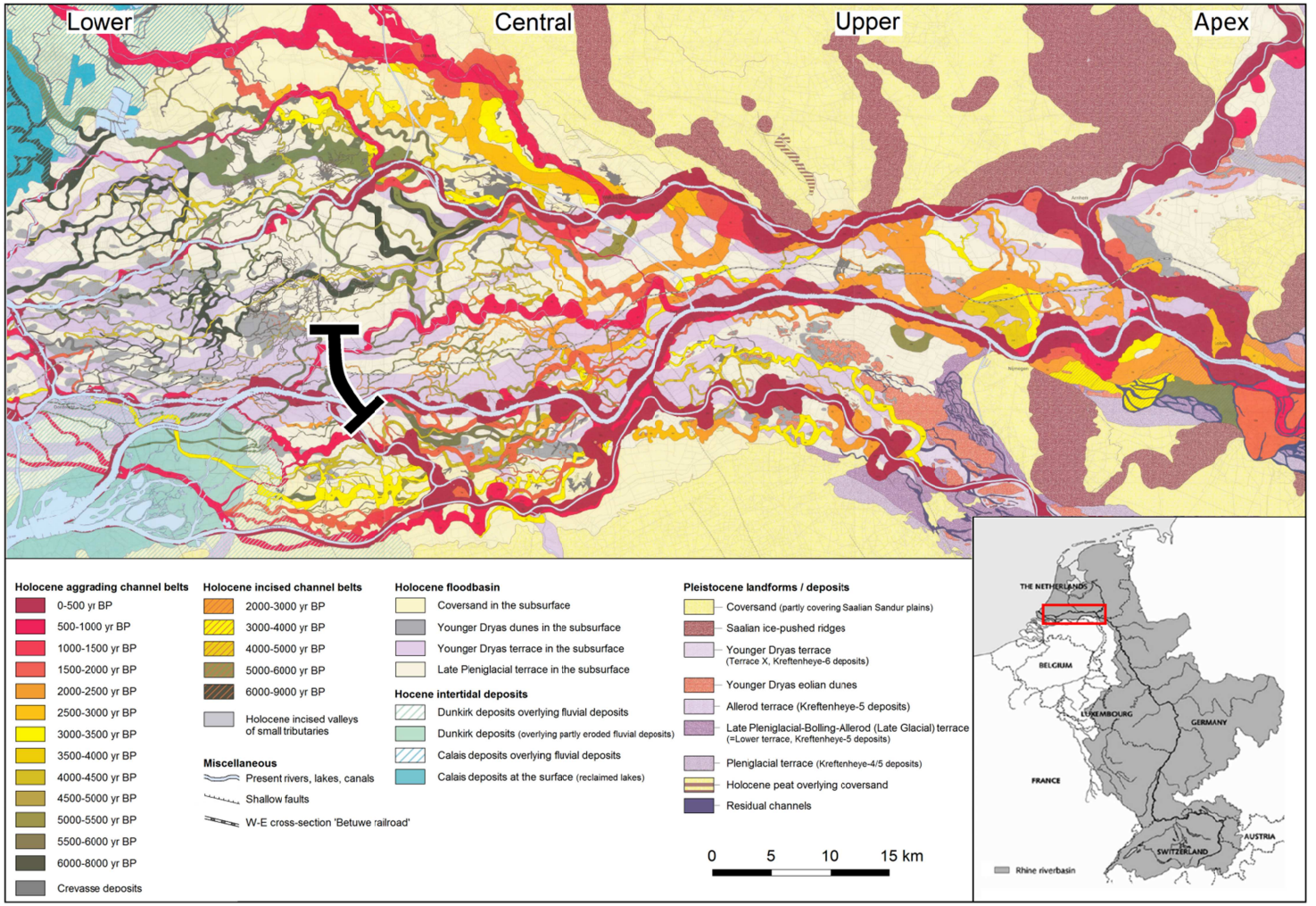
Lower
Central
Upper
Apex
Holocene aggrading channel belts
0-500 yr BP
500-1000 yr BP
1000-1500 yr BP
1500-2000 yr BP
2000-2500 yr BP
2500-3000 yr BP
3000-3500 yr BP
3500-4000 yr BP
4000-4500 yr BP
4500-5000 yr BP
5000-5500 yr BP
5500-6000 yr BP
6000-8000 yr BP
Crevasse deposits
Holocene incised channel belts
2000-3000 yr BP
3000-4000 yr BP
4000-5000 yr BP
5000-6000 yr BP
6000-9000 yr BP
Holocene incised valleys of small tributaries
Miscellaneous
Present rivers, lakes, canals
Shallow faults
W-E cross-section 'Betuwe railroad'
Holocene floodbasin
Coversand in the subsurface
Younger Dryas dunes in the subsurface
Younger Dryas terrace in the subsurface
Late Pleniglacial terrace in the subsurface
Hocene intertidal deposits
Dunkirk deposits overlying fluvial deposits
Dunkirk deposits (overlying partly eroded fluvial deposits)
Calais deposits overlying fluvial deposits
Calais deposits at the surface (reclaimed lakes)
Pleistocene landforms / deposits
Coversand (partly covering Saalian Sandur plains)
Saalian ice-pushed ridges
Younger Dryas terrace (Terrace X, Kreftenheye-6 deposits)
Younger Dryas eolian dunes
Allerod terrace (Kreftenheye-5 deposits)
Late Pleniglacial-Bolling-Allerod (Late Glacial) terrace (=Lower terrace, Kreftenheye-5 deposits)
Pleniglacial terrace (Kreftenheye-4/5 deposits)
Holocene peat overlying coversand
Residual channels
0
5
10
15 km
THE NETHERLANDS
BELGIUM
LUXEMBOURG
GERMANY
FRANCE
SWITZERLAND
AUSTRIA
Rhine riverbasin

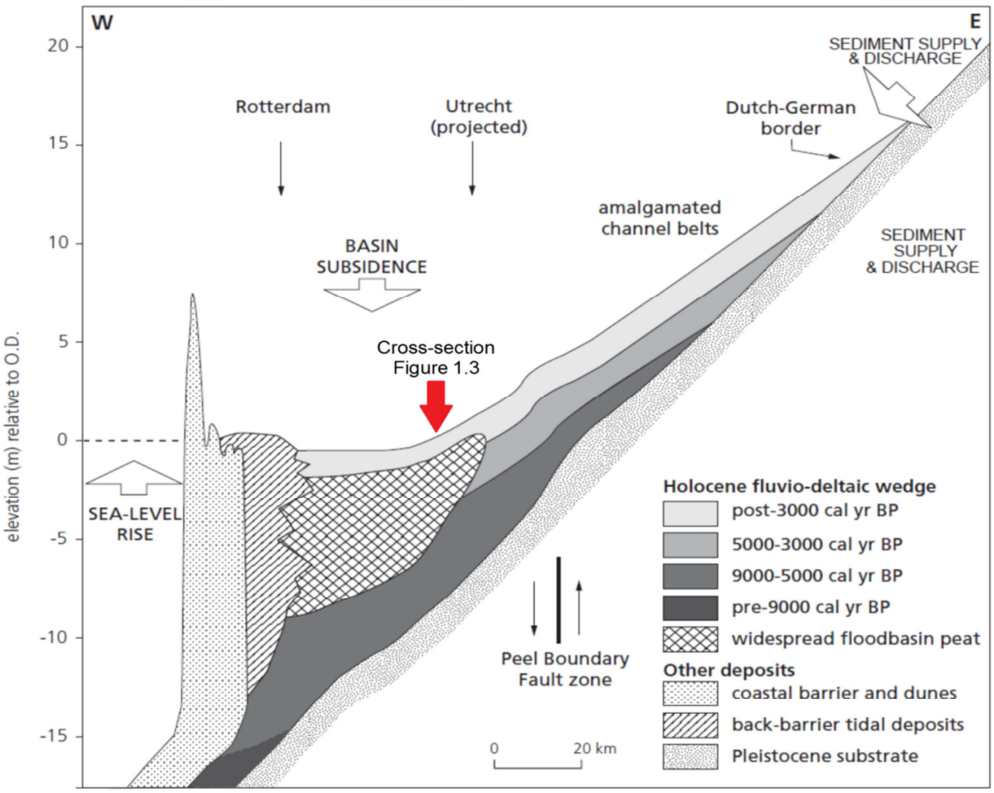

Figure 1.2. West-east cross-section through the Rhine-Meuse delta (after Gouw and Erkens, 2007).

(Middelkoop, 1997; Hesselink, 2002), and local dredging activities were performed. Meanwhile, in the upstream river basin human activities took place that influenced the sedimentary dynamics in the delta channels. These include construction of dams, reforestation and gravel mining (Frings et al., 2009; 2014). Between 1850 and 1920 AD, the delta channels became laterally fixed to a standard width ('normalized') by the construction of a regular array of groynes, preventing lateral channel migration, and leaving vertical accretion by overbank sedimentation as the main deposition process.

1.4 Objectives

This study investigates the increased anthropogenic influence on the sedimentary dynamics in the Rhine-delta. The main objective was to reconstruct the decadal to centennial scale within-channel-belt sedimentary dynamics of the channels in the Rhine-delta, for different periods of increasing human impact. In this investigation, 'building blocks' provided by previous studies

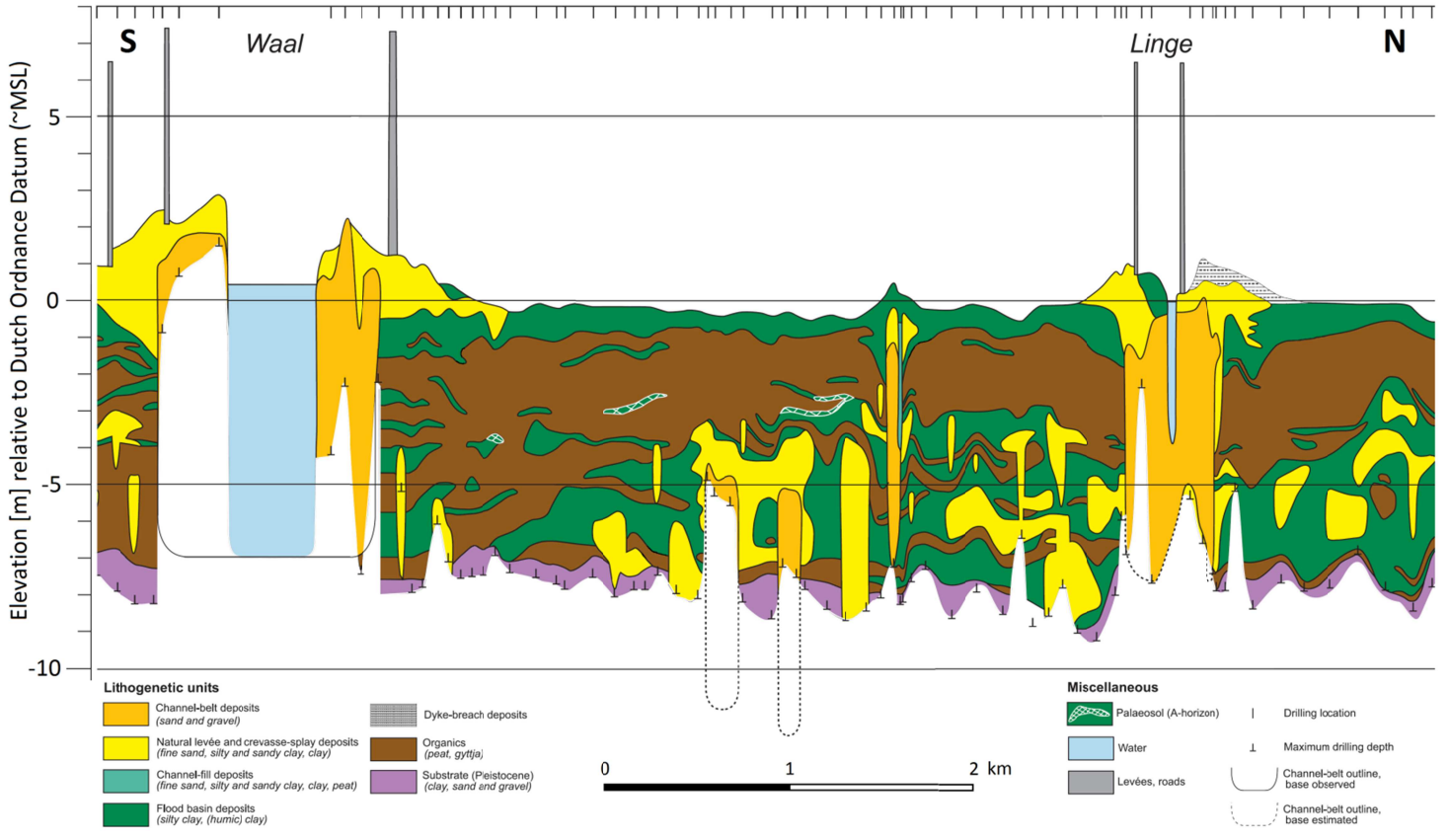

Figure 1.3. Fragment of a south–north cross-section through the Rhine-Meuse delta, showing Holocene floodbasin deposits of clay and peat, on top of the Pleistocene subsurface, intersected by channel belts of different age (Gouw and Erkens, 2007). See Figure 1.1 for location of the cross-section.

were put together, and complemented with new sedimentary and chronological data and reconstructions to quantify erosion and deposition rates at delta scale, and erosion and deposition volumes at century to decadal or event scale.

For three key periods of human impact on the delta, which are the pristine delta, the period after embankment and the recent situation after channelization, a different reconstruction method was required, dependent on the preservation of sediments in the subsurface and the available dating methods. An important prerequisite for reliable sedimentary dynamics reconstruction is the accurate and precise dating of sediment samples. Different dating methods exist for this purpose, depending on age and on a number of environmental variables. A technique that is applied to a wide range of fluvial deposits is Optically Stimulated Luminescence (OSL) dating. However, application of OSL dating to young fluvial deposits is still challenging. Therefore, a secondary objective was to optimize OSL dating of these deposits. Specific research objectives for this research were therefore:

- To develop a protocol to improve OSL dating of young fluvial deposits.
- To quantify for the pristine delta, and the two periods of increased human impact within-channel-belt volumetric erosion and deposition rates, and hence to determine variations in storage, reworking and throughput during the life cycle of a single channel belt.
- To assess the impact of major human interventions in the river system on storage, throughput and reworking of sediments.

1.5 Approach and organisation of the thesis

Three periods of interest were chosen for this study to evaluate the impacts of the two most important human activities on the sedimentary dynamics in the delta (Figure 1.4): (A) the period before the construction of dykes (before ~1300 AD), when natural avulsions occurred and river meanders could develop in a natural way, (B) the period after the construction of dykes, but before the normalization of the rivers (~1300 – 1850 AD), when avulsions no longer occurred while lateral river migration, erosion and deposition were confined between the bordering dykes, and (C) the period after channel normalization (1850 AD – present), in which the bed was fixed by groynes, and overbank deposition became the dominant morphological process in embanked floodplains. For each period the sedimentary dynamics were reconstructed for a channel belt or a channel-belt segment that was representative for the considered period.

To reconstruct the sedimentary dynamics in the three considered periods, high-resolution geochronological data and lithogenetic data were gathered and combined to determine amounts and rates of sediment erosion and deposition. These data were derived from previous studies, and from additional field and laboratory work. The existing chronological data mostly provided the initiation and termination dates of channel belts, but did not allow determination of deposition rates and changes herein during the life-time of the channel belt. Moreover, the 3D mapped sediment bodies of fossil channel belts represent the situation at the terminal phase of the channel belt, and do not show its development over time. To determine rates of change, simple models for erosion and aggradation were established, complemented with additional high-resolution age determination of sediments.

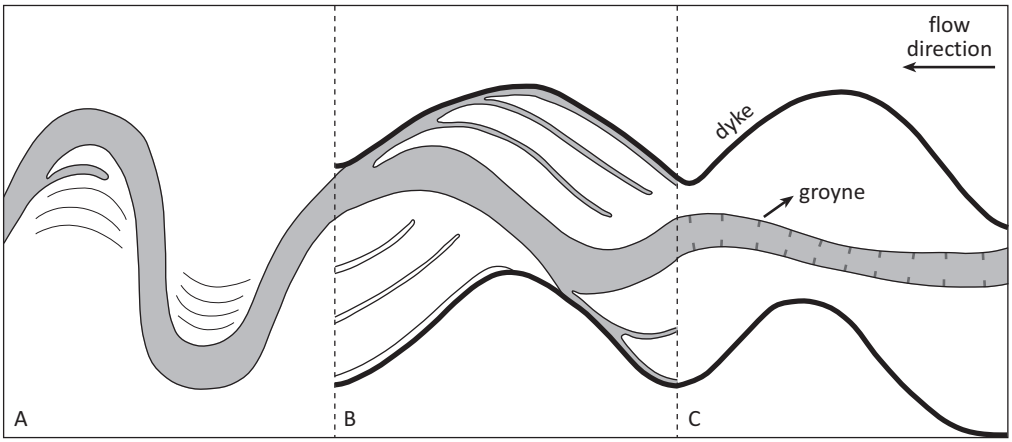

Figure 1.4. The main differences between a natural channel (A), and embanked channel (B), and a normalized channel (C) in the Rhine delta.

One such dating method is Optically Stimulated Luminescence (OSL) dating. This technique has been proven adequate for fluvial deposits in the Rhine-Meuse delta in previous studies (Wallinga, 2001), but its application for dating of young fluvial deposits remained a challenge. Therefore, first a suitable OSL-dating protocol was developed, which improved dating of young fluvial deposits for this project (chapter 2).

Subsequently, the OSL-dating technique was applied to estimate vertical aggradation rates during the most recent period (C) in different floodplain sections of the largest (Waal) and smallest (IJssel) distributary of the Rhine. For comparison of resulting deposition rates, post-normalization sedimentation rates were assessed by three other methods as well: identification of single flood layers, ^{137}Cs dating, and using heavy metal concentrations in the sediments as time markers (chapter 3). These four methods were applied on vertical soil cores from different locations within the embanked floodplains, yielding vertical sedimentation rates on each location. Lithogenetic data were derived from the extensive borehole database of Utrecht University (Berendsen and Stouthamer, 2001), and from new corings. Intercomparison between the methods revealed potential errors associated with each method and indicated the optimal spatial range of application of each method.

OSL dating was also used to reconstruct the sedimentary dynamics of the embanked channels during period B (chapter 4). This was done for a stretch of the river Waal, the largest distributary of the Rhine, particularly in that period. Embanked floodplains contain a sequence of sand bars separated by concave swales, and topped by fine-grained overbank deposits. Based on geomorphological maps, time series of old river maps and lithogenetic cross-sections, the embanked floodplains were subdivided into 'building blocks', representing sediment bodies of similar lithogenetic units. Within these blocks ~50-years isochrones were estimated using heavy metal profiles and OSL dating. Results yielded a series of volumetric erosion and deposition rates for ~50-years time slices between the early 17th century and the late 19th century, which were then related to the many human interventions carried out in this period.

The sedimentary dynamics in a natural channel belt (period A) were calculated for a fossil channel belt in the central part of the delta that was active in the period 3800 – 3000 BP (chapter 5). Detailed lithological cross-sections and geological maps of the preserved channel belt and overbank deposits allowed quantification of net sediment volumes that had accumulated during the channel belt's entire lifetime. Radiocarbon dates provided the age of the start and end of sedimentation, and hence the period of activity. The sedimentary dynamics of several stages within this period of activity were determined using the Bank Stability and Toe Erosion Model (BSTEM). Resulting volumetric erosion and deposition rates provided a generic picture of residence times and pulsing of sediment, and allowed to estimate spatial differences of these dynamics for channel belts across the delta from the apex to the distal zone.

Finally, results of the three periods were combined with those from previous studies and placed in a chronological framework (chapter 6). In this way, all 'building blocks' were integrated to compare the delivery, storage, throughput, and reworking of channel sediments and overbank sediments, from large-scale deposition in the middle Holocene to present-day deposition. These results provide quantitative insight into the natural delta dynamics, and how these have been affected the increased human influence within the delta. Finally, an outline is given of the significance of the results for future delta and river management strategies, which aim at partly restoring the natural dynamics in the presently harnessed channels

2 Sedimentation rates on embanked floodplains determined through quartz optical dating

Jakob Wallinga, Noortje Hobo, Alastair C. Cunningham, Alice J. Versendaal, Bart Makaske, Hans Middelkoop

Manuscript originally published as:
Wallinga, J., **N. Hobo**, A.C. Cunningham, A.J. Versendaal, B. Makaske, H. Middelkoop (2010). Sedimentation rates on embanked floodplains determined through quartz optical dating. **Quaternary Geochronology** *5*:170-175.

Reprinted with permission (Elsevier)

Abstract

We investigate the use of quartz optically stimulated luminescence (OSL) dating for determining fluvial overbank sedimentation rates over decades to centuries. For the study we took 11 samples from three cores from an embanked floodplain along the River Waal (Rhine) near Neerijnen (The Netherlands). We propose a measurement protocol for young fluvial quartz based on the single-aliquot regenerative dose procedure. Parameters for the protocol are chosen to isolate the fast OSL component, eliminate an ultrafast OSL component and avoid thermal transfer. The protocol shows excellent dose recovery and recycling ratios. For each sample, a Gaussian is fitted to the lower part of the equivalent dose distribution to obtain an estimate of the burial dose. We discuss the validity of the OSL ages using internal and external controls, and conclude that there is no evidence for large systematic offsets in the OSL ages. OSL based sedimentation rates are between ~3 and 8 mm/a, in line with previous estimates.

2.1 Introduction

Lowland river deltas are among the most densely populated areas in the worlds, yet they are also vulnerable to flooding. In the case of the Rhine Meuse delta (The Netherlands) flooding risks are expected to increase due to more extreme precipitation events resulting in greater peak discharges. Furthermore, the combined effect of land subsidence and sea-level rise will hamper the discharge of flood water downstream.. In response to these changes, additional flood protection measures are essential to increase the storage capacity and discharge capacity of the fluvial system. New river management strategies in The Netherlands include lowering of the embanked floodplain, widening the embanked floodplain (dike displacement) and digging of additional channels (Enserink, 2004). Many of these measures will lead to enhanced sedimentation, which in the long term will result in a renewed increase of water levels during high discharge. Hence, adequate assessment of such river management strategies requires insight into the dynamics of these fluvial systems during high discharge. In particular, the

mobility of (secondary) channels and the formation of sandy flood deposits on channel banks is poorly understood and cannot be adequately modelled (e.g. Van Vuren et al., 2005). Valuable information can be obtained by studying the geometry and age of sediments on the embanked floodplains, but dating of these sediments, especially sandy deposits, is difficult.

In this study, we investigate the use of optical dating of sand-sized quartz for determining sedimentation rates of natural levee and overbank fines within an embanked floodplain on timescales of decades to centuries. We investigate the optimal procedure for obtaining reliable age estimates on these young fluvial samples, taking into account that limited light exposure prior to deposition and burial of the quartz grains may result in incomplete resetting of the optically stimulated luminescence (OSL) signal. We present optimised measurement and analysis procedures for our samples, and we discuss the validity of resulting OSL ages based on internal and external controls.

2.2 Samples and equipment

For this study we used samples from three cores penetrating overbank deposits of the River Waal in the embanked floodplain of the Rijswaard near Neerijnen (Figure 2.1). Below we present a brief description of the development of our study area after embankment (~ 1300 AD), based on information provided by Middelkoop (1997) and Maas et al. (2003).

The Rijswaard developed as a result of stepwise downstream migration of a meander of the River Waal within the confines of the dykes bordering the embanked system, resulting in a bar and swale morphology. The accretion processes were accelerated by man, by construction of individual groynes and planting of trees. Lateral migration ceased when normalization works fixed the river bed by placing regularly spaced groynes (~ 1850 AD). Deposition of levee and distal fine sediments continued in the embanked floodplain after river normalization during flood events. Our samples originate from the eastern (upstream) part of the Rijswaard where bed sediments were formed during early stages of downstream migration (~ 1300-1700 AD). Overbank deposits were largely formed after ~1600 AD and include natural levee deposits and distal fines. After river normalization a sand bar developed between the groynes; the bar was

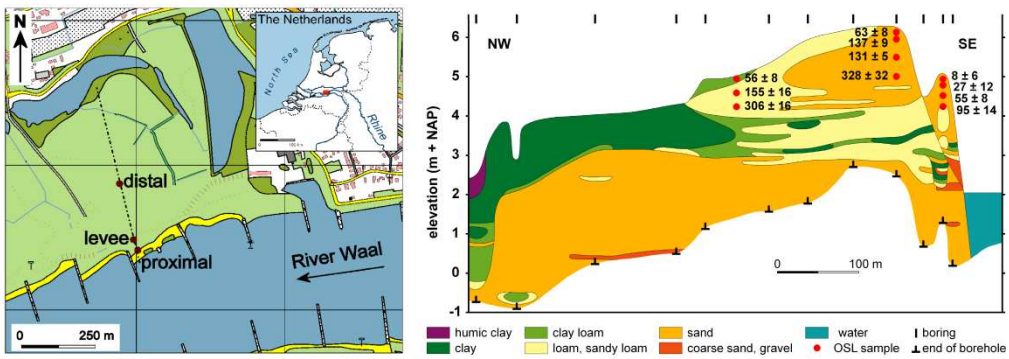

Figure 2.1. Location of the study site and cross section of overbank deposits with quartz OSL ages.

regularly removed until the first half of the 20th century, although it is not exactly clear which parts were removed.

Samples for this study were obtained through driving 10-cm-diameter PVC tubes into the upper few metres of floodplain sediments using a mechanical bailer drilling unit (Oele et al., 1983). Fieldwork was carried out in August 2001. Immediately after coring the sampling tubes were sealed at both ends and stored upright. Shortly after sampling ^{137}Cs profiles were measured on the unopened cores through a core scanning method (Rigollet and De Meijer, 2002). For this study we make use of the interpretation of these profiles as presented by Maas et al. (2003). To obtain additional information on the geometry of the overbank sediments we carried out additional hand corings with an Edelman auger along a cross section (Figure 2.1).

Samples for optical dating were obtained from the cores, which were split in a dark room equipped with subdued orange/red lights in June 2007. For each core, one half was brought into light to describe the sediments and select suitable depth intervals for OSL sampling. The OSL samples were taken from the other half of the core. We sampled sandy intervals and tried to avoid sampling close to lithological boundaries to facilitate estimation of the gamma dose rate. In cases where this was not possible, an additional sample of the adjacent material was taken to allow estimation of the gamma dose rate contribution from that layer.

2.3 Equivalent dose estimation

2.3.1 Equipment and methods

For equivalent dose estimation we employed Risø TL/OSL DA-15 readers (Bøtter-Jensen et al., 2000). Measurements were made on four different readers, each equipped with a Sr/Y beta source (dose rates ranging from ~0.03 – 0.15 Gy/s). Quartz OSL signals were obtained through stimulation with blue LEDs (470 nm, ~30-35 mW/cm^2); infrared (IR) stimulation was provided by IR diodes (875 nm, ~116 mW/cm^2). Signal collection used an EMI9235QA photomultiplier tube shielded by a 7.5 mm Hoya U-340 filter. We used the SAR procedure (Murray and Wintle, 2003) for equivalent dose estimation; suitable parameters for our protocol are discussed in the following sections.

2.3.2 Sample preparation

Upon arrival in the luminescence dating laboratory all samples were split in two; ~200 g of material was used for dose rate analysis, from the remainder (usually ~200 g) we extracted a sand-sized quartz fraction for equivalent-dose analysis. Quartz is the mineral of choice as residual signals for fluvial deposits are usually lower than those for feldspar (Wallinga, 2002a), and because the signal is stable over geological timescales (Wintle and Murray, 2006). We prefer to use sand-size grains over finer grains since this reduces the number of grains per

aliquot, thereby simplifying the interpetation of equivalent dose distributions (e.g. Wallinga, 2002b).

Sample preparation consisted of treatment with HCl and H_2O_2 to remove carbonates and organic material, and wet-sieving to isolate the 180 - 250 μm grain size fraction. The samples were then etched twice with concentrated HF (40%) for 30 minutes to dissolve feldspars and remove the outer layer of the quartz grains. After etching the samples were re-sieved to discard the grains that were heavily damaged by the HF treatment. After this treatment IR responses were negligible for all samples. Unless stated differently, stainless steel discs with the centre 2-3 mm covered with quartz grains were used for OSL measurements.

2.3.3 Selecting signal integration intervals

Following Ballarini et al. (2007) we used an early background (EBG) method, where the net OSL signal is obtained from the initial signal after subtraction of the signal during a similar time interval immediately following it. The advantage of this method over conventional late background (LBG) methods is that the signal is far more dominated by the fast OSL. For this study we routinely obtained the net signal from the first 0.625 s of stimulation minus the signal measured from 0.625 - 1.25 s. As one of our OSL readers has a slightly larger stimulation power, reduced intervals were used for measurements made on that reader (initial: 0 - 0.45 s, background: 0.45 – 0.90 s).

2.3.4 Ultrafast component

We avoided the use of high preheat temperatures for these young (fluvial) samples, as they may lead to an overestimation of the burial dose because of thermal transfer (see section 3.5). The disadvantage of low preheats, however, is that a thermally unstable ultrafast component (UFC) may contribute to the OSL signal in the regenerative measurements (Jain et al., 2008). We investigated the existence of an UFC in our samples through linearly modulated (LM-)OSL measurements (Bulur et al., 1996) on large aliquots (8 mm) following a 10 Gy dose. We found that a small percentage of the aliquots showed a clear UFC (photo-ionization cross-section about 25 times that of fast component). To remove the UFC we employed its large photo-ionization cross-section, and the dependency of relative photo-ionization cross-section on wavelength (Singarayer and Bailey, 2004). Figure 2.2 shows that a 20 s IR exposure at 180°C effectively removes the UFC, whilst only marginally affecting the fast OSL signal. Hence, we adopted a procedure with infrared exposure of the sample during the preheat and cutheat. At the end of the SAR measurements all aliquots were checked for any remaining UFC signal by measuring the LM-OSL signals after an elevated temperature IR treatment. For sample NCL-1107138 ten out of 26 aliquots were rejected for this reason, whereas from all other samples together only two aliquots were rejected. Results on sample NCL-1107138 indicate that elevated temperature IR exposure is not a guarantee for UFC removal and that the method needs to be further optimized.

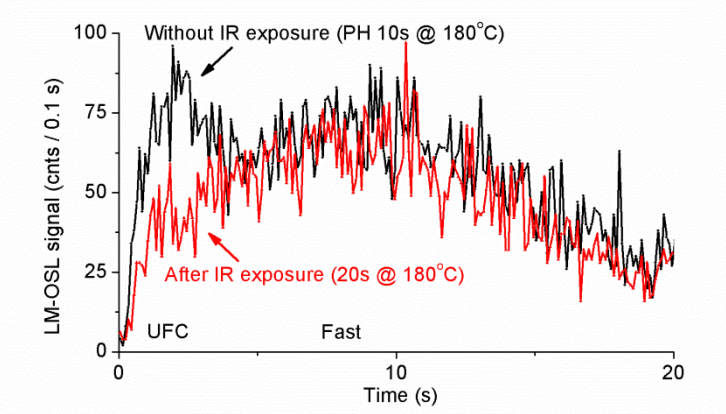

Figure 2.2. LM-OSL measurements on an aliquot of sample NCL-1107144 (deeper sample from levee site, not used for this study) after a 10 s preheat at 180°C (black) and after additional IR exposure (red); note the removal of the UFC with IR exposure.

2.3.5 Thermal transfer

Preheating of the aliquots before each OSL measurement is needed to remove charge from light sensitive shallow traps (e.g. Wintle and Murray, 2006). Heating may however also transfer charge from less light-sensitive traps into the OSL trap(s) used for dating and cause overestimation of the burial dose. For our samples, results of preheat plateau tests would be too scattered to select an appropriate preheat temperature to avoid thermal transfer. Therefore we bleached the fast OSL component of three aliquots of each sample using two 300 s exposures to blue LEDs at 90% power. We preferred bleaching by blue light over using a solar simulator as it resembles the reduced light spectrum under water. After bleaching, the aliquots were heated to 140°C for 30 s, including IR stimulation for the last 20 s. Then their OSL signals were measured for 40 s at 125°C. The same aliquots were then preheated (with simultaneous IR) to 150°C, and measured again; this procedure was repeated for temperatures up to 250°C. The OSL signals were then reset by exposure to blue light at elevated temperature (200°C), after which the OSL response to a 5 Gy dose was recorded. By comparison of the cumulative OSL signal induced by preheating compared to the OSL response to the 5 Gy dose, we obtained a measure of the apparent dose due to thermal transfer. Results indicated that when using EBG, the apparent dose is zero (within uncertainties) up to preheat temperatures of 200°C (Figure 2.3). For comparison, results are also shown when using conventional late background subtraction; it is clear that for LBG thermal transfer effects are larger and start at lower temperatures relative to the effects for EBG, confirming findings of Jain et al. (2003) that medium and slow components are more sensitive to thermal transfer than the fast OSL component.

Our single-aliquot thermal transfer experiment uses repeated heating and thereby differs from other approaches where a separate aliquot is used for each temperature (e.g. Madsen et al., 2007). The advantages of the method used here are that the dependency of thermal transfer on heating temperature is known for the whole temperature range for a single aliquot; that

little material is needed; and that it is time efficient. The drawback of this method is that repeated heating may induce thermal transfer at lower temperatures than during a single heating event (such as that used prior to measurement of the natural OSL signal in the equivalent dose estimation). Yet, absence of a (cumulated) thermal transfer signal at a certain temperature in our experiment is positive evidence that the equivalent dose estimate will not be affected by thermal transfer when using this temperature for the preheat.

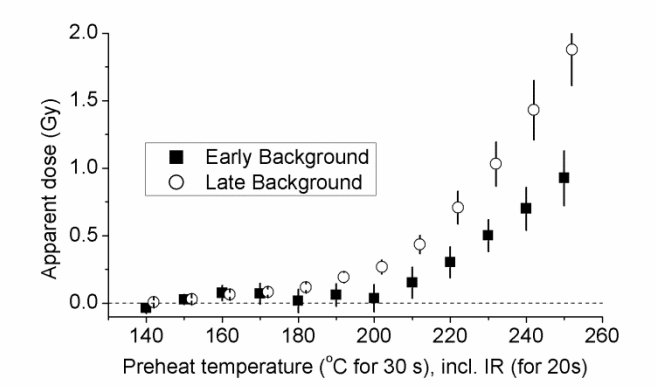

Figure 2.3. Offset in equivalent dose caused by thermal transfer. Average results for all samples are shown; three aliquots per sample were measured. Error bars represent one standard error. Thermal transfer is negligible up to 200°C for the EBG OSL signal, but more severe for conventional LBG methods.

2.3.6 SAR performance

Based on the tests described in the previous sections, we adopted the SAR procedure outlined in Table 2.1. For equivalent dose determination we employed a single regenerative dose point; by adopting such a short procedure we could measure more aliquots and increase the robustness of the equivalent dose distributions. For equivalent dose determination we used linear interpolation between the origin and the regenerated dose point, which induces a systematic overestimation of the equivalent dose by ~3 %. In the light of other uncertainties in dating very young samples we feel such an error is acceptable. Data was accepted for analysis if the recycling ratio agreed with unity within 10%, and the relative error on the test dose OSL signal was less than 10%. The adopted SAR procedure can successfully recover a known laboratory dose (dose recovery ratio: 1.005 ± 0.025; n=30), recycling ratios are near unity (average 1.008 ± 0.005; n=347), and recuperation values are negligible (average in agreement with 0 Gy).

Table 2.1. The SAR protocol used for equivalent dose measurements.

1 – Irradiation (N, 5, 0, 5 Gy)
2 – Preheat 30 s & IR 20s at 200°C
3 – OSL 40 s at 125°C
4 – Testdose (5 Gy)
5 – Cutheat & IR 20 s at 200°C
6 – OSL 40 s at 125°C
7 – OSL 40 s at 220°C
8 – Repeat 1-7 for different doses
9 – Feldspar check
10 – UFC check

2.3.7 Equivalent dose distribution

We assume that the spread in the measured single aliquot equivalent dose values for our young fluvial samples is dominated by incomplete resetting of the OSL signal in some grains. Hence, the burial dose is expected to be at the lower end of the equivalent dose distribution. We obtained palaeodose estimates for our samples by fitting a Gaussian to the lowest peak in the distribution; a second Gaussian was fitted to the remaining data to aid the fitting procedure.

2.4 Dose rate estimation

For dose rate estimation we employed a high-resolution gamma ray spectrometer. Untreated samples were heated to 105°C for 24 h to estimate water content, then ashed for 24 h at 500°C to estimate the organic content, and finally ground to homogenize the samples. The ground sediment was mixed with wax and cast into a puck to retain Rn. U-series activity was determined by measurement of ^{234}Th, ^{214}Pb, ^{214}Bi and ^{210}Pb. Th-series activity was determined from ^{228}Ac, ^{212}Pb and ^{212}Bi. The ^{40}K activity was measured directly and ^{137}Cs activity was obtained from the ^{137}Ba activity. Cosmic dose rates were calculated based on Prescott and Hutton (1994), assuming a constant aggradation rate. For calculation of average gamma dose rate during the burial period we took into account that the gamma dose rate is lower when the burial depth is very small (Aitken, 1985). For samples taken close to lithological transitions (samples NCL-1107139 and 145), we calculated gamma dose rates based on activity concentrations at the sampling depth and those measured on additional samples from adjacent layers (Aitken, 1985). Contributions of anthropogenic ^{137}Cs and excess ^{210}Pb to the overall dose rate are negligible and hence not included. We assumed that dose rates

remained unaltered in the period between taking of the cores and extracting the OSL samples from the cores. Attenuation of beta and gamma dose rates were calculated based on measured moisture and organic contents.

2.5 Results and discussion

2.5.1 OSL-dating results and sedimentation rates

OSL-dating results are provided in Table 2.2; ages are given relative to the time when OSL samples were taken from the core (2007 AD) and with 1-sigma uncertainty. Figure 2.4 shows the probability density functions (PDFs) of the age distributions; to allow comparison between samples, the single aliquot equivalent doses were divided by the sample dose rate. Uncertainties in dose rate are not included in the distributions, but are included in the ages reported in Table 2.2.

The main goal of our study is to use the OSL age data to estimate sedimentation rates of natural levees and overbank fines on the embanked floodplain. With only three or four data points for each core we assume that the sedimentation rate has remained constant over the study period (~100 to 300 a); in reality, sedimentation rates may slightly decrease with time due to gradual rise of the floodplain surface (Middelkoop, 1997). We used two approaches to estimate sedimentation rates for each core from the depth of the samples and the obtained OSL ages: 1) An unweighted linear fit of the data points. The slope of this line provides the sedimentation rate, and the intercept of this line at the surface (zero depth) provides information on whether there is a systematic offset in OSL ages. 2) An unweighted linear fit of the data points, forced through an intercept of 6 years. This intercept was chosen as the

Table 2.2. Quartz OSL dating results with additional information.

Sample	Lithology	Depth [m]	Dose rate information		External dose rate [mGy/a]	
			Water content [%]	Organic content [%]	Beta	Gamma
Distal (Neerijnen 124, x: 147,944; y: 426,436; z: 5.24)						
NCL-1107148	Clay	0.08	35 ± 12	9.6 ± 3.2	1.27 ± 0.14	0.63 ± 0.05
NCL-1107149	Silt	0.44	19 ± 6	2.8 ± 0.9	1.49 ± 0.12	0.89 ± 0.05
NCL-4307150	Silt	0.79	14 ± 5	2.2 ± 0.7	1.45 ± 0.10	0.87 ± 0.05
Levee (Neerijnen 121, x: 147,991; y: 426,242; z: 6.39)						
NCL-1107140	Loam	0.13	14 ± 5	4.4 ± 1.4	1.17 ± 0.08	0.56 ± 0.03
NCL-1107141	Loam	0.31	9 ± 3	2.3 ± 0.8	1.32 ± 0.07	0.70 ± 0.03
NCL-1107142	Sand	0.77	6 ± 2	1.2 ± 0.4	1.42 ± 0.07	0.85 ± 0.04
NCL-1107143	Sand	1.26	4 ± 1	0.5 ± 0.2	1.27 ± 0.06	0.69 ± 0.03
Proximal (Neerijnen 118, x: 148,005; y: 426,200; z: 5.08)						
NCL-1107135	Sand	0.15	13 ± 4	3.0 ± 1.0	1.21 ± 0.08	0.56 ± 0.03
NCL-1107136	Sand	0.31	6 ± 2	1.4 ± 0.5	1.20 ± 0.06	0.58 ± 0.03
NCL-1107137	Sand	0.57	6 ± 2	1.4 ± 0.5	1.03 ± 0.05	0.52 ± 0.02
NCL-1107138	Sand	0.85	10 ± 3	0.9 ± 0.3	0.97 ± 0.06	0.60 ± 0.04

material at the surface is expected to yield zero age at the time of coring (6 years prior to measurement). Results of both fitting exercises are presented in Figure 2.5 and Table 2.3; both methods provide similar sedimentation rates. Sedimentation rates range from ~3 mm/a for the distal core to ~8 mm/a for the proximal core (we prefer the rates determined through the unforced fit as these trend lines show a better fit with the data).

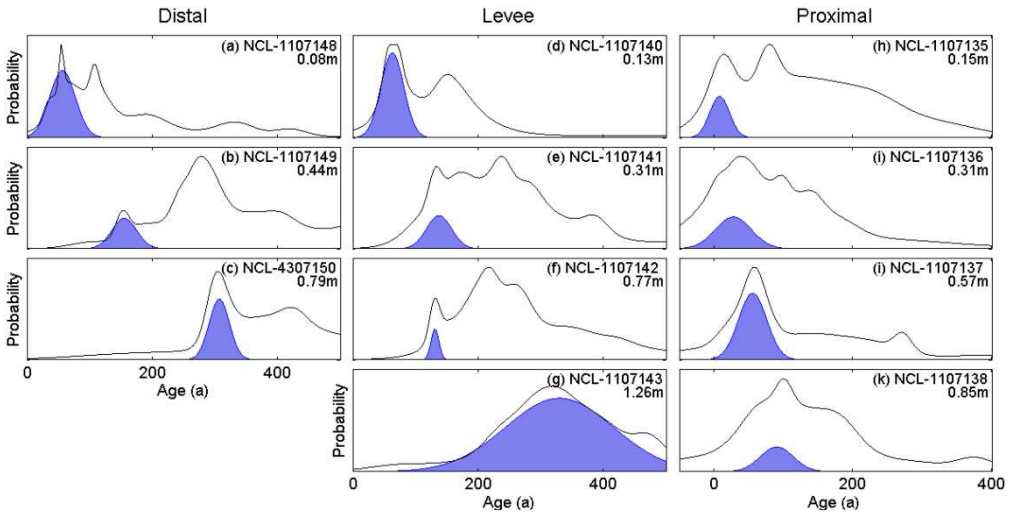

Figure 2.4. Probability density functions (PDFs) of the OSL single aliquot age distributions for all samples. To allow comparison of the samples the age distribution is shown rather than the equivalent dose distributions. Uncertainties in dose rate estimation are not incorporated.

Table 2.2 continued

		Eq. dose [mGy]	D_e – additional information			OSL age [a]
Cosmic	Total		Aliquots		St dev.	
			All	Iterated		
0.28 ± 0.01	2.20 ± 0.15	124 ± 16	36	29	0.25	56 ± 8
0.25 ± 0.01	2.65 ± 0.13	410 ± 36	32	31	0.44	155 ± 16
0.23 ± 0.01	2.57 ± 0.11	787 ± 26	34	26	0.44	306 ± 16
0.28 ± 0.01	2.02 ± 0.08	127 ± 16	28	25	0.11	63 ± 8
0.26 ± 0.01	2.30 ± 0.08	316 ± 17	29	24	0.17	137 ± 9
0.23 ± 0.01	2.53 ± 0.08	331 ± 9	30	25	0.19	131 ± 5
0.21 ± 0.01	2.19 ± 0.06	721 ± 67	33	25	0.17	328 ± 32
0.28 ± 0.01	2.07 ± 0.08	16 ± 13	25	18	0.33	8 ± 6
0.26 ± 0.01	2.06 ± 0.06	57 ± 24	48	38	0.11	27 ± 12
0.24 ± 0.01	1.81 ± 0.06	100 ± 14	26	22	0.15	55 ± 8
0.23 ± 0.01	1.82 ± 0.07	172 ± 24	16	14	0.09	95 ± 14

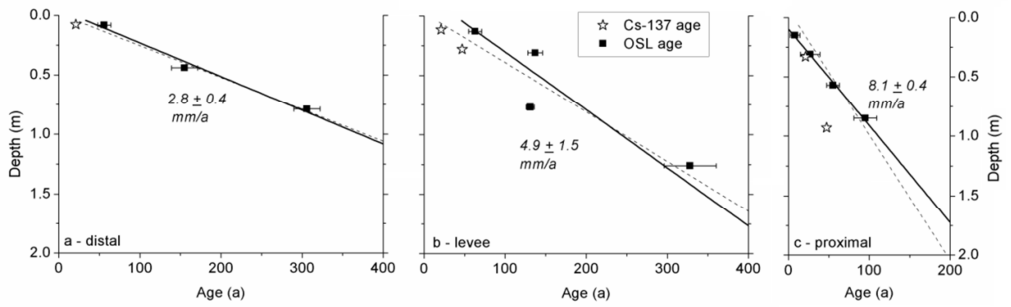

Figure 2.5. Age vs. depth plots indicating OSL ages (squares) and ^{137}Cs ages (stars) for the distal (a), levee (b) and proximal (c) cores. Trend lines indicate results of a linear fit of the OSL data with a forced intercept of 6 years (dashed) and an unforced linear fit (solid bold). Sedimentation rates shown are those for the unforced linear fit.

Table 2.3. Sedimentation rates derived from the OSL ages.

	Intercept of 6 years		Linear fit		
	Sed. Rate [mm/a]	r^2	Intercept [a]	Sed. rate [mm/a]	r^2
Distal	2.7 ± 0.1	0.98	19 ± 24	2.8 ± 0.4	0.98
Levee	4.2 ± 0.6	0.80	38 ± 49	4.9 ± 1.5	0.83
Proximal	10.5 ± 1.1	0.93	-12 ± 3	8.1 ± 0.4	1.00

2.5.2 Internal checks on validity of OSL ages

The first internal check considers the internal consistency. For all cores, OSL ages are internally consistent. For the proximal and the distal core they are in correct stratigraphic order, for the levee core there is a slight age inversion, but results on the two inverted samples agree within error and could also reflect a single deposition event.

The second internal check is whether there is an age offset due to incomplete resetting of the OSL signal, thermal transfer or due to our interpretation of the equivalent dose distributions. Based on the youngest result (sample NCL-1107135: age 8 ± 6 a) any positive age offset should be negligible. For the distal and levee cores the intercept obtained from a linear fit of the OSL ages agrees with an age of 6 years at the surface (Figure 2.5, Table 2.3). For the proximal site the intercept is slightly negative (-12 ± 3 a), which may indicate that our palaeodose extraction method underestimates the true burial dose. However, large sedimentation events in the years just prior to sampling would also lead to such an intercept.

A third internal check is provided by the shape of the equivalent dose distributions as a function of age. For our interpretation of the equivalent dose distributions, we assume that heterogeneous bleaching is the only source of scatter in equivalent doses obtained on small subsamples, i.e. we assume that dose rate heterogeneity does not contribute to the scatter. If this is the case, the width of the equivalent dose distribution should not depend on the age of

the deposit. To check this, we calculated the standard deviation of all equivalent dose distributions. Because the standard deviation is greatly affected by aliquots returning extreme doses, we first cleaned the distribution by iterative removal of single aliquot equivalent dose values that lie further than two standard deviations away from the sample mean (Table 2.2 lists the number of aliquots before and after iteration). For the proximal and levee core, the resulting standard deviation (see Table 2.2) was independent of the equivalent dose (levee) or showed a slight negative dependency (proximal). For the distal core standard deviations were relatively large for all three samples. This may indicate that for these sediments dose rate heterogeneity contributes to the scatter in equivalent dose distributions. We cannot rule out that as a consequence our palaeodose determined through PDF fitting of the lowest peak somewhat underestimates the true burial dose for these samples, although the intercept of the age – depth trend shows no signs of such systematic underestimation (Figure 2.5a).

2.5.3 External checks on validity of OSL ages

External control is provided by age constraints on the deposits. Firstly, the sand bar sampled with the proximal core was likely (partly) excavated until the middle of the 20th century. OSL ages on the top three samples agree with formation after this time, the lower sample indicates an older age but may well originate from a layer that was not excavated.

The second external control is provided by the ^{137}Cs profiles published by Maas et al. (2003). The Cs peaks in the profile are attributed to atmospheric deposition due to bomb tests (~ 1960 AD), and the Chernobyl accident (1986 AD). For the distal core only one peak was observed, which was attributed to 1986 AD. Cs dates are presented together with the OSL data in Figure 2.5. Apart from the 1986 AD Cs result for the proximal core, all Cs ages are younger than the OSL chronologies. This may indicate that Cs has migrated downwards after deposition, a process that has been documented for Chernobyl fallout Cs (e.g. Bunzl et al., 1995) and has recently also been documented by our research team for a site near the Rijswaard where no sedimentation occurred during the past century. Hence, we conclude that Cs chronologies may be erroneous and, unless corrected for downward Cs migration, provide no good control for our OSL ages.

A third control is comparison of the OSL derived sedimentation rates (~3 - 8 mm/a) to those obtained by other methods. For the Rijswaard, sedimentation was measured using sediment traps during a high discharge event in 2001. Results ranged from 1.3 mm for the distal site to 29 mm sedimentation for the proximal site (Maas et al., 2003). For other sites along the Waal River, similar measurements yielded sedimentation values of 1-3 mm in the distal parts, to 5-8 mm in the proximal parts during a high discharge event (70-year recurrence time; Middelkoop and Asselman, 1998). Middelkoop (2002) determined average sedimentation rates using heavy metals contained in the sediments as a tracer for various floodplains of the Waal River. For proximal sites he found sedimentation rates of typically 5 - 11 mm/a, while in the distal parts these rates were 2 - 5 mm/a. We conclude that the OSL derived sedimentation rates are of similar magnitude as those obtained for the Rijswaard and similar settings using other methods.

2.6 Conclusion

We present a SAR protocol which is suitable for quartz OSL dating of very young fluvial deposits. The protocol concentrates on the quartz fast OSL component, eliminates the ultrafast component and avoids thermal transfer. For our samples we obtain excellent dose recovery and recycling ratios. Burial doses obtained by fitting a Gaussian to the lowest peak in the equivalent dose distributions provide ages that are internally consistent. Extrapolation of the age-depth relationships yields zero age at the surfaces for two out of three investigated locations, indicating negligible systematic age offsets. The sedimentation rates obtained decrease with distance from the channel, and range from ~3 - 8 mm/a, which is in line with previous estimates.

Acknowledgements

JW and ACC are supported by an NWO innovative research grant (DSF7552). NH is supported by the BSIK / Delft Cluster 'Safety against Flooding' program (CT04.32.62). This research is part of the strategic research program "Sustainable spatial development of ecosystems, landscapes, seas and regions" which is funded by the Dutch Ministry of Agriculture, Nature Conservation and Food Quality, and carried out by Wageningen University and Research centre.

3 Reconstruction of floodplain sedimentation rates: a combination of methods to optimise estimates

Noortje Hobo, Bart Makaske, Hans Middelkoop, Jakob Wallinga

Manuscript originally published as:
Hobo, N., B. Makaske, H. Middelkoop, J. Wallinga (2010). Reconstruction of floodplain sedimentation rates: a combination of methods to optimise estimates. **Earth Surface Processes and Landforms** *35*: 1499-1515.

Reprinted with permission (John Wiley and Sons)

Abstract

Reconstruction of overbank sedimentation rates over the past decades gives insight into floodplain dynamics, and thereby provides a basis for efficient and sustainable floodplain management. We compared the results of four independent reconstruction methods – optically stimulated luminescence (OSL) dating, ^{137}Cs dating, heavy metal analysis, and flood bed interpretation – applied at three embanked floodplain sites along lower Rhine River distributaries in the Netherlands. All methods indicate significant sedimentation rates on the floodplains, varying between 2-7 mm/a in the distal zones and 3-9 mm/a in the proximal zones. On a rapidly developing sand bar along a natural levee sedimentation rates of 9-25 mm/a were found. Except for some minor inconsistencies in ^{137}Cs dating results, all methods show decreasing sedimentation rates with increasing distance from the river channel. Intercomparison of the results of the different dating methods revealed the potential errors associated with each method, particularly where disagreement among the results were found. Uncertainties may arise due to (1) grain-size dependent downward migration of ^{137}Cs, (2) smoothing of the vertical heavy metal and ^{137}Cs profiles, (3) delayed sediment-associated input of ^{137}Cs in addition to direct atmospheric fall-out, (4) overestimation of the burial age in OSL dating due to incomplete resetting of the OSL signal, or (5) non-linear relationships between sediment deposition and flood magnitude in the count-from-the-top correlation between sediment lamination and past observed flood records. Still, taking the uncertainties associated with each method into account, the results are generally in good agreement. Using the results we indicate the optimal spatial range of application of each method, depending on sediment texture and sedimentation rate. The optimal spatial and temporal ranges differ for each method, but show significant overlap. A combination of the methods will thus provide maximum information for accurate estimation of sedimentation rates on a decadal time scale.

3.1 Introduction

Lowland floodplains are important sinks for suspended sediment transported through a river system. About 10-40% of the annual load entering the system is trapped on the floodplains by overbank deposition during periods of inundation (e.g. Lambert and Walling, 1987; Walling et al., 1998; Walling and Owens, 2003), resulting in vertical accretion of the floodplains. Contemporary accretion rates range from a few millimetres up to several centimetres per year (Rumsby, 2000 and references therein), but large spatial differences exist, dependent on floodplain topography and roughness (e.g. elevation, width, vegetation), overbank flow (e.g. frequency, duration, magnitude, flow velocity) and suspended sediment (e.g. concentration, composition) (Middelkoop and Asselman, 1998; Asselman and Middelkoop, 1998; Thonon, 2006; Straatsma and Baptist, 2008).

On the embanked floodplains of the Rhine in the Netherlands, vertical accretion has been the dominant sedimentation process since the river bed was laterally fixed by groynes around 1850 AD (Hesselink et al., 2003). This has caused the discharge capacity of the embanked floodplains to decrease (Figure 3.1). Due to climate change, however, discharges are expected to increase (Middelkoop et al., 2001; Vellinga et al., 2008), so the reduced discharge capacity threatens the safety of the surrounding low-lying inhabited areas. To ensure safety, a series of landscaping measures have been developed in the last decade. These measures aim to increase the discharge capacity of the river Rhine by removing sediment from the floodplain (e.g. lowering of the floodplains, digging of secondary channels; Silva et al., 2001). Generally, these measures are part of a more dynamic floodplain management strategy that includes the mining of clay, sand and gravel, and also aims to restore nature values (e.g. cyclic floodplain rejuvenation; Peters et al., 2006).

To determine the potential impacts of landscaping measures in a dynamic floodplain management strategy, it is essential to gain insight into the rate of present-day and future floodplain aggradation. This insight can be obtained by the reconstruction of historical sedimentation rates. Previous studies on embanked floodplains of the Rhine have mainly

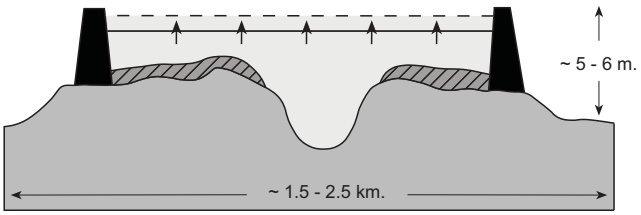

Figure 3.1. Schematic cross section of a river channel with embanked floodplains in the Netherlands during high discharge. Embanked floodplains are bounded by dikes, which restricts the area in which flooding and sedimentation can occur. As a result of embanked floodplain sedimentation (hatching) the discharge capacity decreases and hence the flood water levels rise (arrows), which threatens the safety of the surrounding low-lying inhabited flood basins.

focused on sedimentation at the event scale, for instance by observing the flood deposit thickness in sediment traps (Middelkoop and Asselman, 1998; Maas et al., 2003), or by the estimating sediment accumulation from aerial photographs (Sorber, 1997). In floodplain management, however, the decadal scale is of importance. Hence, several methods have been applied to estimate decadal sedimentation rates in floodplains. One such method is heavy metal analysis, which relates the varying heavy metal concentrations in the sediment profile to known temporal pollution variations in the upstream catchment (Middelkoop, 2000). Other methods make use of fallout radionuclides, such as ^{137}Cs, of which the atmospheric deposition peaks can be identified in the vertical soil profile (Walling and He, 1997; Van den Berg and Van Wijngaarden, 2000), or ^{210}Pb, of which the rate of decrease of the unsupported fraction with depth in the soil profile reflects the average sediment accumulation rate (He and Walling, 1996; Owens et al., 1999). Recently, optically stimulated luminescence (OSL) dating has been introduced to estimate decadal sedimentation rates on floodplains (Wallinga et al., 2010).

Studies of floodplain sedimentation rates are often based on a single reconstruction method. In the present study, we compare four independent methods to estimate the decadal sedimentation rates in the embanked floodplains of the Rhine. The methods we assess are ^{137}Cs-dating, heavy metal analysis, OSL dating, and flood bed interpretation. Our goals are (1) to estimate decadal sedimentation rates at proximal and distal embanked floodplain sites, (2) to assess the applicability and accuracy of the methods through intercomparison of the results, and (3) to determine the optimal spatial and temporal ranges of application of each dating method.

3.2 Study sites

The river Rhine drains a 185,000 km^2 catchment located mainly in Switzerland, Germany, France, and the Netherlands. Its delta is located in the Netherlands, where the river divides into three distributaries: the Waal, the Nederrijn/Lek and the IJssel. Our measurements were carried out on samples from three embanked floodplain sites on the Waal (Rijswaard) and the IJssel (Cortenoever and Vreugderijkerwaard) (Figure 3.2).

The Rijswaard developed as a result of stepwise downstream migration of a meander of the embanked Waal after 1300 AD. Accretion at the upstream part – enhanced by groynes and trees – and erosion at the downstream part have resulted in a series of successively developed bars, separated by secondary channels (Middelkoop, 1997; Hesselink, 2002). On top of these bars a natural levee developed close to the main river channel (Maas et al., 2003). Downstream migration ceased around 1850 AD, when the river bed was fixed by large-scale construction of groynes. Subsequently a sand bar developed between the groynes. We applied our methods in the eastern (upstream) part of the Rijswaard where bed sediments were formed during early stages of downstream migration of the river (~1300-1700 AD). These bed sediments are covered by overbank deposits that were largely formed after ~1600 AD, and include natural levee and distal fine deposits.

Cortenoever is characterized by a bar-and-swale morphology located in an inner bend of a meander of the IJssel. This morphology presumably developed due to increased river discharge between 1200 and 1600 AD (Maas et al., 2003). After 1600 AD discharge

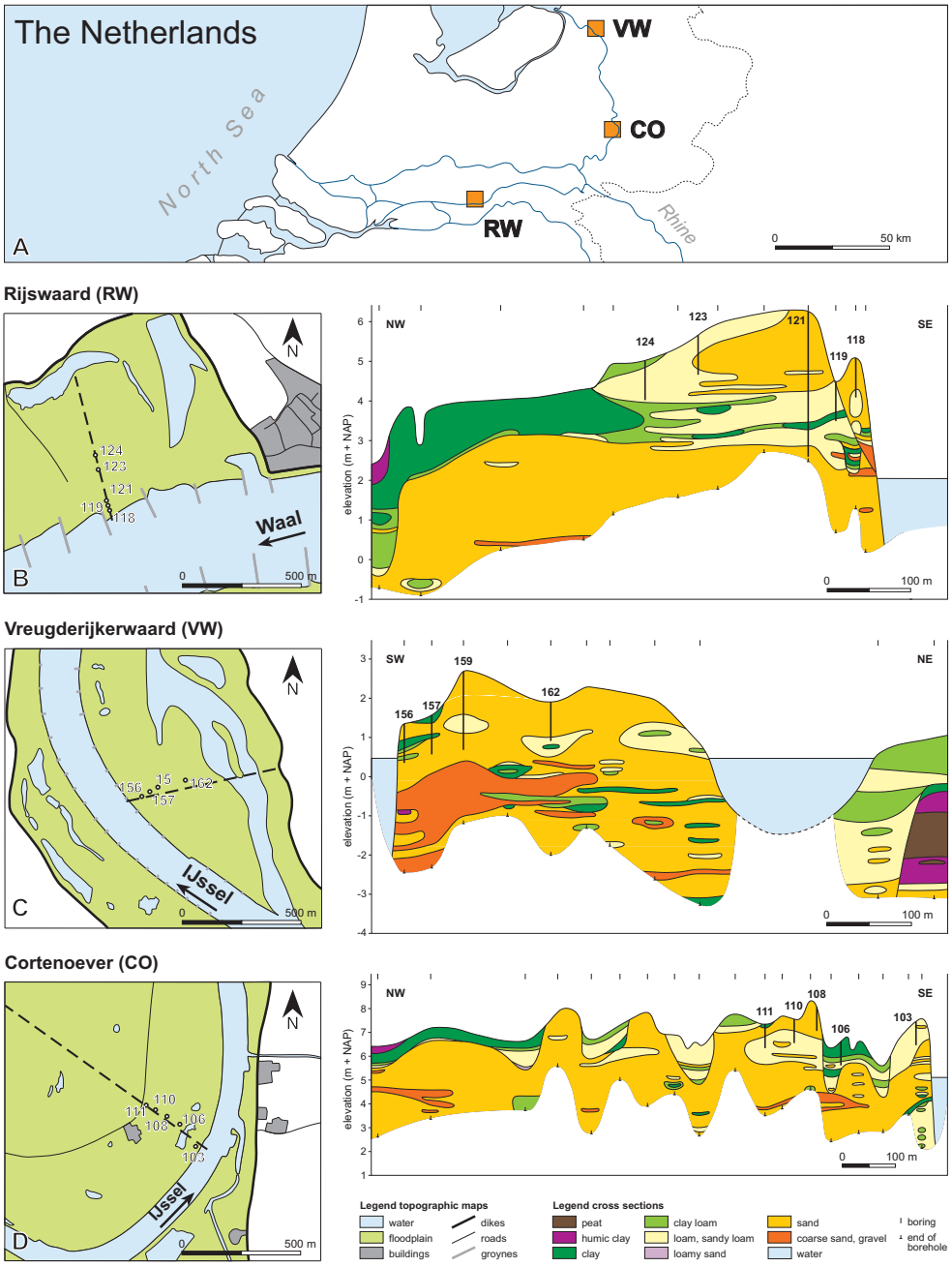

Figure 3.2. Locations of the studied floodplain sites in the Netherlands (A), and topographic maps of the Rijswaard (B), Vreugderijkerwaard (C) and Cortenoever (D) study areas, showing locations of cores (numbered) and the studied transects. To the right, lithological cross-sections along the transects are shown, with the locations of the investigated cores (numbered).

decreased. As a result the development of point bars ceased, and on top of the youngest bar a sandy natural levee developed. The present floodplain, where overbank deposition continues during flood events, shows a relief of 1 to 2 m. Our samples were taken from overbank sediments covering the bars and the swales.

The Vreugderijkerwaard is also characterized by a bar-and-swale morphology, located in an inner bend of an IJssel meander. Point bar formation was accompanied by development of aeolian river dunes on these bars, caused by dominating southwesterly winds. These processes took place until the early 1700s AD. Since then, inner bank erosion dominated in the Vreugderijkerwaard, as the opposite river dike was protected from erosion with groynes (Maas, 1998; Maas et al., 2003). Inner bank erosion ceased due to the construction of large groynes at the beginning of the 19th century. A new sand bar then developed, which became partly covered by silty natural levee deposits. Recently, sand has been mined from parts of the sand bars and river dunes to enlarge the discharge capacity of the embanked floodplains. For sample collection we avoided the aeolian river dunes and disturbed floodplain areas.

3.3 Sample collection

In our research we made use of 14 soil cores from the study of Maas et al. (2003), who used ^{137}Cs dating to estimate sedimentation rates in 1-m-long cores from the three floodplain transects. These floodplain cores were obtained in September 2001 by driving a 10-cm-diametre pvc tube into the soil using a mechanical bailer drilling unit (Oele et al., 1983). Corresponding surface elevations were obtained by levelling to absolute Dutch ordnance datum.

To correct for post-depositional redistribution of ^{137}Cs (e.g. Almgren and Isaksson, 2006) and to determine the amount of local direct fall-out ^{137}Cs, we took reference cores from nearby undisturbed soils outside each floodplain area. The sites were selected from a series of topographic maps dating from the 1950s to the present, and their locations are based on the presence of pastures on all maps. The 25 to 35-cm-long reference cores were taken in November 2008, using a stainless steel tube with a 10-cm-diametre pvc core liner inside, which was hammered into the ground.

In June 2008, we carried out additional corings in the transects with an Edelman auger (Oele et al., 1983) to determine the geometry of the overbank sediments. The vertical elevation of the coring locations was levelled to absolute datum. The locations of the cross-sections and the floodplain cores are plotted in Figure 3.2.

3.4 Dating methods

We applied four different dating methods on 14 cores from three floodplain transects. Table 3.1 summarizes which methods were applied for each core. Selection was mostly based on applicability limitations due to grain size, and for flood bed interpretation on the presence of a bedded profile. Below, a general description of each method will be given.

Table 3.1. The methods applied on each core (c.u. = coarsening upwards, f.u. = fining upwards).

Core	Environment	Lithology	^{137}Cs dating	Heavy metals	OSL dating	Flood beds
Rijswaard						
N118	Sand bar	(Coarse) sand, bedded	X		X	X
N119	Proximal swale	C.u. clay loam to sandy loam	X	X		
N121	Proximal levee	Fine sand	X	X	X	
N123	Distal floodplain	Clay loam / sandy loam	X			
N124	Distal floodplain	F.u. clay loam to clay	X	X	X	
Cortenoever						
B103	Proximal levee	F.u. coarse sand to clay loam	X	X	X	
B106	Proximal swale	Clay loam	X	X		
B108	Distal floodplain	Sandy loam / fine sand	X			
B110	Distal floodplain	F.u. fine sand to sandy loam	X	X		
B111	Distal floodplain	F.u. sandy loam to clay loam	X	X		
Vreugderijkerwaard						
Z156	Proximal levee	Sandy loam / fine sand	X		X	
Z157	Proximal levee	Fine sand / coarse sand	X			
Z159	Proximal levee	Fine sand / coarse sand	X		X	
Z162	Distal floodplain	C.u. clay loam to sandy loam	X	X		

3.4.1 ^{137}Cs dating

^{137}Cs is an artificial radionuclide that entered the environment during the nuclear weapons testing in the 1950s and 1960s, and the Chernobyl nuclear accident in 1986 AD (Cambray et al., 1987). It entered the floodplain soil by atmospheric fallout and by deposition of suspended sediment to which it is bound. In the floodplain soil ^{137}Cs is strongly fixed by clay particles (He and Walling, 1996). The half-life of ^{137}Cs is 30.17 a, and therefore its presence in soils and sediments is still measurable. Hence, ^{137}Cs dating is based on the identification of ^{137}Cs activity peaks in a vertical soil profile, and the correlation of these peaks to the peak years of deposition (Walling and Bradley, 1989). It has proven to be a useful method for estimation of sedimentation rates over the past decades, and has been widely applied in many depositional environments (e.g. Terry et al., 2002). A detailed description of the principles is given by Ritchie and McHenry (1990) and Walling and He (1997).

In our study, we used the results of Maas et al. (2003), who measured vertical ^{137}Cs activity profiles, at 2-cm-thick intervals, on 14 floodplain cores through a core scanning method (Rigollet and De Meijer, 2002). They identified peaks based on at least two successive measurements above a background activity of 10 Bq/kg , and fitted these peaks with a Lorentz function (Hillmann et al., 1996). Subsequently, they estimated sedimentation rates by relating the Lorentz peaks to years of known atmospheric ^{137}Cs deposition (1963 and 1986 AD).

Maas et al. (2003) did not take account of chemical and biophysical processes in the soil, which cause downward migration of ^{137}Cs (Schimmack et al., 1997; Owens et al., 1996), and smooth the vertical ^{137}Cs activity profile. We quantified downward migration by analyzing vertical ^{137}Cs activity profiles in reference cores that were taken from undisturbed, non-depositional environments close to the study sites. We divided these reference cores into 2-cm-

thick samples, homogenized them, and sealed them into 50 ml containers. These containers were measured and analyzed for their ^{137}Cs activity by a HPGe-detector, housed in a low background set-up, in accordance with the Dutch norm on gamma-spectrometric activity concentration determination NEN 5623 (NE01, 2001). In the resulting activity profiles we identified peaks visually, and plotted them with a Lorentz function. The depth of a peak indicates the downward migration of ^{137}Cs between peak year of atmospheric deposition and sampling. We calculated the average migration rate, assuming an initial infiltration of ^{137}Cs in the soil during the deposition event of 1 cm (demonstrated by Owens et al., 1996). This infiltration depth was subtracted from the depth interval used to calculate the average migration rate. The results were used to correct the peak depths in the floodplain cores of Maas et al. (2003).

3.4.2 Heavy metal analysis

Heavy metals occur naturally in river waters. Since approximately 1860 AD, however, urban and industrial waste waters have increased the heavy metal concentration of Rhine water significantly (Middelkoop, 2000). In water, heavy metals become rapidly attached to (fine-grained) sediment, and enter the floodplain by overbank deposition of the contaminated sediments. Long-term variations in pollution history have caused the heavy metal concentrations in the water, and hence in the floodplain sediments, to vary. Middelkoop (2000) reconstructed the temporal variations of zinc, lead, and copper in the Rhine sediments, based on their concentrations in sediments from small ponds within the floodplain area, using historic data and ^{210}Pb dating results for time control. Several characteristic changes could be identified: (1) the first increase in metal concentrations around 1860 AD, (2) the strong increase in concentrations in the early 1900s, (3) a first maximum concentration around 1930, and (4) a second maximum concentration around 1960 (Figure 3.3). Heavy metal analysis relates the varying metal concentrations in a vertical soil profile to this pollution history.

We measured vertical concentration profiles of zinc, lead and copper in eight floodplain cores which had sufficient amounts of fine-grained material (Table 3.1). Samples were collected at 2.5 to 10-cm-intervals, and they were air dried at 40 °C and homogenized with a mortar. The prepared samples were split into two subsamples. One was used to determine the water content by heating to 105 °C, the organic matter content through loss on ignition at 550 °C, and the grain size distribution with a Coulter LS 230 laser particle sizer. The other subsample was analyzed for the contents of zinc, lead and copper, using destruction HNO_3-HCL (aqua regia) ICP-AES Thermo.

The metal concentrations depend on clay and organic matter content, which vary greatly within and between cores. We corrected for this dependency by converting the metal concentrations to a standard sediment of 40% clay and 8% organic matter, on basis of a linear relation between metal concentrations and contents of clay and organic matter (Middelkoop, 1997). In the converted metal profiles we identified characteristic changes from the known pollution history reconstructed by Middelkoop (2000), and assigned ages to the depths of these characteristic changes.

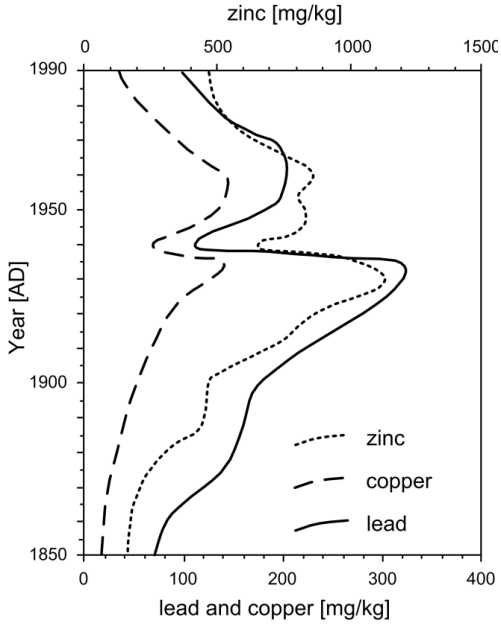

Figure 3.3. Heavy metal concentration in the Rhine sediment. Figure modified from Middelkoop (2000).

3.4.3 Optically Stimulated Luminescence (OSL) dating

Optically stimulated luminescence (OSL) dating is a method that makes use of the charge that is trapped in sand-sized quartz grains by exposure to natural ionizing radiation from the environment.—The accumulated charge gives rise to a luminescence signal that can be measured in the laboratory, and provides a measure for burial time. A comprehensive overview of the OSL-dating principle is given by Wintle (2008) and its application to fluvial deposits is reviewed by Rittenour (2008). The application of OSL dating to young fluvial deposits is challenging. One of the assumptions underlying OSL dating is complete resetting of all trapped charge prior to deposition, which commonly happens by (sun)light exposure during erosion, transport and deposition processes. For fluvial sediments, limited light exposure in the turbid river water may only partially reset the OSL signal. Any remaining signal present at the time of deposition may cause an overestimation of the burial age. This problem is particularly acute for young samples, because the desired OSL signal is relatively small.

We applied OSL dating on six cores (Table 3.1) to determine the time elapsed since sand deposition in the floodplains. Results for 22 samples are used for this study; 11 of these were already reported by Wallinga et al. (2010). The samples were taken from sandy layers in the floodplain cores. The samples were split in a dark room. On one half the natural radionuclide activity concentrations were determined to calculate the dose rates. From the other half quartz grains were extracted for luminescence measurements to determine the equivalent dose. On the dose rate samples water and organic matter content were determined by heating to 105 °C

and 500 °C, respectively. The samples were ground and mixed with wax, and subsequently measured on a high-resolution gamma ray spectrometer. For equivalent dose measurement, we selected sand-sized quartz grains and mounted small aliquots (2-3 mm diameter) to allow detection of heterogeneous bleaching of the OSL signal at the time of deposition the equivalent dose distribution (e.g. Wallinga, 2002b). The grains were extracted by sieving, after removal of carbonates and organic matter, using HCl and H_2O_2 (both 10%), and dissolution of feldspars and etching of the quartz grains by 40% HF. The measurements were employed on Risø TL/OSL DA-15 readers (Bøtter-Jensen et al., 2000). Further details on the measurements are described by Wallinga et al. (2010).

To avoid age overestimation by incomplete resetting we used a measurement protocol developed by Wallinga et al. (2010), that is based on a single-aliquot regenerative dose (SAR) procedure (Murray and Wintle, 2003). With this method, we tried to maximize the proportion of the most light-sensitive stable component (the fast component) in the OSL signal, by subtracting an early background from each OSL decay curve (Ballarini et al., 2007; Cunningham and Wallinga, 2009). To avoid thermal transfer effects we selected a low preheat temperature of 200 °C. As this preheat temperature was not sufficient to eradicate the unstable ultrafast component on the OSL signal, we applied an additional 20 second infrared light exposure prior to the OSL measurements for the Rijswaard samples. This procedure was not used for the Cortenoever and Vreugderijkerwaard samples because there was no evidence of an ultrafast OSL component for these. The resulting dose distributions for each sample were fitted with two Gaussian curves, with the lower peak representing the set of subsamples for which the OSL signal was completely reset at deposition. The position of this peak gives the best estimate of the burial dose, and the width of the peak gives the uncertainty on this estimate. For details we refer to Wallinga et al. (2010).

3.4.4 Flood bed interpretation

In some natural levees individual sediment layers in the vertical soil profile can be identified. Layers that are assumed to have been deposited during one flood event are called here 'flood beds'. Flood bed interpretation involves a count-from-the-top correlation of these flood beds to peak events in the observation record of river water levels that resulted in overbank deposition (Figure 3.4). We applied this method to core N118, the only core in which a markedly bedded profile was observed.

N118 originates from a sand bar on the river bank, in which organic-poor sand or silt layers alternate with organic-rich silt or clay layers. To define flood beds we took samples from all individual layers, and analyzed them for their clay, water and organic matter contents. First, the samples were prepared by air drying at 40 °C, and subsequently by sieving over a 2 mm sieve. Then the prepared samples were measured for their water and organic matter contents, by heating to 105 °C and 550 °C, respectively. Subsequently, grain-size distributions were measured with a Coulter LS 230 laser particle sizer. Finally, we identified flood beds, assuming that one flood bed is a combination of an organic-poor sand or silt layer from the early stage of flooding, followed by an organic-rich silt or clay layer deposited during the recession. Based on their thickness, we distinguished five classes of flood beds (very small: <0.5 cm; small: 0.5-1.5 cm; medium: 1.5-2.5 cm; large: 2.5-3.5 cm; very large: >3.5 cm).

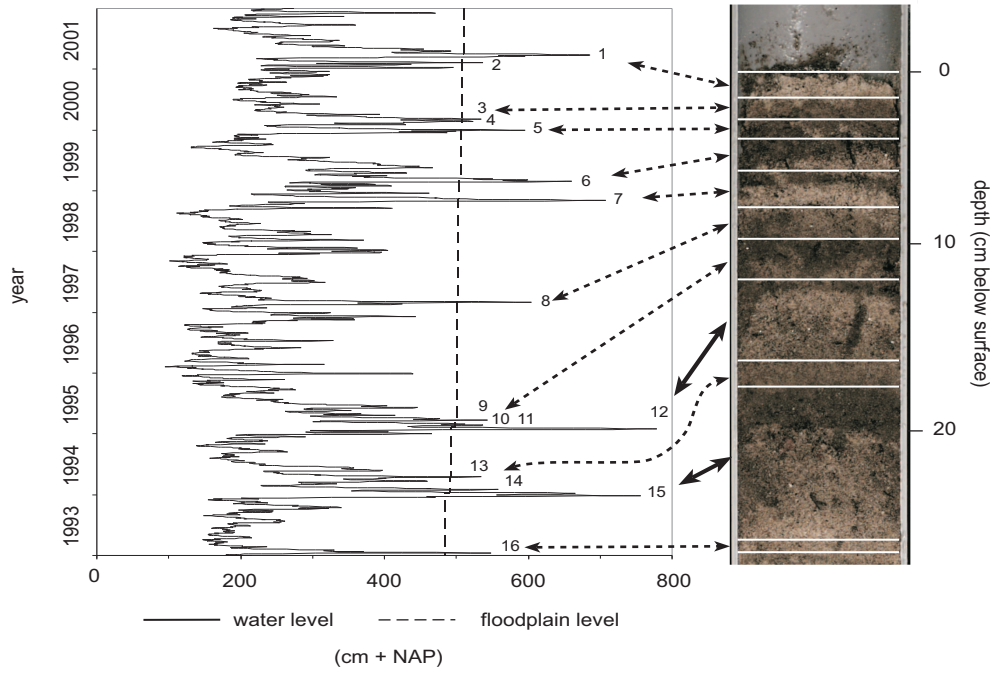

Figure 3.4. Flood bed interpretation, following a two-step count-from-the-top method: (1) correlation of the largest flood beds to the largest flood events, indicated by the solid arrows, and (2) correlation of the smaller flood beds to the smaller flood events, indicated by the dashed arrows. In flood definition, we accounted for changes in floodplain level due to sedimentation.

For reconstruction of water levels, we used data from several nearby gauging stations on the Waal River (V&W, 2008). Daily average water levels for the period 1981-2001 AD at the N118 site were estimated by linear interpolation between upstream (Nijmegen; 47.3 km from the Rijswaard) and downstream (Zaltbommel; 3.0 km from the Rijswaard) gauging station data. Daily average water levels for the period 1951-1981 were estimated by extrapolation from an upstream gauging station (Dodewaard; 33,9 km from the Rijswaard), using the average difference in water level between Dodewaard and N118 at the high stages observed in the 1981-2001 record. Subsequently, flood events were defined as a period in which the water level rises above floodplain surface level. We divided these floods into categories, based on duration (A: >9 days, B: 4-9 days, C: < 4 days) and flooding depth (1: >150 cm, 2: 50-150 cm, 3: <50 cm). We correlated flood beds with flood events on basis of the following assumptions:

- Floods only can result in overbank deposition when the river water level rises above the floodplain surface level.
- The largest floods (concerning both duration and flooding depth) are responsible for deposition of the thickest layers (Sorber, 1997; Middelkoop and Asselman, 1998).

- Small flood events (short and low magnitude) may not result in the deposition of a recognizable layer of sediment.
- Catastrophic events that cause erosion and rework older material do not occur.
- Deposits from two or more flood events in the same hydrological season may sometimes not be identified separately, because sediments are likely reworked during the next flood, unless they are fixed by vegetation during a growing season.

Floodplain elevation, and thus the threshold height for flooding, has increased in time, due to accumulation of sediment. Therefore, correlation was done in an iterative procedure, in which floodplain elevation and flooding depth were adjusted after every step. The floodplain level for 2001 AD, the year of core collection, was obtained from measurements by Maas et al. (2003). Floodplain levels before 2001 AD were obtained by subtracting the thickness of the older sediment layers from the 2001 AD surface level in an iterative procedure. Uncertainty arose in the correlation of the sediment layers to individual flood events in the past, which increases with depth within the profile. Therefore, at an arbitrary depth of 33 cm below surface the iterative procedure was changed into a non-iterative procedure, by estimating past floodplain elevations based on the average sedimentation rate found in the upper 33 cm.

We attempted to correlate flood events with flood beds by a two-step count-from-the-top method. In the first step, the largest flood beds (category large and very large) were correlated with the largest flood events (category A1, B1, and A2). In the second step the smaller intermediate beds were correlated with the smaller events that occurred between the major events (Figure 3.4).

3.5 Results and interpretation

3.5.1 ^{137}Cs dating

Figure 3.5 shows the uncorrected ^{137}Cs activity profiles of the floodplain cores (from Maas et al., 2003) and the reference cores, with the Lorentz fits representing the interpreted 1963 and 1986 AD deposition peaks. The average downward migration rate in the three reference cores is 3.3 mm/a. Corrections for this downward migration of the peak depths in the floodplain cores are indicated by the arrows in Figure 3.5. The precision of the individual ^{137}Cs measurements are one standard deviation. Uncertainties in the peak depths arise from the sample interval (2 cm) and from the correction for downward migration, which may contain some errors due to the relatively coarse increment that is used in the reference cores (also 2 cm) and the large spatial variability in soil mixing process within a floodplain soil. Therefore, an uncertainty range is given with the peak depths, which involves one standard deviation of the average downward migration rate, increased with the sample thickness of the floodplain cores. These, and other uncertainties are addressed in the discussion section.

Depths of the deposition peaks were identified using the criteria described in Maas et al. (2003) (see methods section). For all peaks we scrutinized whether they were not an artifact of the lithology (e.g. ^{137}Cs accumulating in clay layers). This has resulted in rejection of the 1963 AD peak in core Z156. In most floodplain cores both the 1963 and 1986 AD peaks are visible.

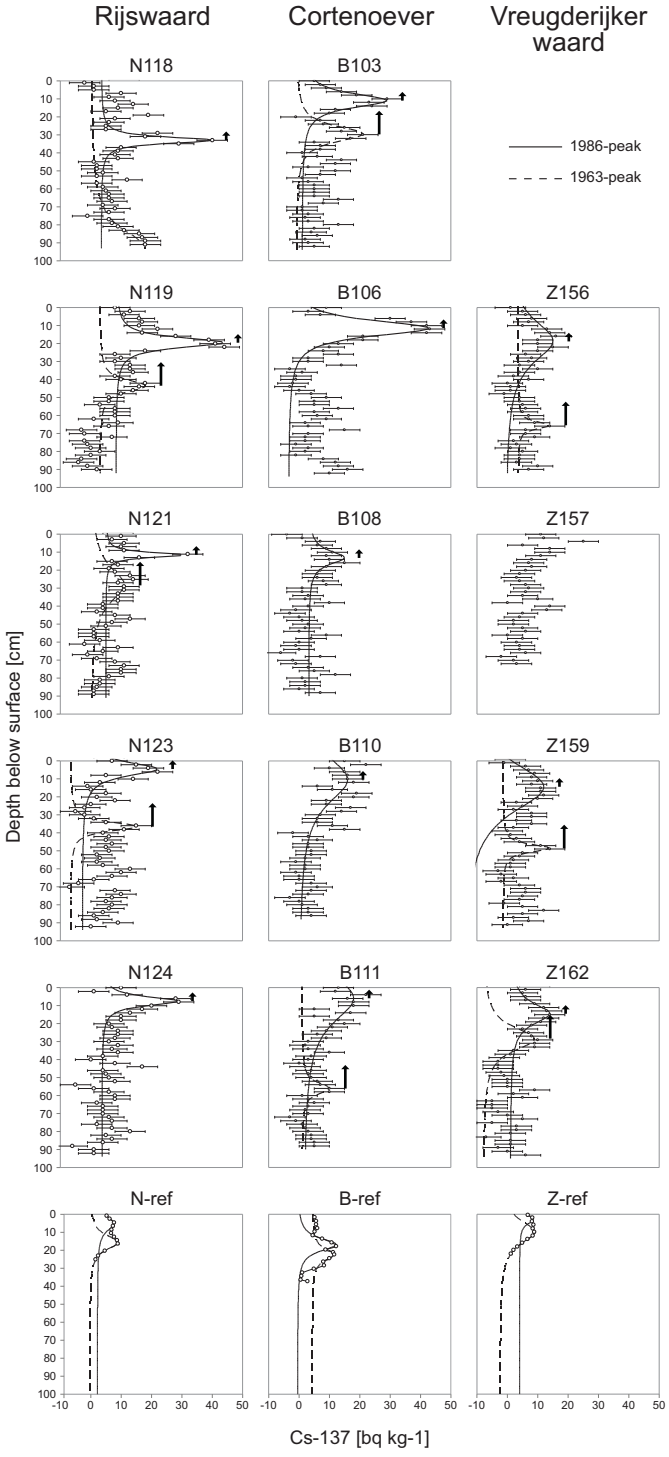
Rijswaard
Cortenoever
Vreugderijker waard
N118
B103
1986-peak
1963-peak
N119
B106
Z156
N121
B108
Z157
N123
B110
Z159
N124
B111
Z162
N-ref
B-ref
Z-ref
Depth below surface [cm]
Cs-137 [bq kg-1]

Some of the floodplain cores show one peak, which was interpreted as the 1986 Chernobyleak. In core N118 the 1963 AD peak is not entirely visible, and may be located below the maximum core depth. Z157 was disturbed and no peak could be identified. In some cores additional peaks were present, but none of these satisfy the criteria for peak identification.

3.5.2 Heavy metal analysis

The heavy metal profiles and the depth of their characteristic changes are shown in Figure 3.6. In most cores, the first increase around 1860 AD and the major increase around 1900 AD are well recognizable. However, all profiles show one peak, which is assumed to represent both the 1935 and 1960 peaks, which merged into a single peak due to by biophysical soil mixing processes, and the relatively coarse sediment increment (2.5 to 10 cm). Cores B110 and N119 do not show any characteristic changes. Core B110 is a sandy core, where heavy metal concentrations are too low to detect changes in the vertical profile, and core N119 may be disturbed at depths where the characteristic changes would be expected.

Uncertainties in the age-depth relations are mainly due to the slight differences between the zinc, copper and lead profiles, and the sample thickness from which the profile was determined. These errors were quantified by giving a depth range for all characteristic changes, and adding the sample thickness to this error (Figure 3.8). Uncertainties in the assignment of the concentration changes in the profiles to the pollution changes of the Rhine in the past century are small, and not included in the uncertainty range.

3.5.3 OSL dating

OSL-ages are obtained by dividing the burial dose by the dose rate. Uncertainties in the age estimate, given as one sigma, include systematic and random errors in both burial dose and dose rate estimation (Table 3.2). Ages range between 8 ± 6 and 565 ± 30 years, and are geologically consistent (i.e. ages are generally in correct stratigraphic order). There is a slight age inversion in N121 and B103, but results agree within the error margins and could also reflect a single depositional event. When calculating sedimentation rates based on the OSL ages we also included uncertainties due to the sample thickness.

Figure 3.5 (previous page). ^{137}Cs activity profiles of floodplain cores and reference cores from the Rijswaard, Cortenoever, and Vreugderijker-waard study sites. Horizontal bars of the individual measurements indicate one standard deviation. Peaks are fitted with a Lorentz function. The arrows indicate correction for downward migration.

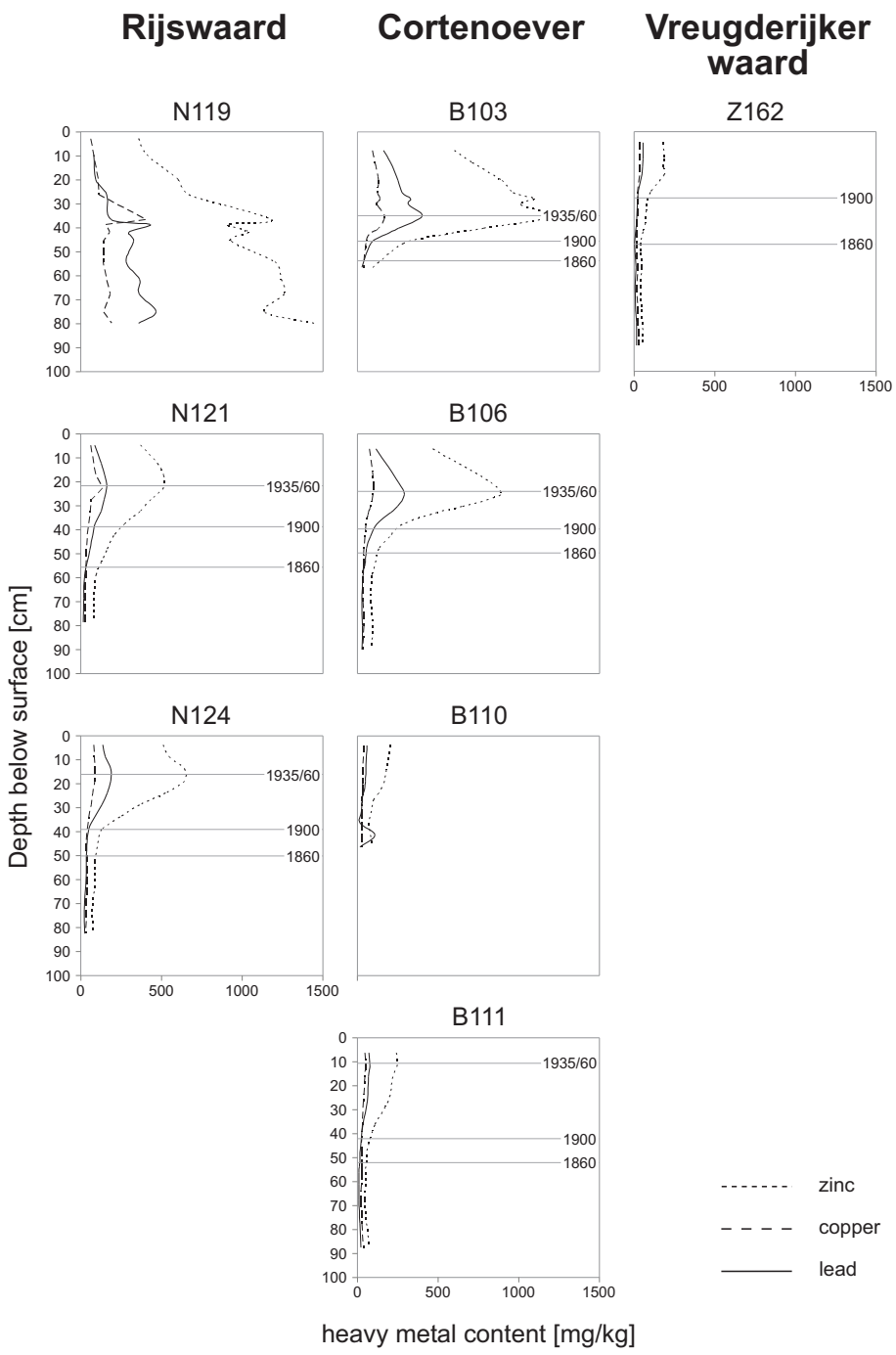

Figure 3.6. Heavy metal profiles of floodplain cores from the Rijswaard, Cortenoever, and Vreugderijkerwaard study sites. Interpreted ages of characteristic changes in the profiles are also given.

Table 3.2. OSL-dating results.

Sample	Lithology	Depth [m]	Total dose rate [mGy/a]	Equivalent dose [mGy]	OSL age [years before 2007]
N118; x:148005, y:426200					
NCL-1107134	Sand	0.15	2.07 ± 0.08	16 ± 13	8 ± 6
NCL-1107136	Sand	0.31	2.06 ± 0.06	57 ± 24	27 ± 12
NCL-1107137	Sand	0.57	1.81 ± 0.06	100 ± 14	55 ± 8
NCL-1107138	Sand	0.85	1.82 ± 0.07	172 ± 24	95 ± 14
N121; x:147991, y:426242					
NCL-1107140	Loam	0.13	2.02 ± 0.08	127 ± 16	63 ± 8
NCL-1107141	Loam	0.31	2.30 ± 0.08	316 ± 17	137 ± 9
NCL-1107142	Sand	0.77	2.53 ± 0.08	331 ± 9	131 ± 5
NCL-1107143	Sand	1.26	2.19 ± 0.06	721 ± 67	328 ± 32
N124; x:147944, y:426436					
NCL-1107148	Clay	0.08	2.20 ± 0.15	124 ± 16	56 ± 8
NCL-1107149	Silt	0.44	2.65 ± 0.13	410 ± 36	155 ± 16
NCL-1107150	Silt	0.79	2.57 ± 0.11	787 ± 26	306 ± 16
B103; x:211797, y:456837					
NCL-4307151	Loam	0.10	2.39 ± 0.11	83 ± 13	35 ± 6
NCL-4307152	Loam	0.29	2.45 ± 0.10	394 ± 47	161 ± 20
NCL-4307153	Loam	0.53	2.45 ± 0.08	454 ± 24	185 ± 12
NCL-4307154	Sand	0.76	2.17 ± 0.06	396 ± 24	183 ± 12
Z156; x:197877, y:503256					
NCL-2107155	Sand	0.15	1.80 ± 0.07	75 ± 13	42 ± 8
NCL-2107157	Sand	0.52	1.71 ± 0.05	142 ± 12	83 ± 8
NCL-2107159	Sand	0.74	1.68 ± 0.05	206 ± 21	122 ± 13
Z159; x:197917, y:503281					
NCL-2107161	Sand	0.22	1.69 ± 0.05	175 ± 12	103 ± 7
NCL-2107162	Sand	0.52	1.87 ± 0.06	328 ± 15	176 ± 9
NCL-2107163	Sand	1.16	1.79 ± 0.05	712 ± 67	397 ± 39
NCL-2107164	Sand	1.67	1.67 ± 0.07	941 ± 34	565 ± 30

3.5.4 Flood bed interpretation

In Figure 3.7a the first step of flood bed interpretation is shown, in which the largest flood beds are correlated with the largest flood events. Close to the surface the uncertainty of the correlations is about 1 or 2 years, but the error range increases with increasing depths of the flood beds. This mainly occurs where large intervals of small flood beds are present (between 48 and 64 cm and between 69 and 80 cm below surface). At a depth of 100 cm below the surface the uncertainty is 10 years: the sediment was most probably deposited between 1952 and 1962 AD. The age-depth plot in Figure 3.7b demonstrates a relatively constant sedimentation rate over the past few decades.

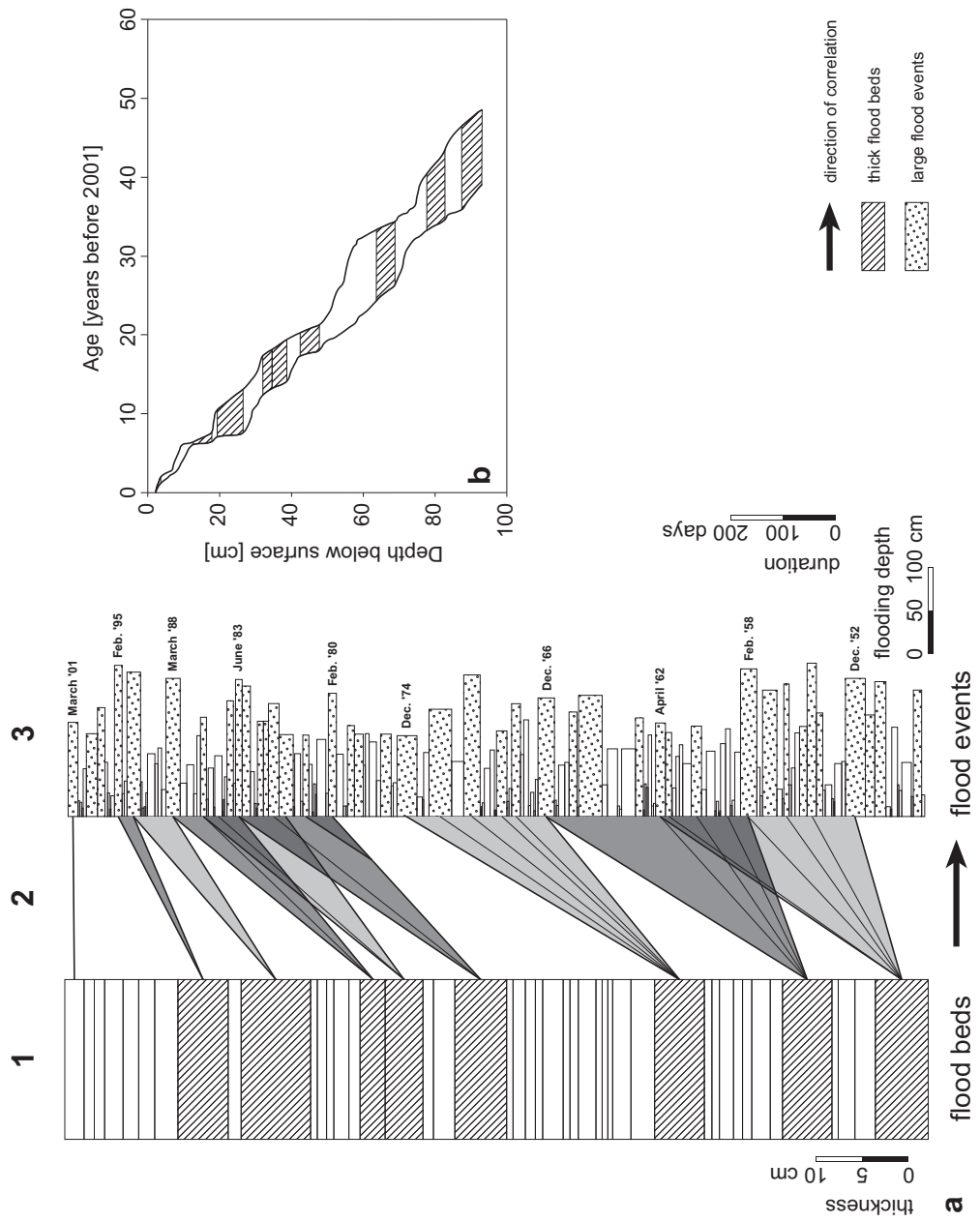

Figure 3.7. (a) In column 1 the flood bed succession in the 1-m-long soil core is schematized and column 3 represents the duration and flooding depth of all flood events that have occurred since 1950 AD. The lines in column 2 connect the flood beds to potential depositional flood events. The increasing distance between the bold lines with increasing depths of the layers shows the increasing uncertainty of the correlations. For clarity, the second step (correlation of thinner flood beds with smaller flood events) is not shown. (b) Age-depth plot of the minimum and maximum age of the large flood beds.

3.5.5 Sedimentation rates and spatial variability

Figure 3.8 shows the results of all methods, plotted in age-depth plots. Sedimentation rates were determined by an unweighted linear fit of the data, forced through zero age at the surface (where zero age is 2001 AD). The same procedure was applied to all minimum and maximum ages and depths to obtain the error range of all sedimentation rates. The resulting sedimentation rates are given in Table 3.3.

Sedimentation rates are expressed as thickness of sediment deposition per unit time [mm/a]. This is the most useful unit for floodplain management, because the thickness of the deposited sediment is directly related to the decrease in discharge capacity of the floodplains.

Sedimentation rates at the study sites vary between 0 and ~25 mm/a. The highest rates are found close to the river, and the rates generally decrease away from the river. This general trend is found with all methods that are applied along transects. At some distal floodplain sites, however, ^{137}Cs-derived sedimentation rates are relatively high (N123, B108 and Z162). This might indeed indicate locally higher sedimentation rates, or (in the case of core Z162) be due to the low precision involved in the ^{137}Cs dating.

Sedimentation rates also differ between the floodplains. Highest sedimentation rates are found in the Rijswaard. Such differences were also found by Middelkoop (2000) and Thonon (2006), and are probably the result of its situation along the River Waal, which is the largest

Table 3.3. Sedimentation rates in mm/a. Best estimates are given for cores in which the results are well in agreement, based on an unweighted linear fit through all data, forced through zero age at the surface.

	Environment	Flood beds	Cesium	Heavy metals	OSL dating	Best estimate[1]
Rijswaard						
N118	Sand bar	19.6 – 24.9	19.9 – 21.8	-	8.8 – 12.1	
N119	Proximal - swale	-	7.4 – 9.3	No value	-	
N121	Proximal - levee	-	3.1 – 5.0	3.4 – 4.3	3.6 – 4.3	3.6 – 4.3
N123	Distal - floodplain	-	4.4 – 6.3	-	-	
N124	Distal - floodplain	-	0 – 3.6	3.2 – 3.8	2.5 – 2.9	2.6– 3.1
Cortenoever						
B103	Proximal - levee	-	3.4 – 5.3	3.9 – 4.8	2.9 – 3.5	3.1 – 3.9
B106	Proximal - swale	-	2.4 – 6.3	3.5 – 4.1	-	3.5 – 4.1
B108	Distal - floodplain	-	3.4 – 7.3	-	-	
B110	Distal - floodplain	-	1.7 – 5.6	No value	-	
B111	Distal - floodplain	-	0 – 2.6	3.0 – 4.2	-	
Vreugderijkerwaard						
Z156	Proximal - levee	-	7.0 – 11.0	-	5.6 – 7.0	5.6 – 7.1
Z157	Proximal - levee	-	No value	-	-	
Z159	Proximal - levee	-	3.0 – 4.9	-	2.8 – 3.2	2.8 – 3.2
Z162	Distal - floodplain	-	8.1 – 10.0	2.9 – 3.4	-	

[1] Best estimates are only calculated for cores that are in good agreement; for all other cores, the total range of sedimentation rates should be considered.

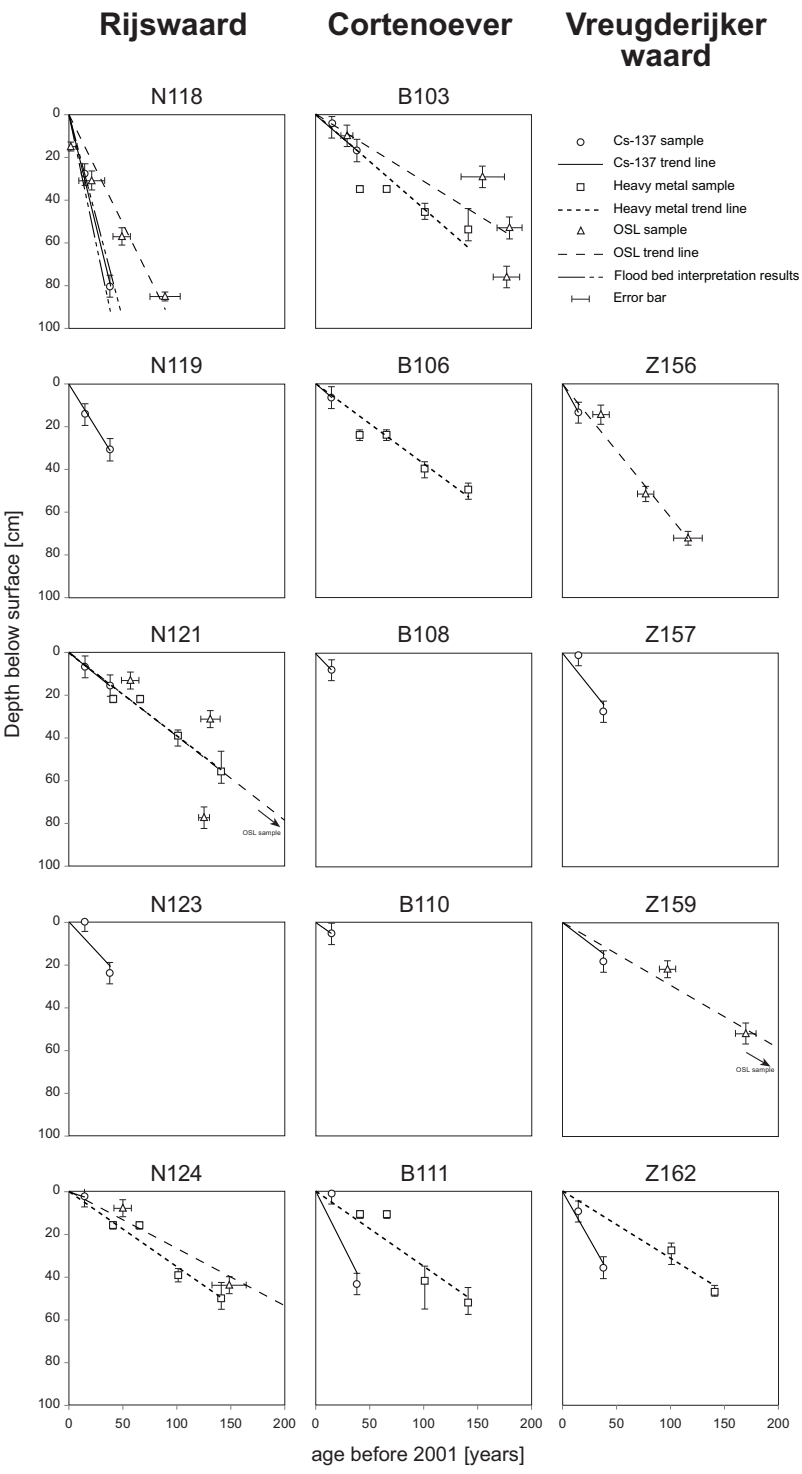
Rijswaard
Cortenoever
Vreugderijker waard
N118
B103
N119
B106
Z156
N121
B108
Z157
N123
B110
Z159
N124
B111
Z162
Cs-137 sample
Cs-137 trend line
Heavy metal sample
Heavy metal trend line
OSL sample
OSL trend line
Flood bed interpretation results
Error bar
OSL sample
OSL sample
Depth below surface [cm]
0
20
40
60
80
100
0
50
100
150
200
age before 2001 [years]

Rhine distributary and carries more water and sediment than the IJssel. Lowest sedimentation rates are found in Cortenoever, of which the floodplain surface is relatively high above the average river water level.

3.5.6 Intercomparison between methods

Sedimentation rates determined using the different methods are generally in good agreement, taking the uncertainty ranges into account. At some sites (N124, B103, Z156), OSL dating tends to yield slightly lower sedimentation rates. Nevertheless, the sedimentation rates mostly agree within their uncertainty ranges.

Disagreement among the dating methods was found in cores N118, B111, and Z162. In core N118, OSL-derived sedimentation rates are lower than ^{137}Cs-derived results that agree well with flood bed interpretation results. For core B111, ^{137}Cs derived sedimentation rates are lower than those based on heavy metal analysis, whereas in core Z162 the opposite is the case. The cores where the different methods agree well are mostly located in the proximal zone (with exception of the sand bar). The distal zone contains many sites where just one method was successfully applied, or where the different methods are in clear disagreement.

Differences in sedimentation rates determined through the applied methods may arise from a change of sedimentation rate over time within a core, as most methods were applied on different sections within the core. However, methods with the longest applicability range, OSL dating and heavy metal profiles, showed no evidence of changes in sedimentation rate over time. Hence, it is more likely that inconsistencies are caused by the assumptions underlying each method. Below, we discuss these assumptions, with a focus on the cores where results disagree (N118, B111 and Z162).

3.6 Discussion

3.6.1 Uncertainties associated with each method

^{137}Cs dating

A first source of uncertainty in the ^{137}Cs dating is related to the catchment-derived input in addition to direct atmospheric fallout. In the upstream basin fine-grained sediments have absorbed fallout ^{137}Cs. During subsequent precipitation and flood events, these grains may be eroded, transported and deposited in a downstream floodplain (Walling and He, 1997).

Figure 3.8 (previous page). Age-depth plots for all investigated cores, showing: (1) the ^{137}Cs activity peaks of 1963 and 1986 AD, corrected for vertical migration (circles), (2) the ages of characteristic changes in the heavy metal profiles (squares), (3) the OSL-dating results (triangles), and (4) the age of the flood events correlated to flood beds (crosses). Linear-fitted trend lines, forced through origin, indicate the average sedimentation rates.

Therefore, the catchment-derived ^{137}Cs peak generally lags behind the atmospheric fallout peak. This effect applies mostly to the 1986 Chernobyl peak, as this is related to a short-duration fallout event. We quantified the amount of catchment-derived ^{137}Cs by subtracting the total amount of ^{137}Cs in the reference cores from the total amount in the floodplain cores, and found a large amount (50-70%) of excess ^{137}Cs due to fluvial deposition. This fluvial sediment-borne ^{137}Cs could have been brought to the floodplain no earlier than during the first flood after 1986, which was in March 1988. This process may result in an age overestimation of the peak in the vertical soil profile, and hence in an underestimation of the sedimentation rate. This may indeed have occurred in N118, where the 1986 AD peak is found on a depth of 28 cm below surface. At this depth a thick flood bed is present, which we correlated with flood bed interpretation with floods from March 1988 or December 1993. The latter is the first large flood event after the Chernobyl accident, and could therefore be held responsible for the deposition of a large amount of ^{137}Cs-contaminated overbank deposits. Correction for this results in sedimentation rates of 18.9 to 21.0 mm/a, which however increases the discrepancy with the OSL-dating results.

After deposition, chemical conditions may cause downward migration of ^{137}Cs in the soil. Errors may have been introduced in the correction for this downward migration. In the reference cores, we found downward migration rates of 1.3 – 7.7 mm/a. These rates are in line with other ^{137}Cs studies, which report downward migration rates between 1 and 10 mm/a (Owens et al., 1996; Schimmack et al., 1997; Almgren and Isaksson, 2006; Clouvas et al., 2007). For correction of the floodplain cores, we assumed an average downward migration rate of 3.3 mm/a. However, true rates depend on several soil and groundwater properties, such as clay type and content, root density, microbiological activity and organic matter content (Schimmack et al., 1997; Almgren and Isaksson, 2006). These properties vary considerably within a floodplain and within the floodplain profiles. Indeed, we found a negative correlation between clay content and downward ^{137}Cs migration rates in our (relatively clayey) reference cores. In most floodplain cores, the clay content is lower than in the reference cores. Therefore, the sandier cores (N118, N121, B108, B110, Z156 and Z159) may have experienced more downward migration than we corrected for, and hence we may have overestimated the sedimentation rates.

Finally, post-depositional bioturbation processes in the soil may cause additional smoothing of the vertical ^{137}Cs profile. As a result, initially separate peaks of ^{137}Cs deposition may have merged into a single one in the floodplain profile. This complicates the assignment of ages to the depth in the profile where the peaks occur, particularly in low sedimentary (distal) environments, where the depth interval between both peaks is relatively small. In core Z162 it is possible that the ^{137}Cs profile has been misinterpreted, as the 1986 event peak is unusually wide compared to the peak representing the 1963 nuclear testing. If this core has been affected by smoothing then the first peak may actually represent both events, in which case our interpretation would lead to an overestimate of the sedimentation rate.

Heavy metal analysis

Biophysical soil mixing also complicates interpretation of heavy metal profiles. In the investigated metal profiles we could not identify the two separate peaks representing the 1930s and 1960s. Therefore, we assigned the average age to the combined peak, which fits well in the age depth plots. The merging of both peaks indicates a severe smoothing, which does not

affect the average peak depth, but causes migration of the first increase in pollution in 1860 AD and the major increase in 1900 AD to slightly greater depths. This results in a minor overestimation of sedimentation rates based on these profile characteristics, as might have occurred for core B111. Downward migration by chemical processes is not expected, as heavy metals are more strongly fixed to the fine-grained sediments than ^{137}Cs under the redox and pH conditions prevailing in the floodplain soils (Scheffer and Schachschabel, 1982).

The merging of both peaks may also be a smoothing effect caused by the relatively coarse sampling intervals (2,5 cm at expected depth of the known time markers to 5 and 10 cm elsewhere in the core). These sampling intervals reflect a balance between feasibility and precision; we expect denser sampling to be of little added value due to soil mixing processes.

OSL dating

For most cores OSL-derived sedimentation rates agree with those obtained through other methods, but for core N118 the rates were substantially lower than those from ^{137}Cs and flood bed interpretation. This discrepancy may be caused by an overestimation of the burial ages, which would occur if in all aliquots grains of which the fast component OSL signal was not completely reset at the time of deposition contribute to the OSL signal. Although we cannot rule out this possibility, several lines of evidence suggest that the OSL ages on this core are accurate. Here we briefly summarize the reasoning presented by Wallinga et al., (2010): (1) the upper sample yields an OSL age of 8 ± 6 years, leaving little space for age overestimation; (2) the four OSL ages on this core are in correct stratigraphic order; (3) a trend line through the OSL dates of this core shows a small negative offset at the surface, which contradicts a positive offset due to incomplete resetting of the signal.

Equivalent dose distributions of all samples show wide scatter, attributed to incomplete resetting of the OSL signal in some of the grains. The Gaussian fitting of probability density functions that we applied for these samples is an attempt to obtain reliable age estimates for these young samples. Dating of such young fluvial deposits remains challenging though, and further methodological developments may enhance the robustness of OSL chronologies in such settings (see e.g. Arnold et al., 2009; Thomsen et al., 2007).

Flood bed interpretation

Flood bed interpretation by count-from-the-top correlation between sediment layers and floods relies on the validity of the underlying assumptions mentioned earlier. One of these assumptions is that the largest floods are responsible for deposition of the thickest layers. However, previous studies showed that the relation between flood event and amount of sediment deposition is complex, and hence not all large floods result in thick sediment layers (Magilligan et al., 1998; Pease et al., 2006). Other important factors are the sediment availability (depletion) and the shape of the flood wave. Furthermore, erosion of previously deposited sediment, during an event or in subsequent events, is hard to determine, but there are no indications of significant erosion in the embanked floodplains studied. Despite the uncertainties, we found sedimentation rates that agree well with the ^{137}Cs-derived sedimentation rates in core N118.

3.6.2 Best estimates of sedimentation rates

In the section "results and interpretation", we showed that at most sites uncertainty ranges of the different methods overlap. If uncertainty ranges overlap the methods are in agreement, and the total uncertainty range must be considered when estimating sedimentation rates. However, at three sites (N118, B111 and Z162) the uncertainty ranges of the different methods show no overlap, i.e. the results are in disagreement. At these sites, we cannot decide what method yields best estimates, because we may have underestimated uncertainty ranges, or there is a systematic error of unknown source in one of the methods.

Best estimates of sedimentation rates are made for all cores where results of the different methods are in good or reasonable agreement (Table 3.3). They are based on an unweighted linear fit, forced through zero surface, through all data of the core, including the uncertainties. Hereby we accept that the results will slightly be biased towards the method with most samples and greatest sample depths. Table 3.4 summarizes the results for the different zones in a floodplain. For the distal and proximal zone, we used the best estimates from Table 3.3, and the results of the cores where only one method was applied. For the sand bar, the whole range of sedimentation rates is given because of the disagreement between the dating methods.

3.6.3 Comparison with other studies

Table 3.4 also presents results from other sedimentation studies in the Rhine embanked floodplains. Middelkoop (2000) applied heavy metal analysis on several floodplains along the Waal. The sedimentation rates he found in the distal zone are in line with our study. In the proximal zone, however, he found slightly higher sedimentation rates. This may be caused by differences in floodplain topography and overbank flow, as the studies concerned different floodplains.

Maas et al. (2003) measured sediment accumulation over an entire flooding season using sediment traps, during a small (February 2001) and a large flood event (March 2001). In all zones, the total sediment accumulation on the traps was smaller than the average yearly sedimentation we found in our study. So, despite the occurrence of a relatively large flood event in 2001 AD, there is just a small contribution of the 2000-2001 flood season to the total deposition of sediment on the floodplain. This suggests that other (larger) floods have contributed most to the total accumulation of sediment (Asselman and Middelkoop, 1998). Two such large events occurred in December 1993 and January 1995. An aerial photo study of Sorber (1997) reported average sand deposition in the Rijswaard natural levee zone of 58 mm in 1993 and 60-64 mm in 1995. This study area encompassed the range where our proximal and sand bar cores were taken. At the sand bar the deposition events described by Sorber (1997) agree with our flood bed interpretation results, which indicate depositions of 54 and 75 mm for the flood beds, which were correlated to the flood events of 1993 and 1995, respectively. However, such large events are rare, and to solve the discrepancy between the event scale and the decadal scale, it seems that these events should occur more often.

Table 3.4. Results compared to other studies results.

	Sand bar near channel	Proximal zone	Distal zone
Our study			
Cores	N118	N119, N121, B103, B106, Z156, Z159	N123, N124, B108, B110
Avg. sedimentation rate	9-25 mm/a	3-9 mm/a	2-7 mm/a
Other reconstruction studies			
Middelkoop (2000): heavy metals		5-11 mm/a	2-5 mm/a
Event studies			
Maas et al. (2003): sediment traps of 2 floods in 2000-2001 flood season	5-30 mm	1-5 mm	0.5-1 mm
Sorber (1997): aerial photos of 1993 and 1995 floods	~ 54-75 mm	~ 54-75 mm	

Another reason for the discrepancy between the event scale and the decadal scale may be a decreased sedimentation rate with time. Aggradation of the floodplains by sedimentation caused their flooding frequency to decrease. This process was enhanced by river bed degradation, which continuously took place over the past decades at a rate of 1 to 3 cm/a (Ten Brinke, 2005; Sieben, 2009). Therefore, contemporary sedimentation rates may be lower than several decades ago, and sediment deposited during the recent 2000-2001 flood season may be less than the average annual sedimentation over the past decades.

3.6.4 Optimal ranges of application

All methods have a different spatial and temporal range in which they are best applicable. Based on the results and the comparison between the methods, and considering all uncertainties associated with each method, we indicate the optimal ranges of the applied methods (Figure 3.9).

Dating using ^{137}Cs is best applicable where sedimentation rates have been sufficiently high to show the peaks in concentrations separately within the profile, in spite of bio-physical soil mixing processes (cf Middelkoop, 2000). Compared to ^{137}Cs dating, heavy metal analysis is better applicable in the slowly aggrading distal parts, as it has a larger age range, and thus a larger depth range. In very sandy (proximal) profiles, the ^{137}Cs and metal concentrations may be too low or too much dependent on minor variations in clay contents to show meaningful profiles in which concentration changes can be correlated to known changes in time. This counts most for heavy metals, as they are only deposited bound to fine-grained sediments, while ^{137}Cs concentrations also result from local atmospheric deposition. Moreover, post-depositional downward migration of ^{137}Cs occurs, which seems to increase with decreasing clay contents. The maximum age range of heavy metals depends on the pollution history of the river; in case of the Rhine it is about 150 years, provided the onset of industrial pollution can be determined in the profiles. The age range of ^{137}Cs dating is about 50 years, corresponding with the introduction of ^{137}Cs into the environment.

OSL dating is applicable over a wide spatial range. We found good results in both the distal and proximal zones, indicating that the presence of a small sand fraction in the clayey distal sites is sufficient for application of OSL dating. The temporal range of OSL dating is also large. We found ages between 8 ± 6 and 306 ± 16 years for the upper metre of the floodplain sediments, and dating well beyond the century scale is also possible (Wallinga, 2002a). However, the uncertainty term for young samples is relatively large.

Flood bed interpretation is only applicable close to the river bed, where individual flood beds are thick enough to be recognized. In our study, flood bed interpretation was only applied in the sand bar, but we expect that this range can be extended to the levee zone, where we also observed bedded profiles. Correlation of flood beds with flood events up to several decades ago is feasible, although the uncertainty range increases with increasing age of sediments. A major difference with the other methods is that it inherently accounts for year-to-year *variation* in sediment deposition, where the other methods provide deposition rates *averaged* over the period of interest. In our study for example, 80 mm of sediment was

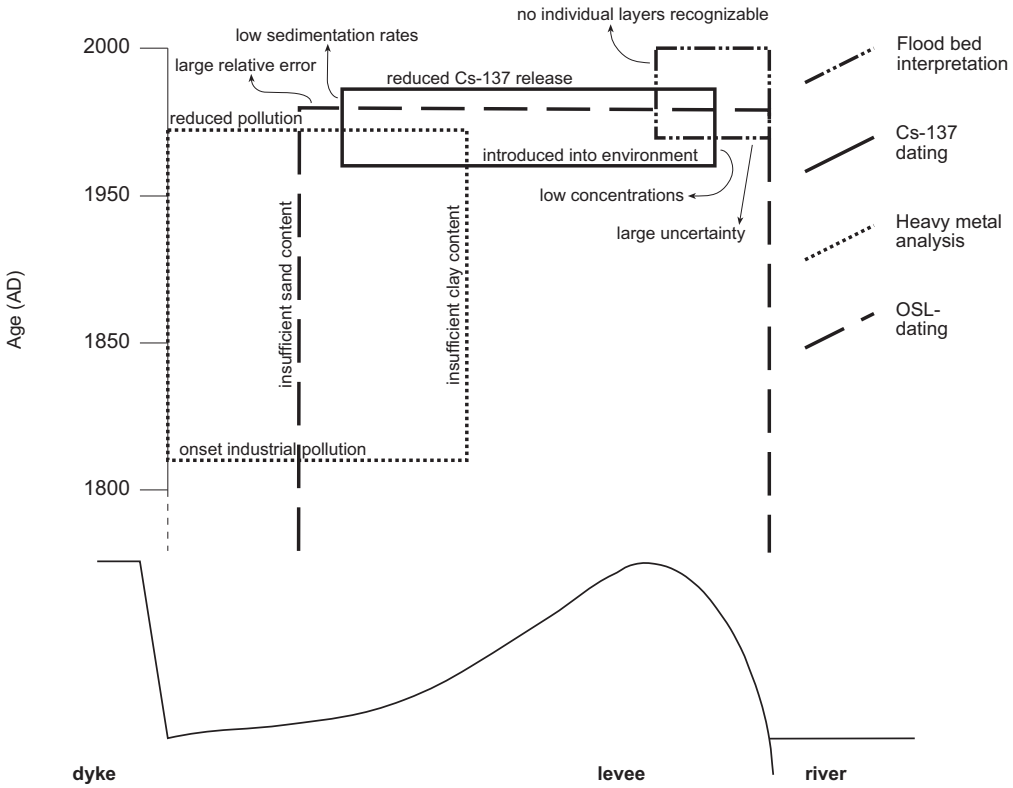

Figure 3.9. Spatial and temporal ranges of application of each method. Reasons for each boundary are also given. Temporal boundaries of both ^{137}Cs dating and heavy metal analysis are based on age markers that can be recognized in a vertical soil core. Of course, these methods can also be used to assess an average sedimentation rate for the period between the last age marker and the present.

deposited in the most extreme flood season, while there were also years without sedimentation.

3.7 Conclusions

We found significant sedimentation on the floodplains, which is important to take into account in floodplain management strategies. Sedimentation rates over the past few decades vary between 2-7 mm/a in the distal zones and 3-9 mm/a in the proximal zones. On a high sand bar along a natural levee sedimentation rates of 9-25 mm/a were found. Except for some minor inconsistencies in the ^{137}Cs dating results, all methods show a similar spatial trend of decreasing sedimentation rates with increasing distance from the river channel.

Intercomparison of the results of the different dating methods revealed the potential errors associated with each method, particularly where disagreement among the results were found. Uncertainties in the age determination may arise due to (1) grain-size dependent downward migration of ^{137}Cs, (2) smoothing of the vertical heavy metal and ^{137}Cs profiles, (3) delayed sediment-associated input of ^{137}Cs in addition to direct atmospheric fall-out, (4) overestimation of the burial age in OSL dating due to incomplete resetting of the OSL signal, or (5) non-linear relationships between sediment deposition and flood magnitude in the count-from-the-top correlation between sediment lamination and past observed flood records. Still, taking the uncertainties associated with each method into account, the results are generally in good agreement. At some sites, OSL dating tends to yield slightly lower sedimentation rates, but results mostly agree within their error ranges. At three sites, results are in clear disagreement, i.e. the uncertainty ranges of the different methods show no overlap. At these sites, we may have underestimated uncertainty ranges or we made a systematic error of unknown source in one of the methods. Therefore, we cannot decide what method yields best estimates.

The optimal spatial range in which each method is more applicable mainly depends on sediment texture and sedimentation rate, which are both related to floodplain elevation and distance from the river channel. OSL dating requires some sand grains, whereas ^{137}Cs dating and particularly heavy metal analysis requires silt and clay-sized sediment. Moreover, ^{137}Cs dating, heavy metal analysis and flood bed interpretation require sites with considerable sedimentation rates for their application. The temporal ranges of ^{137}Cs dating and heavy metal analysis are restricted by their emissions into the environment. For flood bed interpretation the increasing uncertainty with increasing age of the deposits is a limiting factor. For OSL dating the relative uncertainty is large for the youngest deposits. Ultimately, it is the combination of these methods which provides maximum information for the accurate estimation of sedimentation rates on a decadal time scale, and year-to-year variations can be assessed by flood bed interpretation.

Acknowledgements

This research is part of the strategic research program “Sustainable spatial development of ecosystems, landscapes, seas and regions" which is funded by the Dutch Ministry of Agriculture, Nature Conservation and Food Quality, and carried out by Wageningen University and Research centre (grant CT04.32.62). OSL dating of flood deposits is supported by NWO/STW (grant DSF.7553).

4 Reconstruction of eroded and deposited sediment volumes of the embanked river Waal, the Netherlands, for the period 1631 AD – present

Noortje Hobo, Bart Makaske, Jakob Wallinga, Hans Middelkoop

Manuscript originally published as:
Hobo, N., B. Makaske, J. Wallinga, H. Middelkoop (2014). Reconstruction of eroded and deposited sediment volumes of the embanked River Waal, the Netherlands, for the period AD 1631–present. **Earth Surface Processes and Landforms** *39*.

Reprinted with permission (John Wiley and Sons)

Abstract

In the last few centuries humans have modified rivers, and rivers have responded with noticeable changes in sedimentary dynamics. The objective of this study is to assess these responses of the sedimentary dynamics. Therefore, we calculated a sediment budget for eroded and deposited sediment volumes in a ~12-km long floodplain section of the largest semi-natural embanked but still dynamic lower Rhine distributary, for ~50-years time slices between 1631 AD and present. This is the period during which embanked floodplains were formed by downstream migration of meander bends between confining dykes. Our sediment budget involves a detailed reconstruction of vertical and lateral accretion rates and erosion rates of floodplain sediment. To do so, we developed a series of historical geomorphological maps, and lithogenetic cross-sections. Based on the maps and cross-sections, we divided the floodplain into building blocks representing channel bed and overbank sediment bodies. Chronostratigraphy within the blocks was estimated by interpretation of heavy metal profiles and from optically stimulated luminescence (OSL) dating results. Sediment budgets were hence calculated as a change of volume of each building block between time steps. The amount of lateral accretion initially increased, as a result of island and sand bar formation following embankment. From the 18th century onwards, there was a decrease of lateral processes in time, which is a result of straightening of the river by human activities, and a reduction of water and sediment supply due to the construction of a new upstream bifurcation. With straightening of the river, the floodplain area grew. Artificial fixation of the channel banks after 1872 AD prevented lateral activity. From then on, overbank deposition became the main process, leading to a continuous increase of floodplain elevation, and inherent decrease of flooding frequency and sediment accumulation rate.

4.1 Introduction

The sedimentary dynamics of a lowland river comprises the way sediment moves through the system. It can be defined as the whole of processes that involve erosion, transport or deposition of sediment in river systems – including the floodplains – on every possible spatial and temporal scale. Understanding these sedimentary dynamics is relevant for determining storage, reworking and residence times of fluvial sediments and associated contaminants (Macklin et al., 2006) within the river-floodplain system (Lauer and Parker, 2008c), and how these may be influenced by large floods or human activities. At larger spatial and longer temporal scales, knowledge of the sedimentary dynamics contributes to understanding the role of floodplains as secondary sources of sediment and contaminants for the downstream reaches, and to long-term transfer of sediment from catchment to ocean. A key component of the sedimentary dynamics is the sediment budget, i.e. the mass balance between the sediment input, the sediment output and the sediment storage in a unit time and a unit area of a system (Reid and Dunne, 2003; Slaymaker, 2003). In rivers that migrate laterally, this budget is determined by the amounts of sediment deposited laterally within the channel and vertically by overbank deposition versus the amounts eroded from older channel banks in outer bends. Both bed sediments (scroll bars) and overbank fines are involved in these processes. In equilibrium situations, for both types of sediments the reworking mechanisms should result in a mass balance between the amounts entering and leaving a section. Since the newly formed floodplains are generally lower than those eroded at the cut banks, this 'rejuvenation' process replaces high older floodplain parts by lower new floodplains. This elevation imbalance is referred to as 'floodplain shaving' by Lauer and Parker (2008c).

Over the past years many studies have reported on different components of sediment processes and inherent budgets, involving a wide range of spatial and temporal scales. Studies focusing on individual processes over short time scales (individual events to years) considered conveyance loss (Walling and Owens, 2003), overbank deposition (Middelkoop and Asselman, 1998; Thonon, 2006), trapping efficiency (Asselman and Middelkoop, 1998) or bank erosion (e.g. Kummu et al., 2008), contemporary sediment budgets (Brewer and Passmore, 2002; Walling et al., 2006) or sediment erosion or accretion volumes associated with single events (Ten Brinke et al., 1998). Studies on the role of floodplains as secondary source of contaminants typically focused on river reaches on a decadal time scale (e.g., Coulthard and Macklin, 2003; Macklin et al., 2006). Erkens et al. (2006) and Hoffmann et al. (2007) determined net sediment budgets of main river reaches and sinks along the Rhine river at a millennial time scale.

Detailed sediment budgets mostly involve contemporary sediment volumes or cover only a single event, but these budgets cannot be used to evaluate changes in the system over time, for example changes due to human interference. Long-term sediment budgets often result in net volume changes, but the time slices considered are too long to evaluate the dynamics *within* the slices (e.g., Middelkoop et al., 2010). To assess the increasing human influence on the sedimentary dynamics, the time scale of decades to centuries (medium scale) is to be considered. This is the time scale over which humans have modified rivers, and in turn, the rivers' response in terms of changing sedimentary dynamics becomes noticeable. Previous studies on this scale were conducted by, among others, Kesel et al. (1992), Walling et al. (1998) and Latrubesse et al. (2009). However, these studies mostly considered the river bed as the system, with the floodplains as temporary sinks. Exceptions are the studies by Lauer and

Parker (2008a,b), who established a modeling framework for sediment budgeting of meandering rivers, and tested this for a 60-km contaminated river floodplain reach using 19th century contaminants as tracer in floodplain deposits.

In our study, we focus on the floodplains, and we investigate the sediment input and output in the floodplains. Hereby, the floodplains encompass all sediment present between channel and dike, including overbank deposits *and* the channel deposits underneath the overbank deposits. The goal of the present study is to calculate a sediment budget for time slices of about 50 years, involving the eroded and deposited sediment volumes in floodplains in a semi-natural embanked but still dynamic river, on the century timescale. Questions to be answered are: how much sediment enters the floodplains, and how much sediment is eroded from the floodplains? Are there differences over time and, if so, are they related to human activities?

Our research focuses on the river Waal, a lower Rhine distributary (Figure 4.1), in the period after the construction of embankments. In this period many river management measures took place, which had a major impact on the sedimentary dynamics of the river. The river Waal was chosen because of the large amount of data available, in the form of borehole data (Berendsen and Stouthamer, 2001), and numerous published thematic and historic river maps (Table 4.1). Moreover, human interventions on the lower Rhine branches in the past centuries are well documented (e.g., Ploeger, 1992; Van de Ven, 2007).

4.2 Study area

4.2.1 Characteristics of the river Waal and the studied floodplains

The river Waal is the largest distributary of the Rhine in the Netherlands. The average discharge of the Rhine near the Dutch-German border is about 2,300 m^3/s, with an average suspended sediment load of 3.1 x 10^9 kg/year (Asselman, 1999, Middelkoop and Van Haselen, 1999). The Waal receives about two thirds of this discharge and suspended sediment load. Peak discharges of the Waal roughly range between 3,500 and 6,500 m^3/s, and cause complete or partial inundation of the floodplains.

The present river channel of the Waal is about 3 m deep and 300 to 400 m wide at average flow conditions; its banks are artificially fixed. The floodplains are narrow (0.5-1.5 km), and bounded by dykes that were constructed between 1000 and 1350 AD (Hesselink, 2002). Before the construction of dikes, the Rhine was an unconfined meandering river, where overbank deposition could occur over large areas within the entire delta. The embankments prevented river avulsion, confined lateral meander migration to some extent (downstream migration), and limited overbank deposition to narrow areas between the embankments and river channel ('embanked floodplains' cf. Middelkoop, 1997). This situation lasted until about 1850 AD, when 'normalization' works were started: the main channel was narrowed by groynes, and the channel banks were fixed by riprap and small embankments, so that floodplain erosion no longer occurred. In the period between embankment and construction of groynes several other modifications to the Rhine branches were made. These included upstream reforestation, construction of single groynes and planting of trees to enhance sedimentation and reclaim land

from the river bed, meander cut-offs, closure of smaller branches and stabilization of bifurcations, which affected water and sediment distribution over the delta (Ploeger, 1992, Van de Ven, 2007). The present Waal floodplains are almost entirely formed by the pre-normalization downstream channel migration.

The study area comprises a ~12-km-long stretch of the river Waal, consisting of four floodplain sections, which are Gouverneursche polder (GOU), Hiensche uiterwaarden (HIE), Afferdensche en Deestsche waarden (AFF) and Winssensche waarden (WIN), and a part of the floodplains of Wolferensche waard (WOL) and Drutensche waarden (DRU) (Figure 4.1). This section was chosen because the typical embanked floodplain geomorphology formed by downstream migration, is clearly developed, and their formation has been well described in previous studies (Schoor, 1994; Middelkoop, 1997; Maas et al., 1997;Hesselink, 2002; Hebinck, 2008).

The studied floodplains presently comprise a sequence of sand bars and concave swales, topped by a 1-2-m thick clay layer. The swales are in downstream connection with each other and with the present river, forming secondary channels which still carry water in some floodplains. A few sand bars contain scour-holes formed by dike-breach events. At some locations, remnants of a pre-embanked channel belt have been preserved. In all floodplains, large parts have been disturbed by mining of sand and clay, leaving deep pits in the landscape. Other disturbed areas comprise built-up areas and artificially filled swales. In some floodplains, the river bed is bordered by a small dike of 1-2 m in height, which prevents the embanked floodplain from being inundated by minor floods. Land use of the studied floodplain is mostly pasture land, in places alternating with arable land or small wooded sections. In the last two to three decades, some parts of the floodplain have been changed into nature areas, with mixed woodland-grassland vegetation. Despite the considerable disturbance, most floodplains still contain unaffected areas, which were investigated in this study.

4.2.2 Embanked floodplain formation by downstream migration

Embanked floodplain formation was described by Middelkoop (1997) and Hesselink (2002) as lateral accretion of concave sand bars, followed by vertical accretion of overbank fines (Figure

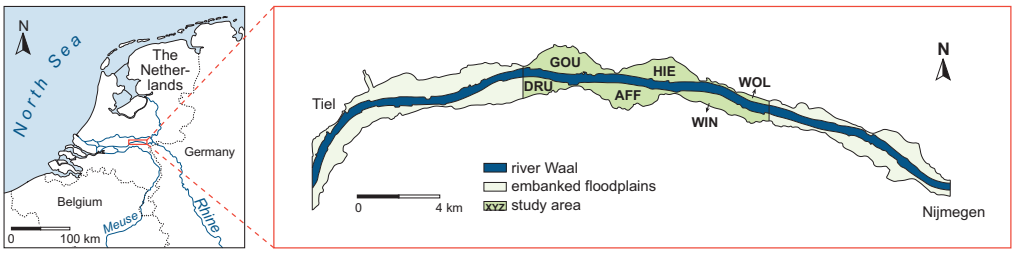

Figure 4.1. Studied floodplains: Gouverneursche polder (GOU), Hiensche uiterwaarden (HIE), Wolferensche waard (WOL), Drutensche waarden (DRU), Afferdensche en Deestsche waarden (AFF) and Winssensche waarden (WIN).

4.2). The sand bars developed laterally in the upstream limb of the outer meander bend, often enhanced by construction of groynes and tree planting. The sand bars were separated from the floodplain by concave swales, functioning as secondary channels during periods of increased discharge. Over a period of several decades, an individual sand bar expanded in a down-channel direction, and aggradated until it became covered by pioneer vegetation. Subsequently, the swale closed-off at the upstream end from the main channel due to sand deposition, and the bar became part of the floodplain. The newly formed floodplain became topped by fine-grained overbank sediments, while vegetation changed from reed to willows and poplar, which were later cut and replaced by meadows. Meanwhile, a new sand bar and swale formed in the river channel at the downstream end of the former sand bar, and the process repeated. The resulting pattern resembles those formed by counterpoint bars (Smith et al., 2009). However, we consider them to be scroll bars, since they consist of sand instead of the finer deposits that characterize counterpoint bars. Due to downstream channel migration within the confinement of the embankment, the sand bars and swales are concave shaped with respect to the direction of channel migration, and swales are in downstream connection with each other. Downstream migration ceased around 1850 AD, when the river bed was fixed by large-scale construction of groynes.

Lateral accretion on one channel bank coincided with erosion of the opposite bank. Due to this erosion, most of the older floodplain parts, formed before embankment, have disappeared. Particularly along the Waal, the present floodplains were mainly formed as the result of stepwise downstream channel migration. They are built-up by a series of successively developed sand bars, separated by filled concave swales, both topped by fine-grained overbank deposits, which are relatively thick due to the lateral confinements by the dikes (Figure 4.2).

4.2.3 Geomorphological elements and associated lithogenetic units

In embanked floodplains, we distinguish for this study three geomorphological elements and related lithogenetic units, all associated with different steps in the downstream migration process (after Hesselink et al., 2003; Figure 4.2). (1) Sand bars are large concave-shaped units (in planform), with an average length of ~1,000-1,500 m and an average width of ~200-300 m, which constitute a large part of the floodplain area (74%). The bars consist of sand and gravelly channel deposits, and developed within the main channel. Often, fining upward sequences can be found, as well as reactivation surfaces or thin clay layers. (2) Swales are the concave, elongated depressions between the sand bars. They are narrower than sand bars (30-70 m), and constitute about 26% of the floodplain area. Mostly, the upstream end of the swales is closed, but at the downstream end they are connected to each other. This results in a secondary channel close to the dyke, often connected to the active channel (Figure 4.2). Concave swales developed as a depression between a growing sand bar and a floodplain. Swale fills consist of sand at their former entrance, and clay and silty and sandy clay in the downstream part of the swales. Most concave swales are now filled depressions, but some still contain water. (3) Natural levees form wedge-shaped layers of sediments, located on top of the sand bars and swales. They cover the whole embanked floodplain. These overbank deposits consist of

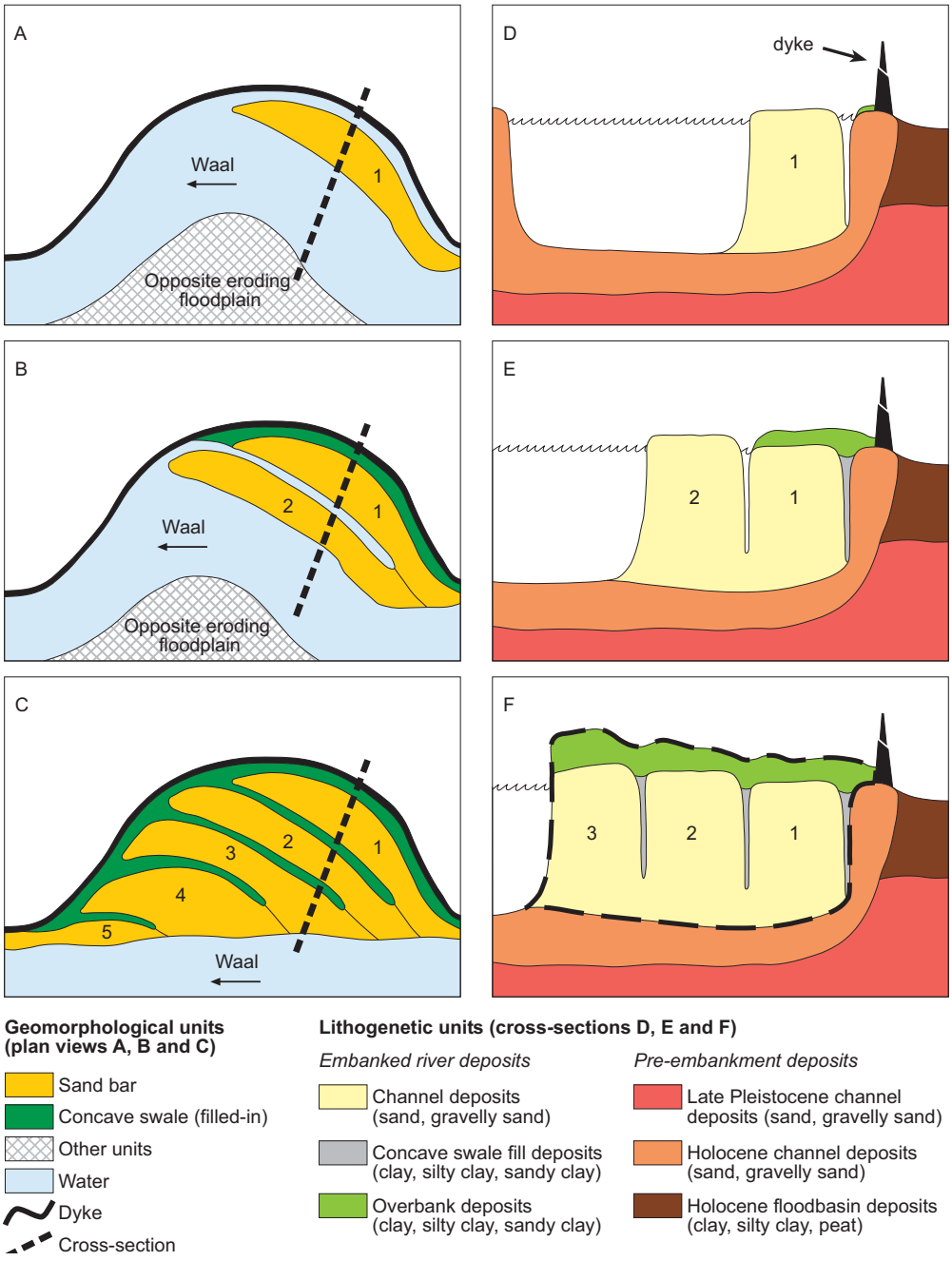

Figure 4.2. Concept of embanked floodplain formation. The plan views (A, B and C) and the cross-sections (D, E and F) represent different stages of embanked floodplain formation by downstream migration along the river Waal. Modified from Hesselink et al. (2003). The purple line in Figure F outlines our definition of embanked floodplain deposits.

laminated clay, silty clay and sandy clay, fining away from the main channel, which have been deposited during periods of high discharge. The overbank deposits are mostly of uniform composition, without sedimentary structures. In the period after normalization, sand deposition only incidentally occurred during extreme floods, as 5-20 cm thick sand sheets close to the river bank. They represent proximal levee deposits of the present river, and thus are also part of the overbank deposits. Other lithogenetic units, like dike-breach deposits and scour-hole fills, are not included, because they comprise a small area within the floodplain. Pre-embanked and artificial deposits are only included for erosion.

4.3 Material and methods

4.3.1 Concept and data

Our sediment budget involves estimates of the volumes of eroded and accreted sediment per unit time during time slices of a few decades length. Accreted sediments are subdivided into lateral accretion deposits, which are the channel deposits, and vertical accretion deposits, which comprise overbank deposits and swale fills. The concept is schematized as shown in Figure 4.3: the floodplains are represented as an architecture of building blocks of uniform lithogenetic composition representing the sand bars or the overbank tops. Its vertical boundaries correspond to geomorphological map units (Figure 4.2c), and horizontal boundaries were determined by lithogenetic composition (Figure 4.2f). In the course of time, the dimensions - and hence the volume - of each building block may change due to erosion, lateral accretion or vertical accretion. For calculation of volume changes of each building block B_i, we need to know its area ($A_{i,t}$) and surface elevation ($H_{i,t}$) at all times t. To determine $A_{i,t}$, we reconstructed a series of historical geomorphological maps, and to determine $H_{i,t}$, we analyzed lithogenetic cross-sections and estimated sedimentation rates depending on floodplain elevation. These were calculated from historical maps, optically stimulated luminescence (OSL) dates and analyses of heavy metal contamination profiles in the floodplain.

Data used in our study were mostly gathered from existing databases, including the extensive borehole database of Utrecht University (Berendsen and Stouthamer, 2001), and published historical and thematic maps and cross-sections of the studied area (Table 4.1). The maps from before the early 18th century are detailed, having scales of about 1:10.000. These were mainly produced for land registration, and cover only limited embanked floodplain sections (Hesselink, 2002). In the 19th century (~1835 AD) systematic topographic mapping of the entire floodplain area took place at a scale of 1:10.000 (Goudriaan, 1830-1835). This resulted in many detailed river maps of the study area, which were updated in ~1870, ~1920, and ~1960 AD (Rijkswaterstaat, 1870-1880; 1965). Moreover, we used a series of topographic maps, from 1870 until present (scale 1:25.000), with ~10 year updates, to locate sand and clay pits. Finally, a high-resolution digital elevation model of the Netherlands was used (AHN; Van Heerd et al., 2000) to map the present-day floodplain surface elevation.

In addition, we used the results of previous river-historical studies, including the geomorphological map of the Netherlands (Koomen and Maas, 2004; floodplains updated in

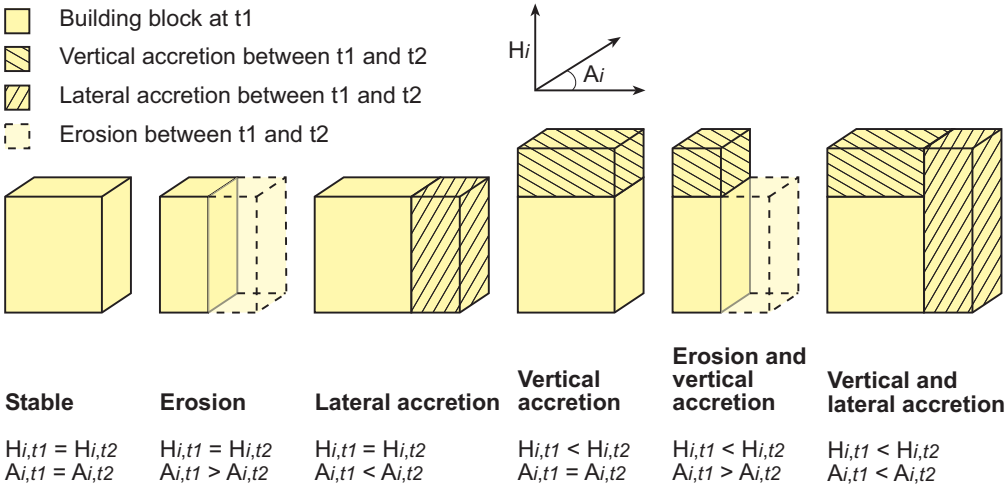

Figure 4.3. Concept of our sediment budget: a building block, representing a part of the floodplain (channel, concave swale or overbank deposits), changes in volume between time step t_1 and t_2. This figure shows the different (combinations of) processes that are responsible for the volume changes.

2007), and reconstructions of the historic development and architecture of the Afferdensche en Deestsche Waarden by Schoor (1994) and of the Winssensche Waarden by Middelkoop (1997) and of the Gouverneursche Polder by Hesselink (2002). From Maas et al. (1997) we obtained land use, vegetation and geomorphology in the floodplains in 1780 and 1850 AD. Finally, maps of floodplain age, clay-cover thickness and sand depths from Hebinck (2008) were used. An overview of the maps and cross-sections used is given in Table 4.1.

To complement these data, fieldwork was carried out. At three locations undisturbed soil cores of 4-5.5 m long and 66 mm in diameter were collected with a Begemann sampler (GeoDelft, 2001). From these cores, samples were taken for heavy metal analyses and optically stimulated luminescence (OSL) dating, which were used for reconstruction of sedimentation rates. Where more detail was needed for preparation of historical geomorphological maps and lithogenetic cross-sections, additional hand borings to a maximum depth of 4 m below the surface were carried out with an Edelman hand auger, following the methods described by Berendsen and Stouthamer (2001) and Oele et al. (1983). The borehole data were described following the description method of Berendsen and Stouthamer (2001).

4.3.2 Planform geomorphology

Geomorphological maps were made for the years of which historical maps were available within the study reach: 1631, 1685, 1723, 1778, 1835 and 1872 AD and the present. All available historical maps were converted to the same geometrical base, following the procedure

Table 4.1. Overview of data from previous studies, used for this research.

Type map	Age [AD]	Floodplain	Reference
Historical map individual floodplain	~1685	WIN	Passavant, 1688
Historical map individual floodplain	1773	HIE	Beijerinck, 1773
Historical map individual floodplain	1778	AFF	Hendrikman and Prilleritz (1776/1778)
Historical map individual floodplain	1778	GOU	Beijerinck, 1778
Historical map individual floodplain	1723	HIE	Couwater, 1723
River maps 1st edition	~1835	All	Goudriaan, 1830-1835; page 4-6
River maps 2nd edition	~1872	All	Rijkswaterstaat, 1870-1880; page 4-6
River maps 4th edition	~1960	All	Rijkswaterstaat, 1965; page 5-6
Topographical maps 1:25.000	1870-1940	All	Topografische Dienst, Emmen
Topographical maps 1:25.000	1950 - present	All	Topografische Dienst, Emmen
AHN	-	All	Van Heerd et al., 2000
Reconstruction Afferdensche en Deestsche waarden (maps and cross-sections)	-	AFF	Schoor, 1994
Reconstruction Winssenche waarden (maps and cross-sections)	-	WIN	Middelkoop, 1997
Investigation Gouverneursche Polder (cross-section)	-	GOU	Hesselink, 2002
Map of 'physiotopes'[*1]	1780	All	Maas et al., 1997
Map of 'physiotopes"	1850	All	Maas et al., 1997
Map of 'ecotopes'[*2]	1780	All	Maas et al., 1997
Geomorphological map floodplains	Present	All	Koomen and Maas, 2004
Chronological map	Present	All	Hebinck, 2008
Clay cover thickness map	Present	All	Hebinck, 2008
Sand depth map	Present	All	Hebinck, 2008
Borehole database Utrecht University	-	All	Berendsen and Stouthamer, 2001

[*1] Physiotope = spatially restricted unit that can be recognized in the landscape based on abiotic characteristics (Maas et al., 1997).
[*2] Ecotope = spatially restricted unit within a physiotope, bound by biotic characteristics (Maas et al., 1997).

described by Hesselink (2002). The geomorphological maps show the geomorphological elements that are present below the overbank deposits: mainly sand bars and concave swales (example in Figure 4.4a). Most of them have developed within our study period, but some sand bars already existed in 1631 AD. Along with these main elements, floodplains contain remnants of pre-embanked floodplains, anthropogenic deposits, and water bodies of various origin. We classified all anthropogenic and pre 1631 AD deposits as 'other unit', because they are not part of the sediment budget of the river. The scour holes and water bodies that originate from digging of floodplain sediments are assumed to be classified as sand bars, because they were created almost exclusively in sand bar deposits.

First, the geomorphological map for the present situation was made. All borehole data were reclassified into three lithogenetic units: 'sand bar', 'concave swale', or 'other unit', and were plotted in a planform map. For all resulting geomorphological map units, the period in which the sand bar developed or in which the residual channel was filled was determined based on their presence or absence on the historical maps.

Then, historical geomorphological maps were reconstructed by stepwise removing the sediment bodies from the geomorphological map for the present. For each time T_j all units younger than T_j were removed, while units older than T_j remained. For the units that were eroded between T_j and the present, the boundaries were reconstructed from the historical maps of T_j. If no historical data were available for this, then its boundary was determined by interpolation, assuming a constant erosion rate estimated from the historical data. The islands are sandbars which are not yet connected to the floodplain, with a surface level equal to the bankfull river water level.

The available maps from 1778 AD to present cover the entire study area. In contrast, the 1723 AD data covered only a part of the study area and data for 1631 and 1685 AD were available for very limited parts of the study reach only. For these years geomorphological maps were reconstructed based on a few assumptions. The primary assumption was that the floodplains were exclusively formed by the downstream migration process; there is no map showing otherwise. A second assumption was that the average river width in the study area did not change during that period. Plots for the recent periods (1778-1872 AD) of river width (measured every 500 m) against age confirmed that there was no significant decrease or increase of river width with time for that period, providing support for our assumption of constant river width.

4.3.3 Lithogenetic composition

The cross-sections show lithogenetic units: channel deposits, concave swale fills, other deposits, and the overbank deposits on top of them (example in Figure 4.4b). We took into account the fact that large amounts of overbank deposits have been excavated in the past. To calculate the amount of this removed clay we measured the clay thickness in the parts of the floodplain that are still intact, and used this thickness to reconstruct the original clay thickness in disturbed units. The lithogenetic units correspond with the planform geomorphology, and can hence be interpreted as the vertical composition of the geomorphological units.

From the planform geomorphology and lithology the building blocks in all time slices were identified. Vertically, the boundaries of the building blocks correspond to the units on the geomorphological map (Figure 4.4a). Horizontally, they are delineated as rectangular blocks of uniform lithogenetic composition, (dashed lines in Figure 4.4b) having the volume of the lithogenetic units. The elevation of these horizontal boundary are derived are derived from the cross-section. However, most cross-sections do not provide a lower boundary of sand bars. According to Maas et al. (1997), the average Waal depth around 1800 AD was 4.4 m below bankfull water level (H_{bf}), in a river stretch located slightly upstream, but overlapping with our study area. We assumed that this depth remained constant over the entire study area and during the entire period 1631-1872 AD, and that H_{bf} is equal to average sand bar thickness. From the cross-sections, we found that the sand bar top elevation depends on both its age and downstream distance along the river, the latter reflecting the channel-belt gradient. We determined these dependencies by multiple regression to infer an average sand bar top elevation. Hence, we estimate sand bar base elevation assuming a sand bar thickness of 4.4 m. This sand bar base elevation provides us the lower boundaries of our sand bar building blocks, however, for the upper boundaries of these blocks, we still use cross-sectional data. For

geomorphological map units that are not represented by a cross-section, these depths were estimated by extrapolation from other units or by a DEM and an existing sand depth map of the area (Cohen et al., 2009).

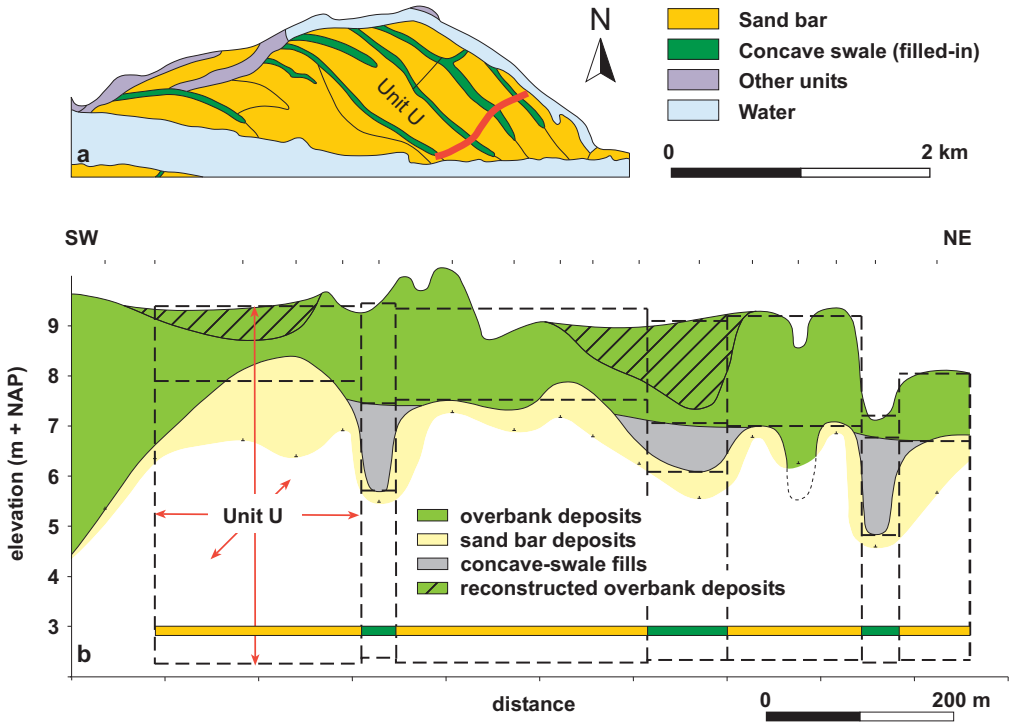

Figure 4.4. Example of a geomorphological map (a) and a cross-section (b). The lower bar in the cross-section demonstrates that lithogenetic units correspond with the geomorphological map units. Hatched lines show where overbank deposits were mined and reconstructed. Dashed lines represent the schematized building blocks. Note that one unit can contain more building blocks.

4.3.4 Age determination

Ages of the building blocks representing the sand bars were obtained from their first appearance on the historical geomorphological maps. The age of the present surface is assumed to be 2000 AD. This is approximately the average age of cross-sections and borehole data of various ages that are involved.

Changes in height of the building blocks over time due to vertical accretion were estimated using sedimentation curves that relate vertical accretion rate of a building block B_i at time T_j to its height $H_{i,j}$. To establish such curves we first determined ages of overbank sediments and sand bars using heavy metal concentrations in floodplain soil profiles and by optically stimulated luminescence (OSL) dating (see Hobo et al., 2010 for methodological details).

Heavy metal analysis is an indirect dating method that relates varying metal contents in a vertical sediment profile with the known pollution history of the river, resulting in an age-depth relation of the profile. Long-term variations in the Rhine pollution history have caused the heavy metal concentrations in the water, and hence in the floodplain sediments, to vary (Middelkoop, 2000). In our study, we were interested in the onset of heavy metal pollution, because this roughly coincides with river normalization works around 1860 AD (Middelkoop, 2000). Heavy metal profiles were determined from soil samples from the Begemann cores, collected at 2.5-5 cm intervals. Contents of zinc, lead and copper in these samples were determined using destruction HNO_3-HCl (aqua regia) ICP-AES Thermo. After sample drying at 105 °C, the organic matter content was determined through loss on ignition at 550 °C, and the grain size distribution was measured with a Coulter LS 230 laser particle sizer. Finally, the organic matter content and the grain size distribution were used to convert the metal concentrations to a standard sediment of 40% clay and 8% organic matter, using a linear relation between metal concentrations and contents of clay and organic matter in floodplain sediments (Middelkoop, 1997). To assess the 1860 AD level in the vertical profiles, we estimated a lower boundary under which samples are almost certainly older, and an upper boundary, above which samples are almost certainly younger than 1860 AD. The lower boundary was determined by the depth of the sample in which heavy metal concentrations going upwards for the first time are more than 10% above background level, and for the upper boundary a value of 50% above background level was used.

For OSL dating samples were taken from the Begemann cores, with a vertical range of 14-19 cm and a spacing of 10-40 cm in the overbank deposits, and a spacing of 1-2 m in the sand bar deposits. On these samples the natural radionuclide activity concentrations were determined to calculate the dose rates, and quartz grains were extracted for luminescence measurements to determine the equivalent dose. The grain-size fractions prepared for analysis varied between samples (180-212 μm, 180-250 μm, or 90-180 μm). Details on the procedure are described by Hobo et al. (2010) and Wallinga et al. (2010). For our young fluvial deposits OSL dating is challenging as light exposure prior to deposition and burial may be too limited to completely reset the OSL signal in all grains. This may lead to an age offset (overestimation) which can be relatively large for young samples. To avoid such age overestimations, we carefully selected suitable measurement parameters and we applied newly developed statistical procedures for data-analysis. With regard to the measurements, we used optimized early-background subtraction methods to obtain signals dominated by the rapidly resetting

fast OSL component of quartz (Cunningham and Wallinga, 2010). Low preheat temperatures were selected to avoid thermal transfer (e.g., Truelsen and Wallinga, 2003) and small aliquots (2 mm; ~75 grains) were measured to obtain meaningful equivalent dose distributions (e.g. Cunningham et al., 2011). Single-grain dating was not attempted as 95% of the grains shows negligible OSL sensitivity. Given the depositional environment and the age range of interest, the burial dose is expected to be reflected by the lower part of the equivalent dose distribution. To obtain a good estimate, we used the Minimum Age Model (MAM; Galbraith et al., 1999) in combination with a recently developed bootstrapping approach (Cunningham and Wallinga, 2012). The bootstrapping approach serves to provide a distribution of possible outcomes, using subsets of the measured equivalent dose estimates and slightly varying the overdispersion parameter for each model run. The bootstrapped MAM outcome is aimed to provide an accurate estimate of the burial age, with an uncertainty that adequately reflects the possibility of incomplete resetting of the OSL signal at the time of deposition.

Age-depth models were established using OxCal (version 4.1.7), which is a Bayesian model that determines the best possible age and a standard deviation for all samples, taking the chronostratigraphical order of the samples into account (Bronk Ramsey, 2008). The model was applied to each profile using all chronostratigraphic data:

- Heavy metal age estimates, only the ones which have an age older or younger than 1860 AD.
- OSL age distributions, as calculated by the bootstrapped Minimum Age Model (following the approach of Cunningham and Wallinga, 2012).
- Top of the overbank deposits and bottom of the sand bar deposits, of which ages were derived from historical geomorphological maps.
- Minimum and maximum ages of the building blocks, derived from historical geomorphological maps. These provide constraints for all other age inputs.

These data were input for a P-sequence model with 4-6 events per meter. We included a model boundary (break) between sand bar deposits and overbank deposits, so sand bar and overbank data were calculated semi-independently from each other. This was done because these units were formed by different processes, and inherently different deposition rates. Moreover, an upper and a lower model boundary were added, to constrain the age model at lower and top end. All these boundaries have no a-priori defined age range; their age is determined by the model from the chronological data (Figure 4.5).

To determine the sensitivity of settings in the Oxcal model, different runs were performed, varying in number of samples, type of boundary, presence of a break or not, and number of deposition events per meter in the stratigraphic section. In total 8 different runs per core were performed, but differences between the results were small and remained within 1 standard deviation from the original run that is assumed to best represent reality. Therefore, only results of the original runs were used for further analysis.

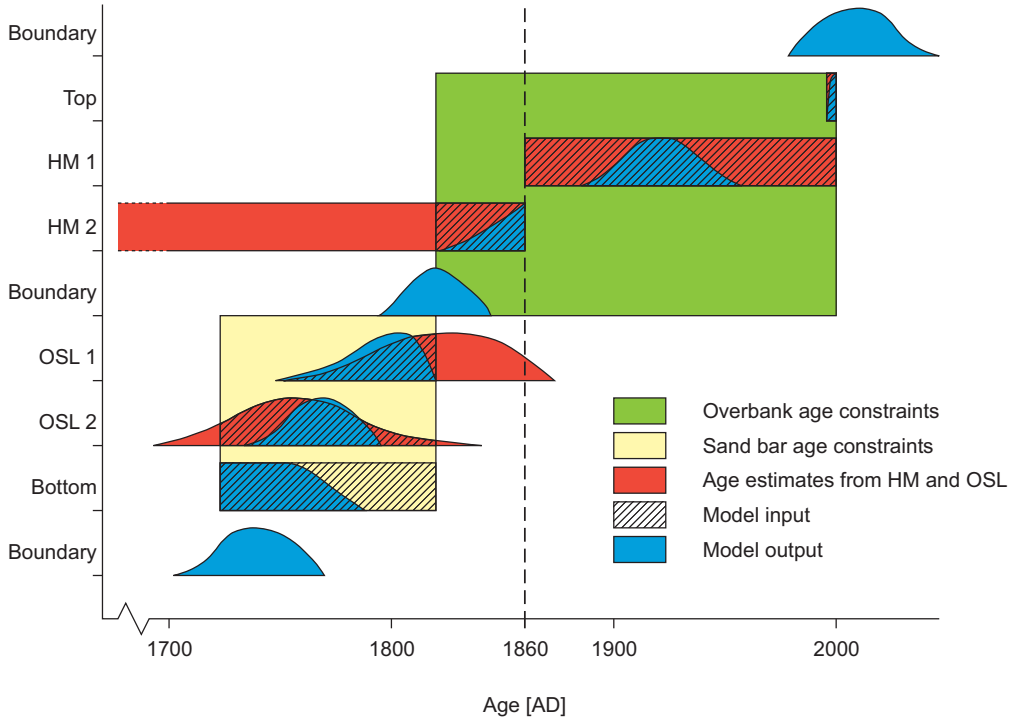

Figure 4.5. Schematic representation of the OxCal model. Age estimates derived from heavy metal analysis (HM) and OSL-dating (both in red), are combined with age constraints (yellow, green). This provides chronological input data for the model (hatching) that is used to calculate the best possible age (blue).

4.3.5 Sedimentation rates

Results from OxCal were used to calculate the increase in height of a building block over time due to deposition, of the form:

$$H_{i,j} = H_{i,0} + dh/dt \cdot t_j \qquad \text{(Eq. 4.1)}$$

where: $H_{i,j}$ = surface elevation of building block i [m+NAP] at time T_j [AD] (NAP = Dutch ordnance datum)
$H_{i,0}$ = surface elevation of building block i [m+NAP], at T_0 (=lower boundary)
T_0 = start time of sedimentation [AD] of building block i
t_j = time passed since start deposition [a] = $T_j - T_0$
dh/dt = sedimentation rate [m/a]

We thereby did not consider variations in sedimentation rate depending on the distance between the main channel and the floodplain section under consideration, nor due to changes

in floodplain vegetation and associated hydraulic roughness. This was because the available data did not allow quantifying such relationship for the historic conditions.

For sand bar blocks SB_i we assumed on average a linear sedimentation rate over the time slice ($dh/dt = c$), resulting in:

$$H_{SB_i,j} = H_{SB_i,0} + c \cdot t_j \qquad \text{(Eq. 4.2)}$$

where: $H_{SBi,j}$ = height of sand bar i [m+NAP] at time T_j [AD]
c = sedimentation rate [m/a]

For the overbank deposits we expect the sedimentation rate on each block OB_i to decrease in time (cf. Middelkoop, 1997). Due to sedimentation, the floodplain aggrades and the average number of days per year that a floodplain is inundated gradually decreases. As first-order approximation, we assumed that the sedimentation amount in a year is proportional to the expected inundation period in that year (Middelkoop, 1997). Then, the relation between floodplain level and annual inundation period has the same form as the relation between water level and the number of days per year that this water level is exceeded. This relation was established using water level data from Nijmegen (located 10 km downstream the investigated reach) between 1800 and 1824 AD (www.waterbase.nl). In Figure 4.6 we fitted a curve through the data points, and found that for high water levels (> bankfull) the annual exceedance time is related to the water level as:

$$\ln(y) = -a \cdot x + b \qquad \text{(Eq. 4.3)}$$

where: y = number of days per year water level x is exceeded [-]
x = water level [m+ NAP]
a, b = regression coefficients

Assuming that y is proportional to the sedimentation rate (dh/dt) and x represents the floodplain elevation above H_0, Equation 4.3 describing how $H_{OBi,j}$ changes between T_0 and T_j becomes:

$$\ln(dh/dt) = -a \cdot h_{i,j} + b \qquad \text{(Eq. 4.4)}$$

where: $h_{i,j} = H_{OBi,j} - H_{OBi,0}$

Combining Equations 4.1 and 4.4 leads to:

$$H_{OB_i,j} = H_{OB_i,0} + \frac{1}{a} \cdot \ln(a \cdot e^b \cdot t_j + 1) \qquad \text{(Eq. 4.5)}$$

Chronological constraints from the OxCal analyses were used to estimate the parameters a, b in Equation 4.5 and c in Equation 4.2 for the three units from which the Begemann cores

were taken. This was done by the software package Origin (OriginLab Corporation), which calculated a best fit through age-depth plots, taking account of the uncertainty of the age results from OxCal. In all other units for which no cores were available, only the ages of the upper and lower boundaries of the building blocks were used to estimate the parameters. This was done by inverse modelling, i.e. adjusting for each building block i the parameter values c_i (for sand bar blocks SB_i) and a_i and b_i (for overbank blocks OB_i) such that the resulting curve fits between the known start and end dates and heights of block i. For sand bar building blocks, the values c_i could be determined in this way, but for the overbank building blocks there is an infinite number of possible combinations of a_i and b_i. Therefore, we kept b constant for all blocks OB_i as the average b from the three Begemann cores, because this turned out to be a more stable parameter for the Begemann cores than a. Using this constant b, we estimated for all overbank blocks the value of a_i.

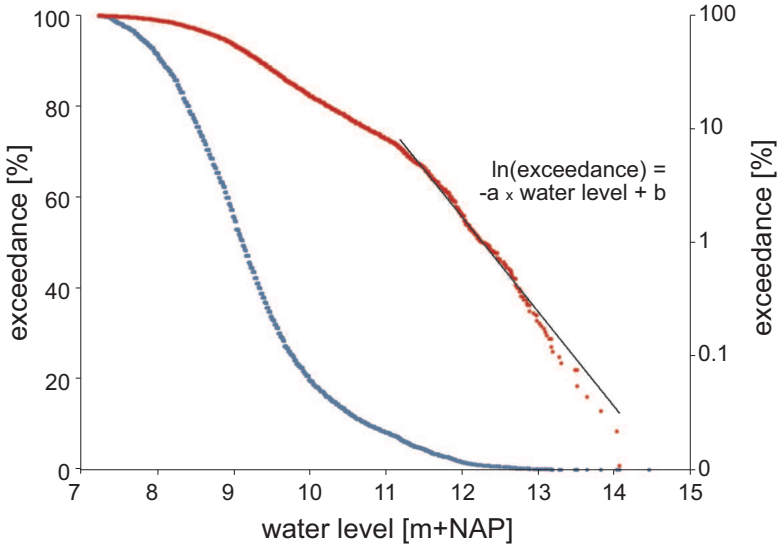

Figure 4.6. The relation between water level and the period per year the water level is exceeded, plotted on a normal (blue) and logarithmic (red) scale. At high water levels, when floods occur, the relation can be described by a logarithmic function.

4.3.6 Sediment budgets

Estimates of the eroded and deposited sediment volumes are based on changes in volume of a building block between two time steps. Volume changes involve a change in area ($dA_{i,t}/dt$) and/or a change in elevation ($dH_{i,t}/dt$) (Figure 4.3). For all building blocks i, $A_{i,j}$ was derived from historical geomorphological maps (Figure 4.7), and $H_{i,j}$ was calculated from the sedimentation curves (Figure 4.8). Hence, for each building blocks B_i and time slice T_1 –T_2 [AD], volumes per year of vertical accretion, lateral accretion and erosion were calculated by multiplying change in area with elevation.

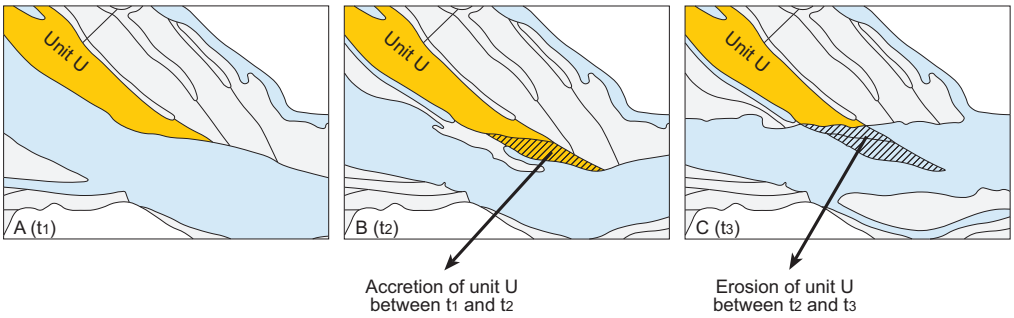

Figure 4.7. Area of erosion or deposition is calculated as the difference in area between two successive time steps.

Lateral accretion takes place when the area at T_2 is larger than the area at T_1 ($A_{i,T2} > A_{i,T1}$; Figure 4.7; a and b). We assume that lateral accretion takes place from the lower boundary of the channel deposits to the surface elevation of B_i at T_2. For each building blocks and time slice lateral accretion volume can be calculated as:

$$V_{AL,i} = \frac{A_{AL,i} \cdot D_{AL,i}}{T_2 - T_1} \qquad \text{(Eq. 4.6)}$$

where: $V_{AL,i}$ = lateral accretion volume [m³/a]
$A_{AL,i}$ = lateral accretion area [m²] = $A_{i,T2} - A_{i,T1}$
$A_{i,Tj}$ = area at time T_j [m²]
$D_{AL,i}$ = lateral accretion thickness [m] = $H_{i,T2} - C_i$
$H_{i,Tj}$ = surface elevation at time T_j [m + NAP]
C_i = lower boundary of channel deposits in SB*i*, or in sandbar block below OB_i or CS_i [m + NAP]

Opposite to lateral accretion, erosion takes place when unit $A_{T1} > A_{T2}$ (Figure 4.7; b and c). We assume that the river always erodes the floodplain for the full river depth. Thus, for every unit the erosion volume was calculated as:

$$V_{E,i} = \frac{A_{E,i} \cdot D_{E,i}}{T_2 - T_1} \qquad \text{(Eq. 4.7)}$$

where: $V_{E,i}$ = erosion volume [m³/a]
$A_{E,i}$ = eroded area [m²] = $A_{T2} - A_{T1}$
$D_{E,i}$ = thickness of eroded area [m] = $H_{T1} - C$

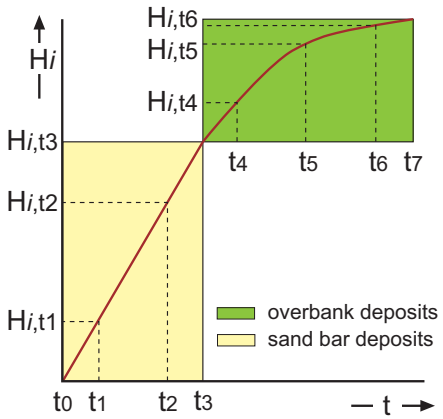

Figure 4.8. From our data, we only know upper and lower elevations of the building blocks (in this example $H_{i,t0}$ $H_{i,t3}$, $H_{i,t7}$). All other $H_{i,tj}$ can be calculated by the sedimentation formulas.

For each unit, vertical growth occurs when $H_{T2} > H_{T1}$ (Figure 4.8). It can take place in all units, independent of whether it is a laterally accreting or eroding unit. In agreement with most observations on old river maps, islands were considered as sand bars, until these have become part of the floodplain and have become covered by vegetation. From then onwards overbank accretion occurs. For every unit vertical accretion volume can be calculated as:

$$V_{AV,i} = \frac{A_{AV,i} \cdot D_{AV,i}}{T_2 - T_1} \qquad \text{(Eq. 4.8)}$$

where: $V_{AV,i}$ = vertical accretion volume [m³/a]
$A_{AV,i}$ = vertical accretion area [m²] = A_{T1} for laterally accreting units, and = A_{T2} for laterally eroding units
$D_{AV,i}$ = vertical accretion thickness [m] = $H_{T2} - H_{T1}$

4.3.7 Floodplain elevation

Along with the estimates of accumulated and eroded volumes, the elevations of all building blocks B_i were determined for all considered times T_j. To determine the changes in floodplain elevation, we calculated for all time slices the floodplain elevation distribution $H_{i,j}$. This shows how the floodplain elevations change as a result of the floodplain shaving and accretion processes (sensu Lauer and Parker 2008ab).

4.4 Results

4.4.1 Planform geomorphology

Figure 4.9 shows the series of historical geomorphological maps of the study area, from 1631 AD – present, with overbank deposits stripped off. In the oldest map, 1631 AD, almost the entire floodplain area consists of other deposits, including sediments deposited before 1631 AD. Still, there are some islands present, which are shown as sand bar. These comprise floodplain deposits that still exist today. Most of the 'other deposits' that exist on the oldest maps were eroded during later time steps. Every next map shows that a part of the floodplain was eroded and that new sand bars were formed, while concave swales were filled. Trends in this process are that every time step the sinuosity decreased, and that islands became smaller and merged with the floodplain, a process that was promoted by the construction of groynes to reclaim land. After 1872 AD the floodplain area hardly changed.

4.4.2 Lithogenetic units

Most lithogenetic cross-sections (Figure 4.10) show a series of channel deposits, forming sand bars that generally increase in elevation from dike to channel, indicating aggradation of the system through time. Furthermore, average sand bar elevation decreases in downstream direction, following the channel-belt gradient. The sand bars are approximately 1000-1500 m long and 200-300 m wide. Their thickness cannot be estimated because of the insufficient coring depth, but is assumed to be equal to the average bankfull water depth of 4.4 m (Maas et al., 2003).

Sand bars are separated by small concave swales that are filled with clayey material. These swales are about 30-70 m wide, and 2.5-4.0 m deep. Their elevation shows the same trend as the sand bars: an increase in elevation in direction of the channel and a decrease in downstream direction. In the cross-sections the width of the sand bars and concave swales is overestimated, because cross-sections are mostly perpendicular to the present channel instead of to sand bars and concave swales.

On top of the concave swales fills and channel deposits a 2-3-m thick layer of clayey overbank deposits is visible. The reconstructed parts the overbank material that has been removed for clay extraction is also shown. Near the dike the clay layer is thicker than near the river, because the older parts of the floodplain near the dike have experienced a longer period of clay deposition and because the top of the sand bars is at lower elevation there.

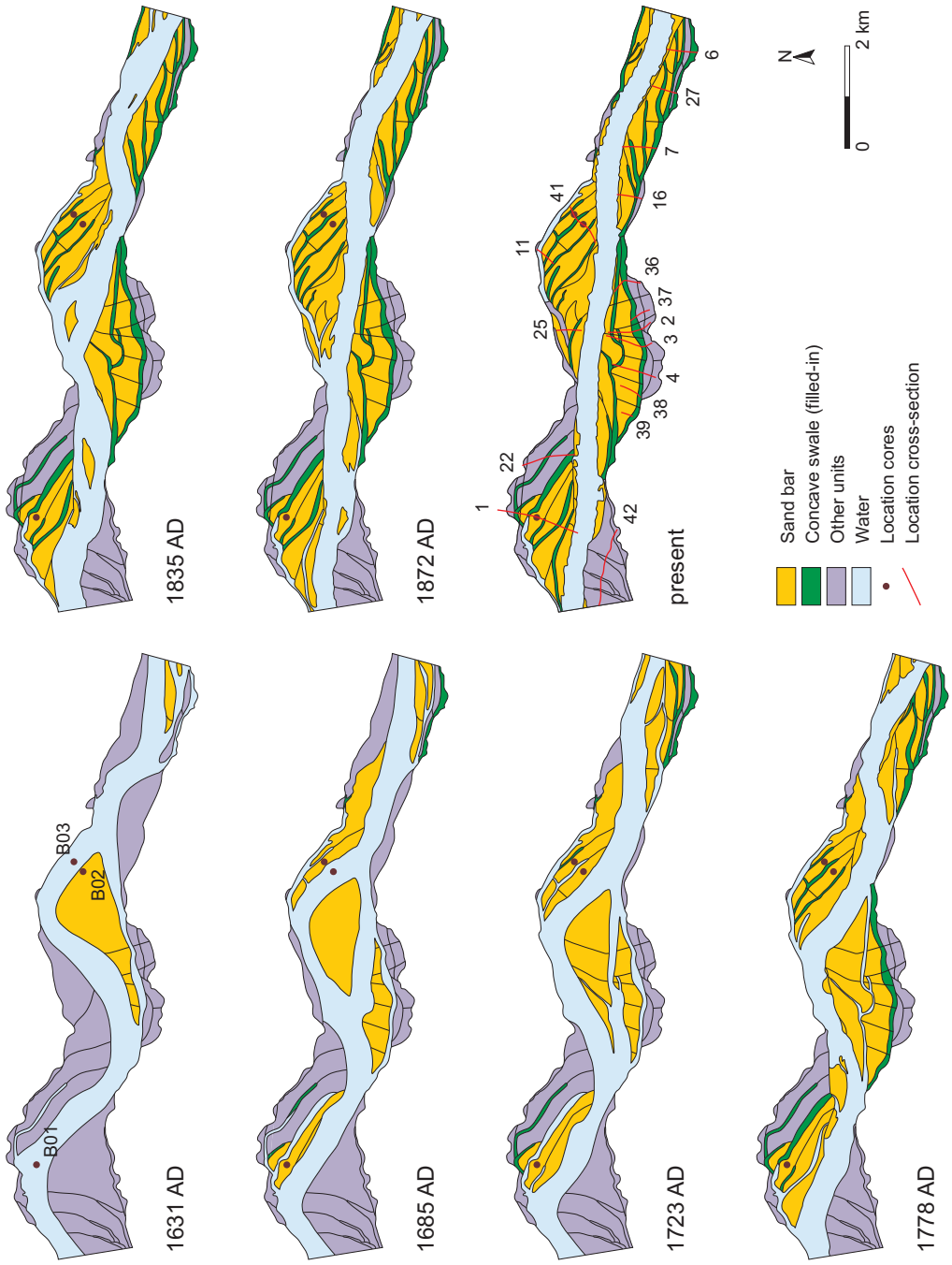

Figure 4.9. Historical geomorphological maps. The red lines in the present map represent all cross-sections given in Figure 4.8. In all maps, the black dots indicate the locations of the Begemann cores.

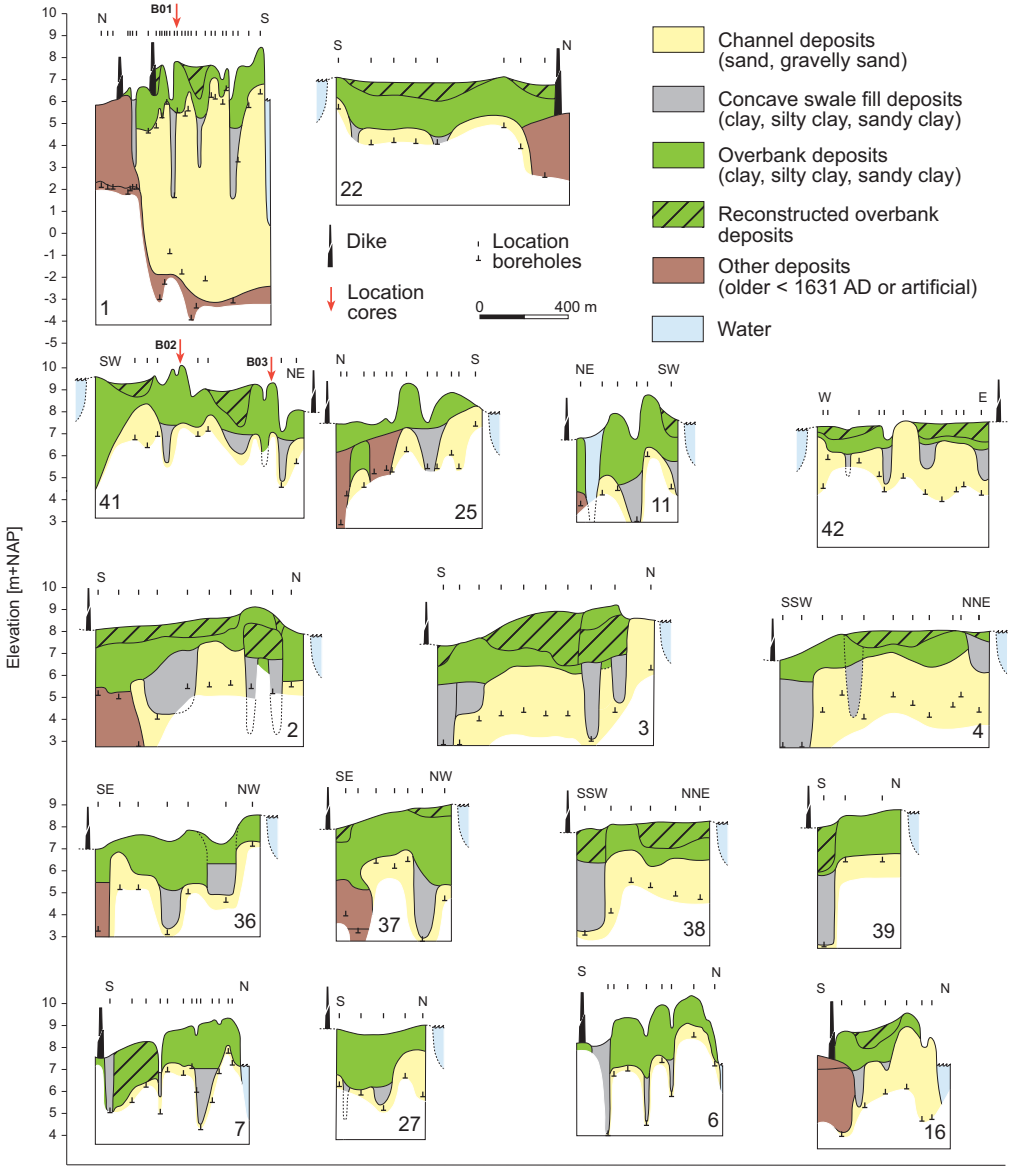

Figure 4.10. Cross-sections, showing the lithogenetic composition of the floodplains. The position of the dike is indicated inside or outside the cross-section. Red arrows indicate the locations of the Begemann cores.

4.4.3 Chronostratigraphy

Figure 4.11 shows the vertical heavy metal profiles of the cores, in which the <1860 AD and >1860 AD boundaries are drawn. In the lower part of all cores heavy metal concentrations are low and slightly fluctuating, but no significant changes occur. These sediments are most likely deposited before 1860 AD. In the upper part of all cores increased heavy metal concentrations are found. These sediments are deposited after 1860 AD.

In Table 4.2 OSL-dating results are presented. Uncertainties in the age estimates, given as one standard deviation, include systematic and random errors in both burial dose and dose rate estimation. Dates range between 1667 ± 20 and 1900 ± 25 AD. These agree with the ages that can be expected from the historical geomorphological maps (Figure 4.9). The ages are not always in correct stratigraphic order, but where age inversion occurs, it is mostly within the uncertainty range of the individual dates. There is no significant age difference on the boundary between overbank deposits and channel deposits.

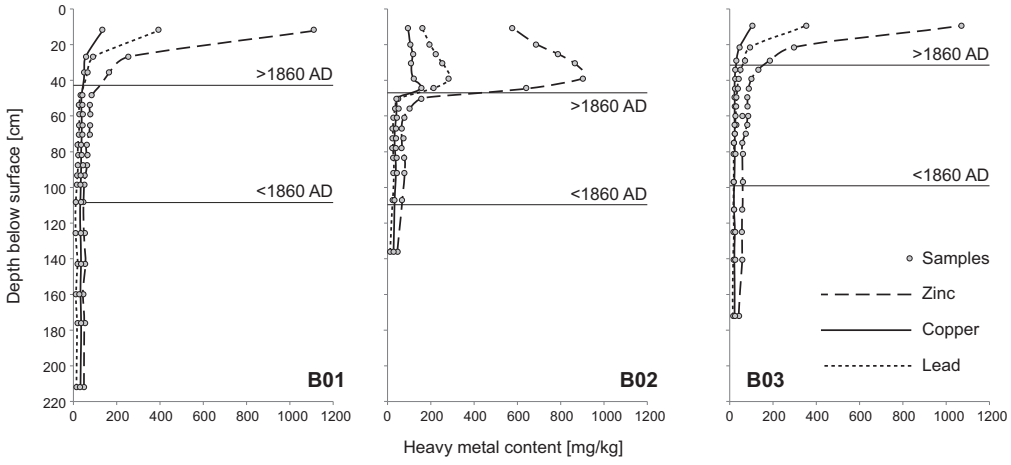

Figure 4.11. Heavy metal concentrations in the floodplain cores, and the estimated upper and lower boundary of 1860 AD.

Table 4.2. OSL-dating results after MAM/bootstrapping analyses.

Sample	Lithogenetic composition	Depth [m]	Total dose rate [mGy/a]	Equivalent dose [mGy]	OSL age [AD]
B01; x:169224, y:435532					
NCL-4110010	Overbank deposits	0.94	2.11 ± 0.14	794	1632 ± 46
NCL-4110011	Overbank deposits	1.61	2.09 ± 0.12	469	1785 ± 135
NCL-4110012	Overbank deposits	1.99	2.06 ± 0.12	644	1696 ± 44
NCL-4110013	Overbank deposits	2.32	2.07 ± 0.13	724	1659 ± 30
NCL-4110014	Overbank deposits	2.91	1.85 ± 0.14	550	1711 ± 25
NCL-4110015	Channel deposits	3.34	1.14 ± 0.06	579	1502 ± 125
B02; x:174937, y:434612					
NCL-4110016	Overbank deposits	0.82	2.47 ± 0.14	514	1801 ± 129
NCL-4110017	Overbank deposits	1.24	1.44 ± 0.05	472	1680 ± 82
NCL-4110018	Overbank deposits	1.63	2.09 ± 0.14	654	1696 ± 10
NCL-4110019	Channel deposits	2.04	1.26 ± 0.06	371	1716 ± 211
NCL-4110020	Channel deposits	3.18	1.59 ± 0.09	492	1700 ± 66
NCL-4110021	Channel deposits	4.47	1.33 ± 0.07	590	1566 ± 102
B03; x:175183, y:434839					
NCL-1110003	Overbank deposits	1.01	2.62 ± 0.17	409	1853 ± 6
NCL-1110004	Overbank deposits	1.56	1.91 ± 0.07	454	1771 ± 62
NCL-1110005	Overbank deposits	1.72	2.27 ± 0.15	584	1752 ± 58
NCL-1110006	Overbank deposits	1.88	1.84 ± 0.07	303	1845 ± 91
NCL-1110007	Overbank deposits	2.07	2.11 ± 0.13	626	1713 ± 53
NCL-1110008	Channel deposits	2.63	1.45 ± 0.07	367	1756 ± 58
NCL-1110009	Channel deposits	4.66	1.37 ± 0.07	374	1736 ± 103

4.4.4 Sedimentation rates

The results of the chronological analyses with the OxCal-model of the three Begemann cores are shown in Figure 4.12 and Table 4.3. The figure gives no information about sedimentation rate because the vertical axis is not scaled. Sedimentation curves fitted through the Begemann core data are shown in Figure 4.13, and the parameters *a*, *b* and *c* (Equations 4.2 and 4.5) belonging to these fits are given. The spread in parameters is large, which means that sedimentation curves vary significantly between cores and do not provide robust values that are valid for all building blocks; separate values for *a* and *c* indeed must be determined for each building block.

Age estimates for the sand bar deposits plot on a straight line, but data is too limited and too scattered to confirm the assumed linear sedimentation rate within a core. Even though, sedimentation rates for sand bars were obtained by fitting a linear trendline through the available age estimates. Results suggest sedimentation rates ranging from 60 to 180 mm/a. In the overbank deposits more age estimates are available for each location. The data indicate a decreasing sedimentation rate, which agrees well with the relation described by Equation 4.5 derived from water level data. However, in all cores there is a slight increase in sedimentation rate in the most recent decades, which was not included in the sedimentation curve. This may be a temporal increase, associated with the occurrence of major peak flows in 1988, 1993 and 1995 (Asselman and Middelkoop, 1998). This high sedimentation rate has a slight effect on these parameters, and may not be fully representative for the general trend. We determined the sedimentation *rates* from these curves, which allowed us to calculate the maximum

sedimentation rate, at start of overbank deposition, and the minimum sedimentation rate, at present time. Results vary considerably between cores. In B01 the sedimentation rate decreases from 38.5 to 3.5 mm/a, in B02 from 6.2 to 5.9 mm/a, and in B03 from 13.2 to 5.0 mm/a.

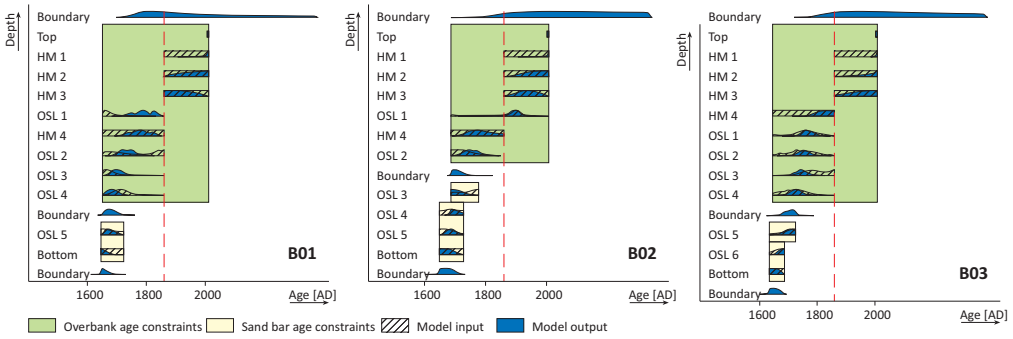

Figure 4.12. Results of the chronological analysis. The principles of this analysis are explained in Figure 4.5. This figure shows the age constraints (yellow and green boxes, red line), the input derived from heavy metal analysis and OSL dating (hatching), and the results derived by the OxCal model (blue). Heavy metal samples were only included if they are certainly older or younger than 1860 AD.

Table 4.3. Results derived by the OxCal model with one standard deviation.

B01			*B02*			*B03*		
Sample	**Age [AD]**	**1σ [year]**	**Sample**	**Age [AD]**	**1σ [year]**	**Sample**	**Age [AD]**	**1σ [year]**
Boundary	1883	131.50	Boundary	2095	182.25	Boundary	2016	178.75
Top	2008	0.63	Top	2008	0.63	Top	2008	0.63
HM 1	1995	13.41	HM 1	1998	9.83	HM 1	1998	10.50
HM 2	1970	38.37	HM 2	1972	32.26	HM 2	1978	30.10
HM 3	1899	37.93	HM 3	1938	35.69	HM 3	1965	41.13
OSL 1	1802	35.44	OSL 1	1894	24.30	HM 4	1833	26.21
HM 4	1781	40.76	HM 4	1778	38.85	OSL 1	1766	22.26
OSL 2	1733	28.85	OSL 2	1752	24.93	OSL 2	1754	21.40
OSL 3	1700	19.54	Boundary	1702	18.25	OSL 3	1743	21.19
OSL 4	1683	17.77	OSL 3	1699	14.60	OSL 4	1726	19.04
Boundary	1676	18.00	OSL 4	1694	13.59	Boundary	1708	17.50
OSL 5	1675	16.60	OSL 5	1683	14.79	OSL 5	1707	15.26
Bottom	1657	11.05	Bottom	1666	19.41	OSL 6	1677	8.47
Boundary	1659	14.00	Boundary	1668	20.00	Bottom	1648	14.02
						Boundary	1651	15.50

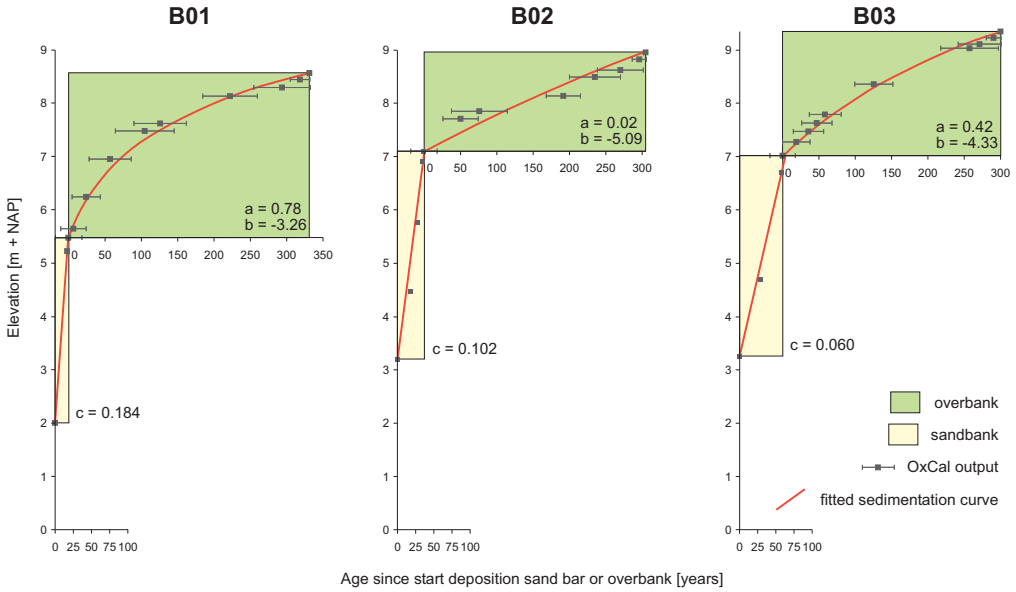

Figure 4.13. A sedimentation curve, forced through upper and lower boundaries, is fitted through the OxCal output data to find parameters a and b for the overbank, and parameter c for the sand bar. For the overbank curve, the uncertainty in the data is included.

4.4.5 Sediment budget

Figure 4.14 shows the isochrones, calculated by the sedimentation curves, in the building blocks that represent cross-section 41. In this figure, the difference in sedimentation rate between the channel deposits and the overbank deposits is clearly visible. The channel deposits and the concave swale fills were deposited in a short time interval, mostly within one time slice, while the overbank deposits have formed much more gradually, and with a decreasing rate.

Estimates of eroded and deposited sediment volumes in m^3 per year are given per lithogenetic unit in Figure 4.15. The estimated amount of accretion decreases from 23,000 to 2,600 m^3/a/km in channel deposits, and increases from 2,500 to 6,500 m^3/a/km in overbank deposits, and from 500 to 2,500 m^3/a/km in concave swale fills. The estimated amount of erosion decreases from 15,000 to 9,000 m^3/a/km in sand bars, from 4,500 to 800 m^3/a/km in overbank deposits, and increases from 0 to 200 m^3/a/km in concave swale fills. A few trends can be recognized. First, the amount of erosion is positively related to the amount of accretion. Mostly, accretion is slightly larger than erosion, resulting in net accretion, and hence an accumulation of sediment in the floodplains. Secondly, there is a general decrease of lateral processes in time. The figure shows a halving of the amount of eroded sediment between ~1631 and 1872 AD, with the largest change around 1723-1778 AD. The amount of accretion initially increased, but from 1778 AD it shows a decreasing trend. In the period 1872-2009 AD hardly any erosion occurred anymore, while accretion processes continued at low rate. Hence,

in the absence of lateral erosion, net overbank deposition is large. In numbers, overall erosion volumes decrease from ~20,000 m^3/a/km to ~10,000 m^3/a/km, and overall accretion from 20,000-30,000 m^3/a/km to 10,000-20,000 m^3/a/km. Thirdly, the amount of vertical accretion continuously increased.Together with the decreased lateral accretion, the proportion of overbank deposition has become larger in time.

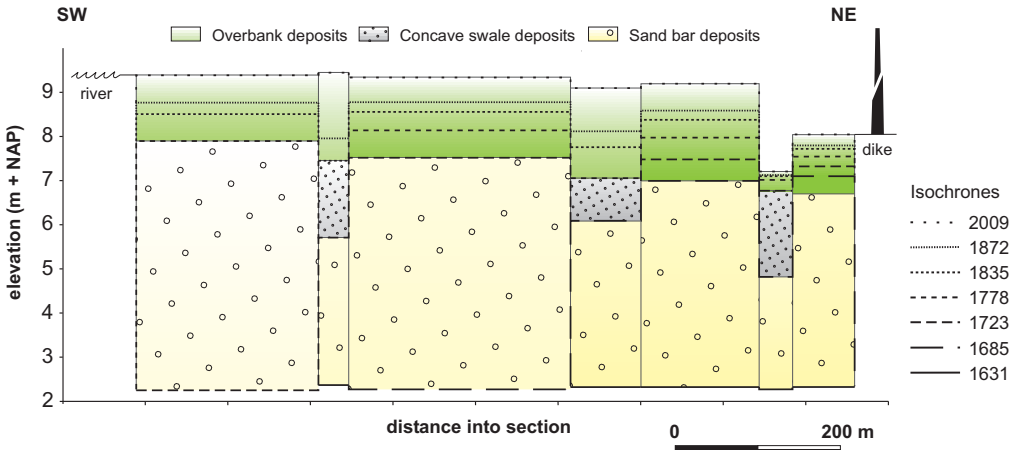

Figure 4.14. Cross-section 41, simplified as building blocks, with isochrones in them. Color gradient represents the decreasing age in both upward direction and riverward direction.

4.4.6 Floodplain elevation

Figure 4.16 shows the change in floodplain elevation through time. In the graph of 1631 AD the floodplain elevation distribution is irregular, caused by the relatively large uncertainties due to deficient historical maps. For the period 1685-1778 AD, floodplain elevation distribution remains quite constant, and there are ample low floodplains present. In this period, downstream migration processes are responsible for the erosion of old, high floodplains, and the formation of new, low floodplains on the opposite site of the river (floodplain shaving concept; Lauer and Parker, 2008c). Meanwhile, the laterally stable parts of the floodplain rose in elevation due to overbank deposition. For the 1835-1872 AD period, the elevation distribution shifts towards higher values, i.e. the average floodplain elevation increased. This is a result of straightening of the river, which reduced lateral dynamics, and fewer old and high floodplain parts were replaced by new low floodplains. In this period, vertical accretion became more important, increasing the average elevation of the floodplains. In the graph of 2009 AD, after normalization, there is a considerable shift of the distribution to higher floodplain elevations. Here, lateral dynamic processes are absent, and floodplain shaving has ceased. Hence, there is no longer rejuvenation of the floodplains, and only vertical accretion processes occur, causing the distribution to move further towards higher values. Moreover, as low floodplains are aggrading more rapidly than higher floodplains, the spread in height is decreasing.

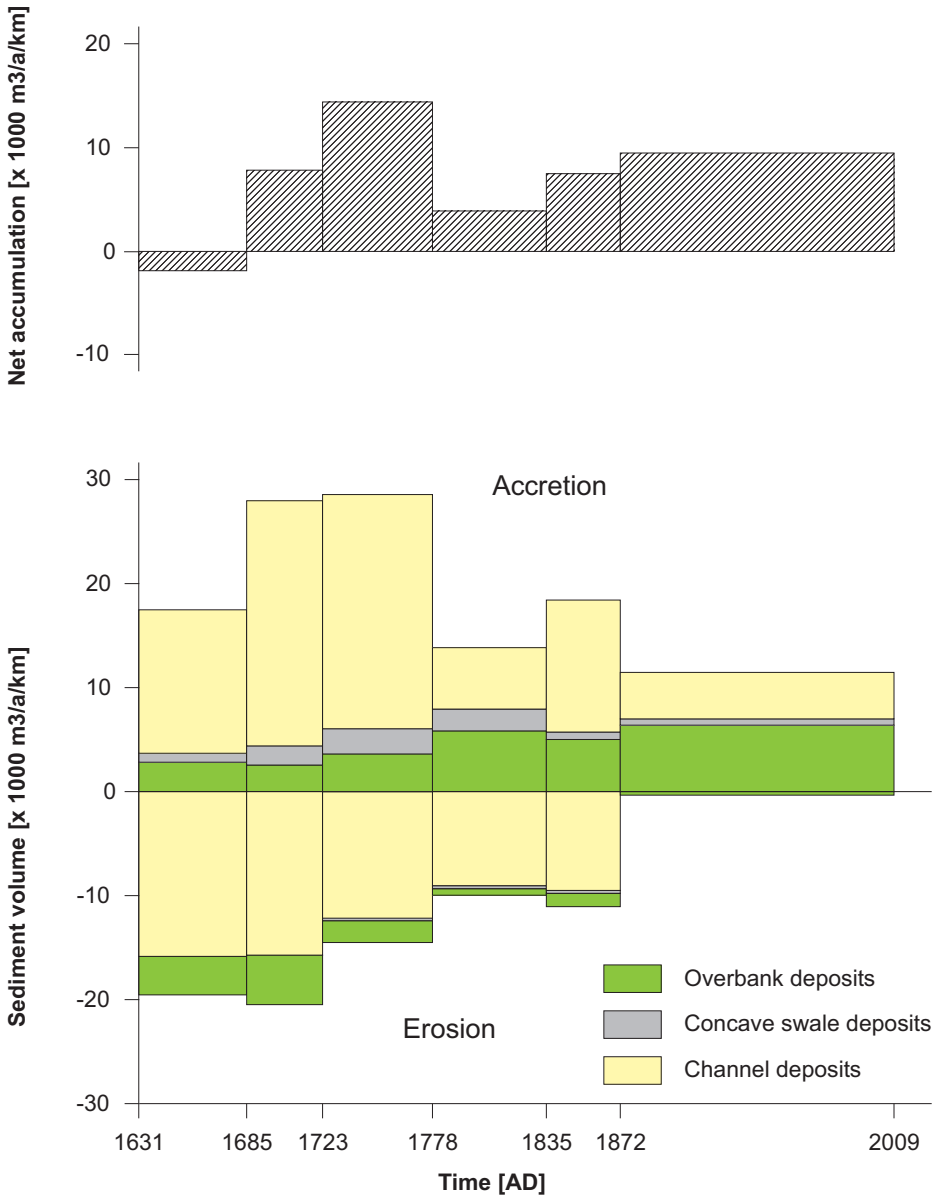

Figure 4.15. Amount of erosion and deposition in the study reach.

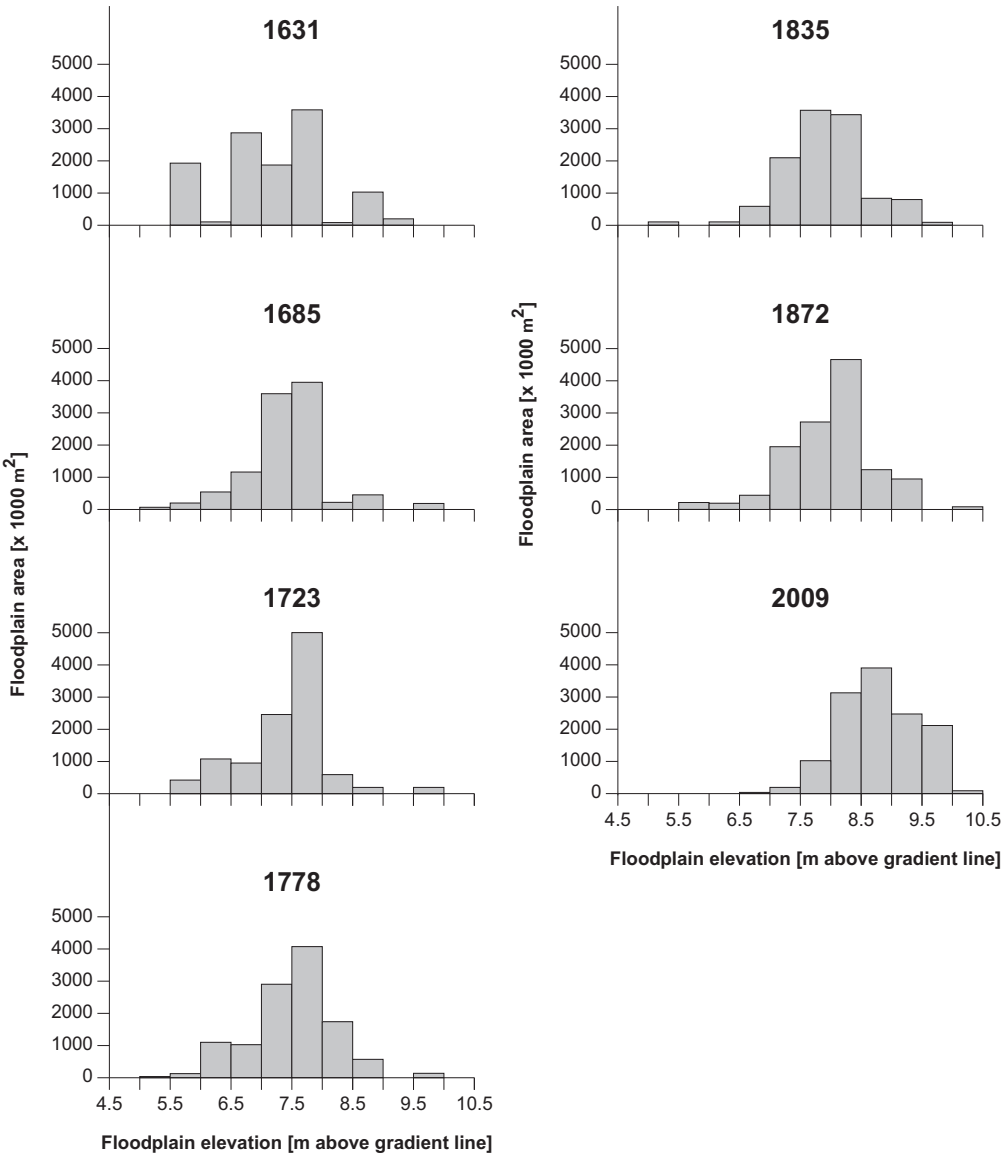

Figure 4.16. The change in floodplain elevation through time, in relation to a gradient line of 10 cm/km that crosses Dutch ordnance level (NAP) at the upstream boundary of the study area.

4.5 Discussion

4.5.1 Historic trends

Important trends in deposition and erosion were observed in the results. In the 17th and 18th centuries lateral processes of erosion and accretion dominated. Channel migration resulted in a positive correlation between the amounts of erosion and accretion, but net accretion occurred. Associated with these early lateral processes concave swale deposits are trapped, which are of importance for the overall sediment accumulation before the river bed was fixed. The amount of lateral accretion of channel deposits initially increased, but after 1778 AD both lateral processes attenuated over time. The amount of vertical accretion of overbank sediments increased continuously (Figure 4.15). Around 1872 AD vertical accretion became more important than lateral processes and from then onwards floodplain elevation has continuously increased. Accordingly, floodplain height distributions show a shift towards higher elevations and a tendency to smaller variation (Figure 4.16).

The near-balance between erosion and deposition in the earliest period suggest that near-equilibrium conditions existed in the early 17th century. Still, already in that time the presence of embankments may have prevented the river reaching such equilibrium. The trends observed during the subsequent period can be largely explained by human modifications, which were abundant in the study period (Table 4.4). The initial increase of lateral accretion may be a result of the development of islands in the channel, which occurred after the river became embanked. Due to the embankments the meander process ceased, sand was no longer deposited in point bars, and instead islands were deposited. The decrease of lateral accretion and erosion volumes in time can initially be related to the straightening of the river. From the 17th century onwards this first occurred by construction of individual groynes to protect the irregular placed dikes against erosion, and to reclaim land from the river (Hesselink, 2002). The groynes promoted lateral accretion, the river straightened, and the floodplain area expanded. With ongoing overbank sedimentation, the contribution of overbank accretion increased.

Another major human impact on the sedimentary dynamics was the construction of the Pannerdensch Canal located 30 km upstream of our study area (Van de Ven, 2007) in 1707 AD, which regulated the discharge distribution of the lower Rhine distributaries. Before construction of this canal, the Waal discharged increasing amounts of Rhine water (up to 90%), at the expense of the Nederrijn and IJssel branches. After construction of the Pannerdensch Canal, the water supply to the River Waal decreased. This resulted in smaller amounts of wash load transported by the Waal, and a lower inundation frequency of the floodplain. Although the distribution of bed load over the branches after the canal was constructed is not known, the transport and erosive capacity of the Waal must have decreased.

Channel normalization and fixation by the end of the 19th century have stopped the 'floodplain shaving' process that existed even during the period of embankment. Since then the floodplains have increased in elevation and therefore they have become increasingly less frequently inundated, and overbank sedimentation rates have decreased. Furthermore, the normalization resulted in a gradual deepening of the main channel due to increased flow velocities.

Table 4.4. Summary of most important human activities along the Waal, and their impact on the sedimentary dynamics.

Human modification	Impact on sedimentary dynamics
Embankments (1000 – 1350 AD)	Lateral accretion volume increased as a result of island formation.
Straightening of the river (1350 – 1850 AD)	Lateral erosion and accretion reduced. Floodplain area grew, and floodplain elevation rose as a result of increased overbank sedimentation.
Construction Pannerdensch Canal (1707 AD)	The discharge through the Waal reduced, and hence the amount of wash load and the inundation frequency decreased.
Normalization works (1850 AD)	Lateral processes ceased. Vertical accretion continues, but without rejuvenation the elevation increases and hence accumulation rates decrease.

Finally, more activities took place that influenced sediment delivery to floodplains to some, but hardly quantifiable, extent. Over the past century or so delivery of sediments to the delta has declined, as a result of reforestation, bank protection measures and building of sediment trapping weirs. Furthermore, channel incision after normalization has slightly decreased the inundation frequency of the floodplains (Ten Brinke et al., 1998). Sand dredging has been an artificial loss of sand from the lower branches.

4.5.2 Accuracy

We realise that we have made many assumptions, leading to uncertainties in our estimated sediment budgets. Uncertainties mainly arise from estimates of the boundaries of our building blocks. Uncertainty in the budgets associated with lateral extent of floodplain segments depends on the planview accuracy of the available maps. For the >1778 AD maps, we have detailed data, but some older maps only show fragments of the floodplains, and thus we had to reconstruct the boundaries based on the overall floodplain configuration arising from the maps. Although we have no verification data for these uncertainties, we consider them smaller than the changes shown in the budgets. Estimates of the amounts of extracted clay cause another major uncertainty. This affects vertical accretion estimates of overbank deposits. The mined sand is part of our accretion budget, but our erosion budget does not include human sand extraction from the channel. Mining might have affected the sediment budget, when lowering of floodplains resulted in enhanced sedimentation.

Other uncertainties are caused by the way we calculated the sediment budget in each time step. Lateral accretion and erosion are two opposite processes, and for every building block only the net result is calculated: either accretion or erosion. This ignores the fact that a building block can have both processes taking place within one time slice. Still, the effect on the sediment budget may be small as we found that this hardly occurred. Another uncertainty arises from relating the sedimentation rate only to elevation. Hereby, we ignore the

occurrences of local minor embankments, changes in vegetation, channel incision, and decreasing overbank deposition amounts at increasing distance from the main channel as relevant factors influencing sedimentation rates (cf. Middelkoop and Asselman, 1998), and hence our sediment budgets. Still, the main trends found in our study will not be much affected. For example, both the elevation and the distance to the river of the floodplain increase through time and they both lead to reduction of the sedimentation rate. This implies that both processes are considered in the calibration of the sedimentation model for each building block.

4.5.3 Comparison to other studies

In this section we compare our results to previous sedimentation and sediment budgeting studies in the Rhine Delta. Erkens et al. (2006) evaluated volumes of preserved flood basin clay and silt in the entire delta, for 1,000-year time slices, since the start of Holocene sediment accumulation 9,000 BP. For the period after 3,000 BP they found an increase in trapped sediment volume, especially in the most recent pre-embankment time slice of 2,000-1,000 BP. They found an estimated overbank deposition rate of 1,220,000 m^3/a, of which 220,000 m^3/a was later eroded by avulsion and meandering processes. The increased deposition was attributed to enhanced sediment delivery from the hinterland to the river system due to deforestation for agriculture (Erkens, 2009). Erkens (2009) assumed that 82% of deposited clay has been preserved. To compare this value to our results, we calculated deposition rate per kilometre river length. Using the paleogeographic map of the Rhine delta for 1500 BP (Berendsen and Stouthamer, 2001) we estimated the total river length in entire Rhine delta to be roughly 500 km. Hence, the overbank deposition rate just prior to embankment becomes about 2,440 m^3/a/km.

In our study, clay deposition rates of 2,500-6,500 m^3/a/km are found for the >1631 AD Waal. Compared to the results of Erkens et al. (2006), this is the same order of magnitude, but slightly larger. This is remarkable, since the environmental conditions were considerably different: Firstly, in the post-embankment period the sediment delivery from upstream was further increased due to intense agricultural land use. However, the embankment may have significantly changed the trapping efficiency of the remaining active floodplain. In the natural river the trapping efficiency was large, because during floods all fine suspended sediment conveyed with the floodwater from the channel over the wide flood basin settled there. The embankment caused flood water levels to become higher than before, resulting in a larger flow over the floodplain, but also coinciding with higher flow velocities. Furthermore, the varying width of the embanked floodplain results at many locations in a return flow of flood water to the main channel, from which not all suspended sediment may have settled. The net effect on deposition rates depends on the hydraulic conditions that resulted from the larger overbank flow combined with higher flow velocities and an enhanced exchange between the channel flow and overbank flow, which are hard to reconstruct for the historic situation. Another difference with the natural Rhine is that preservation of the floodplain deposits became much lower after embankment, due to reworking of the small floodplains by lateral channel migration.

Based on old river maps, Middelkoop et al. (2010) estimated the average annual clay deposition in the period 1300-1850 AD along the lower Rhine distributaries, using crude

estimates of overbank volumes deposited after 1850 AD (30% for the Waal) and percentages of reworked floodplain (90% for the Waal). This resulted in an estimated annual deposition volume of 1.4 10^6 m^3/a, and 0.5 10^6 m^3/a for the lower Rhine distributaries and for the Waal branch, respectively. Per km river length at that time, this yields ~4,400 m^3/a/km for all Rhine branches and 1,600 m^3/a/km for the Waal. These results fall well within the range of our estimated clay deposition rates. However, our values include better estimates of the amounts of clay eroded after normalization, as well as the volume deposited before 1850 AD. We found that only 52% of the floodplain clays was deposited before 1872 AD, and that 71% of the pre-1631 AD sediments has been reworked after 1631 AD. Other pre-1631 AD sediments might have been reworked before 1631 AD. This implies that indeed up to 90% of the Waal floodplains may have been reworked between 1300 and 1850 AD.

In the past century, after the river normalization, removal of sediment only occured through human extraction of sand and clay. Overbank deposition has continued, but rates show a remarkable decrease, resulting in reduced sediment trapping when compared to the preceding pre-normalization period. This is due to the decreasing flooding frequency of the floodplains, on the one hand because their surface becomes increasingly higher, and on the other hand because the discharge capacity of the main channel has increased. Furthermore, in the past century, upstream reforestation has likely decreased sediment supply, whilst channel bank protection and sediment trapping weirs have further reduced sediment delivery to the Rhine delta. Contemporary sedimentation rates of 1-10 mm/a found in related studies for the Rhine (Maas et al., 2003, Middelkoop, 2000, Hobo et al., 2010), are similar to our sedimentation rates.

4.6 Conclusions

We performed a detailed sediment budget estimate for a reach of the largest lower Rhine distributary in the period after it was embanked. Our sediment budget is based on erosion and accretion of the floodplains and in the channel over a period of more than three centuries. With this, we fill the gap between fluvial sediment budget studies (catchment oriented, millennial time scale) and river management studies (river stretch oriented, decadal or event time scale).

Average vertical sedimentation rates in channel deposits were estimated to be 60-180 mm/a. Sedimentation rates in the floodplains decreased during the study period with rising floodplain elevation due to sedimentation, from 6-38 mm/a to 3.5-6 mm/a. Average erosion volumes were estimated to be ~10,000 to 20,000 m^3/a/km, and average accretion volumes were ~10,000 to 20,000 m^3/a/km. These values imply that 0.2 to 0.5% of the total volume of sediments present in the floodplain erodes yearly, and 0.4 to 0.7 % of the total sediment volume accretes. Most of this sediment is involved in the sand bars. In our budget, the accretion volume is larger than the erosion volume, so there is net accumulation of sediment in the floodplains. Apparently, there was no equilibrium state of 'floodplain shaving' (Lauer and Parker, 2008ab): due to the gradual decrease of channel sinuosity and growth of the floodplain area both erosion and accretion volumes decreased, while vertical accretion of overbank fines became relatively more important. After normalization, lateral erosion and accretion have ceased and the natural floodplain shaving mechanism has become inactive. Currently, there is no more rejuvenation of the floodplains, and only vertical accretion processes occur. There is a yearly

accretion of 0.2% of the total floodplain volume, but this percentage will drop as floodplains grow in volume and rates decrease. Along with this development, the variation in floodplain elevation decreased as well.

The observed trends are related to human activities in the past, and cannot be generalized to natural systems. Most importantly, these activities involve straightening of the river, as a result of which lateral dynamics reduces. Moreover, there is reduced sediment delivery. This is caused by upstream works like reforestation, bank protection measures and building of sediment trapping weirs, and by the construction of the Pannerdensch Canal, which reduced the washload supply to the River Waal.

Acknowledgements

The research was partly funded by the BSIK-Delft Cluster programme “Flood protection” and is part of the strategic research program “Sustainable spatial development of ecosystems, landscapes, seas and regions" which is funded by the Dutch Ministry of Agriculture, Nature Conservation and Food Quality, and carried out by Wageningen University and Research centre (grant CT04.32.62). OSL dating of flood deposits is supported by NWO/STW (grant DSF.7553).

5 Decadal to century-scale sediment dynamics in channel belts of the natural Rhine delta

Noortje Hobo, Hans Middelkoop, Maarten Kleinhans, Bart Makaske

Abstract

In a natural delta, avulsions frequently initiate the formation of a new channel, thereby trapping sand in the deltaic plain. The life cycle of this channel can be divided into 4 stages: avulsion stage (Av), in which the channel is formed; channel-belt-building stage (S1), in which floodbasin material is eroded and replaced by channel sand; channel-belt-reworking stage (S2), in which the river's own sediment is reworked; and abandonment stage (Ab), in which the channel gradually fills. The objective of this study was to quantify the sedimentary dynamics during these four stages for a mid-Holocene palaeochannel in the central Rhine delta: the Hennisdijk system. This is a well-documented palaeochannel from which lithogenetic and chronological information is available. The meander migration rates were estimated with the Bank Stability and Toe Erosion Model (BSTEM). The results show that, due to the large resistance of the floodbasin material, meander migration rates were initially low, in the order of 0.1 m/a. But when a transverse bedslope developed, the channel incised into the Pleistocene subsurfacel, and the meander migration rate increased rapidly, reaching rates of 3-3.5 m/a by the end of S1. Reworking rates in S2 were about ~4-4.5 m/a. Finally, we explored the spatial differences in channel belt sediment dynamics within the delta. The meander migration rates, and hence the duration of each stage, are mainly controlled by thickness of the cohesive floodbasin deposits and the proportion of peat in the floodbasin sedimentary succession, which both increase from delta apex to coastal zone. Hence, in the eastern delta meander migration rates are high, and S1 rapidly switches to S2. In the western delta the thick cohesive floodbasin deposits with erosion-resistant peat beds cause low meander migration rates, so that S1 takes a long time and S2 might not be reached within the channel's lifetime.

5.1 Introduction

River dynamics on a fluvial deltaic plain cause erosion, deposition and reworking of sediments. Here we study these sediment dynamics with a combination of detailed data and scenario modelling. On millennial scale, these processes are controlled by the delivery of water and sediment to the delta, and by the availability of accommodation space within the delta. Discharge and sediment load are partly determined by climate. Erosion, deposition and reworking processes of fluvial deltaic sediments results in a change in storage, and a remaining amount of sediment that is transferred to the coastal zone as throughput. The proportion between storage and throughput depends on the availability of accommodation space, which is driven by eustatic sea-level fluctuations and tectonics. Since the middle Holocene human intervention also became an important forcing factor affecting the discharge

and sediment load. For example, in the Rhine-Meuse delta deforestation in the hinterland leads to increased discharge and sediment load, which resulted in a larger deposition in the delta (Erkens et al., 2006). On the other hand, reservoir building has been recognised as world-wide major cause of reduced sediment supply to river deltas and the coastal zone (Syvitski et al., 2009; Giosan et al., 2013).

At a smaller scale, fluctuations in storage, reworking and throughput of sediment in a delta are driven by event-based fluctuations in discharge and sediment load. Peaks in discharge and sediment entering the delta and are smoothed when floodwaters spread across the delta and sediment becomes trapped on the inundated floodplains. Resulting short-term fluctuations in peak flows, storage and throughput are called 'pacing of sediment'. Traces of these event-based fluctuations in discharge and sediment load can be found in sedimentary records, for example in the Lower Rhine (Toonen, 2013).

Pacing of sediment can also be induced by intrinsic processes, without any variations in upstream delivery of water and sediment. This within-delta pacing of sediment may occur due to displacement of delta lobes (Mississippi, Törnqvist et al., 1996; Danube, Giosan et al., 2013). On smaller scale, sediment trapping by the infilling of a floodbasin after avulsion alters the transfer of sediment to the coastal zone (Erkens, 2009). Other intrinsic processes include the development crevasse splays (Smith et al., 2014), the filling of lakes (Bos et al., 2009), bay-head deltas (Hijma et al., 2009), or formation of inland deltas (Kleinhans et al., 2010).

The role of avulsions in pacing sediment flow through a delta is less known. Lauer and Parker (2008c) describe a balance between erosion and deposition of a meandering river. In this balance floodplain shaving and channel extension cause net local erosion of sediments, which is compensated by overbank deposition and deposition in oxbow lakes. Storage and throughput is in balance. However, within a delta, this balance is different. Firstly, overbank fines may be deposited over large distances away from the active channel, resulting in a net loss. Furthermore, new channels are repeatedly formed due to avulsion, which causes an interruption time and shift across the delta in the flow and trapping of the sediment to the coastal zone. After each avulsion a new channel develops over several stages to maturity, and each stage can be identified by its own, specific fingerprint regarding the sedimentary dynamics.

In this study we investigated the storage, throughput and reworking of sediment - which we refer to as sedimentary dynamics - of a channel belt in the fluvial reach of a high-stand delta, in each stage from avulsion to maturity and abandonment, on a time scale of 10^2-10^3 year. Our goal was to establish a detailed sediment budget, that shows the amount of eroded and deposited sediment for a number of time slices within the entire lifetime of the channel. Moreover, we try to answer the question what the contribution of each lithogenetic unit is in this budget. Lithogenetic units are defined as sediment units with alike lithology and genesis. We selected an abandoned prehistoric branch within the Rhine-Meuse delta, with presumably virtually completely natural sediment dynamics. This delta has an exceptionally well-documented avulsion history, fluvial architecture and chronology (Berendsen and Stouthamer, 2001), which allowed us to determine deposited sediment volumes and their ages in detail, and to establish budget estimates. In addition, we used a simple channel bank erosion model that predicts bank retreat rate, to estimate timing of reworking processes within the lifetime of the channel. By doing so we created a novel generic method that can in principle be applied in

many more situations. Finally, we used this budget to explore differences in the timing of pacing between proximal and distal parts of the delta.

5.2 Concept

5.2.1 Stages in channel life cycle

The Holocene Rhine-Meuse delta comprises a floodbasin of peat and clay overlying a Pleistocene fluvial plain, which increases in thickness in a downstream direction. In this floodbasin several fossil channel belts are situated, which are remnants of old meandering and straight anastomosing rivers (section 5.3.2). We simplified the life cycle of the channel belts in the delta by a subdivision in four different stages (Figure 5.1): avulsion (Av), stage 1 (S1) with initial meandering, stage 2 (S2) with reworking meandering and abandonment (Ab). Each of the 4 stages in a channel life cycle is associated with a specific sediment budget, in terms of amounts and rates of erosion of older sediments, and reworking of the channel's own sediments.

In the Avulsion stage (Av) a new channel is formed, thereby eroding the floodbasin of peat and clay from older systems, and eventually the underlying Pleistocene sand. Moreover, remnants of older channel belts that are present in the floodbasin may be eroded. In a relatively short period of time (a few hundred years; Stouthamer and Berendsen, 2001; Stouthamer et al., 2011) this newly formed channel reaches stable dimensions with a sinuosity (p_i) ≥1, but sinuosity index ($p_{ind,i}$) = 1 (Figure 5.1; panels A1 and A2).

In stage 1 (S1), the channel starts meandering through the floodbasin and starts to build a channel belt. Predominantly resistant floodbasin material is eroded by lateral bank erosion from the outer bends, while sand is deposited at the inner bends. This meandering process is controlled by the interaction between flow and channel form in the bends. Due to differences in adaptation length of the flow in the meander bends (Struiksma et al., 1985; Crosato, 2009), the point of maximum bank erosion is not located at the apex of the bend, but more downstream. Hence there is not only a cross-valley component in the erosion direction, but also a downstream component. Similarly, the location of minimum erosion is located downstream of the inflection point between two bends. At the inflection point there is still an erosion component present, only in downstream direction. As a result, the entire channel will migrate in a downstream direction, meanwhile enlarging its amplitude, and increasing its transverse bed slope in the developing meanders. Thereby, eroded floodbasin material in the outer bends is replaced by sand deposited along the inner bends (Figure 5.1; panels B1 and B2). Meanwhile, natural levees develop on the river banks, and during overbank flooding a thin layer of silt and clay is deposited in the floodbasin. This meander migration will occur at a relatively slow rate when highly resistant floodbasin clay and peat must be eroded.

Stage 2 (S2) commences as soon as the process of meander migration has caused a bend to reach the sand deposited by the next downstream bend. Then, the downstream component of erosion no longer occurs in floodbasin material, but in the river's own channel sand. The resistance of this sand is much lower than the resistance in cross-valley direction, where

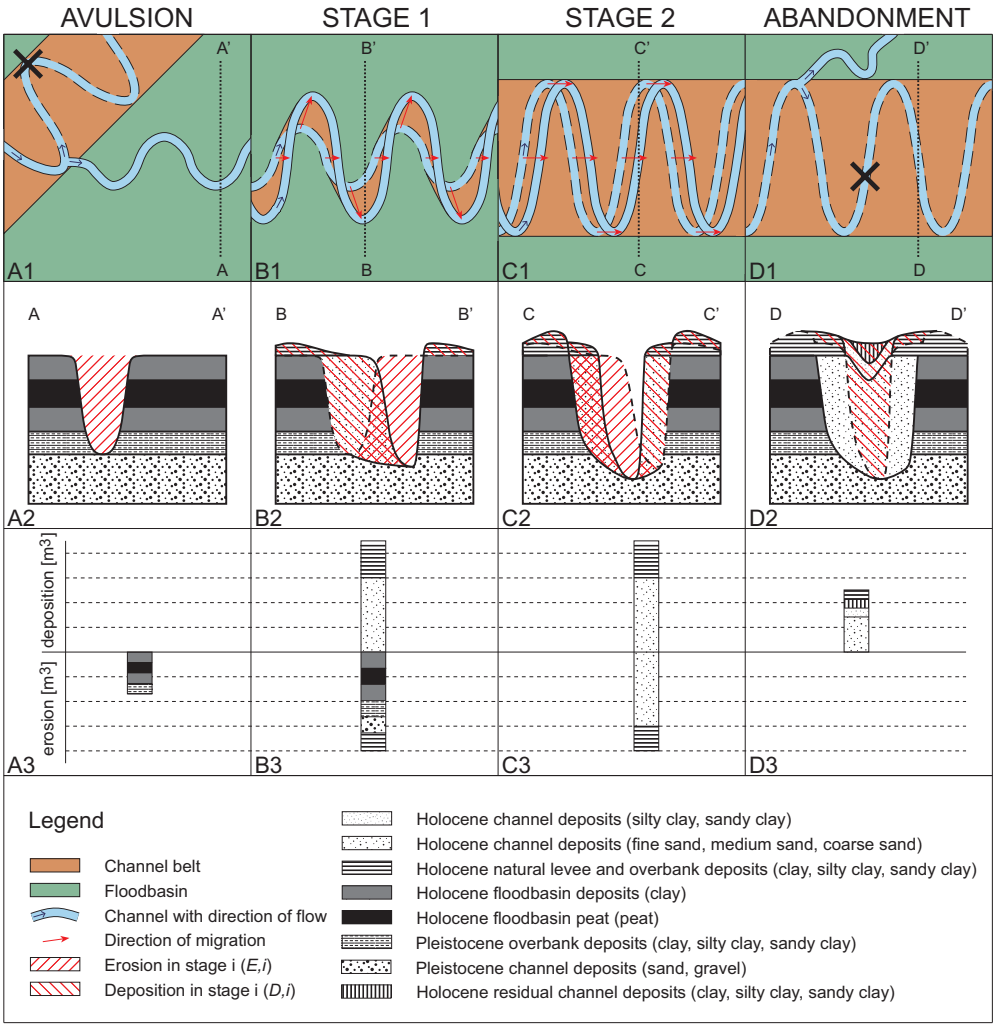

Figure 5.1. A channel in the Holocene Rhine-Meuse delta develops over 4 different stages (A-D). The differences in direction, material and volume between the stages are schematized in a planview (1), a cross-sectional view (2) and a budgetary view (3). Previous river courses are indicated by dotted lines. Time axis is indicative.

floodplain material still exists. As a result, downstream erosion increases to a much higher rate, and meanders start to migrate predominantly in a downstream direction. From this moment onwards, meander migration occurs due to erosion of the river's own previously deposited sand deposits (Figure 5.1; panels C1 and C2). Natural levee development continues. From now on the river is reworking its own sediment, and depending on the meander migration rate and life-time of the branch, the meanders may migrate in a downstream direction over several meander lengths distance.

The abandonment stage (Av) follows after the channel has become abandoned due to upstream avulsion. Reworking of channel deposits stops due to the decreasing flow and erosive power, and the abandoned channel becomes filled in with sand and clay, op top of which some peat may develop (Figure 5.1; panels D1 and D2). The life cycle of the channel has then come to an end.

5.2.2 Sediment budget

The sediment budgets associated with the life-cycle stages are summarized in Figure 5.1 (panels A3 until D3). Here, we plotted for each stage the volume of eroded and deposited sediment. In stage Av, the new channel vertically cuts into the underlying older floodbasin deposits; the total eroded volume of floodbasin material is relatively small, and there is no sand deposition within the channel.

In S1 erosion of floodbasin material continues. The eroded material now also includes silty clay and sandy clay from the natural levee that has started to develop. Sand deposition occurs within the channel, and there is deposition of clay, silty clay and sandy clay on the banks (natural levees) and on the more distal floodbasin (floodplain). Erosion and deposition are not completely balanced; as a result of meander extension, a net erosion of floodbasin material can be expected during S1 (cf. Lauer and Parker, 2008c). The eroded floodbasin material will be redeposited on the floodplains, resulting in a net overbank deposition.

In S2 we assume that floodbasin erosion has become insignificant. Downstream channel migration causes erosion of the river's own channel sand, which is hence replaced by sand from upstream. These processes are in balance, because extension does not occur anymore. The total volume of reworked sediment in S2 increases proportionally with the duration of this stage. There is still a net accumulation in natural levee and overbank sediments, deposited on top of the floodbasin sediments.

In stage Ab there is only deposition. Volume of deposition is larger than the initially eroded volume from the avulsion stage, because the channel has become longer due to meander expansion and deeper due to incision and overbank deposition. As the residual channel may not become entirely filled-in, there is some uncertainty in the total amount of deposition, but the net amount is larger than what is eroded in the avulsion stage.

5.3 Approach and study area

5.3.1 Approach

In our study, we are quantifying the sediment budget as outlined in Figure 5.1 (panels A3 until D3) for channel reaches within the Holocene Rhine-Meuse delta. First, we estimate eroded and deposited sediment volumes based on maps, cross-sections and previous reconstructions. Maps provide information about displacement and dimensions of the channel. Cross-sections add information about the subsurface dimensions and the lithogenetic units that are present. Results are total volumes of eroded and deposited sediment per entire stage. Limitations of

this reconstruction method in view of the objective of quantifying sediment dynamics are that we only calculate net budgets, and that we have no information about erosion rates and temporal differences within a stage. We suspect that the rate of erosion (and hence deposition) processes increase when as a result of meandering the curvature of the bends increases, and a transverse bed slope develops.

In the second part of this paper, we will us a model (BSTEM) to compensate for the limitations of above described reconstruction method. BSTEM allows us to calculate channel bank erosion rates at different steps within a stage. With the results, we calculate reworked surface, reworked volume and duration of the stages, at different steps within S1 and S2. We combine the results of our reconstruction and the BSTEM model results to set-up a detailed sediment budget that shows the temporal differences between and within the stages, for a natural Rhine branch, in which the contribution of each lithogenetic unit is shown.

5.3.2 Holocene Rhine-Meuse delta

The Holocene Rhine Meuse delta is a back-barrier fluvial plain (Berendsen, 1998; Berendsen and Stouthamer 2000, 2001), developed on top of Late Pleistocene sandy and gravelly fluvial sediments deposited by braided rivers. The sand and gravel deposits are topped by 20–50-cm-thick loamy floodbasin deposits deposited during the Bølling-Allerød interstadial and the Preboreal (Berendsen and Stouthamer, 2001).

Holocene delta developed by meandering and straight anastomosing channels. The fluvial deposits of these rivers exist of sandy channel deposits, loamy natural-levee deposits, and clayey floodbasin deposits. Near the river mouths lagoonal deposits formed during the early Holocene transgressive period. Thickness of the Holocene fluviodeltaic deposits increases from about 1 m at the apex in the east, to about 25 m in the west. Intercalated with fluvial overbank clay, peat and humic clay beds occur. Peat abundance and thickness increases towards the coast. As a result of avulsion, many channel belts were formed and abandoned during the Holocene (Stouthamer and Berendsen, 2001). Hence, the delta is now a fluvio-deltaic wedge, consisting of a peaty floodbasin deposits encasing channel sand bodies and associated overbank deposits of former distributaries.

The thickness of the floodbasin material, and hence the percentage of peat and clay, is an important factor determining channel meandering. In the eastern part, channel banks existing of sand from the relatively shallow Pleistocene substrate, which is covered by only a thin layer of floodbasin deposits. Here, bank migration rates were high and channels with large meanders developed, which were rapidly abandoned by meander chute cutoffs. In the western part, there was much more resistance to erosion from the thick clayey and peaty banks preventing rapid meander development. Here, avulsions were the dominating processes for channel relocation (Törnqvist, 1993).

We focus our study on a former channel belt in the high-stand part of natural Holocene Rhine-Meuse delta (Figure 5.2a), which had a relatively short lifetime: the Hennisdijk fluvial system (HEN). This is a well-documented and fully-developed channel belt, which went through all life-cycle stages.

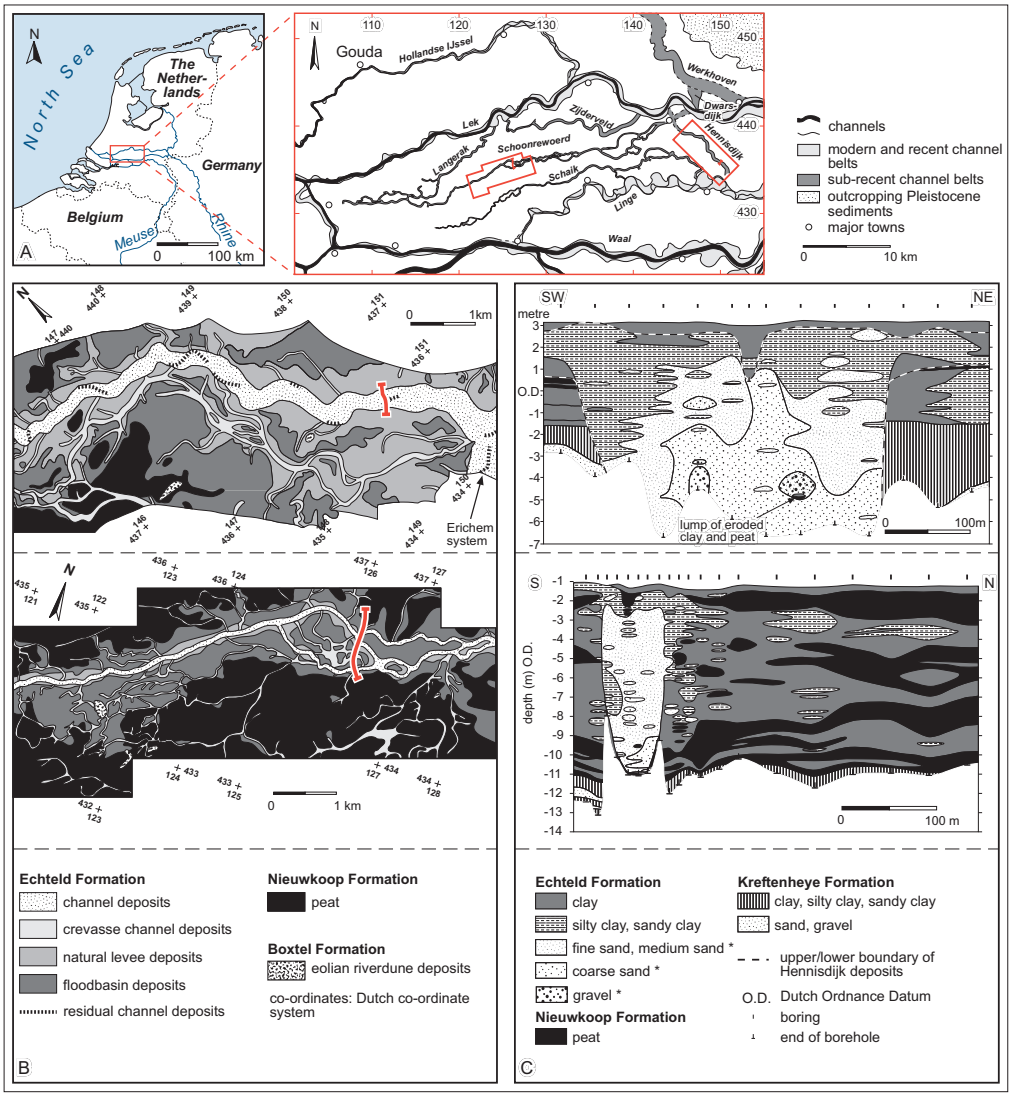

Figure 5.2. Location of the Hennisdijk (HEN) and Schoonrewoerd (SOO) channel belt in the delta (A). In (B), the geological maps of the HEN system (upper) and the SOO system (lower) are presented. The red lines crossing the channel belts indicate the location of the cross-section in (C), where HEN also represents the upper, and SOO the lower cross-section. After Makaske and Weerts (2005) and Makaske et al. (2007).

** Median grain sizes: fine sand = 50-210 µm, medium sand = 210-420 µm, coarse sand = 420-2000 µm, gravel = 2-64 mm.*

5.3.3 The Hennisdijk fluvial system

The Hennisdijk fluvial system was active between 3818 and 2975 ^{14}C years BP (Makaske, 1998; Berendsen and Stouthamer, 2001). A segment of about 10 km length has been preserved in the subsurface, and was reconstructed in detail by Makaske and Weerts (2005). Figures 5.2b and 5.2c show the geological map of the system and a lithological cross-section. The Hennisdijk system comprises a ~360-m-wide belt of channel deposits, in which residual channel deposits occur. These remnants indicate a former meandering channel with a sinuosity index of ~1.35, and a meander wave length of ~700 m. The channel deposits are subsequently bound by natural levees, floodbasin deposits and peat, intercalated by multiple crevasse channel and crevasse splay deposits. The channel deposits are formed by a ~10-m-deep sand body of coarse sand (median grain size 420-2000 μm), fining upward into medium and fine sand (median grain size 50-420 μm). On top of, and laterally to the sand body, a silty and sandy clay package represents the natural levees. These deposits wedge out laterally and grade into floodbasin clay. Humic clay on top of the sand body was interpreted as a residual channel fill. The Hennisdijk system incised into clay, silty and sandy clay, and peat from older systems, and is covered by a ~ 0-0.5-m thick layer of floodbasin clay deposits from a more recent channel belt. Using geological and lithological reconstruction, grain size analysis of soil samples, and sedimentary structures Makaske and Weerts (2005) reconstructed a channel width of about 100 m, a channel depth of about 8.85 m, a slope of about $1.43 \cdot 10^{-4}$, and a bankfull paleo-discharge of about 1000 m^3/s (which is about 40% of the present-day mean annual discharge of the Rhine), and a potential specific stream power of about 7.6 W/m^2 (Kleinhans and Van den Berg, 2011).

5.4 Methods and data

5.4.1 Sediment budget reconstruction based on maps and cross-sections

For the Hennisdijk channel belt we estimated the volumes of eroded and deposited sediment in all stages: the initial erosion after avulsion, the net erosion and deposition in stages 1 and 2, and the filling after channel abandonment. Estimates are based on the geometric data presented in Table 5.5, and the cross-section from Figure 5.2. In the cross-sections, we distinguish four sedimentary architectural units: the channel deposits (CH), the natural levee and other overbank deposits (NL), the intersected floodbasin deposits (FB), and the residual channel deposits (RC). These are further subdivided into eight lithostratigraphic units (u) (appendix A). The channel comprises two lithostratigraphic units: CH1, which contains sand deposited on lower and middle point bars, and CH2, which contains the more muddy deposits near the edges, deposited on upper point bars (Makaske and Weerts, 2005). The floodbasin unit comprises two lithostratigraphic units from the Holocene floodbasin of (FB1) and peat (FB2), and two lithostratigraphic units from the clayey (FB3) and sandy (FB4) Pleistocene subsurface. We estimated volumes of each lithostratigraphic unit by estimating their planview area on the geological maps, and multiplied it with the thickness derived from the cross-

sections. Below, we describe how we determined for each life-cycle stage *i* of the channel belts the resulting amounts of eroded or deposited sediment from these lithostratigraphic units.

Avulsion stage

A channel that is formed by avulsion vertically erodes the floodbasin and removes peat and clay deposits from older systems, and – if present - remnants of older channel belts (Figure 5.3a). Depending on the initial incision depth, underlying Pleistocene deposits may be eroded as well. To reconstruct the composition of the eroded material, we determined the thickness of the different layers of the floodbasins adjacent to the channel belt in the cross-sections. Hence, we estimated the proportion of each unit $E_{Av,u}$ present in the initial erosion volume by averaging the thickness of the layers on both sides. The amount of eroded material (E_{Av}) during the avulsion stage was then calculated as:

$$E_{Av} = E_{Av,FB} \quad \text{(Eq. 5.1)}$$

where: $$E_{Av} = -A_{C,Av} \cdot L_{C,Av} \quad \text{(Eq. 5.2)}$$

$$E_{Av,FB} = E_{Av,FB1} + E_{Av,FB2} + E_{Av,FB3} + E_{Av,FB4} \quad \text{(Eq. 5.3)}$$

$E_{i,u}$ = eroded material at stage *i* unit per lithostratigraphic unit *u* [m^3]
$A_{C,i}$ = channel cross-sectional flow area at stage *i* [m^2]
$L_{C,i}$ = channel length at stage *i* [m]

Stage 1 – channel belt building

Erosion during stage 1 (E_{S1}) comprises floodbasin sediment ($E_{S1,FB1\&2}$) and previously deposited natural levees ($E_{S1,NL}$) removed by bank erosion. Furthermore, due to due to channel incision, also underlying (Pleistocene) deposits may be eroded to greater depth ($E_{S1,FB3\&4}$). The deposited sediment (D_{S1}) includes channel deposits ($D_{S1,CB}$) and natural levee deposits ($D_{S1,NL}$). In our calculation $D_{S1,NL}$ represents only net deposition on the natural levee; we neglect sediments that were deposited but eroded again during S1.

E_{S1} was estimated by subtracting the initial channel volume (E_{Av}) and $E_{S2,FB}$ from the channel belt dimensions. $E_{S2,FB}$ represents a part of the floodbasin and the underlying Pleistocene deposits, that have not been eroded during S1 (Figure 5.3). This component exists because the channel deepens during S1, so in the early stage of S1 riverbank erosion did not reach full depth. Channel deposition ($D_{s2,CH}$) largely compensates erosion, and is hence also calculated by subtracting the channel volume and $E_{S2,FB}$ from the total channel belt volume. However, channel length, and hence channel volume, have increased during S1, so channel deposition is smaller than bank erosion. Moreover, overbank and natural levee sediments have been deposited during S1 ($D_{s1,NL}$). Erosion (E_{S1}) and deposition (D_{S1}) volumes were calculated as:

$$E_{s1} = E_{s1,FB} \quad \text{(Eq. 5.4)}$$

where: $$E_{s1} = -\left(A_{CB,Av} \cdot L_{CB} - E_{Av} - E_{s2,FB}\right) \quad \text{(Eq. 5.5)}$$

$$A_{CB} = W_{CB} \cdot \left(H_{CB} - H_{L,Ab}\right) \quad \text{(Eq. 5.6)}$$

$$E_{s1,FB} = E_{s1,FB1} + E_{s1,FB2} + E_{s1,FB3} + E_{s1,FB4} \quad \text{(Eq. 5.7)}$$

$A_{CB,i}$ = channel-belt cross-sectional area at stage i [m^2]
W_{CB} = channel-belt width (exclusive natural levees) [m]
H_{CB} = channel-belt thickness (exclusive natural levees) [m]
$H_{L,i}$ = levee height at stage i [m]
L_{CB} = channel-belt length [m]

$$D_{s1} = D_{s1,CH} + D_{s1,NL} \quad \text{(Eq. 5.8)}$$

where: $$D_{s1,CH} = D_{s1,CH1} + D_{s1,CH2} = A_{CB,Av} \cdot L_{CB} - A_{C,Ab} \cdot L_{C,Ab} - E_{s2,FB} \quad \text{(Eq. 5.9)}$$

$$D_{s1,NL} = 0.5 \cdot D_{NL} \quad \text{(Eq. 5.10)}$$

$D_{i,u}$ = amount of deposited material at stage i per lithostratigraphic unit u [m^3]
D_{NL} = entire volume of sediment present in the natural levee [m^3]

Stage 2 – channel belt reworking

In stage 2, when the meanders shift in the downstream direction, reworking of channel bed sand of the channel's own belt takes place ($E_{S2,CH}$, compensated by $D_{S2,CH}$). The amount of reworking cannot be calculated from the maps and cross-sections, since these do not indicate over which distance the meanders migrated in downstream direction during S2. Therefore, we determined this volume for a downstream shift over one meander length (Equation 5.13). Finally, some floodbasin and underlying Pleistocene deposits are eroded in S2 ($E_{S2,FB}$), at places where maximum depth is not yet reached (Figure 5.3). Erosion and deposition volumes are calculated as:

$$E_{s2} = E_{s2,FB} + E_{s2,CH} \quad \text{(Eq. 5.11)}$$

where: $$E_{s2,FB} = E_{s2,FB1} + E_{s2,FB2} + E_{s2,FB3} + E_{s2,FB4} = -0.5 \cdot W_{CB} \cdot \left(H_{B,ab} - H_{B,av}\right) \cdot L_{CB} \quad \text{(Eq. 5.12)}$$

$$E_{s2,CH} = E_{s2,CH1} + E_{s2,CH2} = E_{S1} \quad \text{(Eq. 5.13)}$$

$H_{B,i}$ = bank height in stage i [m]

$$D_{s2} = D_{s2,CH} + D_{s2,NL} \quad \text{(Eq. 5.14)}$$

where: $D_{s2,NL} = D_{s2,NL(FB)} = 0.5 \cdot D_{NL(FB)}$ (Eq. 5.15)

$D_{s2,CH} = D_{s2,CH1} + D_{s2,CH2} = -E_{s2,CH}$ (Eq. 5.16)

Overbank deposition

All overbank deposits are captured in one unit (D_{NL}). These deposits involve the silty natural levee deposits, and the finer grained floodplain deposits further away from the channel. The boundary between them is gradual. For our concept, the overbank deposits were subdivided into proximal and distal overbank deposits. Proximal overbank deposits comprise natural levee deposits on top of channel deposits (*NL(CH)*). Distal overbank deposits comprise the natural levee and floodplain deposits on top of older floodbasin deposits (*NL(FB)*), and is present on both sides of the channel belt. The total volume of overbank deposition is:

$$D_{NL} = D_{NL(FB)} + D_{NL(CH)} \quad \text{(Eq. 5.17)}$$

where: $D_{NL(FB)} = 2 \cdot A_{NL(FB)} \cdot L_{CB}$ (Eq. 5.18)

$D_{NL(CH)} = A_{NL(CH)} \cdot L_{CB}$ (Eq. 5.19)

$A_{NL(u)}$ = cross-sectional area of the overbank unit [m^2]

To calculate $A_{NL(FB)}$ we assumed an exponential decrease of overbank aggradation rates away from the channel, and adopted the representation given by Mackey and Bridge (1995) and Törnqvist and Bridge (2002):

$$H_{L,z} = H_{L,0} \cdot e^{\frac{-b \cdot z}{z_m}} \quad \text{(Eq. 5.20)}$$

where: $H_{L,z}$ = levee height at distance z from the channel [m]
$H_{L,0}$ = levee height near the channel [m]
z = cross-sectional distance from the channel [km]
z_m = notional maximum cross-sectional distance from channel [km]
b = rate of decrease [-]

Levee height near the channel was measured from the cross-sections. Z_m and b are site specific variables. In the absence of adequate data for our channels to estimate the value of b, we used the data of Törnqvist and Bridge (2002), who tested this model to overbank deposits from the Rhine-Meuse delta. They used a distance of 5 km for Z_m, and found an average value for b equal to 4. To calculate the cross-sectional area of the levee on top the former floodbasin deposits ($A_{L(FB)}$; Figure 5.3), we integrated Equation 5.20 over the distance z=0 to z=z_m:

$$A_{NL(FB)} = \int_0^{z_m} (H_{L,0} \cdot e^{\frac{-b \cdot z}{z_m}}) dz = H_{L,0} \cdot \left[-\frac{z_m}{b} \cdot e^{\frac{-b \cdot z}{z_m}} \right]_0^{z_m}$$

$$= H_{L,0} \cdot \frac{z_m}{b} \cdot (1 - e^{-b}) \qquad \text{(Eq. 5.21)}$$

The cross-sectional area of the natural levee deposits on top of the channel belt ($A_{NL(CH)}$) was calculated as:

$$A_{NL(CH)} = (W_{CB} - W_C) \cdot H_L \qquad \text{(Eq. 5.22)}$$

The overbank sediments are deposited in both stages, but from the cross-sections we cannot distinguish the proportion of the total amount of deposition belonging to each stage. Hence, we simply assumed that half of the total overbank material was deposited in S1, and the other half in S2 (Figure 5.3).

Abandonment stage

The abandoned channel cross-sectional area is larger than at the end of the avulsion stage, because during stages 1 and 2 natural levees developed. Also, the channel became longer when sinuosity increased. Both effects cause that the final volume of channel fill deposition during the abandonment stage is larger than the amount of sediment eroded during the avulsion stage. The deposited sediment mainly exists of sand and silt, but peat may have developed in the upper parts of the residual channel fill. The amount of each lithogenetic unit of the channel fills was estimated from the cross-sections and corings. Total channel fill deposition (D_{Ab}) was calculated as:

$$D_{Ab} = D_{Ab,RC} + D_{Ab,NL(CH)} \qquad \text{(Eq. 5.23)}$$

where: $D_{Ab,RC} = A_{C,Ab} \cdot L_{C,Ab}$ (Eq. 5.24)

$$D_{Ab,NL(CH)} = 0.5 \cdot D_{NL(CH)} \qquad \text{(Eq. 5.25)}$$

This equation gives an upper estimate, because the residual channel may not be entirely filled after abandonment.

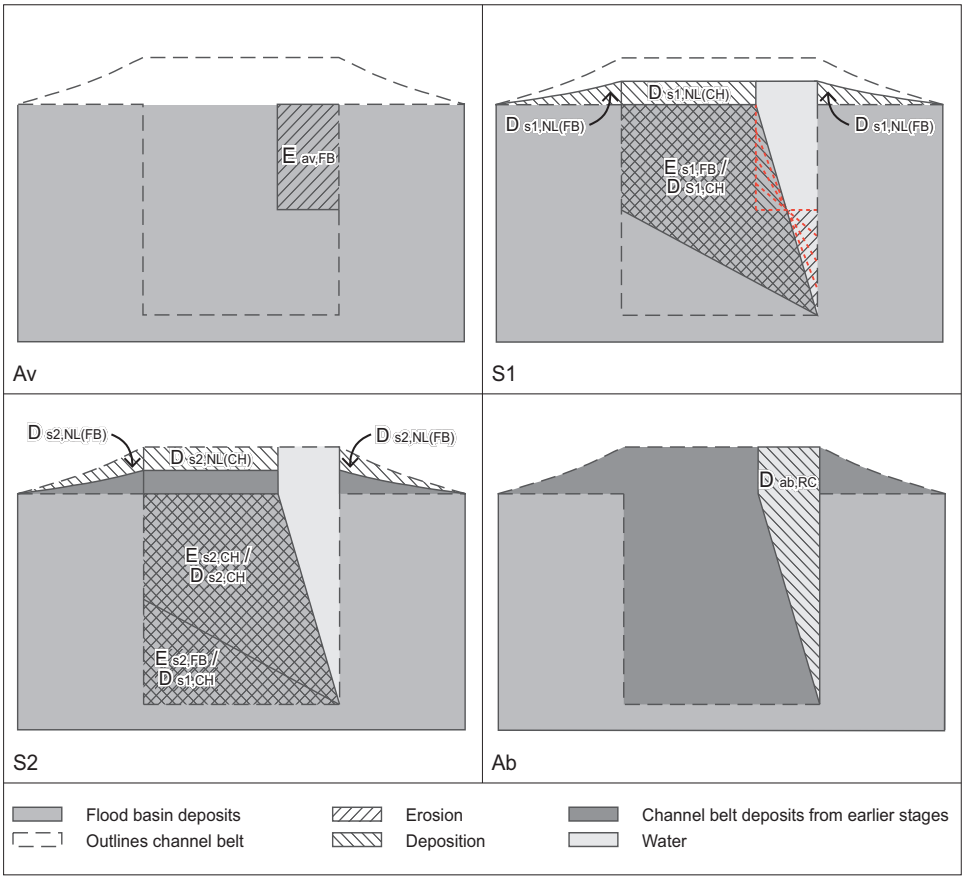

Figure 5.3. The cross-sectional area of deposited and eroded sediment volumes in each stage [m²]. Volumes are obtained when these areas are multiplied with channel (belt) length. The red/dotted lines show the growing transverse bedslope in the channel during S1.

5.4.2 Bank Stability and Toe Erosion Model

For the calculation of time-dependent sediment budgets we needed estimates for bank retreat rate controlling the migration rate of meanders. For this purpose we used the 'Bank Stability and Toe Erosion Model' (BSTEM), a physics-based model (version 5.2), developed at the USDA-ARS National Sedimentation Laboratory (Simon et al., 2000). The model includes two separate models, each representing a distinct process causing bank retreat: the Toe Erosion (TE-) model that calculates erosion of a river bank due to scour of the flow, and the Bank Stability (BS-) model that calculates erosion of a river bank due to mass failure. Both models can be used separately, but also sequentially in an iterative procedure.

Model concept

The TE-model calculates the erosion of the bank, the bank toe and the bed caused by the bed shear stress of the scouring flow. Flow conditions are assumed to be steady and uniform, without sediment import from upstream that could potentially reduce the scour. Furthermore, bed sediment import and export of the considered reach are assumed to be in equilibrium, resulting in constant channel depth. Hence, erosion and transport of material occur at a rate solely controlled by excess shear stress of the flow. As input, the TE-model requires a 2D bank profile with a maximum of five stratigraphic layers of different bank material (Figure 5.4). Bank materials are characterised by their friction angle, cohesion and saturated weight, and are included in the model as averaged literature values (Table 5.1), but can also be replaced by site specific values. Information on vegetation cover, tension cracks and groundwater level can be added to the profile. From a given bank stratigraphy, the TE-model predicts a critical shear stress for all stratigraphic layers and for the bank toe. Using channel and flow parameters (reach length, reach slope, and flow depth and duration), the model calculates boundary shear stresses along the entire submerged bank profile. If a boundary shear stress exceeds the critical shear stress, then erosion takes place, and the model predicts bank retreat, the amount of eroded material from the bank, and returns a new bank profile as output.

Following bank undercutting, the BS-model calculates whether or not an undercut bank fails. This can occur due to different failure mechanisms (see Thorne et al., 1981; Simon et al., 2000), depending on bank material and the degree of undercutting. The model predicts failure of wedge-shaped or cantilevered-shaped blocks, with planar failure surface, eventually initiated by a tension crack. As input, the BS-model requires a 2D bank profile, with parameter data similarly as in the TE-model (Figure 5.4). Whether or not the bank fails is calculated by its factor of safety (*Fs*). *Fs* represents a balance between driving forces and resisting forces along the failure plane. The main driving force is gravity. Resisting forces come from cohesion, normal stress, pore-water pressure and friction angle (Simon et al., 2000). If *Fs* > 1.3 the slope is

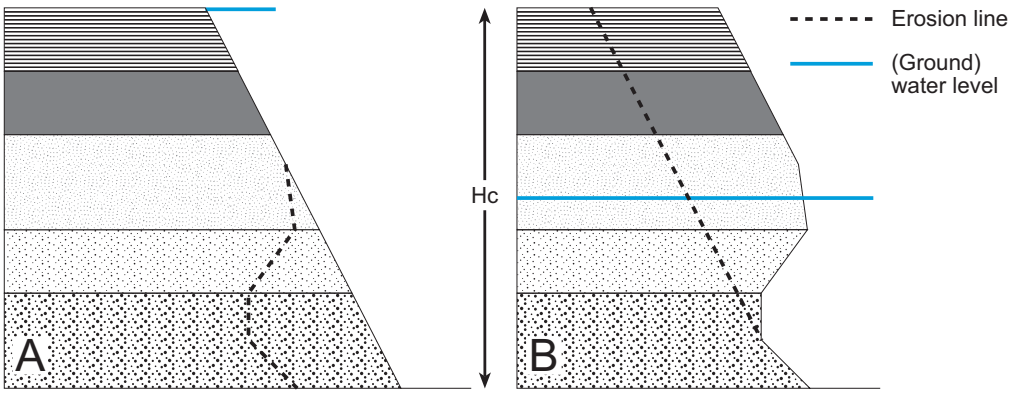

Figure 5.4. Schematical view of the toe erosion model (TE-model; A) and the bank stability model (BS-model; B). For legend see Figure 5.1.

*Table 5.1. Translation of reconstruction data into model data, and the averaged literature values that are part of the model. Moreover, all materials have a saturated unit weight of 18 kN/m³, and an effective angle of internal friction of 15 deg. Critical shear stresses indicated with * are calibrated with own data (see section 5.4.2).*

Cross-section lithology	Model's bank material	Friction angle [deg]	Cohesion [kPa]	Critical shear stress [pa]
Holocene natural levee deposits (silty clay, sandy clay)	Moderate silt	30	3	5.0
Holocene overbank deposits (clay)	Soft clay	25	10	1.8*
Holocene floodbasin peat (peat)	Stiff clay	20	15	2.5*
Holocene channel deposits (silty clay, sandy clay)	Moderate silt	30	3	5.0
Holocene channel deposits (fine sand, medium sand)	Fine angular sand	36	0	0.13
Holocene channel deposits (coarse sand)	Coarse angular sand	36	0	0.51
Pleistocene overbank deposits (clay, silty clay, sandy clay)	Stiff clay	20	15	3.0*
Pleistocene channel deposits (sand, gravel)	Coarse angular sand	36	0	0.51

stable, if $Fs < 1$ the slope is unstable, and for $1 < Fs < 1.3$ the bank slope is conditionally stable. The BS-model calculates *Fs* for soil blocks with failure planes for a range of slopes and corresponding elevations; failure occurs along the plane of smallest *Fs*. From the bank profile and failure slope the amount of failed bank material is calculated and a new bank profile results. A more detailed description of the model and the associated equations is given by a.o. Simon et al. (2009) and Midgley et al. (2012).

Model application

We used BSTEM to determine the meander migration rate in the former active Hennisdijk channel. First, we applied the TE-model to calculate flow erosion along an initial bank profile. Then, the eroded bank profile was used as input for the BS-model, which calculated a new failed bank profile. This failed bank profile was then the input for a new iteration of modelling, in which we assume that all failed material from first iteration has been removed from the bank toe. To calculate a bank retreat rate that is independent of an initial chosen bank profile, we iterated the model 5-12 times, until a constant bank profile shape was reached. The results of the last few cycles in the iteration were averaged, resulting in a value for lateral scour erosion (*Es*) [m], lateral failure erosion (*Ef*) [m], and total lateral erosion ($Et = Es + Ef$).

We applied the model for a single profile along a river bend, at its apex. Along with meander development, this point shifts in lateral direction. The rate at which the profile location – and thus the meander – shifts depends on the bank retreat rate, which is calculated by the model. We therefore calculated the bend migration rate for different *positions* of the

channel, using location-specific input values (bank profile, flow characteristics) as input. We represented the progress of the channel life-cycle stages by the channel *position*. Migration steps during the different stages were indicated as fraction of the distance bridged by the channel during each stage. We calculated bank retreat rates with the BSTEM model at 5 positions during *S1*, referred to as *S1_0*, *S1_25*, *S1_50*, *S1_75* and *S1_100%*. Thus, S1_*0* represents the position of the bank profile at moment the avulsion is completed and the channel at our site starts meandering, *S1_100* represents the position of the bank profile when the channel reaches deposits from the next downstream bend. Due to changing velocity of meander migration, the time interval between equidistant positions is not constant. This space-time relation was determined by interpolation of the bank retreat rates calculated with the BSTEM model.

A priori sensitivity analyses demonstrated that lateral bank erosion during S1 considerably increases if the channel bottom is incised into the underlying Pleistocene sandy deposits (Figure 5.6). Hence, we distinguished a stage S1A that represents the situation in which the channel bank entirely consists of older floodbasin deposits, and S1B in which the lower part of the channel bank consists of sand. In stage 2 the channel bank material consists of previously deposited channel material, and hence bank retreat rate will be higher and more constant than during *S1*. Still, we distinguish between *S12A* and *S12B*, with the boundary after one cycle of complete reworking within *S2*. During *S2A*, the first cycle of reworking, the channel erodes a layer of overbank deposits that were deposited during the longer stage S1. After the first downstream shift over one meander length in S2A – with higher migration rates – overbank deposition thickness on the proximal channel belt will be smaller due to the higher migration rate in stage S2. Therefore, stage S2B represents the subsequent period of channel migration in which less time is available for accumulation of new natural levee deposits on the proximal channel belt, and constant rates of levee deposition and erosion arise.

For each meander position during the life-cycle stages we determined the values for the input variables and parameters of the BSTEM model. Channel geometric data for the start and endpoints of the stages were obtained from the HEN dataset. Bank layer thickness and material were measured from the cross-section. Reach slope and channel depth change during the lifetime of the channel, in particular during S1. Changes in their values during a stage were assumed to be linearly related to the position of the meander (Figure 5.8). Initial bank angle was considered to be irrelevant, because we only include the results when, after a few model cycles, a balanced bank profile has developed. The model runs during S1 were carried out using the composition of the floodbasin material as input, while those for S2 were done using the composition of the channel bed material.

Sensitivity analysis

To explore to which variables the migration rates calculated by the BSTEM model are most sensitive we carried out a sensitivity analysis. First, we modelled a 0-scenario using a simplified profile, with characteristics similar to the true Hennisdijk (HEN) profile. We applied default values included in the BSTEM model for characteristics of the bank materials that correspond to those present in our cross-section lithostratigraphy (Table 5.1). For the duration of flow we used the present number of days per year that the Rhine discharge exceeds bankful, which is about 30 days (Kleinhans et al., 2010). In the TE-model, flow depth is assumed to be

equal to the channel depth and in the BS-model, we assumed a water level at half of the channel depth. Ground water table depth is assumed to be similar to of the channel flow level.

Then we ran the model for a series of scenarios (j) in which each time one of the variables was changed. In these scenarios the variables were varied by a factor 2 to 3 when compared to the 0-scenario (table 5.2). For scenarios HEN-1 and HEN-2, our 0-scenario is a 2-layered bank, consisting of 2 meter coarse angular sand, covered by 4 meter stiff clay, of which the resistance is given as a critical shear stress [Pa]. Here, bank layer thickness was varied through changing the sand layer thickness, and bank layer material was varied by changing the clay resistance. In scenarios HEN-3 to HEN-9, we made a 3-layered 0-scenario, in which a silt layer was added on top of the clay layer, for as that better represents the real HEN profile.

Results of sensitivity scenarios (HEN-1 to HEN-9; Figures 5.5 and 5.6) show how *Es*, *Ef* and *Et* change over a range of input variables. The graphs in Figure 5.6a, b and c show for each scenario the calculated migration rates ($Es_{,j}$, $Ef_{,j}$, $Et_{,j}$), divided by the migration rates from the 0-scenario ($Es_{,0}$, $Ef_{,0}$, $Et_{,0}$) to make them dimensionless. The graphs in Figure 5.6d, e and e show the factor over which the resulting migration rates change ($E_{,j}/E_{,0}$), plotted against the factor over which a variable changes ($V_{,j}/V_{,0}$). So the steeper the line, the more sensitive the model result is for the parameter.

The TE-model is the most sensitive to varying the flow elevation (Figure 5.6). The maximum value is bankfull flow as in the 0-scenario. A smaller flow elevation reduces shear stress, and hence causes *Es* to be small. Subsequently, *Es* determines the width of the scour hole, and hence *Ef*. So, all components of erosion are influenced by this flow elevation. For the same reason, channel depth is a sensitive variable: when channel depth decreases, flow elevation will do, because this elevation cannot be larger than bankfull.

Migration rates are also substantially influenced by flow duration and channel gradient. Flow duration determines the time available for erosion, and thus *Es* increases with flow duration. Increased scour erosion creates a wider scour hole, and hence a larger *Ef*. Reach slope has a similar effect: the steeper the slope, the more energy is available for erosion, enhancing undercutting and failure.

Table 5.2. Scenarios sensitivity analysis.

No#	Variable	0-scenario	Sensitivity analysis range
HEN-1	Sand layer thickness [m]	2	0-6
HEN-2	Clay resistance [Pa]	2	0.1-5
HEN-3	Bank height [m]	6	4-8
HEN-4	Initial bank angle [º]	60	30-90
HEN-5	Duration of flow [hrs]	700	100-1300
HEN-6	Elevation of flow in TE-model [m]	6	2-6
HEN-7	Elevation of flow in BS-model [m]	3	2-6
HEN-8	Water table depth [m-bank top]	3	0-4
HEN-9	Reach slope [-]	$1.0*10^{-4}$	$1.0*10^{-5}$ - $5.0*10^{-4}$

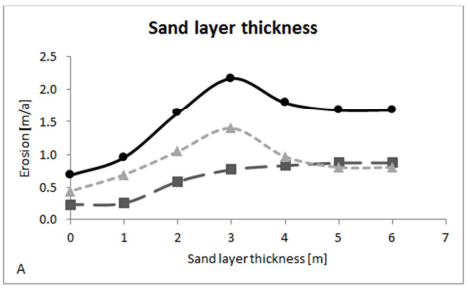
Sand layer thickness
Erosion [m/a]
Sand layer thickness [m]
A

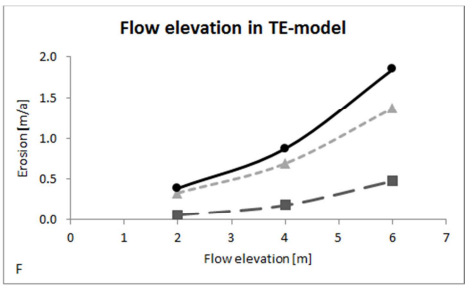
Flow elevation in TE-model
Erosion [m/a]
Flow elevation [m]
F

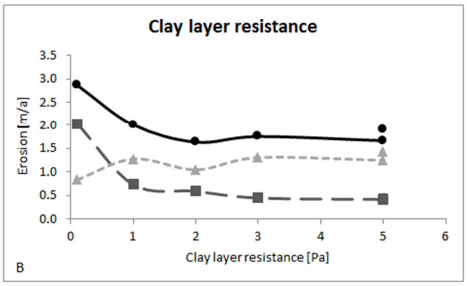
Clay layer resistance
Erosion [m/a]
Clay layer resistance [Pa]
B

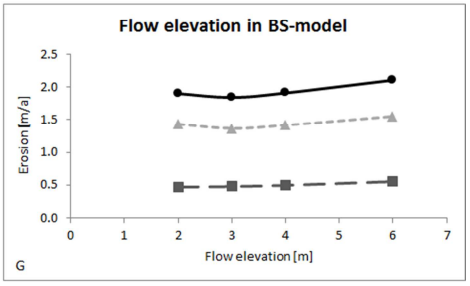
Flow elevation in BS-model
Erosion [m/a]
Flow elevation [m]
G

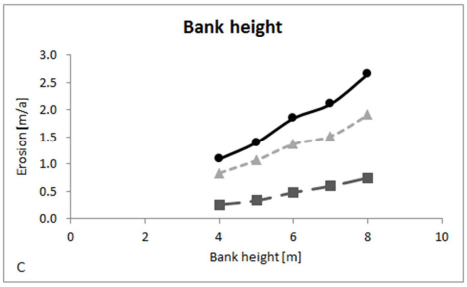
Bank height
Erosion [m/a]
Bank height [m]
C

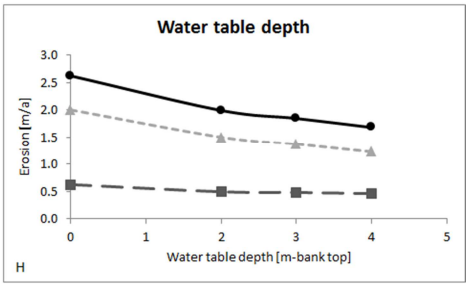
Water table depth
Erosion [m/a]
Water table depth [m-bank top]
H

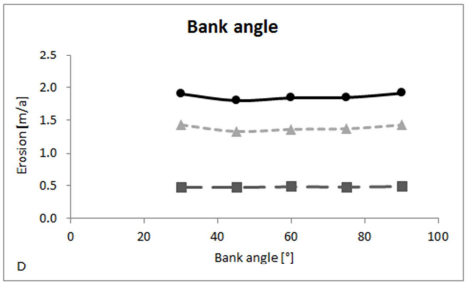
Bank angle
Erosion [m/a]
Bank angle [°]
D

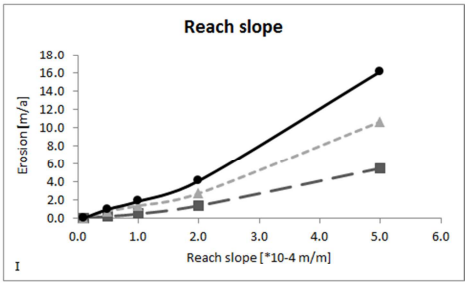
Reach slope
Erosion [m/a]
Reach slope [*10-4 m/m]
I

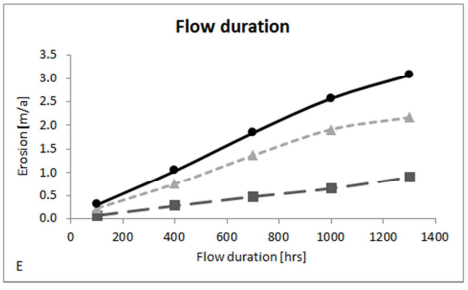
Flow duration
Erosion [m/a]
Flow duration [hrs]
E

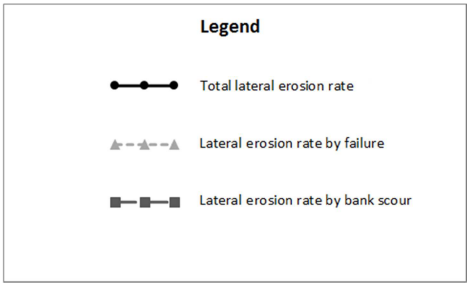
Legend
Total lateral erosion rate
Lateral erosion rate by failure
Lateral erosion rate by bank scour

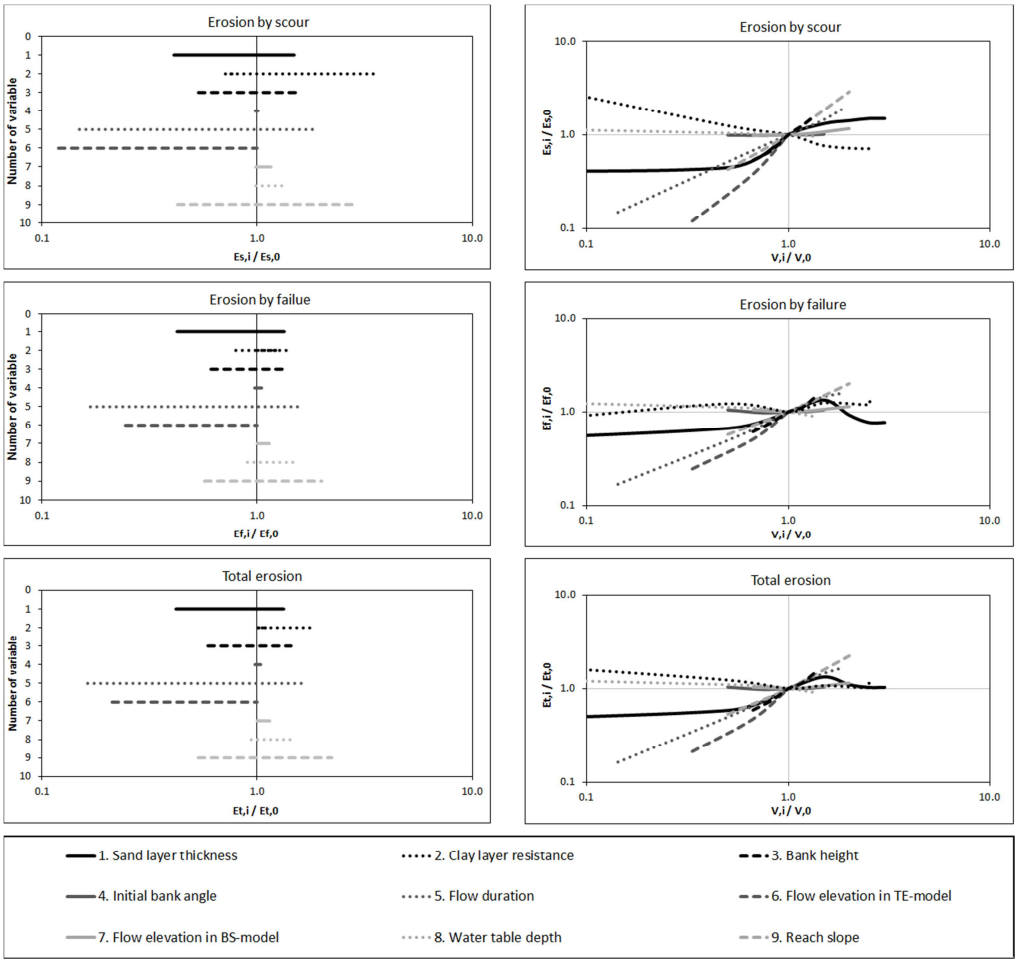

Figure 5.6. Results sensitivity analysis of the Bank Stability and Toe Erosion model (BSTEM). Plots A to C show for each variable the range over which migration rate differs from 0-scenario. As this is dependent on the range of input variables used, plots D to F show for each variable the dimensionless relation between lateral erosion rate and each variable.

Figure 5.5 (previous page). Results sensitivity analysis of the Bank Stability and Toe Erosion model (BSTEM). Each plot shows lateral erosion rate by scour (Es), the lateral erosion rate by failure (Ef) and total lateral erosion rate (Et) as function of a variable.

Maximum erosion occurs when the sand layer thickness is about half the channel depth. Due to its lower critical shear stress than clay, thicker sand layers cause higher scour erosion rates. However, at a certain thickness, *Es* becomes constant, and the maximum erosive capacity of the flow seems to be reached. Erosion by failure occurs when there is enough undercutting to create an unstable bank. A thin sand layer will result in insufficient erosion to cause failure. With increasing thickness of the sand layer more failure occurs. However, there is an optimum (Figure 5.5a): *Es* increases with increasing sand thickness, but scour holes tend to expand more vertically than horizontally. So, a thicker layer of sand leaves a thinner layer of clay to fail, and hence a smaller *Ef*. Clay resistance shows a similar effect (Figure 5.5b). For clay resistances higher than about 3 Pa, clay will not be eroded, and *Es* does not further decrease. Below 3 Pa, *Es* increases with clay erodibility, the scour hole grows vertically, and *Ef* decreases.

The model results were less sensitive for variations in water table depth, flow depth in the BS-model and initial bank angle. The water table depth affects *Ef* more than it does to *Es*. Low water tables generally result in more stable and steeper banks. Increasing flow depth in BS-model increases the factor of safety.

Parameter constraining

Using the default parameter settings, the BSTEM model predicted too small migration rates to create the Hennisdijk channel belt within its lifetime. We therefore performed some calibration of the model. For this, we used data of the Schoonrewoerd channel belt (SOO). This short-lived channel belt in the western delta had a paleochannel which was incised into erosion-resistant floodbasin deposits and which is interpreted to have been very stable laterally (Makaske et al., 2007). Based on the sensitivity analyses we chose to constrain the resistance values – expressed by critical shear stress τ_c – of the bank material by model calibration as follows: the channel belt dimensions and time of activity of the HEN channel belt provide us a *minimum* migration rate. On the other hand, lateral channel migration rates of the SOO paleochannel were so small that the system did not reach the end of S1A during its entire time of activity, which provided us a *maximum* migration rate for SOO.

Calculations of migration rates and associated τ_c were made as follows: HEN was active during about 1016 cal years, in which it fully developed stage 1. Hence, the maximum duration of S1 is 1016 years, in which the channel shifted laterally over a distance of ($W_{CB} - W_C$), and downstream over a distance equal to L_M. According to the model, the channel bottom reaches the Pleistocene sand at about one third of the distance of S1 (S1_32); here is the transition from stage S1A to S1B. We made this subdivision, because based on the sensitivity analysis we expected erosion and resulting migration rates in S1B to be much larger than in S1A. Hence, we supposed the maximum duration of S1A to be 1016 years. The channel shifted laterally during S1A a distance of 0.32 * ($W_{CB} - W_C$) = 74 meter, indicating a minimal migration rate in perpendicular direction (*Et,l*) of 0.07 m/a. The downstream migration distance in S1A is: 0.32 * L_M = 224 meter, indicating a minimal migration rate in downstream direction (*Et,d*) of 0.22 m/a. When we assume that both are components of the vector *Et*, then the angle between *Et* and *Et,d* (α) is 18° and the angle between *Et* and *Et,l* (β) is 72°, and *Et* = ~0.23 m/a. This is the minimum average migration rate during S1 that is necessary to reach S1_32 within 1016 years. We accordingly adapted τ_c for the bank material during S1A to achieve this minimum rate.

SOO shifted laterally over only a few tens of meter, with W_{CB} = ~W_C, during its 300 cal years lifetime. Downstream migration could not be determined, so therefore we assumed it to be the same as the cross-valley distance. This yields a maximum $Et,l = Et,d$ = 0.02-0.31 m/a, with α=β=45°, and Et = 0.02-0.22 m/a. We calibrated the model on this migration rate for the position halfway S1, (S1_50) to find a minimal critical shear stress for clay so that maximal migration rate is not exceeded.

We accordingly adapted τ_c for the bank materials to achieve migration rates within the constraints of the two channel belts during S1A, while preserving relative differences between different materials. This yielded critical shear stresses τ_c = ~1.5 Pa for Holocene floodbasin clay, τ_c = 2.5 Pa for Holocene floodbasin peat, and τ_c = 3.0 Pa Pleistocene clay. Stouthamer et al. (2011) found critical shear stresses along another channel belt (Lek) in the Rhine-Meuse delta of τ_c = 1.8 Pa for moderately soft consolidated clay. The variables that are used for our modelled scenarios are given in Tables 5.3 and 5.4.

Table 5.3. Model setups for stage 1. Layer 1 represents the levee, which increases in height during S1. The lower layers also increase in height.

	S1_0%	S1_25%	S1_50%	S1_75%	S1_100%
Initial bank geometry					
Bank height [m]	3.93	5.01	6.09	7.17	8.25
Bank angle [°]	60	60	60	60	60
Thickness layer 1 [m]	-	0.15	0.30	0.45	0.60
Thickness layer 2 [m]	2.59	2.59	2.59	2.59	2.59
Thickness layer 3 [m]	0.40	0.40	0.40	0.40	0.40
Thickness layer 4 [m]	0.94	1.87	2.14	2.14	2.14
Thickness layer 5 [m]	-	-	0.66	1.59	2.52
Bank material and resistance					
Material layer 1	<----------moderate silt---------->				
Material layer 2	<----------soft clay, 1.8 Pa---------->				
Material layer 3	<----------stiff clay, 2.5 Pa---------->				
Material layer 4	<----------stiff clay, 3.0 Pa---------->				
Material layer 5	<----------coarse angular sand---------->				
Flow conditions TE-model					
Reach slope * 10^{-4} [m/m]	1.43	1.34	1.25	1.15	1.06
Elevation of flow [m]	3.93	5.01	6.09	7.17	8.25
Duration of flow [hrs]	720	720	720	720	720
Flow conditions BS-model					
Elevation of flow [m]	1.97	2.51	3.05	3.59	4.13
Water table [m–bank top]	1.97	2.51	3.05	3.59	4.13

Table 5.4. Model setups for stage 2.

	S2_A	S2_B
Initial bank geometry		
Bank height [m]	8.25	7.90
Bank angle [°]	60	60
Thickness layer 1 [m]	0.60	0.25
Thickness layer 2 [m]	2.30	2.30
Thickness layer 3 [m]	3.50	3.50
Thickness layer 4 [m]	1.85	1.85
Bank material and resistance		
Material layer 1	<----------moderate silt---------->	
Material layer 2	<----------moderate silt---------->	
Material layer 3	<----------fine angular sand---------->	
Material layer 4	<----------coarse angular sand---------->	
Flow conditions TE-model		
Reach slope * 10^{-4} [m/m]	1.06	1.06
Elevation of flow [m]	8.25	7.90
Duration of flow [hrs]	720	720
Flow conditions BS-model		
Elevation of flow [m]	4.13	3.95
Water table [m–bank top]	4.13	3.95

5.4.3 Determination of input variables

Table 5.5 provides an overview of the data from the Hennisdijk channel belt we used for the sediment budget model. Additionally, we used empirical hydraulic and geometric relationships for meandering channels obtained from the literature (Williams 1986), which were consistent with the HEN data.

Channel-belt width (W_{CB}), thickness (H_{CB}) and slope (S_{CB}) were determined using data given in Makaske and Weerts (2005). We calculated the cross-sectional area by assuming a rectangular channel belt, and measured the length along the channel-belt axis from the geomorphogenetic maps scale 1:10,000 of the area (Berendsen and Stouthamer, 2001).

Channel width (W_C), depth (H_C), slope (S_C) and sinuosity index (P_{ind}) were also determined from Makaske and Weerts (2005). They reconstructed two channel depths (7.6 and 10.1 m.), reflecting the uncertainty of the base of the channel deposits. We adopted the average depth for our model. We calculated the cross-sectional flow area (A_C), assuming $A_C = 7/12 * W_C * H_C$ (Figure 5.7), and channel length by multiplying the length of the channel-belt axis by the sinuosity. Moreover, we measured the meander wave length (L_M), amplitude (A_M) and the bend radius (R_M) from the planview maps, and the levee height (H_L) on the cross-sections provided by Makaske and Weerts (2005). Finally, we calculated bank height (H_B), assuming that channel depth is the sum of bank height and levee height: $H_C = H_B + H_L$ (Figure 5.7). Due to the presence of a transverse bedslope, H_B, and hence H_C, are spatially varying along the meanders. We use indices $_{min}$, $_{max}$ and $_{avg}$ to denote the location within the bend. When no index is used, H_B, and H_C represent the maximum depth at the eroding outer bend.

Table 5.5. Data used for the Hennisdijk channel belt, derived from Makaske and Weerts (2005) and Berendsen and Stouthamer (2001). The levee height represents the height of the levee above floodbasin deposits.

	Symbol	Value	Unit	Source
Channel belt characteristics (CB)				
Age	T	843	^{14}C a	Makaske and Weerts (2005)
Grain size	d_{50}	414-432	µm	Makaske and Weerts (2005)
Paleodischarge	Qp	283-1001	m^3/s	Makaske and Weerts (2005)
Width	W_{CB}	330	m	Makaske and Weerts (2005)
Thickness	H_{CB}	8.85	m	Makaske and Weerts (2005)
Cross-sectional area	$A_{CB,Av}$	2525	m^2	Calculated: $A_{CB,Av} = W_{CB} * (H_{CB} - H_{L,Ab})$
Cross-sectional area	$A_{CB,Ab}$	2921	m^2	Calculated: $A_{CB,Ab} = W_{CB} * H_{CB}$
Slope	S_{CB}	$1.43*10^{-4}$	-	Makaske and Weerts (2005)
Length	L_{CB}	11	km	Measured from paleogeographic map (Berendsen and Stouthamer, 2001)
Channel dimension during avulsion (C,AV)				
Width	$W_{C,Av}$	99	m	Makaske and Weerts (2005)
Depth	$H_{C,Av}$	3.93	m	Calculated: $H_{B,i} = H_{C,i} - H_{L,i}$
- Levee height	$H_{L,Av}$	0	m	Assumption: no initial levee
- Bank height	$H_{B,Av}$	3.93	m	Assumption: see model section
Cross-sect. flow area	$A_{C,Av}$	227	m^2	Calculated: $A_{C,i} = 7/12 * W_{C,i} * H_{C,i}$ *(avg)* (see Fig. 5.7)
Channel slope	$S_{C,Av}$	$1.43*10^{-4}$	-	Makaske and Weerts (2005)
Channel length	$L_{C,Av}$	11	km	Calculated: $L_{C,i} = P_{ind,i} * L_{CB}$
Sinuosity index	$P_{ind,Av}$	1	-	Assumption: initial channel follows channel belt
Meander wave length	$L_{M,Av}$	700	m	Assumption: meander wave length remains constant
Meander amplitude	$A_{M,Av}$	0	m	Assumption: initial channel follows channel belt
Bend radius	R_{Av}	0	m	Assumption: initial channel follows channel belt
Transverse bedslope	dz/dy_{Av}	0	-	Assumption: no initial transverse bedslope
Channel dimensions during abandonment (C,AB)				
Width	$W_{C,Ab}$	99	M	Makaske and Weerts (2005)
Depth	$H_{C,Ab}$	8.85	M	Makaske and Weerts (2005)
- Levee height	$H_{L,Ab}$	1.2	M	Measured from cross-section (M. and W., 2005)
- Bank height	$H_{B,Ab}$	7.65	M	Calculated: $H_{B,i} = H_{C,i} - H_{L,i}$
Cross-sect. flow area	$A_{A,Ab}$	296	m^2	Calculated: $A_{C,i} = 7/12 * W_{C,i} * H_{C,i}$ *(avg)* (see Fig. 5.7)
Channel slope	$S_{C,Ab}$	$1.06*10^{-4}$	-	Makaske and Weerts (2005)
Channel length	$L_{C,Ab}$	14.85	km	Calculated: $L_{C,i} = P_{ind,i} * L_{CB}$
Sinuosity index	$P_{ind,Ab}$	1.35	-	Makaske and Weerts (2005)
Meander wave length	$L_{M,Ab}$	700	m	Measured from planview (Makaske and Weerts, 2005)
Meander amplitude	$A_{M,Ab}$	165	m	Calculated: $A_{M,AB} = 0.5 * W_{CB}$
Bend radius	R_{Ab}	300	m	Measured from planview (Makaske and Weerts, 2005)
Transverse bedslope	dz/dy_{Ab}	0.083	-	Calculated (see Struiksma et al., 1985)

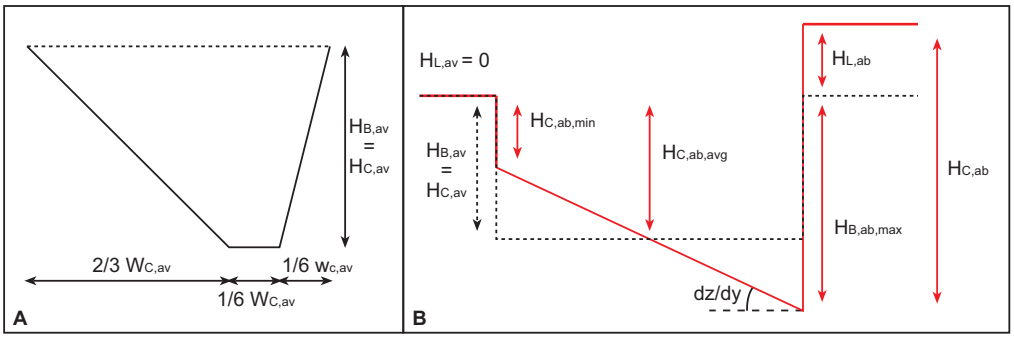

Figure 5.7. Panel A shows the cross-sectional flow area of a Rhine-Meuse channel, which we used to calculate sediment budgets. To calculate transverse bedslope development we used a simplified cross-section which is sketched in panel B. Here, the dotted lines represents the avulsion stage and red/thick lines the abandonment stage. Between these two stages, bank height ($H_{B,i}$) increases by transverse bed slope development (dz/dy), and levee height ($H_{L,i}$) increases by overbank sedimentation. The levee height represents the height of the levee above floodbasin deposits.

The channel dimensions described above are estimates based on the deposits that are present in the subsurface today, which represent the final moment of S2, or the initiation of stage Ab. Channel dimensions during the avulsion stage were estimated based on the following assumptions:

- The initial location of the channel after avulsion is the same as the channel-belt axis that has been preserved to date. Still, although the axis may be curved, sinuosity index during avulsion stage ($P_{ind,Av}$) equals 1, and meander amplitude ($A_{M,Av}$) and bend radius ($R_{M,Av}$) are both 0.
- The channel meanders that form can be represented as having a sinuous shape. Over time, meander wave length remains constant, amplitude increases, and the bends shift in downstream direction.
- Natural levees only start to develop after the avulsion stage ($H_{L,Av}$= 0, and hence $H_{B,Av}$= $H_{C,av}$; Figure 5.7).
- During the avulsion stage the transverse bed slope is zero, so average bank height equals maximum bank height ($H_{B,Av,avg}$ = $H_{B,Av,max}$). In the other stages a transverse bed slope develops in the meander bends, so that $H_{B,Ab,avg} < H_{B,Ab,max}$.
- The average bank height remains constant over time, thus $H_{B,Av,avg} = H_{B,Ab,avg}$.

The latter three assumptions relate to the prediction of the channel depth. The depth measured by Makaske and Weerts (2005) represents the deepest occurrence of channel bed sand from the system. For as channel aggradation cannot be quantified, this is assumed to be the maximum (pool) depth in the fully developed meander ($H_{C,Ab}$). Subsequently, the minimum (riffle) depth and average depth are calculated using the transverse bed slope predictor equation of Struiksma et al. (1985). The channel depth in the initial channel ($H_{C,Av}$) is hence assumed to be equal to the average channel depth in the fully developed meander.

Channel dimensions during stages 1 and 2 were estimated from the avulsion and the abandonment stages, using the following simplifications:

- Channel width and meander wave length remain constant during entire life time of the channel.
- As a result of growing meanders during *S1* sinuosity index, channel length, meander amplitude, bend radius and bank height increase, while reach slope decreases. These variables are all related to the position of the meander, and hence, we assumed them to change linearly over space. During *S2* these variables do not change anymore (Figure 5.8).
- Levee height is not related to time, but to meander position. Although shifting of meander position is not constant over time, for simplicity we assume levee height to be related to meander position.
- Height of the distal natural levee ($H_{L(FB)}$) develops differently from height of the proximal natural levee ($H_{L(CH)}$). Distal natural levees grow continuously during the entire active phase of the river. During S2 proximal natural levees are reworked, and $H_{L(CH)}$ equals the product of average natural levee deposition rate and the time needed for one cycle of reworking during *S2*.
- Channel depth is obtained by adding natural levee height to bank height.

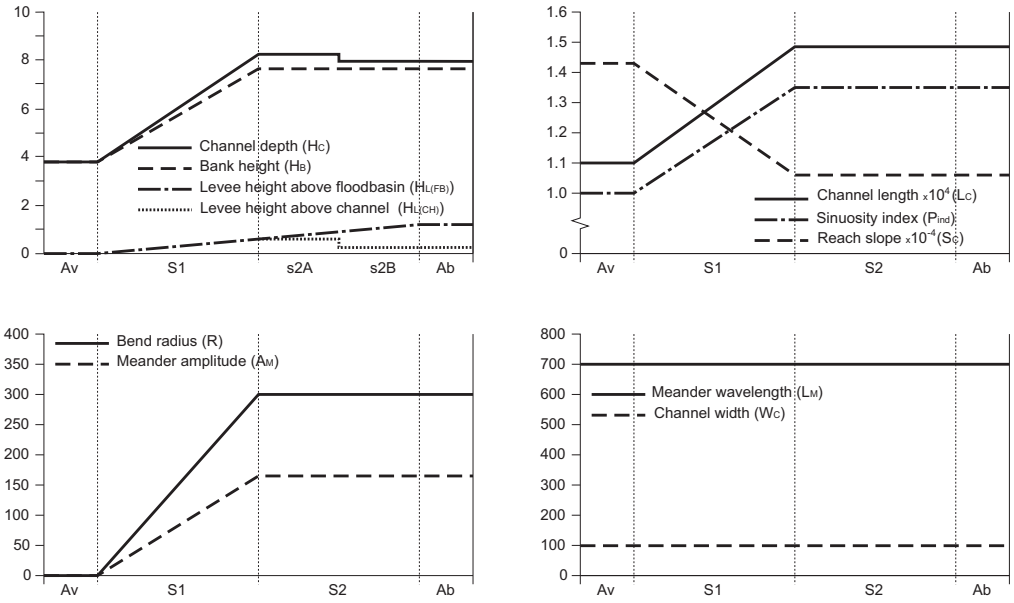

Figure 5.8. Assumed change of the Hennisdijk channel geometric variables, during all stages. The values during the avulsion stage (Av) and the abandonment stage (Ab) are given in Table 6, and the values during S1 and S2 are linearly interpolated. Time axis is indicative.

5.4.4 Calculation of sediment reworking

The resulting migration rate *Et* [m/a], is the rate at maximum bend curvature (Figure 5.9). It is subdivided into a downstream component (*Et,d*) and a lateral component (*Et,l*) (see section 'parameter constraining'). These components are used to calculate reworked surface area and reworked volume.

Surface area
To calculate reworked surface area for every modelled stage S_i, we described the channel shape as a sine at *t*=0 years after the onset of stage *i*:

$$C_{i,0} = A_{M,i,0} \cdot \sin\left(\frac{2 \cdot \pi}{L_M} \cdot x_{i,0}\right) \quad \text{(Eq. 5.26)}$$

where: $A_{M,i,0}$ = meander amplitude at stage *i* [m]
L_M = meander length [m]
$C_{i,0}$ = Cross-valley position of channel, as distance from channel axis [m]
$X_{i,0}$ = Downstream position of channel, as distance along the channel axis [m]

Due to erosion the channel moves downstream and increases in amplitude, and after 1 year of erosion its shape is described as:

$$C_{i,1} = A_{M,i,1} \cdot \sin\left(\frac{2 \cdot \pi}{L_M} \cdot (x_{i,0} - Et_i, l)\right) \quad \text{(Eq. 5.27)}$$

where: Et,l,i = lateral component of bank retreat rate during stage *i*
$A_{M,i,1} = A_{M,i,0} + Et,l,i$
$L_{M,i,1} = L_{M,i,0}$

Then we assumed the reworked surface (RWS_i) of channel C_i between t=0 and t=1 year to be equal to the area between both channels. Hereby, we make a small underestimation in the downstream limbs of the bends in S1, and at the apex in S2 (Figure 5.9).

$$RWS_i = abs\left|C_{i,1} - C_{i,0}\right| \quad \text{(Eq. 5.28)}$$

Sediment volumes
The reworked volumes in the different steps during stages S1 and S2 are subdivided into reworked erosion volume ($RWV_{E,i}$) and reworked deposition volume ($RWV_{D,i}$). These were obtained by multiplying the reworked surface (RWS_i) by the average erosion depth ($H_{E,i}$) or deposition depth ($H_{D,i}$), which vary along with riffle-pool sequences along the meandering channel. $H_{E,i}$ and $H_{D,i}$ are hence the average of the depths at the apex and at the inflection point.

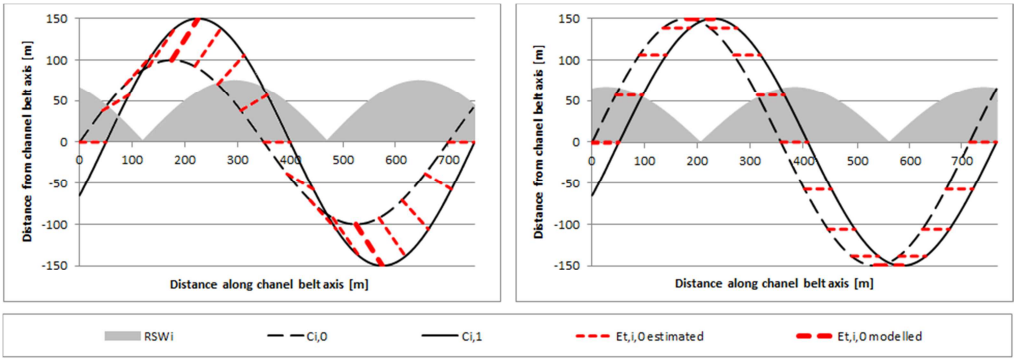

Figure 5.9. Exaggerated representation of the channel as a sinus along the channel-belt axis. Reworked surface (RWS_i) is the area marked by the red/dotted lines, and is approximately equal to $C_{i,1}$-$C_{i,0}$ (grey area).

$H_{E,i}$ is larger than $H_{D,i}$ because erosion includes the levee, whereas deposition only involves the compensation of erosion, which does not include levee development.

$$RWV_{E,i} = RWS_i \cdot H_{E,i} \quad \text{(Eq. 5.29)}$$

$$RWV_{D,i} = RWS_i \cdot H_{D,i} \quad \text{(Eq. 5.30)}$$

where: $H_{E,i}$ = spatially averaged erosion depth per stage i = 0.5 * ($H_{C,i,apx} + H_{C,i,ifl}$)
$H_{D,i}$ = spatially averaged deposition depth per stage i
= 0.5 * ($H_{B,i,apx} + H_{B,i,ifl}$)
$H_{C,i,apx}$ = erosion depth at apex = $H_{B,max,i} + H_{L,i}$
$H_{C,i,ifl}$ = erosion depth at the inflection point = $H_{B,avg,i} + H_{L,i}$
$H_{B,i,apx}$ = erosion depth at apex = $H_{B,max,i}$
$H_{B,i,ifl}$ = erosion depth at the inflection point = $H_{B,avg,i}$

5.5 Results

5.5.1 Reconstructed sediment budgets

Figure 5.10 shows the results of the sediment budget reconstruction based on the HEN maps and cross-sections. Overall, deposition is larger than erosion, reflecting the net aggradation due to natural levee growth. The natural levee deposits include the more distal floodplain deposits into which they laterally grade, and make up a relatively large part of the sediment budget.

The eroded volume in Av and the deposited volume in Ab are relatively small. In Av, about $2.5*10^6$ m^3 older floodbasin peat and clay were eroded. In S1 and S2, Pleistocene sediments became part of the erosion budget, due to channel incision. In S1 $18.5*10^6$ m^3 of floodbasin material was eroded. This was compensated by deposition of sandy channel deposits, but due to extension, floodbasin erosion was ~5% larger than channel deposition. The natural levee and overbank unit contain $17.7*10^6$ m^3 of deposited sediments, of which 91.5% comprised distal overbank sediments deposited in the floodbasin *NL(FB)*.

The amounts of erosion and deposition in S2 (Figure 5.10) are given for one meander length channel shift. In addition to sandy bed sediments a volume of $6.8*10^6$ m^3 of floodbasin material was eroded due to vertical incision. Both volumes were compensated by deposition of

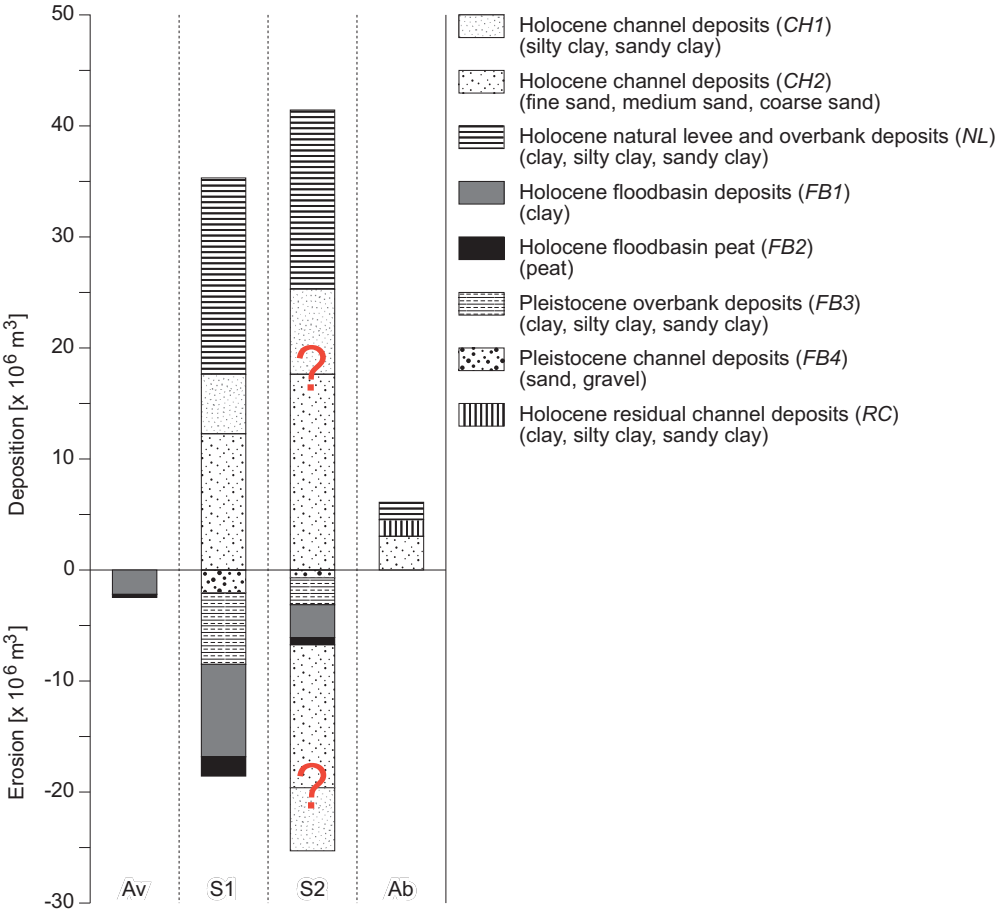

Figure 5.10. Resulting sediment budget from reconstruction based on maps and cross-sections. Channel erosion and deposition in stage 2 are indicative, and estimated based on a downstream migration rate of exactly 1 meander bend during S2.

new channel sediments. Net overbank deposition in S2 amounted $16.2 \cdot 10^6$ m^3, all of which remained preserved in the floodbasin. In stage Ab a large part of the residual channel was filled with sandy and silty material. In total $5.9 \cdot 10^6$ m^3 sediments were deposited, of which 74.3% was deposited within the residual channel. The remaining 25.7% is material deposited on top of the channel sands until maximum levee height was reached ($D_{ab,NL(CH)}$).

5.5.2 Channel migration rates

Figure 5.11 shows for all stages of channel migration *i*, the migration rates by bank erosion ($Es,_i$), bank failure ($Ef,_i$), and the total retreat rate ($Et,_i = Es,_i + Ef,_i$) for the HEN channel belt as calculated using the BSTEM model. In stage S1A the eroding bank consisted solely of resistant clay and peat. Hence, migration rates were low, in the order of 10^{-1} m/a. As a result of transverse bed slope development, the Pleistocene sand in the subsurface became incised, and in stage 1B the retreat rate accelerated along with increasing thickness of the less resistant sand layer in the bank profile to 3-4 m per year. Over the entire stage, the banks mainly consisted of resistant material, and the bank mainly eroded by failure erosion, after undercutting due to scour erosion in the sand layer; hence $Ef > Es$. In stage 2 bank consisted of sand, topped by silty overbank fines. Retreat rates were large, and the most important erosion process was scour

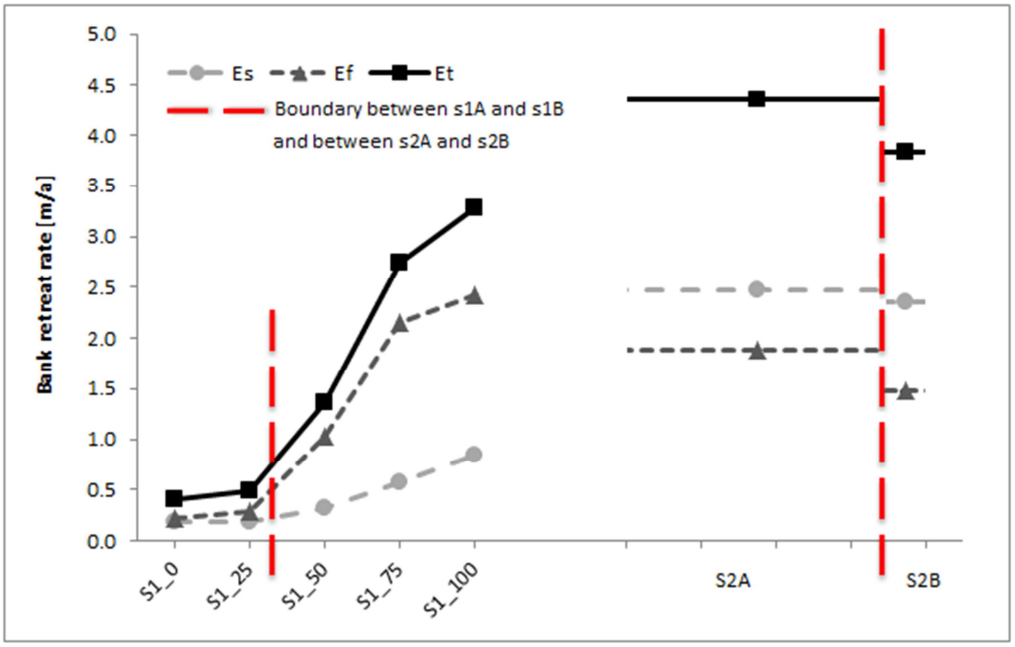

Figure 5.11. Bank retreat rate calculated for the two stages S1 and S2, calculated by the Bank Stability and Toe Erosion Model (BSTEM). The x-axis represents position of the bend apex, which is related to migrated distance.

erosion: E*f* < E*s*. Moreover, E*f* was smaller than in the last phase of S1. The difference between stages S2A and S2B is the decreased average levee height. Since this is related to flow depth, retreat rates gradually decreased between S2A and S2B.

5.5.3 Duration of stages

The period of activity of the Hennisdijk system, which is the period between beginning and ending of sedimentation of the river channel (Stouthamer and Berendsen, 2001) covered 1016 cal years, which is the total duration of stages S1 and S2. The total downstream shift during S1 was 700 m (1 meander length), and the associated downstream shift was 231 m. Using the migration rates calculated by BSTEM we accumulated the channel travel times along its lateral shift during S1, resulting in a total duration for S1 = 827 year for the HEN channel belt. The total duration of S2 was calculated as 1016 years minus the duration of S1, and is 189 years. S2A finished when the whole channel had migrated a downstream distance of L_M = 700 m. Given Et,d = 4.4 m/a, S2A lasted 160 years. Hence, S2B lasted the remaining 29 years, and with an Et,d of 3.8 m/a, the river migrated further to a distance of 109 meter. The total distance travelled in S2 = 810 m. Given L_M = 700 m, the channel belt reworked itself 1.2 times.

The durations of stages Av and Ab were assumed to be 200 years, for as this is the maximum duration of a full instantaneous avulsion, which is the assumed avulsion type responsible for the formation and abandonment of HEN (Berendsen and Stouthamer, 2001). Table 5.6 summarizes the durations of all stages.

5.5.4 Sediment reworking

Reworked volumes show similar trends as the migration rates that are their main controls (Figures 5.10, 5.12). Annually eroded volumes are small during the first stages of S1, but rapidly increase when the channel starts to erode the underlying Pleistocene deposits. During S1, the eroded Holocene floodbasin material and Pleistocene subsurface are replaced by an equal amount of Holocene channel deposits. In S2 annual erosion amounts are relatively high during S2A, and slightly lower during S2A. The channel is now reworking its own sediments: it erodes its previously deposited channel and overbank sediments and replaces these by new channel deposits.

Table 5.6. Duration of each stage.

Stage	Duration [a]	Duration per stage [a]		
Av	200			
S1A	525	0-25%: 414	25-32.5%: 111	
S1B	302	32.5-50%: 147	50-75%: 94	75-100%: 61
S2	189	A: 160	B: 29	
Ab	200			

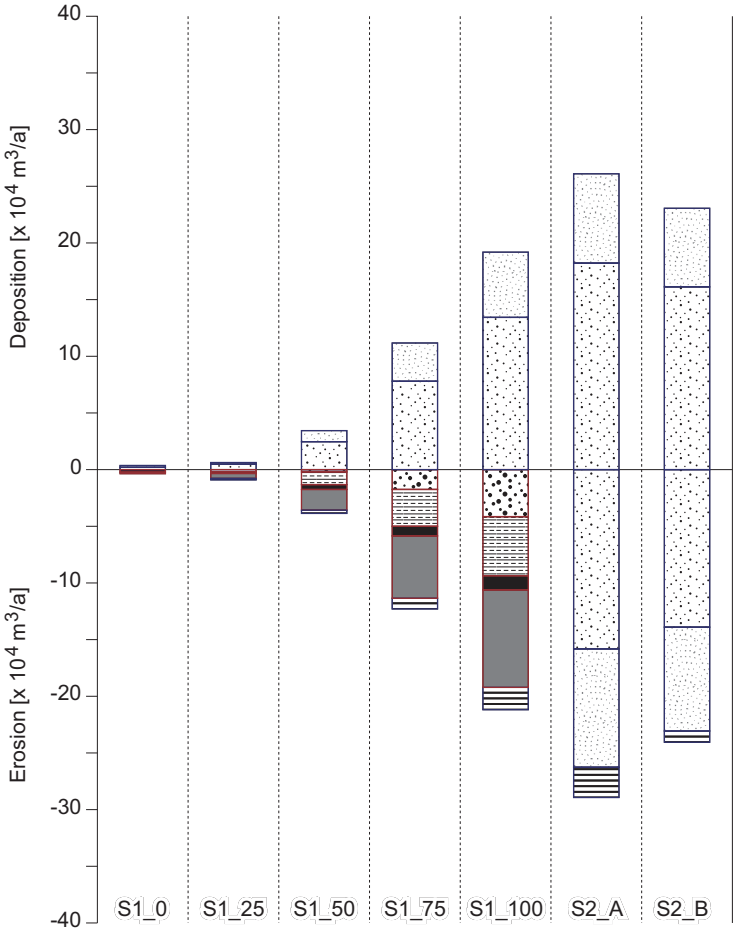

Figure 5.12. Reworked volume [m³/a] for 5 positions for both stages S1 and S2, calculated by the Bank Stability and Toe Erosion Model (BSTEM). Former floodbasin and channel deposits are enclosed by red lines, while channel belts own deposits are enclosed by blue lines. Levee deposition is not included, but assumed to be a sufficient part of the deposition budget. For legend see Figure 5.10.

5.5.5 Sediment budget

Figure 5.13 shows the resulting total volumetric erosion and deposition rates [m³/a], for the 11-km long HEN channel belt. In Figure 5.14 a time axis is added, and the net results are plotted for all units (5.14a), for all units except levee (5.14b), and for levee unit only (5.14c). The results for stages S1 and S2 are derived from the model results, those for Av, Ab, and the levee deposition volume are derived from the reconstruction results. Furthermore, in the model we did not assume a remaining percentage of floodbasin deposits when S2 commenced, so these

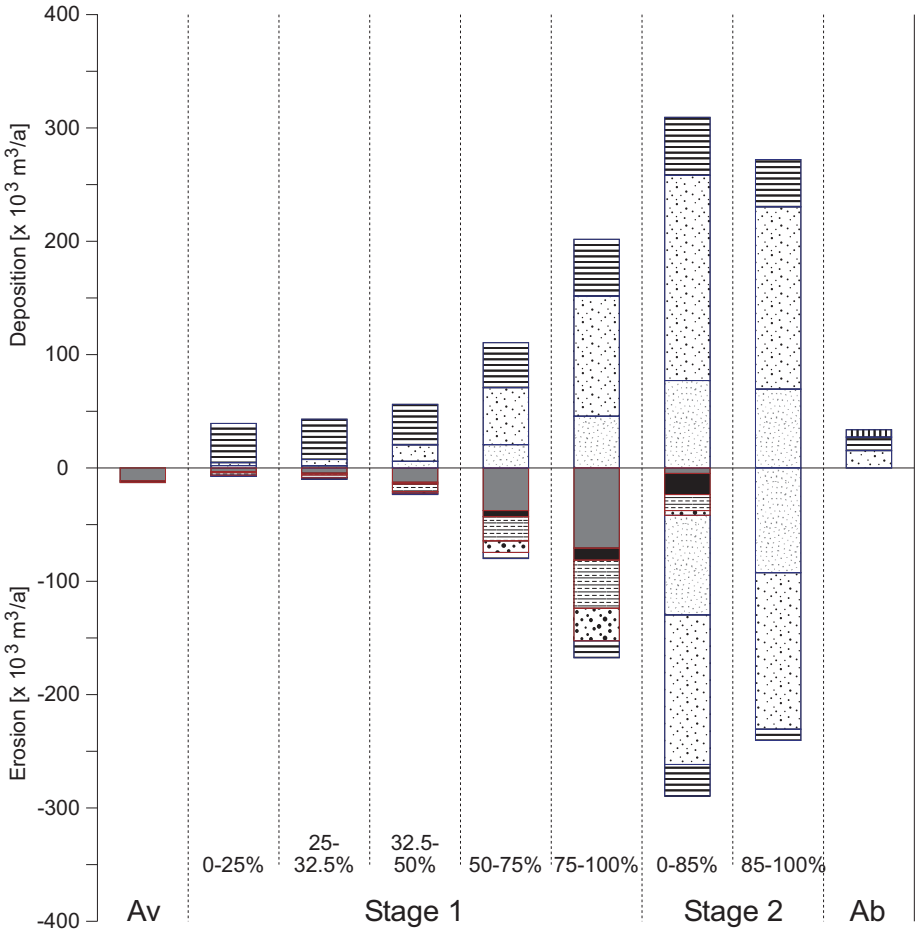

Figure 5.13. Erosion and deposition rates within the Hennisdijk river system, during its entire lifetime. The results are a combination of the reconstruction from maps and cross-sections and from BSTEM. For legend see Figure 5.10.

were derived from the reconstruction results too. Finally, when we assume deposition to be the compensation of the modelled erosion, we disregard extension. So, when estimating depositional volumes, we used the extension percentage calculated in the reconstruction section.

Figure 5.14 (next page). Total erosion, total deposition and net deposition within the Hennisdijk river system, during its entire lifetime. For all units (A), for all units except levee (B), and for levee units only (C).

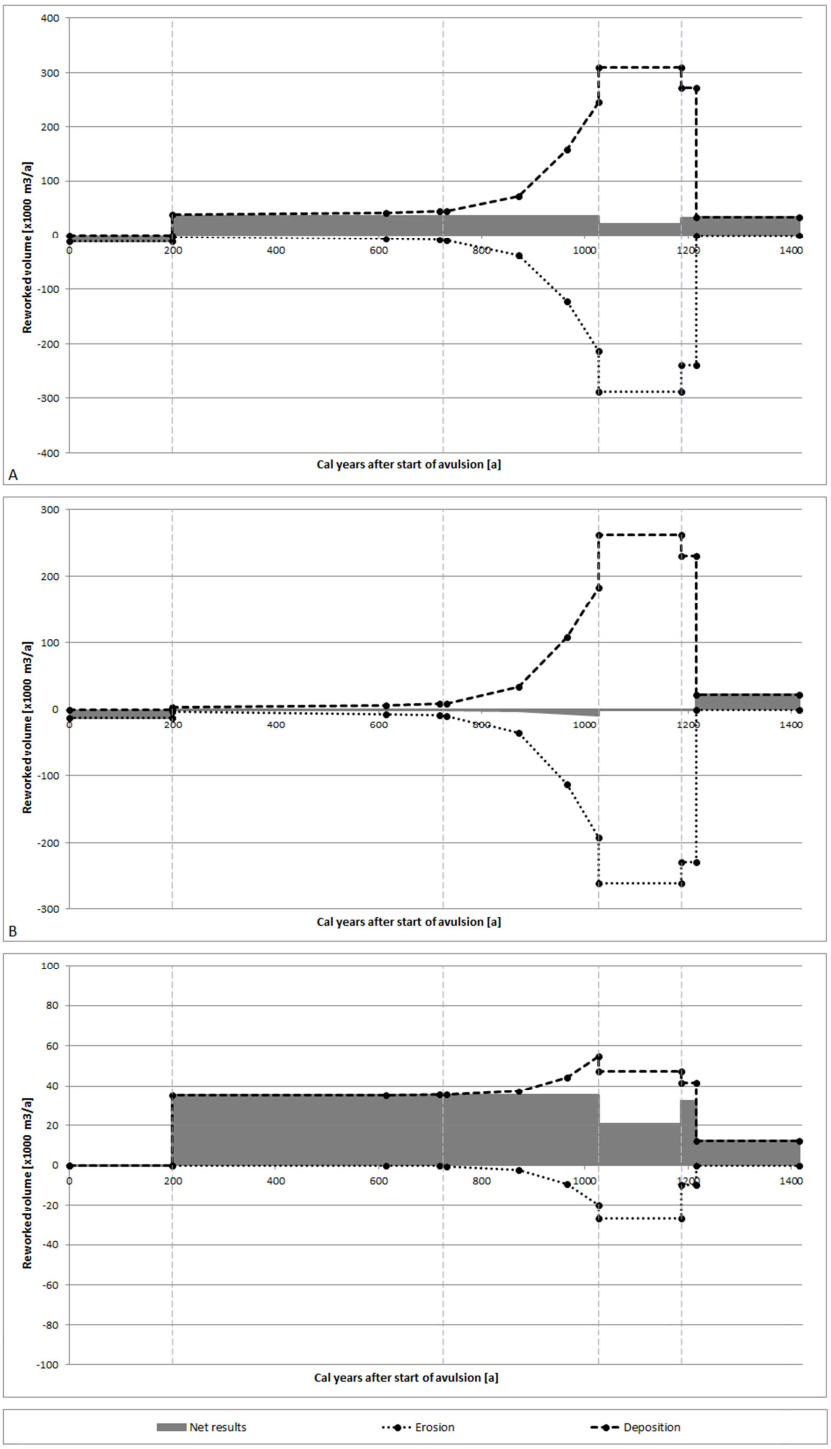
A
Reworked volume [x1000 m3/a]
Cal years after start of avulsion [a]
B
Reworked volume [x1000 m3/a]
Cal years after start of avulsion [a]
Reworked volume [x1000 m3/a]
Cal years after start of avulsion [a]
Net results
Erosion
Deposition

Total annual erosion and deposition volumes are related to *Et*. Since migration rates are low in the early parts of S1, the associated volumetric erosion and deposition rates increase during this stage, reaching high values in S2. In S1 there is small net erosion in the non-levee deposits as a result of extension, but in S2 the non-levee deposition fully compensates its erosion. Overall, there is net deposition, resulting from a net overbank deposition on the floodplain, and the surplus of deposition in the abandoned channel in stage Ab versus the initial erosion volume in stage Av.

Overbank deposition started in S1; in the course of time during S1 the amount of levee erosion due to bank retreat increased as levee height increased. Since S1 lasted much longer than S2 considerably more levee material was deposited in S1 than in S2. This means that in Figure 5.10, which is based on the assumption that half of the levee was deposited in S1 and the other half in S2, we underestimated the levee volume in S1 and overestimated it in S2. During S2A and S2B levee erosion was assumed to be constant, but in S2A erosion is larger than in S2B, because in S2A remaining levee material from S1 is eroded, while in S2b there is less levee material available.

Figure 5.15 shows the total accumulation per lithogenetic unit. In total, an amount of $7.28 * 10^6$ m^3/km sediment has been eroded by HEN. Net erosion of floodbasin material is $2.89 * 10^6$ m^3/km. This comprises Pleistocene (39%) and Holocene (61%) floodbasin material which is not renewed. The remaining $4.39 * 10^6$ m^3/km is hence the reworking of sediment from the system itself. Most of this involves channel deposits (87%) and a smaller amount (13%) involves erosion of the overbank deposits. Total deposition was about $10.6 * 10^6$ m^3/km. Net deposition of new material was $6.19 * 10^6$ m^3/km. This is mainly overbank sediment (48%), and channel sand (42%), and the remaining residual channel (10%). Over the lifetime of the channel, $2.89 * 10^6$ m^3/km of floodbasin material has been eroded, replaced by $6.19 * 10^6$ m^3/km new sediment, which is a surplus of $3.30 * 10^6$ m^3/km.

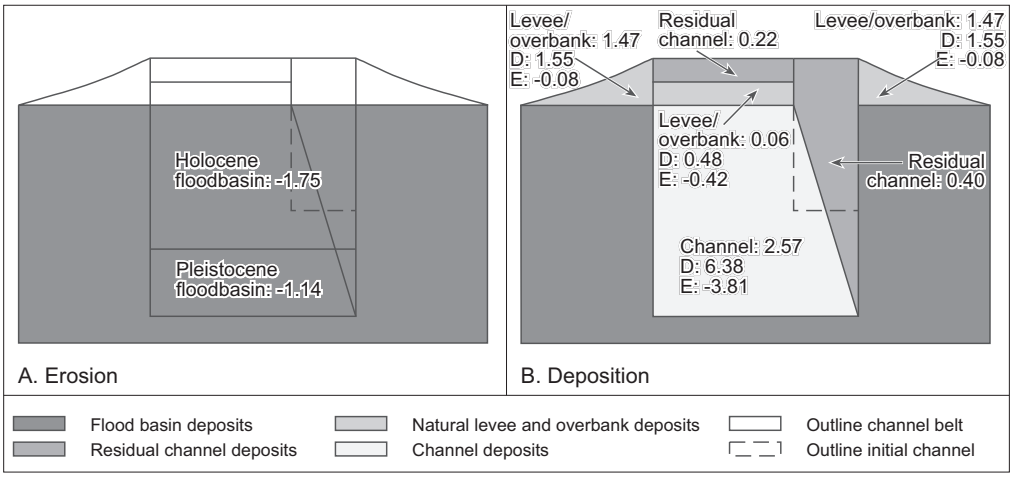

Figure 5.15. Net volumetric erosion (A) and deposition (B) rates, per kilometre channel-belt length [10^6 m^3/km].

5.6 Discussion

5.6.1 Channel-belt life-cycle stages

We presented a novel, generic method to calculate the sedimentary dynamics of a channel belt in the Holocene Rhine delta during its entire lifetime, from avulsion to abandonment. During the Holocene, many channel belts have been present in the delta, which vary greatly in size, age, duration of activity, discharge, sediment supply and bank material. In our study, we tested this concept to the Hennisdijk channel belt (HEN), which is a well-documented minor channel belt in the centre of the delta that was active during the middle Holocene.

Detailed lithological cross-sections and geological maps of the preserved HEN channel belt and overbank deposits allowed quantification of net sediment volumes that had accumulated during the channel belt's entire multiple centuries lifetime. Radiocarbon dates provided the age of the start and end of sedimentation, and hence the period of activity. We identified four stages in the channel life cycle: avulsion (Av), stage 1 (S1), stage 2 (S2), and abandonment (Ab). Determination of erosion and deposition rates, and sediment reworking within this life cycle requires estimates of channel migration rates during stages S1 and S2, which we determined using the Bank Stability and Toe Erosion Model (BSTEM). Our concept and methods entail a number of simplifications necessary to provide such estimates from the sedimentary archive, of which the most important ones are discussed below.

Crevasse-splays

In many deltas, avulsion starts with the formation of large-scale crevasse-splays that over time evolves into one meandering channel (Morozova and Smith, 2000). Sandy crevasse-splay deposits may make up a considerable part of the sediment budget. These deposits are not included in our concept, which is hence only applicable in deltas from the beginning of the avulsion stage, i.e. when scour of a dominant channel has started. However, the concept can be extended for crevasse-splay deposits, by adding a crevasse stage, preceding the avulsion stage. This may be relevant in alluvial systems where thick crevasse splay deposits are found, which make up a large part of the sand budget. This is for example the case in the Cumberland Marshes (Morozova and Smith, 2000). In the Rhine-Meuse delta crevasse splays are also present. For example, a large complex of crevasse deposits is found to the southwest of the Hennisdijk channel belt and seems to originate from the Hennisdijk avulsion point (Figure 5.2). Roughly estimated, the preserved sandy crevasse deposits from HEN are in the order of 6 * 10^6 m^3, which is about 10-20% of the net amount of sand trapped in the channel belt.

Bank erosion

Lateral erosion rates of floodbasin material along the channel banks as we estimated using BSTEM for stage S1 depend on the material's resistance to erosion. Default values for the resistance of each type of floodbasin material as suggested in the BSTEM software appeared not valid for our study. Moreover, these values do not include the role of vegetation on bank stability in the model. During the mid-Holocene, the channel banks in the Rhine delta were covered by forest, which may have influenced bank stability in two opposite ways: on the one hand, tree roots stabilize the banks, but on the other hand the weight of the trees destabilizes

them (see Thorne, 1990). In the absence of adequate default resistance values for each floodplain material type and reliable data on the effect of bank vegetation, we calibrated the effective long-term averaged bank resistance, using the minimum and maximum bank retreat rates from different sites, based on maps and cross-sections. The resulting values hence indirectly included vegetation, and agree with literature values of similar bank material types. In turn, our exercise yielded improved estimates of effective resistance values as alternative to the default values for BSTEM calculations when applied over longer time scales.
In our model we did not consider the situation in which the channel starts to laterally erode channel deposits from an older fossil channel belt, that is dissected by the new channel belt. Obviously, at those locations, bank erosion rate will accelerate due to the lower resistance of the sandy material. Also, the model does not consider the reoccupation of an older channel. In that case, the reoccupying new channel directly commences in stage S2 of the model.

Channel migration during stage S2 is simplified to meanders which migrate in downstream direction, with a spatially and temporally constant migration rate. We did not consider the possible occurrence of chute cut-offs and meander cut-offs, because only few residual channels have remained preserved to indicate such events, and it is not likely that chute bars formed in this type of low specific stream power channels (cf. Van den Berg, 1995; Kleinhans and Van den Berg, 2011).

In both stages there are spatial and temporal variations influencing migration rates, like year-to-year variations in discharge and along-channel variations in bank height, composition of the river bank material [e.g. due to occurrence of counterpointbar deposits (Smith et al., 2009)]. Such variations may result in an irregularly shaped channel. However, our purpose was to estimate an average (decade – century) migration rate for the entire channel over multiple meander wavelengths. We therefore considered spatial and temporal variations of less importance, and by representing the channel planform shape by a sine, we could extend the results of a point model along the entire channel, and hence estimate an average budget for the entire channel belt.

As consistency check we compared the calculated floodbasin erosion volume resulting from the reconstruction part with the total floodbasin erosion volume resulting from the model simulations. The erosion volume from the model is 12% larger than the results from the reconstruction, which is assumed to be an artefact of the assumptions to represent the channel as a sine curve.

5.6.2 Sedimentary dynamics

The sedimentary dynamics of a channel varies considerably on different spatial and temporal scales. In this section we discuss these variations, based on the results obtained for the Hennisdijk channel belt. Then we compare our results to data on larger scale variations, within the delta and during the Holocene.

Channel belts
Erosion, deposition and reworking of sediment during the channel belt lifetime varied within the four stages of its life cycle. This results in a characteristic sequence of sediment erosion, trapping and throughput, which can be seen as a 'fingerprint' of the channel development

stages in its sediment budget. Figure 5.16 represents this fingerprint for the active phase of a channel schematically: an initial period with low floodbasin erosion rates (S1A), followed by an exponential increase during S1B, reaching peak values at the end of S1B, and rapidly decreasing to zero in its mature stage (S2). Channels sand deposition mirrors floodbasin erosion. Moreover, there is a continuous amount of overbank deposition which is not shown in the graph. The graph represented here was derived from a small channel belt in the central part of the delta. The active phase is preceded by a crevasse stage, in which sand is trapped in the floodbasin, and an avulsion stage, in which floodbasin material is eroded. Furthermore, the active phase is followed by a period of abandonment, in which the residual channel is filled. The amount of sediment eroded or deposited in these stages is relatively small, and not related to the position in the delta.

The durations of the stages, and amounts of sediment involved in this fingerprint are likely to vary across the delta, from the apex towards the coastal zone. A major control is the downstream increase in thickness of the erosion-resistant upper layer of floodbasin clay and peat, along with a decreasing channel slope. This strongly reduces the ability of a channel to erode its banks and create meander bends, particularly when the channel does not incise into the underlying Pleistocene sand. This effect is well demonstrated by Schoonrewoerd channel belt of which the banks are formed by thick resistant floodbasin peat and clay, and that is not incised into in the Pleistocene subsurface (Makaske et al., 2007). As a result, SOO erosion rates in stage S1 were so small, that the channel did not reach stage S2 before it was abandoned. On the other hand, the Old Rhine channel belt in the distal part of the delta between the present-day city of Utrecht and the coast completed stage S1 and reached stage S2. This branch was active during ~5000 years (Van Dinter, 2013; Berendsen and Stouthamer, 2001), allowing it to reach stage S2 in spite of low migration rates during S1. In the delta zone closer to the apex, floodbasins contain less peat and are thinner; here the channel banks are mostly formed by more erodible sand. Accordingly, large meanders were formed here, and bank erosion rates were high. Reconstructions of meander development from historic maps. demonstrated that meander migration rates could be as high as 10-20 m per year, while no or little floodbasin sediment was eroded (see also Kleinhans et al., 2011).

Holocene delta accumulation

The presented reconstructions and model refer to varying sediment dynamics during a single channel belt life cycle. At the scale of the entire Rhine delta, there was a net accumulation of sediment, during the entire Holocene. This is caused by tectonics and sea-level rise, creating accommodation space, and by climate change, controlling water and sediment supply (Berendsen and Stouthamer, 2000; Blum and Törnqvist, 2000). The surplus of sediment includes natural levee deposits and overbank fines. Erkens et al. (2006) found an increase in accumulation rate, especially from 4000-2000 BP onwards, which they attributed to human activities in the hinterland, leading an increased sediment delivery to the delta.

We compared our results to previous sedimentation and sediment budgeting studies in the Rhine-Meuse delta. Erkens et al. (2006) calculated a clay deposition rate in the period 4,000 – 3,000 BP of about 450,000 m^3/a, over the entire delta. Given a delta area of 1500 km^2 (Erkens et al., 2006), this corresponds to a deposition rate of 300 m^3km^{-2}/a. When we add the results of all our stages, we find an average net deposition rate of about 20,000 m^3/a, over a depositional area of 110 km^2 (the entire channel-belt length of 11 km multiplied by a width of 5 km per side

of the channel), resulting in a deposition rate of 178 m^3km^{-2}/a. Our results are about twice as low, which may be explained by the factors below.

- We only included sediments that were deposited within a distance of 5 km from the edge of the channel, apparently missing sediment trapped in the more distal floodplain areas.
- The HEN system was a secondary distributary of the Rhine, while the budget of Erkens et al. (2006) is based on the deposition of all Rhine channels in the delta. Assuming that the HEN channel discharged was less than half the total Rhine discharge, both estimates agree surprisingly well.

Our estimates can be considered complementary to the budgets for the entire delta of Erkens et al. (2006). While Erkens' estimates are aggregated values over large delta compartments and 500-year time steps, our results show the variations in net sediment trapping both at the level of individual channel belts as well as during a channel belt life cycle.

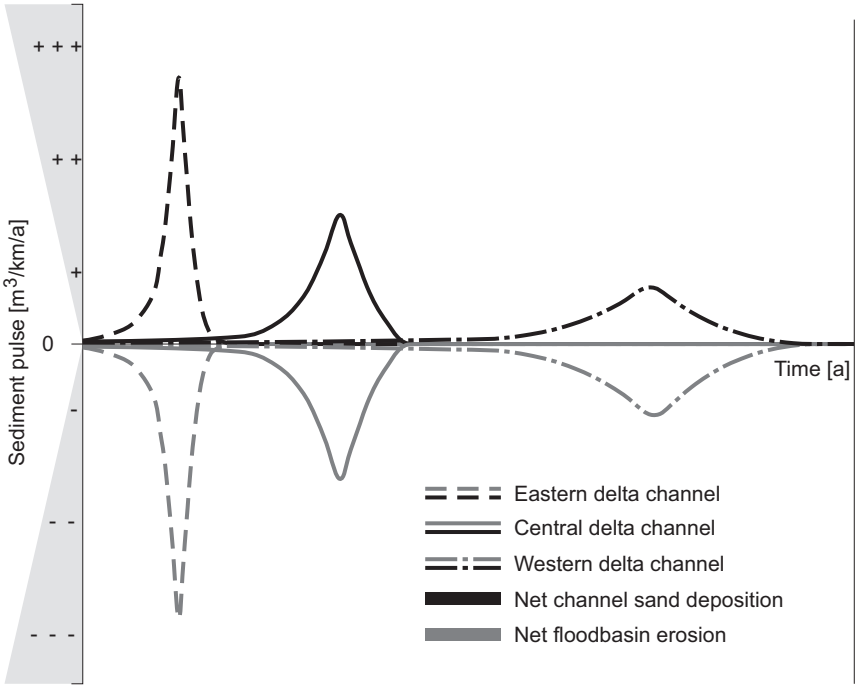

Figure 5.16. Conceptual sediment pulse, indicating the replacement of floodbasin material by channel sand, during the active stages of a channel (S1 and S2).

5.7 Conclusion

In this study we reconstructed sediment budgets with refined time resolution sufficient to recover the internal sediment dynamics of a natural channel belt in the Rhine delta. Such channel belt develops through several stages, including stage 1 (S1), in which the river erodes

floodbasin clay and peat and replaces them by bed sediments, and stage 2 (S2), in which the river reworks its own bed sediments.

Our study was performed at an abandoned mid-Holocene channel in the central Rhine delta: the Hennisdijk channel belt. We used geological maps, lithogenetic cross-sections, and a bank retreat model to calculate reworked volumes in S1 and S2, i.e. the volumetric erosion rate of floodbasin sediments (S1) or channel sediments (S2), and the in-channel depositional volume that compensates the erosion. Moreover, overbank deposition was estimated. Early in S1 reworked volume was about $0.5 * 10^3$ m^3/km/a. This volume increased gradually, and after a knickpoint it started to increase rapidly, reaching $13 * 10^3$ m^3/km/a at the end of S1. This knickpoint is the point where due to incision the sandy Pleistocene subsurface is reached, i.e. the boundary between S1A and S1B. During S2 reworking volumes were rather constant, ~21–$23 * 10^3$ m^3/km/a. Average overbank deposition volume was ~$3 * 10^3$ m^3/km/a.

The eroding riverbank is highly sensitive to the presence of sandy sediments. Due to scour erosion in the erosive sandy bottom layer, the overlying resistant peat and clay layers are undercut, an unstable bank is created, and the river bank fails. This process increases the bank retreat rate, and hence the reworked volume. Another factor is the resistance against erosion of the Holocene floodbasin material in the river bank, which generally increases with proportion of peat. Meander migration involves a decrease in bend radius, and hence an increase in outer bank scour depth. Therefore, high resistant river banks slow down the outer bank scouring rate, and hence the timing of incision into the Pleistocene subsurface.

Sand trapping within a channel is most efficient when it is incised into Pleistocene sand (S1B). Before, (S1A) reworking rates are substantially smaller, and in S2 only channel's own sand is reworked, which has no net trapping effect. Channels with most effective stages 1B are expected to be found in the central delta. In the upstream delta the Pleistocene subsurface is relatively high, so too much sand will be reworked. In the downstream delta the Pleistocene subsurface is deep, and unlikely to be reached because of the high resistance of the overlying layers. Sand trapping in the entire delta is most efficient when frequent avulsions take place, shortly after channels fulfilled S1B. Trapping of overbank sediments is less dependent on channel belt development stage.

The characteristic sequence of sediment dynamics in each channel, forms the channel's own specific fingerprint. These fingerprints are likely to vary across the delta. In this paper a fingerprint for the Hennisdijk channel belt was reconstructed. A next step is to quantify how the sediment fingerprint changes across the delta, and to combine this with the channel avulsion history given by Stouthamer et al. (2011) to reconstruct the internal sediment pacing in the Rhine delta due to avulsion.

6 Changing sedimentary dynamics under increasing human influence (synthesis and conclusion)

6.1 Introduction

The Rhine-Meuse delta forms a sedimentary wedge that has been built by sandy channel belts, which are intersecting floodbasins with clay and peat. Deposition of this deltaic wedge was accommodated by relative sea-level rise, which created space for deposition of the delta sediments and peat formation. Variations in upstream delivery, storage, throughput and reworking (i.e., sedimentary dynamics) determined the distribution of sediments in the delta. These sedimentary dynamics have been strongly influenced by human activities.

The main objective of this thesis *was to reconstruct the decadal time-scale sedimentary dynamics of the Rhine delta, and to assess the role human of activities in the delivery, storage, throughput and reworking of sediment.* These human activities comprised building of a diversity of engineering constructions, and altering river courses, thereby – often unintendedly - influencing discharge and sediment load. Roughly, the history of human influence can be divided into three periods, in which the sedimentary dynamics strongly differed due to major human modifications:

- *The natural Rhine*, before 1100 AD (Period A). In this period, the Rhine was free to meander naturally.
- *The embanked Rhine*, between 1100 and 1850 AD (Period B). Between 1100 and 1350 AD the active channels in the Rhine delta were embanked for flood protection and land reclamation purposes (Van de Ven, 1993; Berendsen and Stouthamer, 2000). After embankment the river migrated laterally between the dykes, but erosion and deposition were laterally confined. Moreover, the embanked channels were not able to avulse, and remained active without the ability of being abandoned.
- *The normalized Rhine*, after 1850 AD (Period C). River straightening was completed when halfway the 19th century a regular array of groynes was constructed along the Rhine distributaries, which completely fixed the channels. These normalization works were carried out to improve the navigability and the discharge capacity of the river, but they also affected the sedimentary dynamics, as lateral activity no longer occurred.

Reconstruction of the past sedimentary dynamics of a river requires detailed information about lithology and chronology of the sediments. From previous studies, a substantial amount of data from the Rhine delta was already available for all three periods. However, the method by which these data were achieved differed per period, depending on preservation of sediments in the subsurface, and the application range of the used dating methods. Therefore, this thesis also had a methodological objective, which was to develop for each of the above periods a method to reconstruct the sedimentary dynamics, which is adequate for the age and data availability of that period.

This final chapter addresses the research objectives specified in chapter 1.3. Firstly, 6.2 reflects on the applied methods to determine erosion and deposition rates from chronological and lithological data. Sections 6.3, 6.4 and 6.5 give a synthesis of how sedimentary dynamics

have changed through time as a result of human activities. Results of the case studies described in chapters 3, 4 and 5 of this thesis, combined with information from previous studies on the Rhine-Meuse delta, provided the building blocks; these are put together to compare the delivery, storage, throughput and reworking of sediment, as well as the changes in trapping efficiency and residence time, for the three periods mentioned above. Thereby, a distinction is made between channel sediments (section 6.3) and overbank sediments (section 6.4). Organic floodbasin deposits are not taken into account in this thesis. In the natural delta (period A), the focus is on high-stand delta, which is the period from 5500 years BP onwards, because then the influence of eustatic sea-level rise does not affect the comparison to the human-affected delta (Periods B and C). Section 6.6 concludes this thesis and addresses the implications of the results for future floodplain management.

6.2 Estimating sedimentary dynamics

Over the past decades, detailed lithogenetic and chronological information of the Rhine delta has been collected in a high-resolution database, in the form of borehole descriptions (Berendsen and Stouthamer, 2001), lithological cross-sections (Gouw and Erkens, 2007), different types of thematic maps (Maas et al., 1997; Koomen and Maas, 2004; Hebinck, 2008), dating results (Berendsen and Stouthamer, 2001), and reconstructions of channel belts (Schoor, 1994; Middelkoop, 1997; Hesselink, 2002; Makaske and Weerts, 2005; Makaske et al., 2007), complemented with coring data collected in the present study. Combining lithological and chronological information provided total volumes of eroded and deposited sediment within the specified period. To estimate the within-channel sedimentary dynamics, not only *volumes*, but also *rates* of erosion and deposition processes were required. This section explains how erosion and deposition rates were obtained for each period from lithological and chronological data.

Life-cycle stages

The simple model that describes the life cycle of a channel belt in four stages (chapter 5) provided an adequate framework to investigate internal rates reworking of sediment by a river channel:

- Avulsion stage (**Av**): within a relatively short period of time, a new channel is formed, which scours into a floodbasin of mainly peat and clay from earlier Holocene systems.
- Channel-belt building stage (**S1**): the newly formed channel starts to form meanders. Thereby, floodbasin material exposed in the banks is eroded and replaced by sandy channel deposits. Hence, the channel belt widens and meanders also migrate in a downstream direction. S1 is subdivided into **S1A** and **S1B**. In S1A the channel bank entirely consists of clayey floodbasin deposits and peat, whereas in S1B the lower part of the channel bank consists of Pleistocene sand.
- Channel-belt reworking stage (**S2**): in this stage, a downstream migrating bend has reached channel deposits from the next downstream meander of the same river. This channel-belt sand is far less resistant to erosion than floodbasin clay and peat, so downstream migration supersedes lateral migration. The downstream migrating river starts to rework the channel-belt sand deposited during S1. S2 is subdivided into **S2A** and

S2B. S2A represents the first cycle of reworking, in which the channel erodes a layer of relatively thick overbank deposits that were deposited during the longer stage S1. S2B represents the subsequent period of channel migration in which constant and relatively high rates of levee deposition and erosion arise.

- Abandonment stage (**Ab**): the equilibrium of S2 is interrupted by a new avulsion that causes upstream abandonment of the channel. The discharge gradually decreases and the channel loses its sediment transport capacity. This results in a net deposition of sand and finer grained deposits, until the channel is completely filled in. At that point the sedimentary dynamics associated with the channel life cycle came to an end.

Period A, natural Rhine

The data on fossil channel belts from the period before human impact from the Rhine database provides information on the beginning and ending of active phase of the channel belt, the composition of the floodbasin that has been intersected by the channel belt, and the lithogenetic composition of the channel belt as it has been preserved after its abandonment. This information tells us in which period a body of sediment was deposited or eroded, but does not provide direct estimates of the duration of the life-cycle stages it went through, neither of *within-life-cycle* variations in erosion and deposition rates. Therefore, the duration of stages Av and Ab was determined from the average avulsion durations in the Rhine-Meuse delta (Stouthamer and Berendsen, 2001). The duration of stages S1 and S2 depends on the rate of lateral erosion and accretion within S1 and S2. These erosion rates, and hence the duration of these stages, were estimated using the bank retreat model "Bank Stability and Toe Erosion Model" (BSTEM). Application of this model required calibration of the parameters for bank resistance, which was performed for two channel belts (chapter 5): Hennisdijk (HEN) and Schoonrewoerd (SOO). HEN is a well-developed channel belt that was active between 4191 and 3175 years BP and completed all life-cycle stages. Hence, the HEN total lifetime and dimensions data provided maximum bank retreat rates during the channel-belt building stage. SOO was a laterally almost immobile channel, which did not reach the channel belt reworking stage. Hence, it's channel belt dimensions provided minimum bank retreat rates for this stage.

Period B, embanked Rhine

When chronological data is available at high temporal resolution, within-channel belt erosion and deposition rates can be determined. Historic river maps provided detailed chronological information to calculate decadal-scale lateral erosion and accretion rates. Vertical accretion rates were determined from interpolation of high-resolution dated samples from the vertical sediment profiles. Hereby, the underlying model for interpolation was the assumption that vertical accretion rate was directly proportional to flood duration. The latter was derived from historic time series of water-level measurements along the Waal river. Optically Stimulated Luminescence (OSL) dating appeared to be an adequate method for dating fluvial sediments at this time scale.

Period C, normalized Rhine

For period C, only vertical accretion rates were determined, because lateral erosion and deposition have become zero. Detailed vertical floodplain soil profiles were dated at high resolution, resulting directly in sedimentation curves. Comparison of different methods

allowed to derive optimal ranges in space and time for their application (chapter 3). One such method was Optically Stimulated Luminescence (OSL) dating. This method was not previously applied to fluvial sediments of this age, and its application on young fluvial sediments has been improved (chapter 2). Resulting sedimentation rates agree with age constraints from maps, and with sedimentation rates from other methods.

6.3 Sedimentary dynamics of channel sediments

6.3.1 Holocene delta

During the Holocene many channels were active in the Rhine delta, transporting sandy sediments from upstream channels and from the Pleistocene subsurface to the coastal zone. Part of this sand was deposited in the channel beds, and has been preserved within the delta. Erkens (2009) calculated the net amount of channel sediment that was deposited in all Holocene channels. His results show that over the last 5500 years $6.9 * 10^{12}$ kg of bed sediment was trapped in the Rhine delta. When omitting the most recent period of strong human-influence, total channel bed storage due to deposition was $6.4 * 10^{12}$ kg in 4700 years. Assuming a dry bulk density of 1700 kg m^{-3} (Erkens, 2009), this equals a volume of $3.8 * 10^{9}$ m^3, or on average $0.80 * 10^{6}$ m^3/a. The upstream supply of bed sediments into the delta and the downstream loss are uncertain; nevertheless, it is assumed that the supply rate has been rather constant in time, as no fluctuations were proven (Erkens, 2009). Present-day annual input of coarse sediment at the Dutch-German border is between 0.66 and $0.85 * 10^{9}$ kg/a (Ten Brinke, 2005; Frings, 2014), which equals a volume of $0.4 – 0.5 * 10^{6}$ m^3/a, when all would be deposited in the channels. This input is smaller than the net Holocene channel deposition rate.

Holocene trapping of bed sediments within the delta varied in time and space, suggesting a variable delta trapping efficiency, and inherent variable throughput to the coastal zone. Erkens (2009) determined variations in sediment storage along eight north-south segments across the Rhine delta for 10 time slices of about 500 years (Figure 6.1). Net average channel deposition during the Holocene varied between about 0.8 and $2.0 * 10^{9}$ kg/a, with the higher values after 3000 years BP. This increase may be related to an increase in channel belt area as a result of delta area growth, and to an increasing thickness of floodbasin sediment replaced by sand. Furthermore, differences in trapping between the 500-year periods do not necessarily primarily reflect variations in sediment delivery from the upstream basin. Instead these can be attributed to the formation of new channels within the delta due to avulsion, as shown by Stouthamer et al. (2011). Hereby, not only the avulsion frequency, but also the avulsion location within the delta, and the length of the new channel have determined the variation in amounts of sand trapped in the delta.

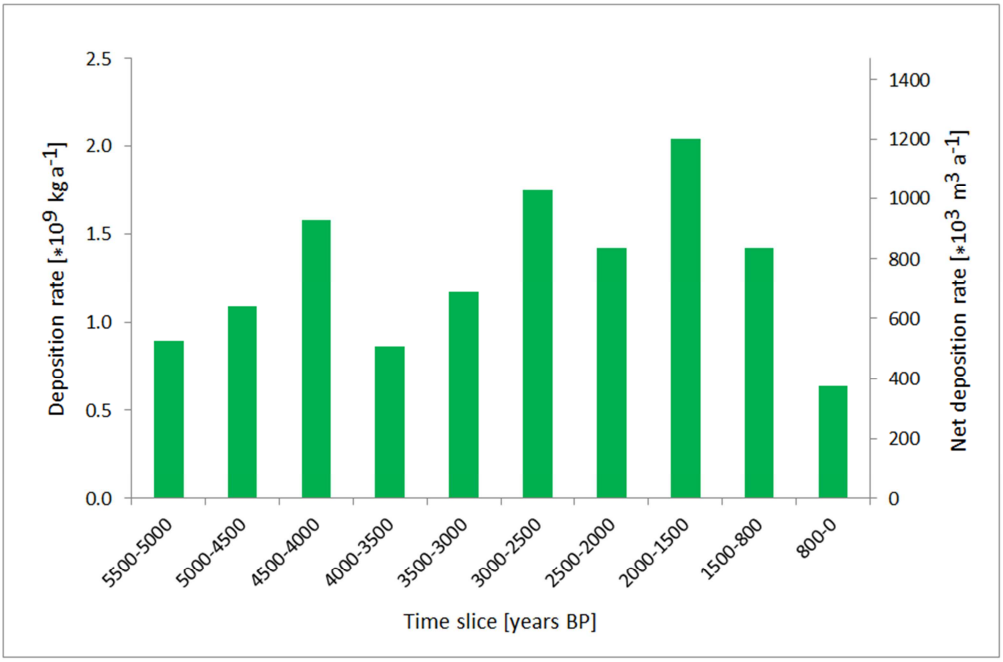

*Figure 6.1. Net Holocene channel deposition in the Rhine delta per time slice in [*10⁹ kg/a] along the left y-axis, and in [*10³ m³/a] along the right y-axis (adapted from Erkens, 2009).*

6.3.2 Natural channel belts

The results of Erkens (2009) do not show what happened within the life cycle of a channel belt, in which internal reworking of sand plays a considerable role. Exploration of this effect requires insight into the trapping of sediment during the life cycle of a channel, and how this varied across the delta.

Hennisdijk case study

The Hennisdijk (HEN) case study (chapter 5) demonstrated how the rate of erosion and deposition processes during the different stages of a channel belt's life cycle were reconstructed. HEN was a mid-Holocene channel belt in the central delta. It was a minor channel, as it presumably discharged 10-30% of the mid-Holocene Rhine discharge. Most of the HEN channel sediment is sand, but a part of it is finer material. The silty counterpoint deposits present along the edges of the channel belt (Makaske and Weerts, 2005; Smith et al., 2009), and the fine-grained deposits in the upper part of the residual channels are considered as channel deposits.

The amount of bed sediment that has been preserved in the investigated 11-km Hennisdijk channel belt reach is $31 * 10^6$ m³. This is 0.8% of the total amount of all channel sediments present in the high-stand Rhine delta. This may seem a small amount, but is considered a consistent value when accounting for the facts that the HEN channel width was

only one fifth of the channel width at the apex (~500 m; Toonen, 2013), was active during ~20% of the high-stand delta building period, and had a length of 11 km while the entire delta is ~150 km long. Most channel sediment (90%) was deposited during the active phase of the HEN channel, replacing older floodbasin deposits and the Pleistocene subsurface, mainly during stage S1B (59%), but also in stages S1A (9%) and S2A (22%) (Figure 6.2a). The remainder comes from infilling after abandonment, which mainly compensates the initial avulsion volume, but is slightly larger because the channel had become larger than during stage Av. These numbers all represent the first presence of sand; the total amount of deposition that occurred was considerably larger: $73 * 10^6$ m^3, which includes erosion and deposition of the channel's own deposits during stage S2 (Figures 6.2b and 6.2c).

Figure 6.3a shows the sand deposition, erosion and throughput rates associated with these stages. No deposition occurs during stage Av, when the new channel incised into the floodbasin. During S1, the deposition rate increased from 0.5 to $13 * 10^3$ m^3/a/km. Erosion of older Pleistocene bed material was initially zero, but slightly increased to $3.0 * 10^3$ m^3/a/km along with vertical channel incision. During S2 channel erosion rates, and hence deposition rates, rapidly increased and became in balance in S2B, with erosion and deposition rates of about $21 * 10^3$ m^3/a/km. After abandonment no erosion occurred, and the residual channel was largely filled with channel deposits.

The upstream delivery rate is unknown, but it is estimated by scaling the total Rhine load according to channel width (Bolla Pittaluga et al., 2003). The paleo-channel width at the apex is ~500 m (Toonen, 2013), and the average Holocene trapping rate – which is approximately the upstream delivery rate – is $750 * 10^3$ m^3/a (Figure 6.1). By scaling this amount to the 99-m-wide HEN channel (Table 5.5), it delivered about $150 * 10^3$ m^3/a of channel sediment. Throughput is calculated as the upstream delivery minus the net storage. During S1 trapping of upstream supplied sediments temporarily reduced the throughput of bedload sediments to the coastal zone. During S2 bed deposition rates are even higher; however, this is all reworked material of the channel-bed sediments from S1. Hence, there is neither net deposition, nor uptake of Pleistocene sand, and the throughput of bedload sediments to the coastal zone equals the upstream delivery (Figure 6.3b).

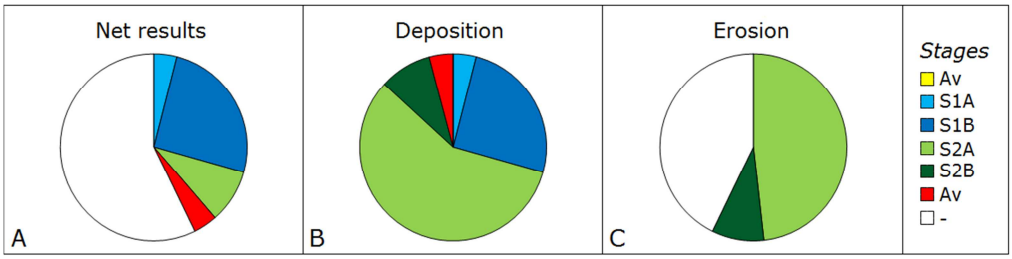

Figure 6.2. Erosion and deposition of channel sediments in the Hennisdijk channel belt, as percentage of the total amount of deposition (100% = $73 * 10^6$ m^3). Eroded amounts of Pleistocene sand are relatively small and not taken into account in this figure. Stages are explained in section 6.2.

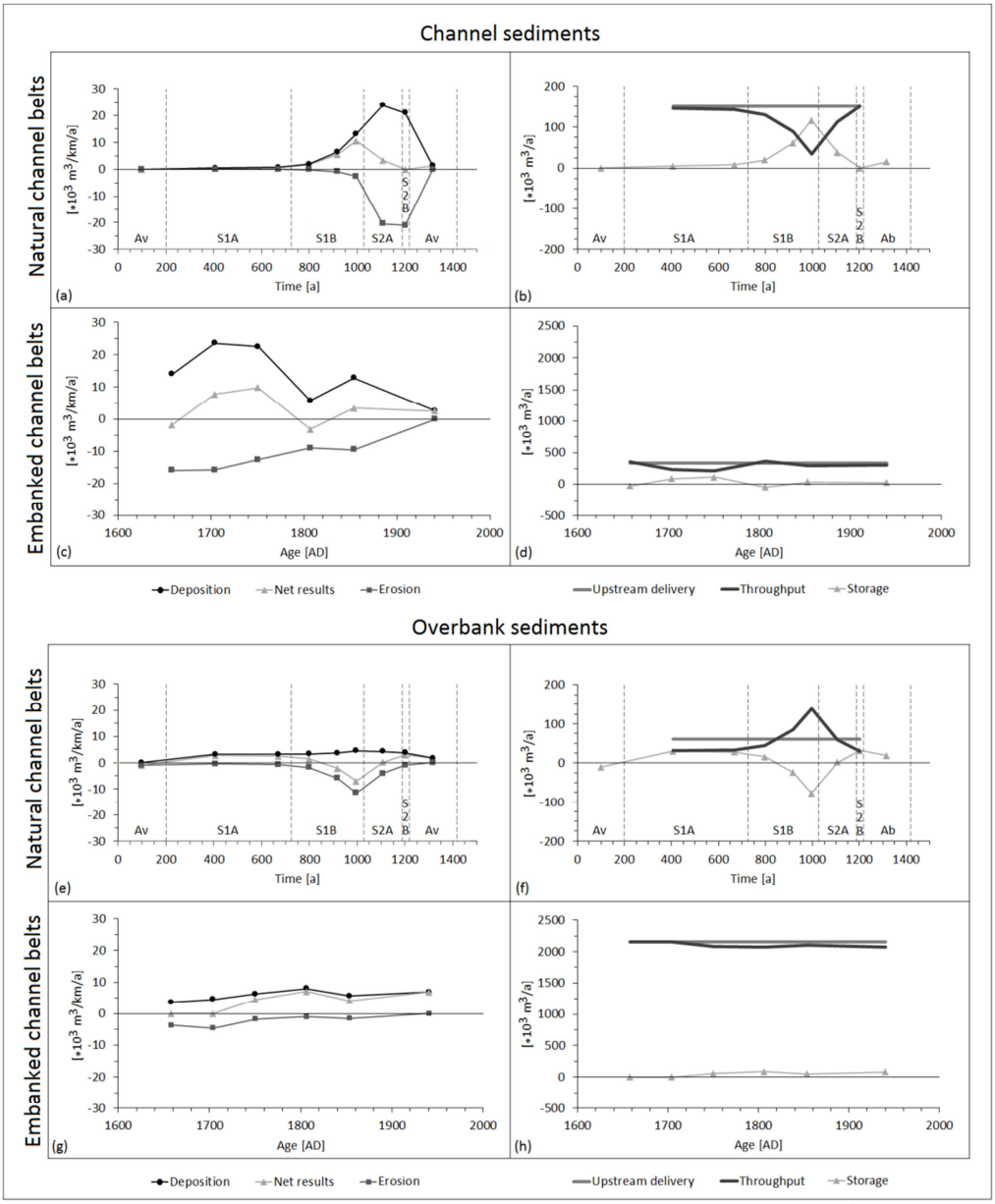

Figure 6.3. Total deposition, total erosion and net accumulation (left-hand graphs: a,c,e,g) and upstream delivery, storage and throughput (right-hand graphs: b,d,f,h) of channel sediments and overbank sediments in the natural Hennisdijk channel belt, and in the embanked Waal. In all situations we assume that upstream delivery rate remains constant.

Spatio-temporal variations across the delta

The HEN case study demonstrates the general sedimentary dynamical pattern within the life cycle of a single channel: bed sediment deposition is related to bank retreat rate, for as it compensates bank erosion. In S1A this is a low rate, due to resistant river banks of clay and peat that are hard to erode. But meandering goes together with transverse bed slope development, and in the outer bend the channel deepens. When due to deepening the channel incises into Pleistocene deposits, then erosion rate rapidly increases (S1B). This is a result of the mechanism of undercutting: due to scour in the erosive Pleistocene sand layer, the overlying resistant peat and clay layers are undercut, an unstable bank is created, and the weight of the overlying layers causes failure of the riverbank. In S2, the eroding river bank consists of channel deposits. These are far less resistant against erosion, and sand is reworked at high rates.

The above described within-channel sedimentary dynamics are likely to vary across the delta (Table 6.1). Major controls are the depth of the sandy Pleistocene subsurface, and the resistance of the overlying bank material. These are correlated, as the resistance depends on the thickness of the floodbasin deposits on top of the Pleistocene subsurface, and on the proportion of peat in this floodbasin. Both increase from the apex towards the coastal zone, thereby strongly reducing the ability of a channel to erode its banks and create meander bends. In the upper delta the Pleistocene subsurface is at relatively shallow depth, bank retreat rates are large, and hence meander bends are well developed. However, much Pleistocene sand will be reworked, so bedload trapping efficiency and residence times are small. Oppositely, in the lower delta, the Pleistocene subsurface is deep, and the overlying Holocene deposits contain resistant peat layers. Meanders develop slowly, incision rate is low, and it takes a long time for the channel belt to reach the sandy Pleistocene subsurface. These channels are short-lived and relatively straight, and do not efficiently trap bed sediments (S1A). Only some long-lived

Table 6.1. Main spatial differences in channel deposition and erosion across the natural delta.

Characteristic	**Lower delta**	**Central delta**	**Upper delta**
Depth Pleistocene subsurface	11 – 18 m	6 – 11 m	0.5 – 6 m
Proportion peat in floodbasin (P)	Many/thick peat layers $P >> 0\%$	Few/thin peat layers $P > 0\%$	No peat layers $P = 0\%$
Sinuosity index (p_i)	Straight channels $p_i < 1.3$	Low sinuosity $p_i > 1.3$	High sinuosity $p_i >> 1.3$
Sand trapping efficiency	No efficient sand trapping, because lateral erosion rates are small	Efficient sand trapping, especially when channels are in stage 2	No efficient sand trapping, because there is much reworking of sand
Residence time of channel deposits	Long	Medium	Short

channels may reach the Pleistocene subsurface (S1B), and then bedload trapping becomes more important.

Thus, sediment trapping within a channel belt will be most efficient when it is located in the central delta, where S1B is easily reached, whereas at the same time a thick-enough cover of fine sediments exists that can be eroded and replaced by channel belt deposits. However, in the entire delta, not only the location of a channel belt is of importance, but also the number of active channels, the length of these channels, and in which stage of development these are. A delta with long-lived channels, which are in S2 for a long period of time, is not an efficient bedload trapper. Bedload trapping is most efficient when avulsions take place frequently, in the central part of the delta, and occur shortly after channels have completed the built-up of their channel belt in stage S1B.

6.3.3 Embanked channel belts

The remaining active Rhine channels after embankment were in stage S1 (Lek, Waal) or S2 (Nederrijn, IJssel). Within the confinement of the dykes a downstream channel migration process evolved (chapter 4), which eroded remnants of older floodbasin material, and trapped bed sediments in sand bars at the opposite side of the river. This process continued until total reworking of all floodbasin sediment within the embanked floodplains was reached. From then onwards there was only reworking of channel sand, and the channel remained in stage 2. However, the embanked channels could not develop channel belts as wide as in the natural situation, and erosion processes continuously threatened the dykes. To protect the dykes, and to promote accretion to reclaim land for agricultural purposes, many individual groynes were created along the channel banks, resulting in a gradual straightening of the river (Middelkoop 1997).

Middle Waal case study

In chapter 4, erosion and deposition rates from the 17th century onwards were calculated for a floodplain section at a 12-km-long stretch along the river Waal. By then, most of the older floodbasin deposits had disappeared, and only few remnants of older material were left. In the early 17th century there was a near-balance between sand deposition and erosion (Figure 6.3c). There was much reworking of bed sediments, reaching erosion and deposition rates of about $200 * 10^3$ m^3/a. From the late 17th century onwards, erosion rates continued to decrease, while deposition rates remained constant, resulting in net deposition. This is a result of channel straightening, due to which floodplain area grew. By 1800 AD, lateral activity had nearly attenuated, and there was almost a balance between erosion and accretion rates again.

The net bedload trapping rate during the study period was $34 * 10^3$ m^3/a (Table 6.3). The present-day mean annual input of coarse material at the Dutch-German border is $0.4 – 0.5 * 10^6$ m^3. The river Waal transports about two-third of this, which is about $0.33 * 10^6$ m^3/a. This means that bedload trapping rate in the studied section is about 10% of all coarse sediment transported through the Waal River. This may be a relatively high percentage, because it applies to a limited reach of the river, and not all bedload will be trapped. Apparently, the studied section concerns a relatively upstream located and active segment, trapping substantial amounts of sand. Figure 6.3d suggests that a trapping efficiency of maximal 30%

during study period. In downstream direction, embanked channel belts become considerably smaller and less channel sediment was trapped.

On average, the total bed erosion rate was ~13 * 10^3 m^3/a/km, and the total bed deposition rate was ~15 * 10^3 m^3/a/km (Table 6.3). These reworking rates are small compared to the reworking rate of HEN during S2, which was ~21 * 10^3 m^3/a/km (Figure 6.7; compare scaled results). This may reflect the impact of embankment: the Waal River was embanked in its stage S1, preventing further lateral extension. So, when stage S2 was reached, the channel belt had laterally less extended than it would have in a natural situation, with accordingly lower reworking rates.

Spatio-temporal variations across the delta

The major effect of human activities is that various stages in the life cycle of the channel belt cease to exist. After embankment the avulsion and abandonment stages can no longer occur. S1 continues shortly after embankment, until S2 is reached. In this period the river Waal is the largest and most dynamic channel in the embanked Rhine delta. However, reworking rates are smaller than they would have been in a natural situation. Moreover, the magnitude of erosional processes decreases with time, because floodplains are protected against lateral erosion, while deposition continued. This resulted in a straightening of the channel.

Planform dynamics of the embanked Waal river shown on historic maps suggest that sedimentary dynamics occurred along most of the river Waal, with little differences between upstream and downstream channel stretches. The main difference was a decrease in volumetric erosion rate, which was related to the decreasing width of the embanked floodplain. As in the natural situation, the highly resistant floodplains prevented rapid lateral channel migration in the lower reaches even before embankment. Differences between Rhine-delta distributaries were larger than the within-channel-belt variations. Particularly before the Pannerden Canal was dug (Van de Ven, 1976), the Nederrijn and IJssel discharged considerably less water than the Waal river. The rivers Nederrijn and Lek reworked parts of their embanked floodplains, but in the river IJssel discharge was so small, that no sediment reworking occurred (Maas et al., 1997). Here, overbank deposition was the dominant process.

6.3.4 Normalized channel belts

Along the normalized channels, no lateral erosion or deposition of bed sediments occurs, and overbank deposition has remained as the dominant sedimentation process on the embanked floodplains. Erosion and deposition of sand are limited to the channel bed; sand is transported through the river without being temporarily stored in the embanked floodplains (Figure 6.6c), and is transported to the lower delta, where it is deposited within the channels. Dredging is required to prevent loss of navigation depth (Ten Brinke, 2004). So, due to normalization works all stages previously discussed have ceased to exist, and a new type of stage emerged: the fixed channel stage.

Lower Waal case study

In Figure 6.3c, the most recent points represent the normalized river. Erosion of sand amounts 0.1 * 10^3 m^3/a/km (1.3 * 10^3 m^3/a), total deposition amounts 2.5 * 10^3 m^3/a/km (30 * 10^3 m^3/a), and

hence net deposition is 2.4 * 10^3 m^3/a/km (29 * 10^3 m^3/a). These rates are much smaller than in the preceding periods, but still indicate activity. Part of this surplus of sand represents the lateral activity in the period overlapping with construction of the groynes (late 19th century). Moreover, during peak flow some occasional overbank deposition of sand occurs at some locations close to the channel bank. In an embanked river, flow velocity remains relatively high between the confining dykes. This flow is capable to carry bedload sediment into the groyne fields or onto the floodplain, where small natural levees are formed. At such locations average vertical aggradation rates of 9-25 mm/a may occur (chapter 3). During extreme events, this rate may be up to 50-75 mm/a (Sorber, 1997). This deposition occurs on a small part of the embanked floodplain area. Assuming that 4% of the Rijswaard was covered with sandy natural levees (Ten Brinke et al., 1998), the net volumetric sand deposition rate amounts 0.9 – 2.6 * 10^3 m^3/a, which is insignificant when compared to the annual amount of sand entering the delta. Erosion of floodplain sand does not take place anymore, and sand only disappears from the floodplain due to mining activities.

Spatio-temporal variations across the delta

As a result of normalization, sandy bed sediments, which would in natural circumstances remain in the channel, are deposited on the embanked floodplains near the channel edge. If not removed by artificial extraction and mining, the residence time of these sediments becomes infinite, as no more erosion of embanked floodplains occurs. The amount of sand deposition varies strongly between different Rhine branches. These variations are caused by differences in configuration of groynes, presence of river bank protection measures and dams, and the magnitude of water and sediment supply (Kater et al., 2012). On average, along the river Waal sand deposition covers an area of 4% of the floodplain area, and along the river IJssel sand deposition covers an area of 1% of the floodplain area (Ten Brinke et al., 1998).

Apart from very small amounts of overbank deposition, the only other temporary sink of sand along the lower Rhine distributaries are groyne fields. During peak flow, sand deposition occurs on sandy beaches between groynes (Ten Brinke, 2005). The residence times of these sediments are in the order of a year, as these sediments are removed in the course of the year by currents and waves from ships. Ten Brinke (2005) estimated that along the river Waal this navigation induced erosion of sand between groynes is ~1000 m^3/a/km. Most bedload material is transported to the coast. In the upper and central delta the channel deepens due to incision, while in the lower delta sedimentation occurs and dredging is required (Ten Brinke, 2005). Assuming that the annual volume of sand entering the river Waal at its upstream end moves every year during peak flow about 5 km in a downstream direction (Frings et al., 2009), it takes about 30 years before it reaches coastal reaches 150 km downstream, where it is dredged. Residence times in the Nederrijn and IJssel branches are slightly longer, due to lower flow velocities and longer river branches.

6.4 Sedimentary dynamics of overbank sediments

6.4.1 Holocene delta

In the entire high-stand Rhine delta a total amount of $7.8 * 10^{12}$ kg of overbank deposits has been trapped (Erkens, 2009). However, $2.0 * 10^{12}$ kg has been eroded by avulsion and meandering processes; thus, only $5.8 * 10^{12}$ kg is still present. The amount of overbank sediment trapping depends on suspended sediment delivery and on trapping efficiency.

In contrast to bedload supply, suspended load supply to the Rhine delta has been very variable during the Holocene (Erkens, 2009). Early Holocene delivery of suspended sediment was large from the barely vegetated hillslopes, but from the Early to Middle Holocene the hillslopes became forested, and suspended load delivery declined. From the Middle to Late Holocene suspended load delivery increased by ~60-70%, as a result of human interference and climate change (Erkens, 2009). Moreover, eroded overbank sediments were resuspended and reintroduced elsewhere in the delta floodbasins, so part of the present-day overbank deposits consists of reworked Holocene and Pleistocene clay. Trapping of suspended sediment has been very efficient throughout the Holocene, and is largely coupled with base level. Erkens (2009) found that Early Holocene trapping efficiency was relatively large (~90%) as a result of rapid relative sea-level rise. However, between 5000 and 3000 years BP, relative sea-level rise decreased, and only 70% of the sediment supply from upstream was trapped. During the Late Holocene trapping efficiency increased, due to delta extension in the apex region and the northeast (Erkens, 2009). Because of the large trapping efficiency, the sediment throughput of fine sediment to the sea has been relatively low during most of the Holocene, and no significant contribution to development of the coastal zone was found (e.g., Beets and Van der Spek, 2000). The peak in the amounts of sediment trapped during the Late Holocene (Figure 6.4) is related to increased sediment delivery, for as trapping efficiency was no restricting factor, and almost all delivered sediment could be trapped. In the most recent time slice there is a large dip in trapping of suspended sediment. This is not the result of decreased delivery, but of a reduction in trapping efficiency due to construction of dykes.

Between 5500 and 1000 years BP the average overbank trapping rate amounted $1.3 * 10^6$ m^3/a. Assuming a dry bulk density for overbank sediments of 1300 kg m^{-3} (Erkens, 2009), this equals a mass trapping of $1.2 * 10^9$ kg/a. After about 3000 years BP, a maximum trapping rate of $1800 * 10^3$ m^3/a or $2.4 * 10^9$ kg/a was reached (Figure 6.4). In the most recent decades, the annual input of suspended load at the Dutch-German border was in the order of 2.5 to $3.4 * 10^9$ kg (Ten Brinke, 2005).

The data of Erkens (2009) show that average Holocene reworking of overbank sediments was ~22%, but spatial and temporal differences existed. In eastern sections reworking was larger (36%), and in western sections smaller (10%). Early Holocene (9000-6000 years BP) reworking rate was high, because then aggradation rate was high, and relatively many new channel belts formed. In Middle Holocene (6000-3000 years BP) there was less reworking, but in the Late Holocene, the reworking intensified again. This was related to an increase in avulsion frequency (Stouthamer, 2001), and the much thicker body of floodbasin deposits that were eroded by new channel belts. Erkens (2009) determined for 500-year time slices the

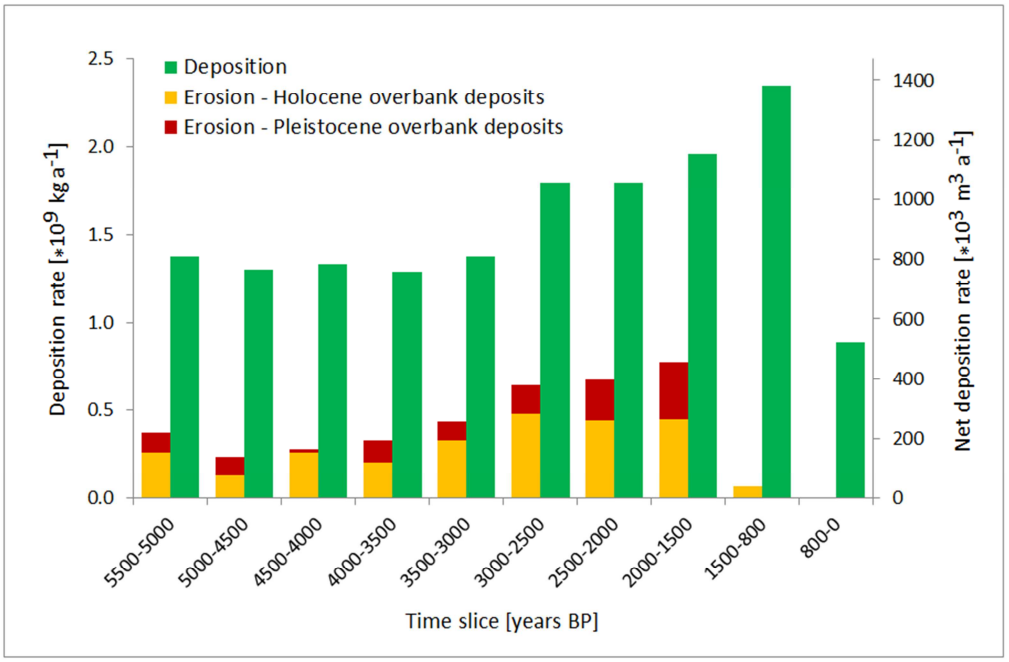

Figure 6.4. Net Holocene overbank deposition per time slice in [10^9 kg/a] (left y-axis), and in [*10^3 m^3/a] (right y-axis). (Adapted from Erkens, 2009).*

amounts of deposited and eroded overbank sediments along different transects across the delta. In this study, these data were used to calculate average residence times and half-lives for several segments between the apex and distal part of the delta. The results show a strong downstream increase: in the upper delta the half-life time of fine-grained overbank deposits amounts ~2,000 years, while in the lower delta half-life times of ~40,000 years were obtained. As the latter value is much longer than a high-stand period, this indicates that preservation potential of overbank fines in the downstream part of the delta is considerably higher than in the upstream parts.

6.4.2 Natural channel belts

Erosion and deposition of overbank sediments varied considerably during the life cycle of a natural channel belt. These variations are reconstructed in the natural Hennisdijk channel belt.

Hennisdijk case study

Erosion and deposition of overbank sediments also vary during the life cycle of single channel belt (chapter 5). In the case study of the 12-km-long Hennisdijk (HEN) channel reach, a distinction was made between proximal and distal overbank deposits. Proximal overbank deposits are the silty and sandy clay deposits close to the river, on top of the sandy channel

deposits and prone to reworking during the river's life cycle. Distal overbank deposits are the finer-grained clays further away from the channel, which are deposited on top of peat and clayey overbank deposits from older channel belts. The results presented in this study include distal deposits up to 5 km from the channel edges, although overbank deposition may extend over longer distances.

The total amount of overbank deposits trapped along the HEN system during its lifetime is ~43 * 10^6 m^3 (Figure 6.5a). Most of this was trapped in the distal floodbasin (D; 79%). The remainder was trapped in the proximal natural levee zone (P) during the active phase of the river (S1 and S2; 12%) and during abandonment (9%). Part of channel's own overbank deposits were eroded during the active phase of the river. These eroded sediments mainly involve the proximal overbank deposits that were eroded during S2, and distal overbank deposits that were eroded during S1 (Figure 6.5a). The total erosion amounted ~29 * 10^6 m^3. Most of this was floodbasin material of overbank sediments from older systems (48%), and clay from the Pleistocene subsurface (30%), eroded during Av and S1. The remainder (22%; given in Table 6.3) involved the reworked overbank deposits of the channel itself. Shortly after completion of the abandonment stage, the net amount of overbank fines deposited by the HEN river was ~37 * 10^6 m^3 (Figure 6b).

Floodbasin deposits from earlier Holocene and Pleistocene systems (referred to as 'older deposits') make up the major part of the erosion budget (Figure 6.5), and were mainly eroded during stage S1. During S1 the total volumetric erosion rate, including the older deposits and the channel's own distal deposits, increased from 0.5 to 11.5 * 10^3 m^3/a/km (Figure 6.3e). Net overbank deposition rate was assumed to be constant through time. During S2, there was no more erosion of the older and distal deposits. After removal of the proximal overbank deposits from stage S1 in stage S2A, erosion and deposition of proximal overbank deposits were in balance in S2B, and there was a net deposition of distal overbank deposits.

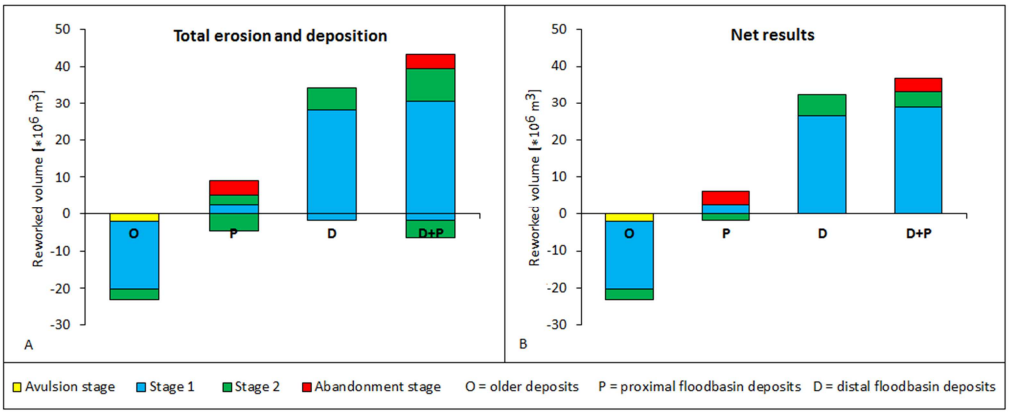

Figure 6.5. Total erosion, total deposition and net results of overbank deposits in the Hennisdijk channel belt during its entire lifetime.

The HEN system was active during the middle Holocene, when an estimated 70% of all suspended sediment that was delivered from upstream was trapped in the delta (Erkens,

2009). Assuming that the ~43 * 10^6 m^3 of overbank deposits trapped by the HEN system was also 70% of the amount delivered, the suspended sediment delivery to the Hen system was ~62 *10^6 m^3. Or, taking the duration into account, 61 * 10^3 m^3/a. Figure 6.3f shows that at the end of S1B the throughput was larger than the upstream delivery. Evidently, erosion of older floodbasin deposits was then so large that it was a temporary net sediment source into the system.

The average trapping rate of overbank fines in the entire delta during the lifetime of the HEN system (~4000-3000 years BP) was ~1000 * 10^3 m^3/a (Figure 6.4). The average trapping rate by the 12-km long HEN stretch was 42 * 10^3 m^3/a (total) or 36 * 10^3 m^3/a (net), which is about 4% of average trapping rate in entire delta during that time (Table 6.3). Assuming that overbank trapping rate is roughly proportionally to discharge, this small proportion can be well explained by the small proportion of the total Rhine discharge drained by the HEN system (~10 to 30%), and the limited length of the considered HEN section when compared to the entire delta length of ~150 km. Moreover, in the HEN budget, overbank sediments deposited farther than 5 km from the channel were not considered.

Spatio-temporal variations across the delta

Erosion of fine-grained floodbasin sediments is strongly determined by the bank retreat rate. In S1, when the floodbasin and the underlying Pleistocene sediments are eroded, volumetric erosion rates are largest, due to erosion of these older deposits. This process ceased during S2, which strongly reduced the volumetric erosion rates. Erosion of channel's own deposits is a relatively small component, but continues during S2. Deposition of overbank deposits causes a net accumulation of sediment in the delta.

Likewise the trapping of channel-belt sand, spatial variation in the total amount of eroded fines by different channel belts across the delta (Table 6.2) is controlled by the downstream increasing thickness of the body of Holocene overbank deposits from earlier systems. In the upstream part of the delta, erosion rates are high, but the available source of older floodbasin deposits is small. Oppositely, in the lower delta the amount of Holocene overbank deposits is much larger, while bank retreat rates are smaller. Erosion rates will therefore be largest in the central part of the delta. The total amount of eroded overbank sediments depends mainly on the availability of these sediments in the river bank. When downstream channels have enough time to complete S1, then the total amount of overbank sediment erosion will increase from upstream to downstream. Overbank deposition is less spatially dependent. It depends on flooding magnitude and frequency, and on available accommodation space, the latter increasing in downstream direction.

6.4.3 Embanked channel belts

Embankments reduced the area of overbank deposition and erosion processes to a ~500 to 1500 m zone along the river. Between the confining dykes, the downstream shifting channel laterally eroded older floodplain parts, while forming new floodplain areas along opposite banks on which overbank deposition started. These proximal overbank deposits include the concave swale fills separating the successively developed floodplain areas, and the layer of

Table 6.2. *Main spatial differences in overbank deposition and erosion across the natural delta.*

Characteristic	Lower delta	Central delta	Upper delta
Bank retreat rates	Low bank retreat rates.	Initially low bank retreat rates, but these increase rapidly when the sandy Pleistocene subsurface becomes incised.	High bank retreat rates.
Duration of stage S1	Long stage S1.	Long stage S1A, short stage S1B.	No stage S1A. Short stage S1B
Stages of coeval active channels.	Mainly stage S1 channels. Stage S2 will only be reached in long-lived channel.	Stage S1 and stage S2 channels.	Mainly stage S2 channels.
Reworking efficiency	Potentially, there is a large amount of floodbasin fines to erode, but it is restricted by the duration of stage S1.	A substantial amount of floodbasin fines will be eroded.	Small amount of floodbasin fines will be eroded.
Trapping of fine sediments	No spatial differences.	No spatial differences.	No spatial differences.

fine-grained sediments topping the embanked floodplain. Erosion of Holocene and Pleistocene floodbasin fines was limited to a few remaining spots within the embanked floodplains.

Middle Waal case study

In the Waal, initial overbank deposition rates were high: in the order of 6 to 39 mm/a. Deposition rates decreased locally over time with increasing floodplain elevation. However, in the downstream migrating river there was rapid reworking of floodplain area, and on the relatively low-lying newly developed floodplain area overbank deposition rates were relatively high again (Lauer and Parker, 2008c). So, when considered over the entire Waal stretch, there was little variation in volumetric overbank erosion and deposition rates before the 19th century (Figure 6.3g).

In the course of the 19th century, lateral erosion rates decreased as a result of bank protection measures. Overbank deposition continued, and average vertical accretion rates decrease to 3 to 6 mm/a. The decrease in lateral erosion resulted in net overbank deposition. Between ~1630 and ~1870 AD the total amount of overbank sediment present in the studied reach increased from ~8.5 to ~18.5 $*$ 10^{6} m^{3}, which was a net volumetric deposition rate of 40 $*$ 10^{3} m^{3}/a. To the entire delta, 19th century delivery rate of fine suspended sediment was ~4.2 $*$ 10^{9} kg/a (Van Urk and Smit, 1989). Assuming that suspended sediment delivery was proportional to discharge, and that dry bulk density was 1300 kg m^{-3}, then the river Waal, which discharged two thirds of the Rhine discharge, had a fine suspended sediment delivery

rate of 2150 * 10^3 m^3/a. If this is assumed to have been constant over the entire study period, then trapping efficiency of the considered 12 km Waal stretch was ~2-5% (Figure 6.3h). Over a 100-km reach this would add up for the Waal to a total trapping efficiency of ~20-40%.

The net deposition was a result of an average lateral erosion rate of 2.4 * 10^3 m^3/a/km, and an average vertical aggradation rate of 5.8 * 10^3 m^3/a/km. These are high rates compared to the natural HEN channel, for which these values were 0.6 * 10^3 m^3/a/km and 3.9 * 10^3 m^3/a/km (Table 6.3). This is partly explained by the 3 to 5 times larger discharge of the river Waal. Moreover, volumetric erosion rates were higher, because in the embanked Rhine there is a much thicker layer of overbank deposits to erode. Trapping of overbank sediment is less efficient than along the natural HEN channel, but average volumetric deposition rates may have been higher because of the higher suspended sediment delivery rates. Given a floodplain area of ~14 km^2, the average vertical accretion rate in the embanked floodplains was ~2.9 mm/a. Compared to the HEN channel belt, where the average overbank deposition rate amounted 0.33 mm/a, this is about 9 times higher.

The construction of embankments thus strongly accelerated overbank deposition of fine-grained sediments. Moreover, due to increased flow velocity and water level above the embanked floodplain (Hesselink et al., 2003; Ten Brinke, 2004), overbank deposits were generally coarser than in the natural distal floodplains. Initially, floodplains were continuously being reworked, and average overbank deposition rates remained fairly constant. Accordingly, residence times of embanked channel overbank deposits were relatively small, and there was only a small net storage of sediments. However, when humans started to prevent lateral bank erosion, net volumetric overbank deposition increased due to increasing floodplain area, and in the absence of erosion. Hence, residence time of overbank sediments became longer. By the end of the 19th century the sedimentary dynamics slow down. Less new floodplain area is formed, and accretion rate decreased.

Spatio-temporal variations across the delta

Spatial differences in erosion and deposition of fine-grained overbank material in the embanked floodplains depended on the floodplain width and extent of downstream channel migration. Along the upper and central Waal lateral erosion rates were relatively large, resulting in rapid reworking of overbank sediments. Moreover, in these embanked floodplains concave swales were formed, which were filled with sediments belonging to fine-grained overbank deposits. In the lower delta there was hardly any activity, just as in other Rhine channels. Even after embankment the IJssel river had wide floodplains, while the channel hardly eroded its banks. Here trapping efficiency was likely to be high, although absolute volumes were low, due to the small amount of water discharged by this distributary.

6.4.4 Normalized channel belts

The floodplains along the laterally fixed channels are not renewed anymore, and their elevations keep increasing in time. This causes the flooding frequency, and hence the vertical overbank deposition rates to decrease. Because inundation of embanked floodplains is associated with higher flow velocities, the transported material is coarser than in a natural

situation. This coarser material may also be deposited on the floodplain, and even sand may be deposited close to the channel edge (section 6.3.4).

Lower Waal case study

Recent overbank deposition rates, reconstructed for several locations within the Waal and IJssel floodplains, decrease with increasing distance to the river. Close to the river (proximal zone) rates are about 3 to 9 mm/a. Further away from the river (distal zone) rates are 2 to 7 mm/a. Based on the cross-sections and topographic maps in chapter 5 the floodplain area for which each measurement location is representative was calculated. Hence, the average overbank deposition rate for each floodplain section was estimated. Along the Waal this rate amounts 3.0 to 3.5 mm/a, which equals 0.4 to 0.5 * 10^9 kg/a, and along the IJssel it amounts 1.5 to 4.0 mm/a, or 0.2 to 0.5 * 10^9 kg/a. Presently, the annual input of suspended load at the Dutch-German border is 2.6 to 3.4 * 10^9 kg. When it is assumed that suspended sediment load is distributed proportionally to discharge, the Waal receives 1.7 to 2.3 * 10^9 kg/a of suspended load, and the IJssel receives 0.3 to 0.4 * 10^9 kg/a. This results in a trapping efficiency for the Waal of 20 to 30%, and for the IJssel of 50 to 100%. These results are consistent with previous modelling studies by Asselman and Van Wijngaarden (2002) and Middelkoop et al. (2010), who estimated a sediment trapping efficiency of 20 to 30% for the river Waal and ~80% for the river IJssel. This larger efficiency for the IJssel is mainly due to its wide and low floodplains when compared to the Waal.

Due to increasing floodplain elevation, overbank deposition rates decreased with time. This process is enhanced by river bed degradation. Since normalization higher flow velocities occur, which causes incision of 1 to 3 cm/a (Ten Brinke et al., 1998; Sieben, 2009). A study of Maas et al., (1997) confirmed this decrease. They found that event-related sedimentation on sediment traps is less than the long term (decadal) average, and Middelkoop (2000) found that average sedimentation rates over the past century are five times as high as present sedimentation rates. In chapter 4 sedimentation rates trendlines are fitted for the overbank deposits, and in chapter 3 age-depth plots are presented. These curves and plots confirm the decrease in sedimentation rate through time. However, the different sedimentation curves varied significantly, and did not provide robust values to generalize curves to the entire floodplain.

The net overbank deposition rate in the normalized Waal (3.0 to 3.5 mm/a) is higher than in the preceding embanked Waal, where net overbank deposition rate was ~3 mm/a (cf. Figure 6.8, where the most recent data point represents the embanked period). In the embanked Waal there was still much reworking, and most of deposited overbank sediments were eroded. At present, the reworking has ceased, and sediment is only removed from the floodplain by human activities. Van der Meulen et al. (2009) estimated the post-1850 clay extraction rate to be ~1.1 * 10^6 m^3/a, and current extraction rate to be ~0.7 * 10^6 m^3/a. The latter is higher than the current deposition rate of ~0.4 * 10^6 m^3/a. Clay extraction causes floodplain lowering, and hence locally increased flooding frequency leading to increased overbank deposition rates.

Spatio-temporal variations across the delta

The main sedimentary process in normalized rivers is overbank deposition. The rate of this process is expected to decrease with time. However, human removal of sediments may change

this pattern, for as on the lowered floodplains flooding frequency, and hence overbank deposition rates, increases.

Spatial differences in overbank deposition rates are mainly related to the amount of human interventions within a floodplain. This includes the frequency of removal of sediments, but also the presence of structures. Minor dykes for example, have a trapping-enhancing effect: water that flows over a minor dyke onto the floodplain is not able to flow back, and all sediments will settle (Thonon, 2006). Spatial differences between Rhine-delta channels are also related to the flooding frequency and to the amount of sediment available. Within a single flood event the floodplains of the river Waal receive more sediment than floodplains of the river IJssel. Along the Waal sediment trapping is more effective due to the trapping-enhancing effect of minor dykes. However, the river IJssel experiences more flood events each year, so the average annual deposition rate is higher for the IJssel (Thonon, 2006). Moreover, the IJssel has larger floodplains compared to main channel, and traps relatively large amounts of sediment (Asselman and Van Wijngaarden, 2002).

6.5 Comparison between channel and overbank sedimentary dynamics

In this study the sedimentary processes within the life cycle of a channel belt were quantified in terms of volumetric changes in storage, throughput and reworking of channel and overbank sediments. Moreover, trapping efficiency and residence times were qualitatively estimated. The sedimentary dynamics for channel sediments were considerably different from those for overbank sediments. Results are summarized in Table 6.3 and in Figures 6.6 and 6.7.

Volumetric erosion and deposition amounts and rates from the entire Holocene delta represent the average rates of many natural channel belts (Table 6.3). Their total channel length was unknown, and not all components were calculated. Still, the Holocene delta shows similar results as the natural Hennisdijk channel belt: in natural channel belts net amounts of trapped channel sediments and overbank sediments are similar; however, the total amount of erosion and deposition strongly differs, due to reworking of sandy channel sediments during the life cycle of the channel belt, while overbank deposits are deposited at larger distances from the channel, well away from its erosive action.

Erosion and deposition volumes of individual channel belts have decreased through time under increasing human influence, for both channel and overbank deposits. When calculated over the entire lifetime of a channel belt, sediment reworking rates for the embanked Waal are larger than for the natural Hennisdijk channel belt. This is because the embanked river Waal was in its 'reworking stage' S2, while the Hennisdijk results in Table 6.3 represent the average rates of all stages. Vertical accretion rates within individual channel belts have increased through time, as processes became limited to small zones. Moreover, channel normalization results initially in artificially high net vertical accretion rates due to the absence of reworking, but average rates dramatically decreased in the course of time along with progressive floodplain accretion.

To compare results from a natural delta channel belt to human-influenced channel belts, results from this thesis have been standardized in Figure 6.6: volumetric erosion and deposition rates were divided by the length of the studied segment, and were scaled for discharge. Thereby - for simplicity - it was assumed that the distribution of the total amount of bed load sediment entering the delta was distributed over the delta channels proportionally to the width of these channels (Bolla Pittaluga et al., 2003). Furthermore, the amounts of incoming sediment into the natural reach were not corrected (reduced) for upstream deposition losses. Hence, the large differences in upstream supply reflect increased erosion from hillslopes due to human interventions is clear. This figure summarises how the dynamics, and eroded and deposited sediment volumes within a channel belt have decreased due to embankment and normalization.

Volumetric erosion and deposition

In a natural channel belt overbank deposition rate remains rather constant, while the channel deposition rates vary considerably during a channel's life cycle (Figure 6.7; a1). During the stage of channel belt building (S1), amounts of deposited channel sediments are initially small, but when the channel incises into the sandy Pleistocene subsurface, the bank retreat rate, and hence the sand deposition rate, rapidly increase. Since both bank resistance and the depth of the Pleistocene subsurface increase from upper to lower delta, channel deposition rates decrease in a downstream direction, along with a delay in reaching the maximum rate. Erosion rates of older overbank sediments show a similar downstream trend, with a peak during stage S1 and decreasing to almost zero at the onset of the reworking stage S2, when only the channel's own proximal overbank deposits are eroded. During stage S2 sand deposition rates are constant, and are no longer varying across the delta, because reworking of sand is not dependent on resistance of the floodbasin. Instead, the reworking in stage S2 involves erosion of previously deposited channel sediments (Figure 6.7; a2).

Along the embanked channels sediment reworking of both channel and overbank deposits occurs. However, reworking rates decrease in time, as human interventions increasingly protect the floodplains against erosion (Figure 6.7; b2). Channel deposition is stimulated, but the amount of newly gained embanked floodplain area decreases in time. Hence, due to the increased floodplain area, overbank deposition increases (Figure 6.7; b1). After complete fixation by groynes, reworking rates of sediment decrease to almost zero (Figure 6.7; c2), and overbank deposition becomes the dominant process, with decreasing deposition rates over time due to increasing floodplain elevation (Figure 6.7; c1).

Table 6.3 (next page). Total erosion and deposition volumes, and time-averaged volumetric erosion and deposition rates of channel sediments and overbank sediments in the Rhine delta.

		HOLOCENE DELTA	NATURAL CHANNEL BELT *(Hennisdijk)*	EMBANKED RHINE STRETCH *(Waal)*	NORMALIZED RHINE FLOODPLAIN *(Waal and IJssel)*
Characteristics					
Study period	[-]	5500–800 BP	4191–3175 BP	1631–1872 AD	1872–2009 AD
Duration	[a]	4700	1016	241	137 [*4]
Bankfull discharge	[$m^3 s^{-1}$]	2500–3000	283-1001	1700-2000	300–2000 [*5]
Channel length	[km]	-	11	12	2.4 – 3.6 [*5]
Floodplain area	[km^2]	2300–3300 [*1]	111	14	1.4 – 3.3 [*5]
Channel deposits					
Dry bulk density	[kg m^{-3}]	1700	1700	1700	1700
Total erosion volume	[m^3]	Not calculated	$-42 * 10^6$ [*2]	$-36 * 10^6$	No erosion
Total deposition volume	[m^3]	Not calculated	$73 * 10^6$	$44 * 10^6$	$0.15 * 10^6$
Net deposition volume	[m^3]	$3.8 * 10^9$	$31 * 10^6$	$8.0 * 10^6$	$0.15 * 10^6$
Net deposition mass	[kg]	$6.4 * 10^{12}$	$53 * 10^9$	$14 * 10^9$	$0.26 * 10^9$
Net vertical deposition	[$m^3 m^{-2}$]	1.3	0.28	0.6	1.5 [*6]
Total erosion rate	[m^3/a]	Not calculated	$-41 * 10^3$ [*2]	$-150 * 10^3$	No erosion
Total deposition rate	[m^3/a]	Not calculated	$72 * 10^3$	$184 * 10^3$	$0.7–2.1 * 10^3$ [*7]
Net vol. deposition rate	[m^3/a]	$0.80 * 10^6$	$31 * 10^3$	$34 * 10^3$	$0.7–2.1 * 10^3$
Net mass deposition rate	[kg/a]	$1.4 * 10^9$	$52 * 10^6$	$58 * 10^6$	$1.0–2.7 * 10^6$
Net vert. deposition rate	[mm/a]	0.29	0.28	2.4	9-25
Total erosion rate	[m^3/a/km]	Not calculated	$-3.7 * 10^3$ [*2]	$-13 * 10^3$	No erosion
Total deposition rate	[m^3/a/km]	Not calculated	$6.5 * 10^3$	$15 * 10^3$	$0.21–0.59 * 10^3$
Net vol. deposition rate	[m^3/a/km]	Not calculated	$2.8 * 10^3$	$2.8 * 10^3$	$0.21–0.59 * 10^3$
Overbank deposits					
Dry bulk density	[kg m^{-3}]	1300	1300	1300	1300
Total erosion volume	[m^3]	$-1.5 * 10^9$	$-6.4 * 10^6$ [*3]	$-6.9 * 10^6$	No erosion
Total deposition volume	[m^3]	$6.0 * 10^9$	$43 * 10^6$	$17 * 10^6$	$0.7-1.5 * 10^6$
Net deposition volume	[m^3]	$4.5 * 10^9$	$37 * 10^6$	$9.7 * 10^6$	$0.7-1.5 * 10^6$
Net deposition mass	[kg]	$5.8 * 10^{12}$	$48 * 10^9$	$13 * 10^9$	$0.9-1.9 * 10^9$
Net vertical deposition	[$m^3 m^{-2}$]	1.6	0.33	0.70	0.42-0.52
Total erosion rate	[m^3/a]	$-0.32 * 10^6$	$-6.3 * 10^3$ [*3]	$-29 * 10^3$	No erosion
Total deposition rate	[m^3/a]	$1.3 * 10^6$	$42 * 10^3$	$69 * 10^3$	$5.2–11 * 10^3$ [*7]
Net vol. deposition rate	[m^3/a]	$0.95 * 10^6$	$36 * 10^3$	$40 * 10^3$	$5.2–11 * 10^3$
Net mass deposition rate	[kg/a]	$1.2 * 10^9$	$47 * 10^6$	$53 * 10^6$	$6.8–14 * 10^6$
Net vert. deposition rate	[mm/a]	0.11	0.33	2.9	3.1–3.8 [*7]
Total erosion rate	[m^3/a/km]	Not calculated	$-0.6 * 10^3$ [*3]	$-2.4 * 10^3$	No erosion
Total deposition rate	[m^3/a/km]	Not calculated	$3.9 * 10^3$	$5.8 * 10^3$	$1.8–2.8 * 10^3$
Net vol. deposition rate	[m^3/a/km]	Not calculated	$3.3 * 10^3$	$3.4 * 10^3$	$1.8–2.8 * 10^3$

[*1] Deltaic area increases during the Holocene.

[*2] This only includes erosion of river's own channel deposits. Additionally, $3.6 * 10^6$ m^3 of Pleistocene sand was eroded.

[*3] This only includes erosion of river's own overbank deposits. Additionally, $9.0 * 10^6$ m^3 of Pleistocene fines and $14 * 10^6$ m^3 of Holocene floodbasin deposits from earlier systems were eroded.

[*4] Aggradation rates calculated in chapter 5 are not the average rates over the entire period, but only of the upper layers deposited in the most recent period.

[*5] Three individual floodplain sections were studied, which differ in size and discharge. Average results from three sites are given.

[*6] A rough estimate based on cross-sectional data.

[*7] In chapter 5 vertical accretion rates were calculated. These are recalculated into volumetric accretion rates, assuming 80% of distal floodplain area, and 20% of proximal floodplain area. Along the Waal a sand bar is present, which takes 4% of floodplain area.

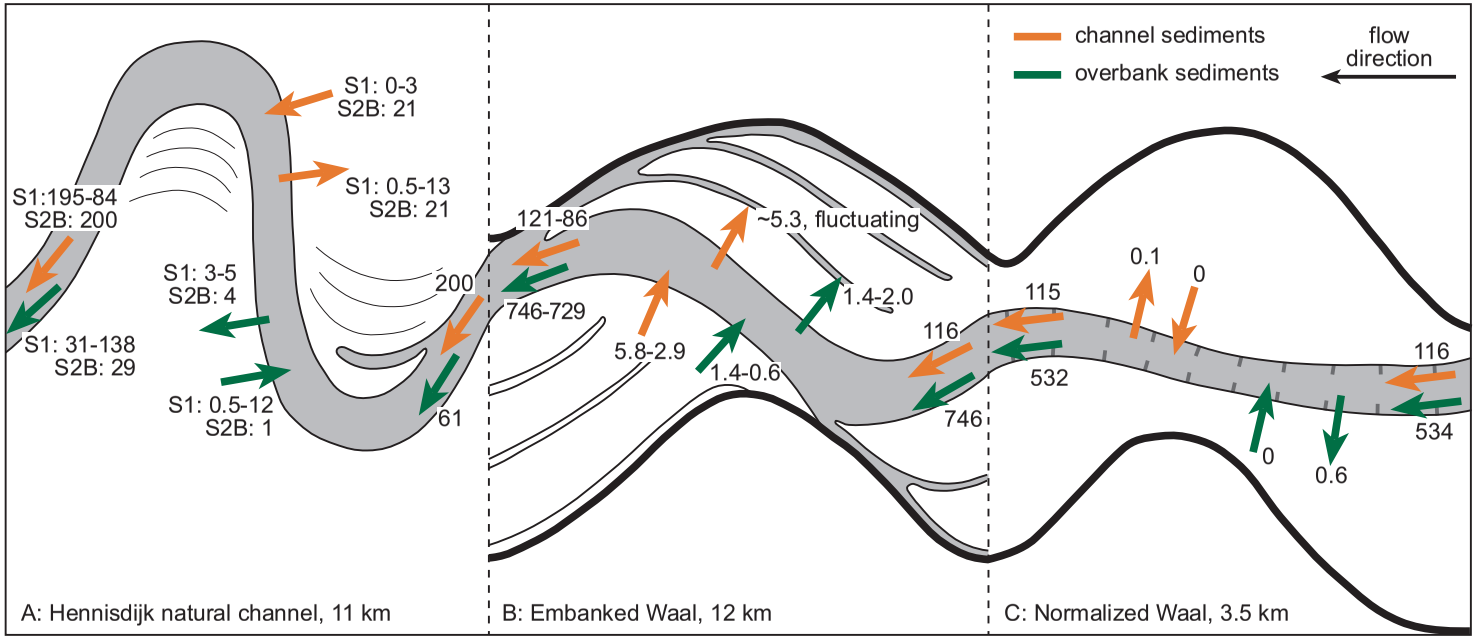
channel sediments
overbank sediments
flow direction
S1: 0-3
S2B: 21
S1: 0.5-13
S2B: 21
S1:195-84
S2B: 200
S1: 3-5
S2B: 4
S1: 31-138
S2B: 29
S1: 0.5-12
S2B: 1
200
61
121-86
746-729
5.8-2.9
~5.3, fluctuating
1.4-0.6
1.4-2.0
116
746
115
532
0.1
0
0
0.6
116
534
A: Hennisdijk natural channel, 11 km
B: Embanked Waal, 12 km
C: Normalized Waal, 3.5 km

Trapping efficiency and residence times

Trapping efficiency and residence times were only qualitatively described, and are schematically represented in Figure 6.7. Trapping efficiency concerns the net volumetric deposition rate, as percentage of the upstream sediment supply rate. Upstream supply of channel deposits has been rather constant, while net channel deposition strongly decreases in the human-influenced periods. Although not shown, in Figure 6.7, channel incision due to channel narrowing, decreasing upstream delivery of bed sediments, and dredging have caused a net erosion of channel-bed sediments in the past century. Upstream supply of overbank sediments strongly increases in the three stages, associated with upstream agriculture expansion, while deposited volumes decrease (Figure 6.7). Hence, for both channel and overbank sediments the trapping efficiency decreases when human interventions increased. Although not shown, in Figure 6.7, upstream supply of channel deposits has been rather constant, while channel incision due to channel narrowing, decreasing upstream delivery of bed sediments, and dredging have caused erosion of channel-bed sediments in the past century. Upstream supply of overbank sediments strongly has increased over the entire study period, while deposited volumes decreased (Figure 6.7). Hence, for both channel and overbank sediments the trapping efficiency decreased when human interventions increased.

Upstream supply rates within a period are here assumed to be constant during each of the periods, so changes in trapping efficiency are related to changes in net deposition. In the natural channel belt, trapping efficiency of channel sediments is depended on the stage the channel is in: during stage S1 the trapping efficiency is high, along with the development of the channel belt, while during stage S2 net trapping is nil (Figure 6.7; a3). Trapping of overbank deposits is dependent on flooding frequency and sediment delivery, and hence shows less variation associated with the life-cycle stages of a channel, and is less dependent on

Figure 6.6 (previous page). Changing sedimentary dynamics through time as a result of human activities in the delta. Panel (a) represents the Hennisdijk channel belt, while panels (b) and (c) represent a segment of the Waal. All results are standardized to Hennisdijk channel width. Orange arrows represent the channel sediments, and green arrows represent the overbank sediments. Input and throughput rates are given in 10^3 m^3/a, while erosion and deposition rates are given in 10^3 m^3/a/km. The range given for some arrows indicates the increase or decrease during the study period.

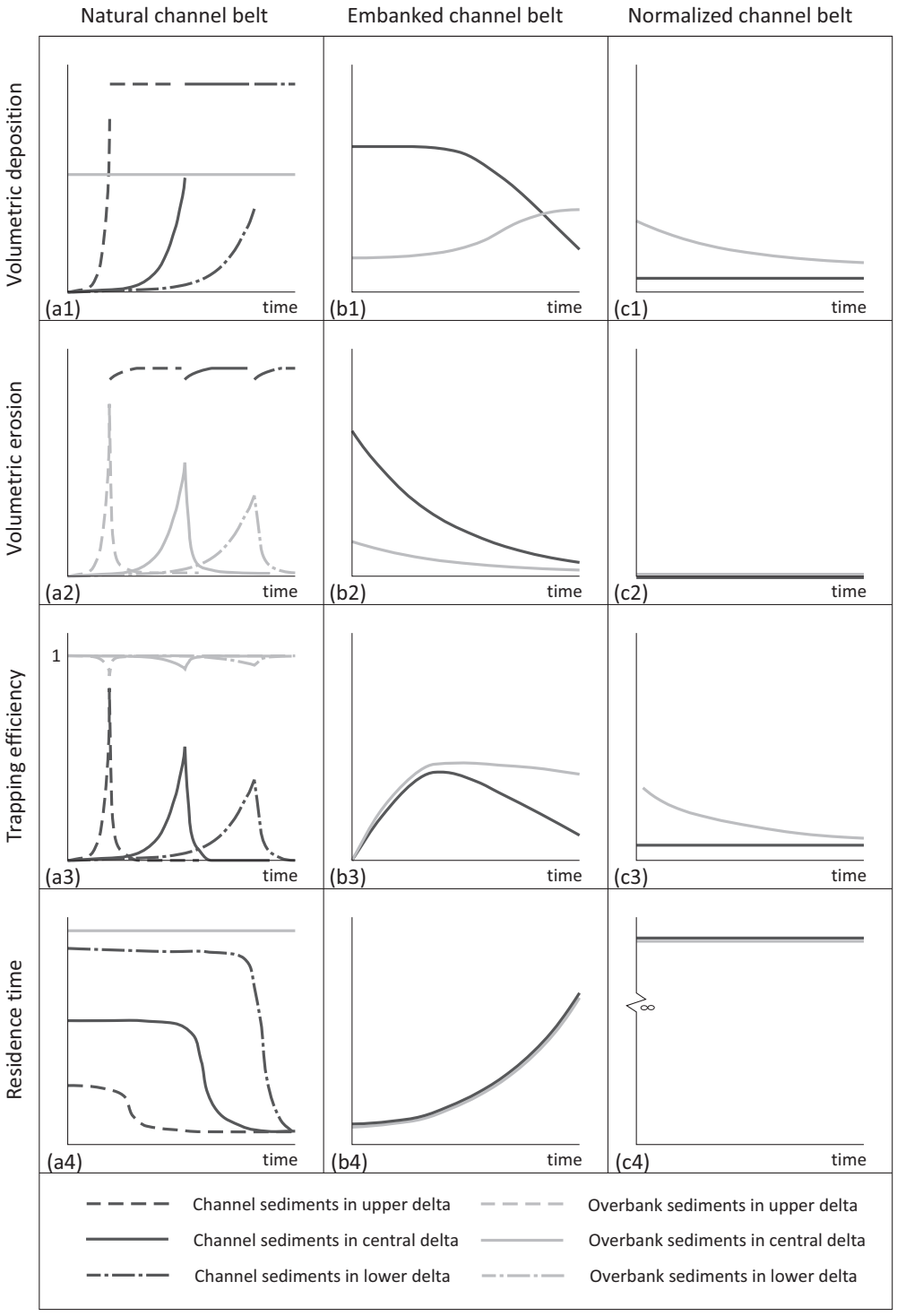
Natural channel belt
Embanked channel belt
Normalized channel belt
Volumetric deposition
Volumetric erosion
Trapping efficiency
Residence time
(a1)
(b1)
(c1)
(a2)
(b2)
(c2)
(a3)
(b3)
(c3)
(a4)
(b4)
(c4)
time
1
Channel sediments in upper delta
Channel sediments in central delta
Channel sediments in lower delta
Overbank sediments in upper delta
Overbank sediments in central delta
Overbank sediments in lower delta

location within the delta. Within embanked channels variations in trapping efficiency depends on human interventions. Trapping of both channel and overbank sediments increases when deposition is promoted (Figure 6.7; b3), but trapping efficiency decreases as the river straightens and less new low-lying floodplain area with high accretion rates form. In normalized channels, erosion has stopped, and trapping efficiency is related to the total volumetric deposition (Figure 6.7; c3).

Residence times are strongly related to reworking rate: intensive sediment reworking sediments results in short average residence times. Along active natural channels residence times for overbank deposits are continuously high. Across-delta variations in average residence time of overbank deposits depend on avulsion frequency and location within the delta, and show a decrease from order of century in the upstream parts of the delta, a few millennia in the central part to more than a single high-stand period in the distal parts of the delta. Residence times of channel-bed sediment associated with the life cycle of a channel belt show considerable shorter-term variation. Channel sediments deposited during the earliest stages of S1 my remain deposited for a substantial amount of time, before these are re-eroded during stage S2, when rapid reworking causes a decrease in residence time (Figure 6.7; a4). Across-delta differences are related to the duration of stage S1. Once abandoned, the residence time becomes dependent on the possibility of the material to become eroded by younger systems, which is determined by the frequency and location of avulsion and the increase in accommodation space (not in figure). Since embankment prevents channel avulsion, residence times of overbank sediments still present in the Holocene floodbasin have increased potentially to infinity. However, continuous and intensive reworking along the embanked channels causes residence times of channel bed and overbank sediments to be low here. When during period B erosion decreases due to construction of individual groynes, the residence times increase (Figure 6.7; b4). After normalization reworking stops, and the residence time of the embanked floodplain overbank sediment also increases to potentially infinity (Figure 6.7; c4). Residence times of sediments that remain in the channel are not evaluated in Figure 6.7; assuming these are dredged, their residence times within the delta are in the order of a few years.

Figure 6.7 (previous page). Schematic overview of changes in sedimentary dynamics as a result of increased human intervention. The x-axes represent the life cycle of a channel belt, and the y-axes represent the unscaled intensity of a process. The natural delta is characterised by large spatial differences, and in the panels for period A (left graphs) curves for an upper, a central, and a lower delta channel belt are sketched. In the human-influenced delta spatial differences between channel belts are smaller and the central channel belt is plotted.

6.6 Application

Many deltas in the world are threatened by flooding. This is not only caused by increased flood levels due to climate change, but also by a sediment deficit, as artificial damming in upstream courses prevent sediments to reach the delta. Hence, it is made impossible for the delta to cope with flooding threats in a natural way. Therefore, sustainable delta management must take into account sedimentary dynamics. Restoration of sedimentary dynamics requires references and benchmarks for the amounts of sediment trapped in the natural delta, and for where, when and how this sediment was trapped.

The research in this thesis provides insight into the natural sedimentary dynamics, and the changes in sedimentary dynamics caused by human activities in the Rhine delta, but can be applied to other deltas too. In the natural Rhine delta sand could be trapped by frequent formation of new channel belts after avulsions. Moreover, fine-grained suspended sediment could be trapped over the entire width of the delta. This has resulted in an average Holocene trapping rate of 800 * 10^3 m^3/a for channel sediments and 1000 * 10^3 m^3/a for overbank sediments. In the present Rhine delta less sediment is trapped, because a large part of the flood basin has been isolated by dykes. Van der Meulen et al. (2009) estimated the present overbank deposition rate of fine sediments to be 229 * 10^3 m^3/a; the remainder is deposited in the lower river channels and has to be dredged. In the Rhine-Meuse delta, present-day river management focuses on restoration of the natural dynamics of the river. Obviously, this is only partly achievable, because several economical functions have to be maintained, like maintenance of a minimal water depth for navigation, and extraction of clay, sand and gravel. Moreover, safety of the dyke-protected floodplains against flooding has to be ensured. This is threatened by aggradation of the floodplains, which reduces the discharge and storage capacity of the river and its embanked floodplains. Therefore, floodplain management strategies primarily involve enhancement of discharge capacity.

One strategy that combines enhancement of discharge and storage capacity with improvement of ecological quality of the embanked floodplains is 'cyclic floodplain rejuvenation' (CFR, Peters et al., 2006). This strategy involves a number of measures that replace natural erosion and deposition processes associated with meandering rivers. CFR includes a number of measures that lead to a form of sediment 'reworking'. Such measures include floodplain lowering by excavation, digging of secondary channels, opening levees and removal of floodplain forest. When periodically a part of the embanked floodplain is rejuvenated, then a landscape with different vegetation succession stages evolves. At the same time this periodic removal of overbank deposits or vegetation enhances the discharge capacity of the river. Baptist et al. (2004) applied a CFR model to the river Waal. They demonstrated that when about 15% of the total floodplain area is rejuvenated with a return period of 25 to 35 years, then safe flood levels will be sustained, and a diverse floodplain vegetation distribution will develop that largely complies to the historical reference for the river Waal. This area corresponds to the semi-natural lateral embanked floodplain erosion rate between 1780 and 1830 AD, which is ~0.4% of the floodplain surface per year (Wolfert, 2001). However, the volumetric erosion rate involved in CFR is considerably less: in the model of Baptist et al. (2004) the volume of removed sediment amounts 17 * 10^6 m^3, over a 50-km-long stretch along the river Waal, or 10 to 14 * 10^3 m^3/a/km, while in the semi-natural embanked Waal a volumetric erosion rate of 29 * 10^3 m^3/a/km occurred (chapter 5). Moreover, these amounts even

less resemble reworking in a natural channel belt, where amounts of eroded and deposited sediment volumes are larger. A fundamental difference is that CFR involves vertical lowering of the floodplain surface by 1 to 2 m (which in fact resembles going back in time) instead of lateral erosion of the entire floodplain sediment body as occurring in the natural floodplain shaving process.

When restoring sedimentary processes, measures should not only be applied on a regional scale, but the entire delta must be included, as regional measures can have large-scale influence on the sedimentary dynamics. Therefore, it should be considered on a large scale where the sediment is needed, where it is available, and how it gets where it is needed. An example can be found in the Mississippi delta, where wetland loss is a major problem. Wetlands are threatened by land subsidence due to compaction (Törnqvist et al., 2008) and relative sea-level rise, while the supply of sediment has been dramatically reduced due to construction of upstream reservoirs (Kesel, 1989). Restoration aims to transfer water and sediment to areas that have experienced wetland loss (Day et al., 2007). In embanked deltas with polders, however, there is little room for re-allowing floodplain sedimentation to compensate for soil subsidence. Still, local projects of re-opening polders might benefit from such knowledge.

6.7 Conclusions

Human activities have had great impact on the sedimentary dynamics in the Rhine-delta channel belts. In the Rhine delta, a wide range of human activities was carried out in the past millennium, of which river embankment and channel normalization had dramatic impacts on the sedimentary dynamics of the delta. To quantify these impacts, this study reconstructed and compared the sedimentary dynamics within the life cycle of a channel belt for the natural delta, and for two periods of increased human impact.

Determination of sedimentary dynamics not only requires age determination, and sediment budgeting over discrete time slices, but also estimation of deposition *rates*. In addition to using different dating methods over different time scales, this also requires modelling of lateral erosion and vertical accretion rates. Of the dating methods used in this study, OSL dating has the largest range of application, and this range is now extended to young fluvial deposits by a novel method that accounts for incomplete bleaching.

The life cycle of a natural channel belt can be subdivided into four stages in which, respectively, incision, building, reworking and infilling takes place. There are fundamental differences in sedimentary dynamics between these stages. The avulsion stage involves erosion of older floodplain sediments. Subsequently, a channel-belt building stage occurs, in which older floodbasin sediments are replaced by channel-belt sand, and in which overbank deposition occurs. When the channel has shifted one meander length in a downstream direction, it starts to rework its previously deposited sediments. Replacement of older floodbasin sediment by new channel-belt sand then stops, while overbank deposition continues. Finally, after abandonment of the channel, active overbank deposition stops, and the channel gradually fills up with increasingly finer material.

River embankment and channel straightening dramatically changed the occurrence, duration and sedimentary dynamics of these stages:

- Natural delta channels experience all four stages, while their sedimentary dynamics show large spatial and temporal variations across the delta. Channel belts in the central parts of the delta are most capable of trapping new channel-bed sediment, which occurs during the channel-belt building stage. Total bedload trapping within the entire delta also depends on the number of active channels, and the length of these channels. Hence, bedload trapping in a delta is most efficient when avulsions take place frequently, and occur in the central part of the delta, shortly after channels have completed the channel-belt building stage. Oppositely, overbank deposition occurs in a more uniform way, both during channel-belt stages (temporally) and within a delta (spatially).
- Embankment causes strong reduction of sedimentary dynamics. Its spatial dimension reduces because dykes exclude the majority of the floodplain from erosion and deposition processes, and its temporal dimension reduces because life-cycle stages are eliminated, and only the reworking stage continues to exist. However, reworking rates are smaller than they would have been in a natural situation, because the channel belt is laterally less extended. Moreover, the magnitude of erosional processes decreases with time, because floodplains are often protected against lateral erosion, while deposition continues. Embankment accelerates vertical aggradation of fine-grained overbank sediments. When embanked floodplains are intensively being reworked, sediment residence times are short, resulting in a small net storage of overbank sediments. However, when humans prevent lateral bank erosion and support lateral accretion, the floodplain area increases, resulting in longer residence times.
- Normalization causes further reduction of sedimentary dynamics. All stages cease to exist, and a new type of stage emerges: the *fixed channel* stage, in which overbank deposition is dominant. Sand deposition becomes reduced to local overbank deposition directly bordering the main channel during major flood events. In the absence of lateral channel bank erosion, overbank sediments continue to accumulate on the floodplain, with gradually decreasing rates.

Insight into the changing sedimentary dynamics is essential for evaluation of the potential effect of delta and river restoration measures. The amounts of overbank sediments removed in cyclic floodplain rejuvenation (CFR), a new floodplain management strategy which is promoted for the embanked floodplains in the Netherlands, are substantially smaller than those associated with downstream migration processes in the semi-natural embanked equivalent river. Moreover, CFR involves vertical lowering of the floodplain surface instead of lateral erosion of the entire floodplain sediment body as occurring in the natural floodplain shaving process.

Summary

Chapter 1. General introduction

Human activities have increased the vulnerability of deltas to flooding. Anthropogenic influence on global warming has caused a global eustatic sea-level rise, while excessive land drainage and extraction of oil, natural gas and water have caused subsidence of deltas. Moreover, human engineering has dramatically limited the natural mechanisms for delta aggradation: upstream sediment trapping in reservoirs has reduced the amounts of sediment reaching deltas, and artificial levee building of river distributaries has isolated large parts of deltas from sediment input and deposition. Present-day river management focuses therefore on flood protection and restoration of the natural sedimentary dynamics in rivers. Sedimentary dynamics is defined as the whole of processes that involve erosion, transport and deposition of sediment in a river – including its floodplain – across a range of spatial and temporal scales. Evaluation of the potential effects of restoration measures requires tools to predict their morphodynamic and ecological effects, and raises the need to define references and benchmarks for these effects. This requires insight into and understanding of the natural sedimentary dynamics within deltas, and how these have been affected by past human activities.

The main objective of this study was to investigate the increased anthropogenic influence – mainly embanking, straightening and stabilisation of the channel – on the channel-belt sedimentary dynamics in the Rhine delta (chapter 6). To make this investigation, the sedimentary dynamics during the life cycle of a channel belt were reconstructed for three key periods of increasing human impact, which are: (A) the pristine delta (chapter 5), (B) the period after embankment (chapter 4), and (C) the recent situation after channelization (chapter 3). Reconstruction of the sedimentary dynamics required detailed lithogenetic and chronological data. One method that was used to collect chronological data is Optically Stimulated Luminescence (OSL) dating, and a secondary objective was to optimize this method for dating of young fluvial deposits (chapter 2). Specific research objectives were:

- To develop a protocol to improve of OSL dating of young fluvial deposits.
- To quantify for the pristine delta, and the two periods of increased human impact, within-channel-belt volumetric erosion and deposition rates, and hence to determine variations in storage, reworking and throughput during the life cycle of a single channel belt.
- To assess the impact of major human interventions in the river system on storage, throughput and reworking of sediments.

Chapter 2. Sedimentation rates on embanked floodplains determined through quartz optical dating

Quartz grains in fluvial sediments that are deposited in a channel belt become buried and shielded from sunlight by overlying sediments. Due to exposure to natural ionizing radiation

of the surrounding sediment, charge is trapped inside the quartz crystal. This charge accumulates over time and gives rise to a luminescence signal that provides a measure for burial time. Application of OSL dating to young fluvial deposits is challenging because limited light exposure of the grains during fluvial transport may cause age overestimation: under subdued light conditions in turbid river water the OSL signal may be reset incompletely, and any remaining signal at the time of deposition causes an age offset. This effect will be relatively large for younger samples.

To improve OSL dating for young fluvial deposits, a modified Single-Aliquot Regenerative dose (SAR) protocol was developed, and applied on a suite of samples from an embanked floodplain of the river Waal near Neerijnen. In the newly developed protocol, any poorly bleached signal was minimized by improved isolation of the most light-sensitive component (fast component) of the signal by subtracting the early background (slow and medium component) from the initial signal. Moreover, to avoid transfer of charge from light insensitive traps to the OSL trap used for dating (thermal transfer), a low preheat temperature was applied. To eliminate an unstable (ultrafast) component that remains present in the signal after low preheat temperatures, samples were briefly exposured to infrared light prior to OSL-measurement. Finally, the dose distribution of a set of subsamples was plotted as a probability density function, to which two Gaussian peaks were fitted, of which the lower peak represents the set of subsamples for which the OSL signal was completely reset at deposition. Based on internal controls (internal consistency, negligible age offset) and external controls (age constraints and comparison with other dating methods), it was concluded that there was no evidence for large systematic offsets in the OSL ages, and that the OSL-dating method can be applied on a wide range of spatial and temporal scales to derive chronological data of fluvial sediments.

Chapter 3. Reconstruction of floodplain sedimentation rates: a combination of methods to optimize estimates

The present-day lower Rhine branches in the Netherlands have been laterally fixed by groynes since the end of the 19th century. Consequently, no lateral channel accretion or erosion processes have occurred since then, and vertical accretion is presently the dominant natural sedimentary process in the embanked floodplains. Vertical overbank accretion rates were estimated using four independent reconstruction methods, applied at three different floodplain sections: (1) chronostratigraphic interpretation of flood layers, which involves a correlation of individual layers to peak flow events in the discharge record, (2) ^{137}Cs-dating, which relies on correlation of ^{137}Cs peaks in a vertical sediment profile to years with peak deposition of ^{137}Cs, (3) heavy metal analyses, in which varying metal contents in a vertical sediment profile are correlated with the known pollution history of the river, and (4) optically stimulated luminescence (OSL) dating, which uses the accumulated charge that is trapped in sand-sized quartz grains that are shielded from the light to determine the time of deposition and burial.

Vertical accretion rates found on the floodplains vary between 2-7 mm/a in the distal zones, and 3-9 mm/a in the proximal zones. On a rapidly developing sand bar along a natural

levee sedimentation rates of 9-25 mm/a were found. Except for some minor inconsistencies in ^{137}Cs dating results, all methods show decreasing sedimentation rates with increasing distance from the river channel. Intercomparison of the results of the different dating methods revealed the potential errors associated with each method. Still, the results are generally in good agreement. The optimal spatial and temporal ranges of application for each method differed, depending on sediment texture and sedimentation rate, but showed significant overlap. Flood layer interpretation is only applicable close to the river, where individual flood layers can be recognized. ^{137}Cs dating yields best results on the natural levee and proximal parts of the embanked floodplain, where sedimentation rates are sufficiently high to distinguish between the peaks of 1960 and 1986 AD. Heavy metal analysis is best applicable in the distal parts, where fine grained sediments to which heavy metals are bound are deposited. Finally, OSL dating used in sandy natural levee deposits can date sediments well beyond the century scale. A combination of the methods will thus provide maximum information for accurate estimation of sedimentation rates on a decadal time scale.

Chapter 4. Reconstruction of eroded and deposited sediment volumes of the embanked River Waal, the Netherlands, for the period AD 1631–present

In the semi-natural embanked but still dynamic river Waal, embanked floodplains were formed by downstream migration of meander bends between confining dykes. This process resulted in a sequence of successively developed sand bars, separated by concave swales, and topped by fine-grained overbank sediments. To calculate the vertical and lateral accretion rates and the lateral erosion rates that were involved with this downstream migration, the floodplains were modelled as an architecture of 'building blocks' of uniform lithogenetic composition, representing sand bars, concave swales or overbank tops. The boundaries between blocks were determined by interpretation of a series of historical maps and lithogenetic cross-sections. Chronostratigraphy within the blocks was estimated by interpretation of heavy metal profiles and from optically stimulated luminescence (OSL) dating results. Volumetric changes were hence calculated as a change of volume of each building block between time steps.

Novel results were a series of volumetric erosion and deposition rates for ~50-year time slices between the early 17th century and the late 19th century. Changes of these rates in time were then related to human interventions carried out. The amount of lateral accretion initially increased, as a result of island and sand bar formation following embankment. From the 18th century onwards, there was a decrease of lateral processes in time, which was a result of straightening of the river by human activities, and a reduction of water and sediment supply due to the construction of a new upstream bifurcation. With straightening of the river, the floodplain area grew. Artificial fixation of the channel banks after 1872 AD prevented lateral activity, leaving overbank deposition as the main process in sedimentary dynamics.

Chapter 5. Decadal to century-scale sediment dynamics in channel belts of the natural Rhine delta

In the natural Rhine-delta, new channels were frequently formed by avulsion. These new channels often developed a new channel belt through meandering, thereby eroding floodbasin material from earlier channel belts, while trapping sand in point bar complexes. In this chapter the sediment budget of the natural Hennisdijk channel belt in the central part of the delta was calculated. Detailed lithological cross-sections and geological maps of the preserved channel belt and overbank deposits were used to quantify net sediment volumes that had accumulated during the channel belt's entire lifetime. Radiocarbon dates provided the ages of the start and end of sedimentation, and hence the life time of the channel. To determine the variations within the life cycle of a natural channel, this cycle was divided into four stages: avulsion stage (Av), in which the channel is formed; channel-belt-building stage (S1), in which floodbasin material is eroded and replaced by channel sand; channel-belt-reworking stage (S2), in which the river's own sediment is reworked; and abandonment stage (Ab), in which the channel gradually fills up. For the main stages (S1 and S2), volumetric erosion and deposition rates were calculated using the Bank Stability and Toe Erosion Model (BSTEM).

The results show that, due to the high resistance to erosion of the floodbasin material, meander migration rates were initially low, in the order of 0.1 m/a. When the channel incised into the sandy Pleistocene subsurface, the meander migration rate increased rapidly, reaching rates of 3-3.5 m/a by the end of S1. Bank erosion rates in the reworking stage S2 remained more or less constant, and were about ~4-4.5 m/a. Furthermore, spatial differences in channel-belt sediment dynamics within the delta were explored. Meander migration rates, and hence the duration of each stage, are mainly controlled by the thickness of the cohesive floodbasin deposits and the proportion of peat in the floodbasin sedimentary succession, which both increase from delta apex to coastal zone. Hence, in the upstream part of the delta meander migration rates are high, and S1 rapidly switches to S2. In the downstream area the thick cohesive floodbasin deposits with erosion-resistant peat beds cause low meander migration rates, so that S1 takes a long time and S2 might not be reached within the channel's lifetime.

Chapter 6. Changing sedimentary dynamics under increasing human influence (synthesis and conclusion)

In this chapter, results obtained in this study for the three periods were combined with those from previous studies. All results were placed in a chronological framework, in order to assess the impact of major human interventions on the sedimentary dynamics within delta channels. Thereby, a distinction was made between channel sediments and overbank sediments.

In the natural Holocene delta, trapping of sandy channel sediments has been very variable in space and time, due to the formation of new channel belts by repeated avulsion. However, the channel-belt trapping efficiency varied greatly among different channels, depending on length, duration of activity, and location within the delta. As channel sediments were mainly trapped in the channel-belt-building stage – in which floodbasin material is eroded and replaced by sand – sediment trapping was most efficient in the central delta, where the

presence of the sandy Pleistocene sediments in the banks enabled sufficiently high bank retreat rates, and where a thick-enough cover of floodbasin deposits existed to become replaced by sand. After embankment of the rivers by humans, no new channels formed anymore. The existing channels remained in their reworking stage, in which erosion and deposition rates were high, but where net trapping of channel sediment was nil. After normalization reworking stopped, and sand is now only deposited as overbank material on a limited area near the channel edge during major flood events.

Trapping of overbank deposits has been less variable during the life cycles of a channel belt. In a natural channel belt overbank fines were largely deposited far away from the erosive action of the channel, resulting in relatively long residence times. In contrast, after embankment, deposition became limited to a relatively small embanked floodplain between dykes. These embanked floodplains were reworked, and overbank sediments now were part of this reworking cycle, resulting in short residence times. When lateral activity stopped, erosion stopped, but overbank deposition has continued. However, along with rising floodplain elevation overbank deposition rates have decreased. Potential residence times within the present-day embanked floodplains are infinite - because erosion stopped – except when clay is excavated for brick production, dike enforcing or nature restoration projects. The fines that are not deposited on the floodplains settle in the lower estuary, where they have to be dredged; this sediment resides less than a year in the delta.

Insight into the changing sedimentary dynamics of channel and overbank sediments is essential for adequate river and floodplain management in the Rhine delta, but also in other deltas in the world. In the first place, it helps understanding to what extent earlier human interference and engineering measures have changed the natural sedimentary dynamics that have built our modern deltas. Furthermore, deltas that suffer from serious sediment starvation due to upstream reservoir trapping require a careful management of the remaining material to prevent a delta from rapid drowning. And finally, regional restoration measures may have large-scale impact on sedimentary dynamics within a delta. Hence, this insight is of crucial importance to provide references and benchmarks, and to predict direct and long-term morphodynamic effects of the measures.

Samenvatting

Hoofdstuk 1. Algemene inleiding

Als gevolg van menselijke activiteiten is het overstromingsrisico in delta's sterk toegenomen. De antropogene opwarming van de aarde heeft een eustatische zeespiegelstijging teweeg gebracht, terwijl drainage en de winning van grondstoffen als olie en gas juist een bodemdaling hebben veroorzaakt. Door het aanleggen van diverse constructies is de delta bovendien niet meer in staat om de bodemdaling op een natuurlijke manier te compenseren: bovenstrooms wordt het sediment vaak vastgehouden in reservoirs, en benedenstrooms heeft de aanleg van dijken ervoor gezorgd dat een groot gedeelte van de delta buiten het bereik van riviersedimentatie ligt. Het huidige deltabeheer is gericht op de bescherming tegen overstromingen, en op het herstellen van de natuurlijke sedimentatiedynamiek in de rivieren. Sedimentatiedynamiek wordt gedefinieerd als het geheel aan erosie-, transport- en depositieprocessen van sediment in de rivieren en op de overstromingsvlakten, op verschillende tijd- en ruimteschalen. Om het effect van herstelmaatregelen te kunnen beoordelen, is het noodzakelijk dat men de morfodynamische en ecologische effecten van deze maatregelen kan voorspellen. Ook zullen er natuurlijke referentiekaders geschetst moeten worden. Inzicht in en begrip van de sedimentatiedynamiek in natuurlijke delta's, en in toenemende mate door de mens beïnvloede delta's, is hiervoor van essentieel belang.

Het hoofddoel van dit onderzoek was om de toegenomen antropogene invloed – met name het bedijken, rechttrekken en stabiliseren van de rivierbedding – op de sedimentatiedynamiek in de rivieren en de riviervlakten van de Rijndelta vast te stellen. Om dit te onderzoeken is de sedimentatiedynamiek binnen de levensduur van een rivier gereconstrueerd voor drie verschillende situaties van antropogene invloed: (A) de natuurlijke delta, (B) de delta met bedijkte rivieren, en (C) de delta met door kribben vastgelegde rivieren. Om de sedimentatiedynamiek te kunnen reconstrueren zijn gedetailleerde lithogenetische en chronologische gegevens nodig. Een methode die gebruikt kan worden om chronologische gegevens te verkrijgen is 'optisch gestimuleerde luminescentiedatering' (OSL-datering). Een tweede doel was om de toepassing van deze methode op jonge rivierafzettingen te optimaliseren. Specifieke doelen waren:

- Een protocol ontwikkelen om OSL-dateren van jonge rivierafzettingen te verbeteren.
- Voor elk van de genoemde perioden de volumetrische erosie- en sedimentatiesnelheden binnen een stroomgordel kwantificeren, en vervolgens daarmee de variaties in de opslag, doorvoer en herwerking van het sediment binnen de levenscyclus van een individuele rivier vaststellen.
- Het effect van enkele grote menselijke ingrepen in het riviersysteem op de opslag, de doorvoer en het herwerken van sedimenten in de delta beoordelen.

Hoofdstuk 2. Sedimentatiesnelheden in de uiterwaarden bepaald door het OSL-dateren van zandkorrels

Zandkorrels die in een stroomgordel worden afgezet, raken bedekt met jongere sedimenten, en ontvangen daardoor geen zonlicht meer. De kwartskorrels in het zand absorberen radioactieve straling vanuit de omgeving, en bouwen zo een luminescentiesignaal op. Zolang deze korrels niet worden blootgesteld aan licht, wordt dit signaal steeds groter. Door in het laboratorium de grootte van het luminescentiesignaal en het tempo waarmee het signaal is opgebouwd te meten (OSL-dateren), kan het moment van afzetting en begraving berekend worden. De toepassing van deze dateringsmethode op jonge rivierafzettingen brengt echter wat problemen met zich mee. In het troebele rivierwater worden de zandkorrels slechts beperkt blootgesteld aan zonlicht, zodat het signaal bij afzetting mogelijk niet helemaal op nul gezet (gebleekt) is. Hierdoor kan een overschatting van de ouderdom ontstaan, die relatief groot is voor jonge sedimenten.

Om het OSL-dateren van jonge rivierafzettingen te verbeteren, is in dit onderzoek een bestaand protocol (het zogenoemde 'Single-Aliquot Regenerative dose' protocol) aangepast om geschikt te maken voor deze afzettingen, en toegepast op een set monsters uit de uiterwaarden van de Waal bij Neerijnen. Het nieuwe protocol bevat vier stappen om overschatting van de ouderdom te voorkomen. Ten eerste is het aandeel van slecht gebleekte korrels geminimaliseerd door zoveel mogelijk de meest lichtgevoelige component van het signaal (snelle OSL-component) te gebruiken. Dit is gedaan door de bijdrage van minder lichtgevoelige componenten (langzame en gemiddelde OSL-componenten) van het totale signaal af te trekken. Om te voorkomen dat er signaal vanuit de niet-lichtgevoelige component naar de componenten die voor OSL-dateren gebruikt zijn wordt overgeheveld (thermische overheveling), is een relatief lage voorverwarmingstemperatuur gebruikt. Deze voorverwarming is nodig om signalen die langzaam in de natuur worden opgebouwd te kunnen vergelijken met signalen die in het lab worden opgewekt. Door het gebruik van deze lage temperaturen blijft er echter een onstabiele, ultrasnelle component achter. Deze is geëlimineerd door de monsters, voordat de OSL-meting plaatsvond, kort bloot te stellen aan infrarood licht. Tenslotte zijn de resultaten van een aantal submonsters in een 'probability density'-grafiek geplot. Hierin zijn twee Gaussische functies geplot, waarvan de lage piek de submonsters voorstelt die compleet gebleekt zijn afgezet.

Op basis van interne controles (interne consistentie, slechts kleine afwijkingen in ouderdom) en externe controles (onafhankelijke ouderdomsinformatie) kon worden geconcludeerd dat het nieuwe protocol geen systematische afwijkingen in OSL-ouderdommen oplevert, en dat OSL-dateren een bruikbare methode is om chronologische data van riviersedimenten te verzamelen, over een groot temporeel bereik.

Hoofdstuk 3. Reconstructie van sedimentatiesnelheden in uiterwaarden: een combinatie van methoden om de resultaten te optimaliseren

Aan het eind van de 19e eeuw zijn de Nederlandse Rijntakken volledig vastgelegd met kribben. Als gevolg hiervan zijn laterale erosie- en depositieprocessen gestopt, en is verticale opslibbing van de uiterwaarden het dominante depositieproces geworden. In dit hoofdstuk zijn deze verticale opslibbingssnelheden berekend met behulp van vier verschillende reconstructiemethoden, die zijn toegepast op drie verschillende uiterwaarden. Deze methoden zijn: (1) chronostratigrafische interpretatie van overstromingslaagjes, waarbij individuele laagjes van grof sediment worden gecorreleerd met pieken in de afvoergrafiek, (2) ^{137}Cs-datering, waarbij gemeten ^{137}Cs-pieken in een verticaal sedimentprofiel worden gecorreleerd met de jaren waarin de neerslag van ^{137}Cs maximaal was (1960 en 1986 AD), (3) zwaremetalenanalyse, waarbij variaties in zwaremetalengehalte in een verticaal sedimentprofiel worden gecorreleerd met de bekende vervuilingsgeschiedenis van de Rijn, en (4) optisch gestimuleerde luminescentiedatering (OSL-datering), waarbij het luminescentiesignaal dat wordt opgebouwd in kwartskorrels, wanneer deze door andere sedimenten bedekt raken, wordt gebruikt om de ouderdom van de afzetting te berekenen.

De verticale opslibbingssnelheden die gevonden zijn variëren van 2 tot 7 mm/jaar in de distale delen, en van 3 tot 9 mm/jaar in de proximale delen van de uiterwaarden. Op een zandbank vlak naast de rivier werden zelfs snelheden van 9 tot 25 mm/jaar gevonden. Op wat kleine tegenstrijdigheden in de ^{137}Cs-resultaten na, laten alle methoden zien dat de sedimentatiesnelheid afneemt naarmate de afstand tot de rivier toeneemt. Door onderlinge vergelijking van de verschillende methoden konden de potentiële fouten die elke methode met zich meebrengt in beeld worden gebracht. De resultaten zijn over het algemeen goed in overeenstemming. Het optimale bereik per methode verschilt zowel ruimtelijk als temporeel, afhankelijk van de textuur van het sediment en de depositiesnelheid, maar er is ook een aanzienlijke overlap. Chronostratigrafische interpretatie van overstromingslaagjes kan alleen dicht bij de rivier gebruikt worden, omdat alleen daar individuele overstromingslaagjes onderscheiden kunnen worden. ^{137}Cs-datering levert het beste resultaat op in de oeverwallen en in de proximale delen, waar sedimentatiesnelheden groot genoeg zijn om de twee piekjaren in ^{137}Cs-neerslag te kunnen onderscheiden. Zwaremetalenanalyse is daarentegen het best bruikbaar in de distale delen, waar het fijnere sediment waaraan zware metalen zich binden wordt afgezet. OSL-dateren is tenslotte het best toe te passen in zandige oeverafzettingen, en heeft verreweg het grootste temporele bereik. Een combinatie van de verschillende methoden zal daarom de meeste informatie opleveren wanneer sedimentatiesnelheden op de decenniaschaal berekend moeten worden.

Hoofdstuk 4. Reconstructie van geërodeerde en gedeponeerde sedimentvolumes in de bedijkte Waal-stroomgordel, in de periode 1631 AD – heden

In de seminatuurlijke – bedijkte, maar toch dynamische – Waal werden uiterwaarden gevormd door het stroomafwaarts migreren van meanderbochten in de beperkte ruimte tussen de dijken. Het migratieproces heeft geresulteerd in een aaneenschakeling van zandbanken, die van elkaar waren gescheiden door concave kronkelwaardgeulen, en die bedekt raakten met een laag fijne oever- en komafzettingen. In dit hoofdstuk zijn de laterale erosievolumes en de verticale en laterale depositievolumes berekend, die gepaard gaan met het proces van stroomafwaartse migratie. Daarvoor zijn de uiterwaarden opgedeeld in 'bouwstenen' van uniforme lithogenetische samenstelling, die elk een zandbank, een kronkelwaardgeul, of een laag oever- en komafzettingen vertegenwoordigen. De grenzen van deze bouwstenen zijn bepaald aan de hand van een reeks historische kaarten en lithologische dwarsprofielen. De chronostratigrafie binnen een blok is geschat met behulp van zwaremetalenprofielen en OSL-dateringen, waarmee vervolgens horizontale en verticale tijdslijnen binnen een bouwsteen zijn geschat. De erosie- en depositievolumes zijn berekend uit het verschil tussen twee opeenvolgende tijdslijnen.

Het resultaat bestaat uit een reeks volumetrische erosie- en depositiesnelheden voor tijdstappen van ~50 jaar, van begin 17^{e} eeuw tot heden. De veranderingen die hierin te zien zijn, zijn vervolgens gerelateerd aan menselijke interventies in de delta. In het begin van de bestuurde periode neemt de hoeveelheid laterale depositie iets toe, wat een gevolg is van de vorming van eilanden en zandbanken na de bedijking. Vanaf de 18^{e} eeuw neemt de intensiteit van de laterale processen echter af, vanwege het rechttrekken van de rivier door de mens en de afname van de toevoer van water en sediment door de aanleg van het Pannerdensch Kanaal. Door het rechttrekken van de rivieren is het oppervlak aan uiterwaarden toegenomen. Nadat rond 1872 AD de rivieren volledig zijn vastgelegd door kribben is de laterale activiteit helemaal verdwenen en is verticale uiterwaardafzetting het belangrijkste sedimentaire proces.

Hoofdstuk 5. Sedimentatiedynamiek van natuurlijke rivieren in de Rijndelta, op een tijdschaal van decennia tot eeuwen

In de natuurlijke Rijndelta werden, als gevolg van avulsies, regelmatig nieuwe geulen gevormd. Vaak groeiden deze geulen uit tot een nieuwe stroomgordel, waarbij ze als gevolg van meanderprocessen fijn sediment van oude komafzettingen in de ondergrond erodeerden, en grof sediment invingen in kronkelwaarden. In dit hoofdstuk is het sedimentbudget van de natuurlijke Hennisdijkse stroomgordel berekend, welke is gelegen in het centrale deel van de delta. Met behulp van gedetailleerde lithologische dwarsprofielen en geologische kaarten van restanten van de stroomgordel konden de netto sedimentvolumes in de stroomgordel worden gekwantificeerd. ^{14}C-dateringen zijn gebruikt om de ouderdommen van het begin en eind van sedimentatie, en dus de levensduur van de stroomgordel, te schatten. Om de variaties binnen de levenscyclus van een natuurlijke stroomgordel te kunnen analyseren is deze levenscyclus

onderverdeeld in vier fasen: De avulsiefase (Av), waarin de geul wordt gevormd; de opbouwfase (S1), waarin de oude komafzettingen worden geërodeerd, en vervangen wordt door zand; de herwerkingsfase (S2), waarin de rivier zijn eigen sediment herwerkt; en de verlatingsfase (Ab), waarin de geul langzaam weer opgevuld wordt met sediment. Voor de hoofdfases (S1 en S2) zijn volumetrische erosie- en depositiesnelheden berekend met behulp van het 'Bank Stability and Toe Erosion Model' (BSTEM).

De resultaten laten zien dat de migratiesnelheden van meanderbochten initieel laag zijn, namelijk in de orde van grootte van 0.1 m/jaar. Dit is het gevolg van de aanwezigheid van cohesieve komafzettingen in de oevers. Als de geul echter door insnijding de zandige pleistocene ondergrond bereikt, nemen de migratiesnelheden snel toe, en aan het einde van fase S1 bedragen deze 3 – 3.5 m/jaar. In de herwerkingsfase S2 is de oevererosie min of meer constant geworden, namelijk ~4 – 4.5 m/jaar. Daarnaast zijn ook de ruimtelijke verschillen binnen de gehele delta verkend. De migratiesnelheid van een meanderbocht en duur van fase S1 zijn vooral afhankelijk van de dikte van de laag cohesieve komafzettingen, en de hoeveelheid zeer erosieresistent veen in het sedimentpakket, welke beide toenemen vanaf de delta-apex (het meest stroomopwaartse punt van de delta) naar het kustgebied. Daarom zijn in het bovenstroomse gedeelte van de delta migratiesnelheden van meanderbochten hoog, en gaat fase S1 snel over in fase S2. In de benedenstroomse delta zorgt het dikke pakket cohesieve komafzettingen, afgewisseld met erosieresistente veenlagen, voor lage migratiesnelheden van meanderbochten. Fase S1 duurt hier aanzienlijk langer, en fase S2 wordt vaak niet eens bereikt binnen de levensduur van een stroomgordel.

Hoofdstuk 6. Veranderingen in sedimentatiedynamiek onder toenemende invloed van de mens (synthese en conclusie)

In dit laatste hoofdstuk zijn de resultaten van de verschillende perioden uit deze studie gecombineerd met resultaten uit eerdere studies. Alle resultaten zijn in een chronologisch kader geplaatst, om zo de invloed van de mens op de sedimentatiedynamiek in delta's te evalueren. Hierbij is onderscheid gemaakt tussen enerzijds beddingsediment en anderzijds oever- en komafzettingen.

Als gevolg van het herhaaldelijk optreden van avulsies is het invangen van zand in de natuurlijke Holocene delta in zowel tijd als ruimte erg variabel geweest. De invangcapaciteit verschilde bovendien per stroomgordel, en was afhankelijk van de lengte en de levensduur van de rivier, en van zijn locatie in de delta. Beddingzand werd voornamelijk ingevangen tijdens de opbouwfase, waarin komafzettingen (klei en veen) werden vervangen door beddingzand. De invang van zand was daarom het meest efficiënt in de centrale delta, waar enerzijds de aanwezigheid van pleistoceen zand in de ondergrond aanzienlijke oevererosiesnelheden veroorzaakte, en waar anderzijds voldoende komafzettingen aanwezig waren om door het zand te worden vervangen. Nadat de rivieren werden bedijkt, zijn er geen nieuwe avulsies meer opgetreden en dus geen nieuwe rivieren ontstaan. De bestaande rivieren bleven in de herwerkingsfase, waarin erosie- en depositiesnelheden hoog zijn, maar waarin nauwelijks netto zand wordt ingevangen. Na de normalisatie is ook het herwerken gestopt, en

sindsdien wordt er alleen maar zand afgezet tijdens extreme hoogwaters, op de oevers nabij de geul.

De invang van oever- en komafzettingen gedurende de levenscyclus van een rivier is veel minder variabel geweest dan die van beddingzand. In een natuurlijke riviervlakte werd fijn suspensief materiaal tot op grote afstanden van de rivier afgezet, buiten het erosieve bereik van de rivier. De verblijftijd van dit sediment was relatief lang. Na de bedijking werd de zone waar de rivier sediment kwijt kon sterk gereduceerd, en kon het alleen in de uiterwaarden worden afgezet. Omdat deze uiterwaarden geheel werden herwerkt door laterale migratie van de rivier, werd ook het fijne, vanuit suspensie afgezette, materiaal weer geërodeerd en namen de verblijftijden van dit sediment sterk af. Na normalisatie stopte laterale activiteit, en nu vindt er voornamelijk verticale opslibbing in de uiterwaarden plaats, die door een toenemende hoogte van het uiterwaardoppervlak steeds minder snel gaat. Door afwezigheid van erosie zijn de potentiële verblijftijden van het sediment in de huidige uiterwaarden oneindig, behalve wanneer klei wordt gewonnen voor de productie van bakstenen, voor dijkversterking, of voor natuurherstel. Het fijne sediment dat niet in de uiterwaarden wordt afgezet bezinkt in de estuaria, waar het gebaggerd moet worden; dit sediment verblijft vaak niet langer dan een jaar in de delta.

Inzicht in de veranderende sedimentatiedynamiek is van essentieel belang voor een adequaat rivierbeheer in de Rijndelta, maar ook in andere delta's over de hele wereld. In de eerste plaats is het van belang om inzicht te krijgen in de mate waarin het menselijk ingrijpen in de delta de natuurlijke sedimentatiedynamiek heeft veranderd. Daarnaast zijn er veel delta's met een aanzienlijk sedimenttekort als gevolg van het bovenstrooms vasthouden van sediment in reservoirs, zodat een zorgvuldig beheer van het overgebleven sediment nodig is. Tenslotte hebben lokale herstelmaatregelen een grote invloed op de rest van de delta. Inzicht in de sedimentatiedynamiek van cruciaal belang om natuurlijke referentiekaders te schetsen, en om langetermijneffecten van de maatregelen op morfodynamiek en ecologie in te schatten.

References

Aitken, M.J., 1985. Thermoluminescene dating. Academic Press, London.

Almgren S., M. Isaksson, 2006. Vertical migration studies of ^{137}Cs from nuclear weapons fallout and the Chernobyl accident. *Journal of Environmental Radioactivity* 91: 90-102.

Arnold L.J., R.G. Roberts, R.F. Galbraith, S.B. DeLong, 2009. A revised burial dose estimation procedure for optical dating of young and modern-age sediments. *Quaternary Geochronology* 4: 306-325.

Asselman N.E.M., H. Middelkoop, 1998. Temporal variability of contemporary floodplain sedimentation in the Rhine-Meuse delta, The Netherlands. *Earth Surface Processes and Landforms* 23: 595-609.

Asselman N.E.M., 1999. Suspended sediment dynamics in a large drainage basing: The River Rhine. *Hydrological processes* 13: 1437-1450.

Asselman, N.E.M., M. Van Wijngaarden, 2002. Development and application of a 1D floodplain sedimentation model for the River Rhine in the Netherlands. *Journal of Hydrology* 268: 127-142.

Auerbach, L.W., S.L. Goodbred Jr, D.R. Mondal, C.A. Wilson, K.R. Ahmed, K. Roy, M.S. Steckler, C. Small, J.M. Gilligan, B.A. Ackerly, 2015. Flood risk of natural and embanked landscapes on the Ganges–Brahmaputra tidal delta plain. *Nature Climate Change* 5: 153-157.

Ballarini M., J. Wallinga, A.G. Wintle, A.J.J. Bos, 2007. A modified SAR protocol for optical dating of individual grains from young quartz samples. *Radiation Measurements* 42: 360-369.

Baptist, M.J., W.E. Penning, H. Duel, A.J.M. Smits, G.W. Geerling, G.E.M. van der Lee, J.S.L. van Alphen, 2004. Assessment of the effects of cyclic floodplain rejuvenation on flood level and biodiversity along the River Rhine. *River research and applications* 20: 285-297.

Beets, D.J., A.J.F. van der Spek, 2000. The Holocene evolution of the barrier and the back-barrier basins of Belgium and The Netherlands as a function of late Weichselian morphology, relative sea-level rise and sediment supply. *Geologie en Mijnbouw / Netherlands Journal of Geosciences* 79(1): 3-16.

Beijerinck A., M. Beijerinck, 1773. Kaart van alle de Buyte Landen des Kerspels Hien en Buertschap Wely, mitsgaders den Doodeweerdse Schaardijk, alle gelegen in het Ampt van Nederbetuwe onder het Nijmeegse Quartier. *Rijksarchief Gelderland*, algemene kaarten verzameling 18.

Beijerinck M., W. Beijericnk, 1778. Kaarten van de metinge der buitenlanden in den Ampte van Nederbetuwe. Atlas mat 6 kaarten, blad 1: Hien-Wely-Doodeweerd, blad 2: Doodeweerd-Ochten, blad 3: IJzendoorn-Echteld. *Rijksarchief Gelderland*, algemene kaarten verzameling 18.

Berendsen, H.J.A., 1998. Birds-Eye View of the Rhine-Meuse Delta (The Netherlands). *Journal of Coastal Research* 14(3): 740-752.

Berendsen, H.J.A., E. Stouthamer, 2000. Late Weichselian and Holocene palaeogeography of the Rhine–Meuse delta, The Netherlands. *Palaeogeography, Palaeoclimatology, Palaeoecology* 161: 311–335.

Berendsen H.J.A., E. Stouthamer, 2001. Palaeogeographic development of the Rhine-Meuse delta, The Netherlands, Assen: Koninklijke Van Gorcum, 268 pp.

Bird, G., P.A. Brewer, M.G. Macklin, M. Nikolova, T. Kotsev, M. Mollov, C. Swain, 2010. Dispersal of Contaminant Metals in the Mining-Affected Danube and Maritsa Drainage Basins, Bulgaria, Eastern Europe. *Water Air and Soil Pollution*. 206: 105–127.

Blum, M.D., T.E. Törnqvist, 2000. Fluvial responses to climate and sea-level change: a review and look forward. *Sedimentology* 47(1): 2-48.

Bolla Pittaluga, M., R. Repetto, M. Tubino, 2003. Channel bifurcation in braided rivers: Equilibrium configurations and stability. *Water Resources Research* 39(3): 1046.

Bos, I.J., H. Feiken, F. Bunnik, J. Schokker, 2009. Influence of organics and clastic lake fills on distributary channel processes in the distal Rhine–Meuse delta (The Netherlands). *Palaeogeography, Palaeoclimatology, Palaeoecology* 284: 355–374.

Bøtter-Jensen, L., E. Bulur, G.A.T. Duller, A.S. Murray, 2000. Advances in luminescence instrument systems. *Radiation Measurements* 32: 57-73.

Brewer, P.A., D.G. Passmore, 2002. Sediment budgeting techniques in gravel-bed rivers. *Geological Society London Special Publication* 191: 97-113.

Bronk Ramsey C,. 2008. Deposition models for chronological records. *Quaternary Science Reviews* 27: 42–60.

Bulur, E., 1996. An alternative technique for optically stimulated luminescence (OSL) experiment. *Radiation Measurements* 32: 141-145.

Bunzl, K., W. Schimmack, S.W. Krouglov, R.M. Alexakhin, 1995. Changes with time in the migration of radiocesium in the soil, as observed near Chernobyl and in Germany. *Science of the Total Environment* 175: 49–56.

Cambray R.S., P.A. Cawse, J.A. Garland, J.A.B. Gibson, P. Johnson, G.N.J. Lewis, D. Newton, L. Salmon, B. Wade, 1987. Observations on the radioactivity from the Chernobyl accident. *Nuclear Energy* 6: 77-101.

Chan, F.K.S., G. Mitchell, O. Adekola, A. McDonald. 2012. Flood Risk in Asia's Urban Mega-deltas: Drivers, Impacts and Response. *Environment and Urbanization Asia* 3: 41-61.

Church, M., P. Biron, A. Roy (eds.), 2012. Gravel Bed Rivers: Processes, Tools, Environments. Wiley & Sons, Chichester, 512 pp.

Clouvas A, S. Xanthos, G. Takoudis, M. Antonopoulos-Domis, G. Zinoviadis, T. Vidmar, a. Likar, 2007. Twenty-year follow-up study of radiocesium migration in soils. *Radiation Protection Dosimetry* 124: 372-377.

Cohen, K.M., 2005. 3D geostatistical interpolation and geological interpolation of palaeo-groundwaterrise within the coastal prism in the Netherlands. In L. Giosan and J.P. Bhattacharaya (Eds.), *River Deltas: Concepts, models, and examples*: 341-364 (502 pp.) Tulsa, Oklahoma: SEPM (Society for Sedimentary Geology).

Cohen, K.M., E. Stouthamer, W.Z. Hoek, H.J.A. Berendsen, H.F.J. Kempen, 2009. Zand in banen – zanddieptekaarten van het rivierengebied en het IJsseldal in de provincies Gelderland en Overijssel. Arnhem: Provincie Gelderland. 130 pp.

Coulthard T.J., M.G. Macklin, 2003. Modeling long-term contamination in river systems from historical metal mining. *Geology* 31: 451-454.

Couwater J., 1723. Caarte van de uijtterweerde en rijsweerde gelegen onder Hien, in den Ampt van Neder Betouw, toestendig aan de weduwe de Bongaarde. *Rijksarchief Gelderland*, Archief gedeputeerden Nijmegen 54.

Crosato, A., 2009. Physical explanations of variations in river meander migration rates from model comparison. *Earth Surface Processes and Landforms* 34: 2078–2086.

Cunningham A.C., J. Wallinga, P.S.J. Minderhoud, 2011. Expectations of scatter in equivalent-dose distributions when using multi-grain aliquots for OSL dating. *Geochronometria* 38(4): 424-431.

Cunningham A.C., J. Wallinga, 2009. Optically stimulated luminescence dating of young quartz using the fast component. *Radiation Measurements* 44: 423-428

Cunningham A.C., J. Wallinga, 2010. Selection of integration time intervals for quartz OSL decay curves. *Quaternary Geochronology* 5: 657-666.

Cunningham A.C., J. Wallinga J, 2012. Realizing the potential of fluvial archives using robust OSL chronologies. *Quaternary Geochronology* 12: 98-106.

Day Jr., J.W., D.F. Boesch, E.J. Clairain, G.P.Kemp, S.B. Laska, W.J. Mitsch, K. Orth, H. Mashriqui, D.J. Reed, L. Shabman, C.A. Simenstad, B.J. Streever, R.R. Twilley, C.C. Watson, J.T. Wells, D.F. Whigham, 2007. Restoration of the Mississippi Delta: Lessons from Hurricanes Katrina and Rita. *Science* 315: 1679-1684.

Enserink, B., 2004. Thinking the unthinkable - the end of the Dutch river dike system? Exploring a new safety concept for the river management. *Journal of Risk Research* 7: 745-757.

Erkens, G., 2009. Sediment dynamics in the Rhine catchment: Quantification of fluvial response to climate change and human impact. PhD thesis, Utrecht University. Netherlands Geographical Studies 388. 278 pp.

Erkens, G., K.M. Cohen, M.J.P. Gouw, H. Middelkoop, W.Z. Hoek, 2006. Holocene sediment budgets of the Rhine Delta (The Netherlands): a record of changing sediment delivery. In: Rowan, J.S., R.W. Duck, A. Werritty (Eds.). *Sediment Dynamics and the Hydromorphology of Fluvial Systems*. IAHS Publ. 306: 406-415.

Frings, R.M., B.M. Berbee, G. Erkens, M.G. Kleinhans, M.J.P. Gouw, 2009. Human induced changes in bed shear stress and bed grain size in the river Waal (The Netherlands) during the past 900 years. *Nederlandse Geografische Studies* 368: 95-116.

Frings, R.M., R. Döring, C. Beckhausen, H. Schüttrumpf, S. Vollmer, 2014. Fluvial sediment budget of a modern, restrained river: The lower reach of the Rhine in Germany. *Catena* 122: 91–102.

Galbraith R.F., R.G. Roberts, G.M. Laslett, H. Yoshida, J.M. Olley, 1999. Optical dating of single and multiple grains of quartz from Jinmium rock shelter, northern Australia, part 1, Experimental design and statistical models. *Archaeometry* 41:339-364.

Geleynse, N., J.E.A. Storms, D.J.R. Walstra, H.R.A. Jagers, Z.B. Wang, M.J.F. Stive, 2011. Controls on river delta formation; insights from numerical modelling. *Earth and Planetary Science Letters* 302: 217–226.

Geleynse, N., J.E.A. Storms, M.J.F. Stive, H.R.A. Jagers, D.J.R. Walstra (2010). Modeling of a mixed-load fluvio-deltaic system. *Geophysical Research Letters* 37(5): (L05402).

GeoDelft, 2001. Sample disturbance of a soft organic Dutch clay. Report no.: CO-710203/20, GeoDelft, Delft. 27 pp.

Giosan, L., S. Constantinescu, F. Filip, B. Deng, 2013. Maintenance of large deltas through channelization: Nature vs. humans in the Danube delta. *Anthropocene* 1: 35–45.

Giosan, L., J. Syvitski, S. Constantinescu, J. Day. 2014. Protect the world's deltas. *Nature* 516(729): 31-33.

Goudriaan B.H., 1830-1835. Kaart van de rivieren de Rijn, de Waal en Merwede, de Oude Maas en Dordtsche Kil. Utrecht: Utrecht University, Faculty of Geographical Sciences, The Netherlands. Map collection, Invenory number VIIIBb92.

Gouw, M.J.P., 2008. Alluvial architecture of the Holocene Rhine–Meuse delta (the Netherlands) *Sedimentology* 55: 1487–1516.

Gouw, M.J.P., G. Erkens, 2007. Architecture of the Holocene Rhine-Meuse delta (the Netherlands) - A result of changing external controls. *Geologie en Mijnbouw/Netherlands Journal of Geosciences* 86(1): 23-54.

Gouw, M.J.P., W.J. Autin, 2008. Alluvial architecture of the Holocene Lower Mississippi Valley (U.S.A.) and a comparison with the Rhine-Meuse delta (The Netherlands). *Sedimentary Geology* 204: 106–121.

He Q., D.E. Walling, 1996. Interpreting particle size effects in the adsorption of ^{137}Cs and unsupported ^{210}Pb by mineral soils and sediments. *Journal of Environmental Radioactivity* 30: 117-137.

Hebinck, K.A., 2008. Databank van de lithologische opbouw en morfologische ontwikkeling van de uiterwaarden van de Midden-Waal. Alterra-rapport 1678, Alterra, Wageningen. 37 pp.

Hendrikman H.G., P. Prilleritz, 1776/1778. Specifique caart van de Buijten Landen onder de kerspels Deest, Afferden en Winssen. *Rijksarchief Gelderland*, archief Verpondingskaarten 195.

Hesselink A.W., H.J.T. Weerts, H.J.A. Berendsen, 2003. Alluvial architecture of the human-influenced river Rhine, The Netherlands. *Sedimentary Geology* 161: 229-248.

Hesselink, A.W., 2002. History makes a river: morphological changes and human interference in the river Rhine, The Netherlands. PhD thesis Utrecht University. Netherlands Geographical Studies 292, 177 pp.

Hesselink, A.W., H.J.T. Weerts, H.J.A. Berendsen, 2003. Alluvial architecture of the human-influenced river Rhine, The Netherlands. *Sedimentary Geology* 161: 229-248.

Hijma, M.P., K.M. Cohen, G. Hoffmann, A.J.F. Van der Spek, E. Stouthamer, 2009. From river valley to estuary: the evolution of the Rhine mouth in the early to middle Holocene (western Netherlands, Rhine-Meuse delta). *Netherlands Journal of Geosciences*, 88(01), 13 – 53.

Hillmann U, W. Schimmack, P. Jacob, K. Bunzl, 1996. In situ γ-spectrometry several years after deposition of radiocesium; Part I. Approximation of depth distributions by the Lorentz function. *Radiation and Environmental Biophysics* 35: 297-303.

Hobo N., B. Makaske, H. Middelkoop, J. Wallinga, 2010. Reconstruction of floodplain sedimentation rates: a combination of methods to optimise estimates. *Earth Surface Processes and Landforms* 35:1499-1515.

Hoffmann T., G. Erkens, K.M. Cohen, P. Houben, J. Seidel, R. Dikau, 2007. Holocene floodplain sediment storage and hillslope erosion within the Rhine catchment. *Holocene* 17(1):105–118.

Hoyal, D., B.A. Sheets, 2009. Morphodynamic evolution of experimental cohesive deltas. *Journal of Geophysical Research* 114: (F02009).

Hung, N.N., J.M. Delgado, A. Güntner, B. Merz, A. Bárdossy, H. Apel, 2014a. Sedimentation in the floodplains of the Mekong Delta, Vietnam. Part I: suspended sediment dynamics. *Hydrological Processes* 28: 3132–3144.

Hung, N.N., J.M. Delgado, A. Güntner, B. Merz, A. Bárdossy, H. Apel, 2014b. Sedimentation in the floodplains of the Mekong Delta, Vietnam. Part II: deposition and erosion. *Hydrological Processes* 28: 3145–3160.

Hutton, E.W.H., J.P.M. Syvitski, 2008. Sedflux 2.0: an advanced process-response model that generates three-dimensional stratigraphy. *Computers and Geosciences*. 34: 1319–1337.

IPCC, 2013. Climate Change 2013. The Physical Science Basis. Contribution of Working Group I to the Fifth Assessment Report of the Intergovernmental Panel on Climate Change. Stocker, T.F., D. Qin, G.K. Plattner, M. Tignor, S.K. Allen, J. Boschung, A. Nauels, Y. Xia, V. Bex and P.M. Midgley (eds.) Cambridge University Press, Cambridge, United Kingdom and New York, NY, USA, 1535 pp.

Jain, M., J.H. Choi, P.J. Thomas, 2008. The ultrafast OSL component in quartz: Origins and implications. *Radiation Measurements* 43: 709-714.

Jain, M., A.S. Murray, L. Bøtter-Jensen, 2003. Characterisation of blue-light stimulated luminescence components in different quartz samples: implications for dose measurement. *Radiation Measurements* 37: 441-449.

Kater E., B. Makaske, G.J. Maas, 2012. De kansrijkdom van morfodynamische processen in het rivierenlandschap. OBN rapport 2012/OBN154-RI, Den Haag. 98 pp.

Kesel R.H., E.G. Yodis, D.J. McCraw, 1992. An approximation of the sediment budget of the lower Mississippi River prior to major human modification. *Earth surface processes and landforms* 17: 711-722.

Kesel, R.H. ,1989. The role of the Mississippi River in wetland loss in southeastern Louisiana, U.S.A. *Environmental Geology and Water Sciences* 13: 183-193.

Kim, W.S., D. Mohrig, R.R. Twilley, C. Paola, G. Parker, 2009. Is it feasible to build new land in the Mississippi River delta? *Eos Trans. AG* 90: 373–374.

Kleinhans, M.G., J.H. Van den Berg, 2011. River channel and bar patterns explained and predicted by an empirical and a physics-based method. *Earth Surface Processes and Landforms* 36: 721–738.

Kleinhans, M.G., K.M. Cohen, J. Hoekstra, J.M. IJmker, 2011. Evolution of a bifurcation in a meandering river with adjustable channel widths, Rhine delta apex, The Netherlands. *Earth Surface Processes and Landforms* 36: 2011-2027.

Kleinhans, M.G., H.J.T. Weerts, K.M. Cohen, 2010. Avulsion in action: reconstruction and modelling sedimentation pace and upstream flood water levels following a Medieval tidal-river diversion catastrophe (Biesbosch, The Netherlands, 1421-1750 AD). *Geomorphology* 118 (1-2): 65-79.

Kolker, A.S., M.D. Miner, H.D. Weathers, 2012. Depositional dynamics in a river diversion receiving basin: The case of the West Bay Mississippi River Diversion. *Estuarine, Coastal and Shelf Science* 106: 1-12.

Komori, D., S. Nakamura, M. Kiguchi, A. Nishijima, D. Yamazaki, S. Suzuki, A. Kawasaki, K. Oki, T. Oki, 2012. Characteristics of the 2011 Chao Phraya River flood in Central Thailand. *Hydrological Research Letters* 6: 41-46.

Koomen, A.J.M., G.J. Maas, 2004. Geomorfologische Kaart Nederland (GKN). Achtergronddocument bij het landsdekkende digitale bestand. Wageningen. Alterra-rapport 1039.

Kummu M., X.X. Lu, A. Rasphone, J. Sarkkula, J. Koponen, 2008. Riverbank changes along the Mekong River: Remote sensing detection in the Vientiane–Nong Khai area. *Quaternary International* 186: 100–112.

Lambert C.P., D.E. Walling, 1987. Floodplain sedimentation: A preliminary investigation of contemporary deposition within the lower reaches of the River Culm, Devon, UK. *Geografiska Annaler. Series A, Physical Geography* 69: 393-404.

Latrubesse E.M., M.L. Amsler, R.P. De Morais, S. Aquino, 2009. The geomorphologic response of a large pristine alluvial river to tremendous deforestation in the South American tropics: The case of the Araguaia River. *Geomorphology* 113 (3-4): 239-252.

Lauer J.W., G. Parker, 2008a. Modeling framework for sediment deposition, storage, and evacuation in the floodplain of a meandering river: Application to the Clark Fork River, Montana. *Water Resources Research* 44: W08404.

Lauer J.W., G. Parker, 2008b. Modeling framework for sediment deposition, storage, and evacuation in the floodplain of a meandering river: Theory. *Water Resources Research* 44: W04425.

Lauer J.W., G. Parker, 2008c. Net local removal of floodplain sediment by river meander migration. *Geomorphology* 96: 123–149.

Maas G.J., 1998. Historisch-geomorfologische ontwikkeling van enkele riviertrajecten langs de IJssel. SC-DLO report 620, DLO-Staring Centrum, Wageningen.

Maas, G.J., H.P. Wolfert, M.M. Schoor, H. Middelkoop (1997): Classificatie van riviertrajecten en kansrijkdom voor ecotopen; een voorbeeld studie vanuit historisch-geomorfologisch en rivierkundig perspectief. SC-DLO rapport 552, Wageningen. 157 pp.

Maas G.J., B. Makaske, P.W.F.M. Hommel, B.S.J. Nijhof, H.P. Wolfert, 2003. Verstoring en successie; Rivierdynamiek en stroomdalvegetaties in de uiterwaarden van de Rijntakken. Alterra report 759, Alterra, Wageningen. 100 pp.

Mackey, S.D., J.S. Bridge, 1995. Three-dimensional model of alluvial stratigraphy: theory and application. *Journal of Sedimentary Research*, B65(1): 7–31.

Macklin M.G., P.A. Brewer, K.A. Hudson-Edwards, G. Bird, T.J. Coulthard, I.A. Dennis, P.J. Lechler, J.R. Miller, J.N. Turner, 2006. A geomorphological approach to the management of rivers contaminated by metal mining. *Geomorphology* 79: 423–447.

Macklin, M.G., K.A. Hudson-Edwards, E.J. Dawson, 1997. The significance of pollution from historic metal mining in the Pennine orefields on river sediment contaminant fluxes to the North Sea. *The Science of the Total Environment* 194/195: 391-397.

Madsen, A.T., A.S. Murray, T.J. Anderson, 2007. Optical dating of dune ridges on Rømø, a barrier island in the Wadden Sea, Denmark. *Journal of Coastal Research* 23: 1259-1269.

Magilligan F.J., J.D. Phillips, L.A. James, B. Gomez, 1998. Geomorphic and sedimentological controls on the effectiveness of an extreme flood. *Journal of Geology* 106: 87-95.

Makaske B., H.J.T. Weerts, 2005. Muddy lateral accretion and low stream power in a sub-recent confined channel belt, Rhine-Meuse delta, central Netherlands. *Sedimentology* 52: 651-668.

Makaske, B., 1998. Anastomosing rivers: forms, processes and sediments. PhD thesis Utrecht University. Netherlands Geographical Studies 249, 298 pp.

Makaske, B., H.J.A. Berendsen, M.H.M. Van Ree, 2007. Middle Holocene avulsion-belt deposits in the central Rhine-Meuse delta, the Netherlands. *Journal of Sedimentary Research* 77: 110–123.

Manh, N.V., N.V. Dung, N.N. Hung, M. Kummu, B. Merz, H. Apel, 2015. Future sediment dynamics in the Mekong Delta floodplains: Impacts of hydropower development, climate change and sea-level rise. *Global and Planetary Change* 127: 22-33.

Marriner, N., C. Flaux, C. Morhange, D. Kaniewski, 2012. Nile Delta's sinking past: Quantifiable links with Holocene compaction and climate-driven changes in sediment supply? *Geology* 40: 1083-1086.

Middelkoop, H., 1997. Embanked floodplains in the Netherlands; geomorphological evolution over various time scales. PhD thesis, Utrecht University. Netherlands Geographical Studies 224. 341 pp.

Middelkoop, H., M. van der Perk, 1998. Modelling spatial patterns of overbank sedimentation on embanked floodplains. *Geografiska Annaler* 80A: 95–109.

Middelkoop, H., N.E.M. Asselman, 1998. Spatial variability of floodplain sedimentation at the event scale in the Rhine-Meuse delta, The Netherlands. *Earth Surface Processes and Landforms* 23: 561-573.

Middelkoop H., C.O.G. Van Haselen, 1999. Twice a river: Rhine and Meuse in the Netherlands. RIZA-Rapport, 99(3). Ministerie van Verkeer en Waterstaat, Directoraat-generaal Rijkswaterstaat (RWS), Rijksinstituut voor Integraal Zoetwaterbeheer en Afvalwaterbehandeling (RIZA): Arnhem. ISBN 9036952239. 127 pp.

Middelkoop, H., 2000. Heavy-metal pollution of the river Rhine and Meuse floodplains in the Netherlands. *Netherlands Journal of Geosciences* 79 (4): 411-428.

Middelkoop H., K. Daamen, D. Gellens, W. Grabs, J.C.J. Kwadijk, H. Lang, B.W.A.H. Parmet, B. Schädler, J. Schulla, K. Wilke, 2001. Impact of climate change on hydrological regimes and water resources management in the Rhine basin. *Climatic Change* 49: 105-128.

Middelkoop, H., 2002. Reconstructing floodplain sedimentation rates from heavy metal profiles by inverse modelling. *Hydrological Processes* 16: 47-64.

Middelkoop, H., G. Erkens, M. van der Perk, 2010. The Rhine delta - a record of sediment trapping over time scales from millennia to decades. *Journal of soils and sediments* 10: 628-639.

Midgley, T.L., G.A. Fox, D.M. Heeren, 2012. Evaluation of the bank stability and toe erosion model (BSTEM) for predicting lateral retreat on composite streambanks. *Geomorphology*, 145–146: 107–114.

Morozova, G.S., N.D. Smith, 2000. Holocene avulsion styles and sedimentation patterns of the Saskatchewan River, Cumberland Marshes, Canada. *Sedimentary Geology* 130: 81–105.

Murray, A.S., A.G. Wintle, 2003. The single aliquot regenerative dose protocol: potential for improvements in reliability. *Radiation Measurements* 37: 377-381.

NE01, 2001. Bepaling van de activiteit van gammastraling uitzendende nucliden in een telmonster met behulp van halfgeleider-gammaspectrometrie, Nederlandse Norm, NEN5623, 2001.

Oele, E., W. Apon, M.M. Fischer, R. Hoogendoorn, C.S. Mesdag, E.F.J. De Mulder, B. Overzee, A. Sesören, W.E. Westerhoff, 1983. Surveying The Netherlands: sampling techniques, maps and their applications. In: Van den Berg, M.W., Felix, R. (Eds.), Special Issue in the Honour of J.D. de Jong. *Geologie en Mijnbouw* 62: 255-372.

Owens P.N., D.E. Walling, Q. He, 1996. The behaviour of bomb-derived caesium-137 fallout in catchment soils. *Journal of Environmental Radioactivity* 32: 169-191.

Owens P.N., D.E. Walling, G.J.L. Leeks, 1999. Use of floodplain sediment cores to investigate recent historical changes in overbank sedimentation rates and sediment sources in the catchment of the River ouse, Yorkshire, UK. *Catena* 36: 21-47.

Panin, N., 2003. The Danube Delta. Geomorphology and Holocene Evolution: a Synthesis. *Géomorphologie: relief, processus, environnement* 4: 247-262.

Passavant G., 1688. Caart van de rijsweerden van de heren van Winssen en Doddendael in't Rijck van Nijmegen onder Euuik [= Ewijk] aen de Waelkant gelegen.

Pease P., S. Lecce, P. Gares, C. Rigsby, 2007. Heavy metal concentrations in sediment deposits on the Tar River floodplain following Hurricane Floyd. *Environmental geology* 51: 1103-1111.

Peters, B.W.E., E. Kater, G.W. Geerling, 2006: Cyclisch beheer in uiterwaarden: Natuur en veiligheid in de praktijk. Centrum voor Water en Samenleving, Radboud Universiteit, Nijmegen. 206 pp.

Ploeger B., 1992: Bouwen aan de Rijn; Menselijke ingrepen op de Rijn en zijn takken. Ministerie van Verkeer en Waterstaat, rapport 53.

Prescott, J.R., J.T. Hutton, 1994. Cosmic ray contributions to dose rates for luminescence and ESR dating: large depths and log-term time variations. *Radiation Measurements* 23: 497-500.

Reid L.M., T. Dunne, 2003. Sediment budgets as an organizing framework in fluvial geomorphology. In Tools in fluvial geomorphology, Kondolf GM, Piegay H. (eds.). Chichester: Wiley, 463-499.

Rigollet, C., R.J. De Meijer, 2002. PHAROS: A pluri detector, high-resolution, analyser of radiometric properties of soil. *Nuclear Instruments and Methods in Physics Research* 488: 642-653.

Rijkswaterstaat, 1870-1880. Rivierkaart, 1e herziening. Emmen: Topografische Dienst.

Rijkswaterstaat, 1965. Rivierkaart, schaal 1:10.000. Archive Rijkswaterstaat, The Netherlands.

Ritchie, J.C., J.R. McHenry, 1990. Application of radioactive fallout cesium-137 for measuring soil erosion and sediment accumulation rates and patterns: a review. *Journal of Environmental Quality* 19: 215-233.

Rittenour, T.M., 2008. Luminescence dating of fluvial deposits: applications to geomorphic, palaeoseismic and archaeological research. *Boreas* 37: 613–635.

Rumsby B., 2000. Vertical accretion rates in fluvial systems: a comparison of volumetric and depth-based estimates. *Earth Surface Processes and Landforms* 25: 617-631.

Scheffer F., P. Schachtschabel (eds.), 1982. Lehrbuch der Bodenkunde. Stuttgart: Ferdinand Enke Verlag.

Schimmack W., H. Flessa, K. Bunzl, 1997. Vertical migration of Chernobyl-derived radiocesium in Bavarian grassland soils. *Naturwissenschaften* 84: 204-207.

Schoor, M.M., 1994. De geomorfologie en het ontstaan van de Afferdensche en Deestsche waarden. Rijkswaterstaat nota 94.002. RIZA, Amhem, 48 pp.

Sieben, J., 2009. Sediment management in the Dutch Rhine Branches. *River Basin Management* 7(1): 43-53.

Silva, W., F. Klijn, J. Dijkman, 2001. Room for the Rhine in The Netherlands. RIZA report 2001.033. RIZA, Arnhem.

Simon, A., A. Curini, S.E. Darby, E.J. Langendoen, 2000. Bank and near-bank processes in an incised channel. *Geomorphology* 35: 193–217.

Simon, A., N. Pollen-Bankhead, V. Mahacek, E.J. Langendoen, 2009. Quantifying reductions of mass-failure frequency and sediment loadings from streambanks using toe protection and other means: Lake Tahoe, United States. *Journal of the American water resources association* 45 (1): 170-186.

Singarayer, J.S., R.M. Bailey, 2004. Component-resolved bleaching spectra of quartz optically stimulated luminescence: preliminary results and implications for dating. *Radiation Measurements* 38: 111-118.

Slaymaker O., 2003. The sediment budget as conceptual framework and management tool. *Hydrobiologica* 494: 71-82.

Smith, D.G., S.M. Hubbard, D.A. Leckie, M. Fustic, 2009. Counter point bar deposits: lithofacies and reservoir significance in the meandering modern Peace River and ancient McMurray Formation, Alberta, Canada. *Sedimentology* 56: 1655-1669.

Smith, N.D., G.S. Morozova, M.R. Gibling, 2014. Channel enlargement by avulsion-induced sediment starvation in the Saskatchewan River. *Geology* 42: 355-358.

Sorber, A.M., 1997. Oeversedimentatie tijdens de hoogwaters van 1993/1994 en 1995. RIZA-rapport 97.015, RIZA, Arnhem. 40 pp.

Stouthamer, E., 2001. Holocene avulsions in the Rhine-Meuse delta, The Netherlands. PhD thesis Utrecht University. Netherlands Geographical Studies 283, 211 pp.

Stouthamer, E., H.J.A. Berendsen, 2001. Avulsion frequency, avulsion duration, and interavulsion period of Holocene channel belts in the Rhine-Meuse delta, The Netherlands. *Journal of sedimentary research* 71(4): 589–598.

Stouthamer, E., K.M. Cohen, M.J.P. Gouw, 2011. Avulsion and its implications for fluvial-deltaic architecture: insights from the Holocene Rhine-Meuse delta. In: From River To Rock Record: The Preservation Of Fluvial Sediments And Their Subsequent Interpretation. *SEPM Special Publication* 97: SEPM, 215–231.

Stouthamer, E., H.J. Pierik, K.M. Cohen, 2011. Erodibiliteit en kans op het ontstaan van zettingsvloeiing als maat voor stabiliteit van oevers, onderwatertaluds en rivierbodem van de Lek. (49 p.). Utrecht: Dept. Fysische Geografie / Universiteit Utrecht.

Straatsma M.W., M.J. Baptist, 2008. Floodplain roughness parameterization using airborne laser scanning and spectral remote sensing. *Remote sensing of environment* 112: 1062-1080.

Struiksma, N., K.W. Olesen, C. Flokstra, H.J. De Vriend, 1985. Bed deformation in curved alluvial channels. *Journal of Hydraulic Research* 23(1): 57–79.

Syvitski, J.P.M., 2008. Deltas at risk. *Sustainable Science* 3: 23–32.

Syvitski, J.P.M., A.J. Kettner, I. Overeem, E.W.H. Hutton, M.T. Hannon, G.R. Brakenridge, J. Day, C. Vörösmarty, Y. Saito, L. Giosan, R.J. Nicholls, 2009. Sinking deltas due to human activities. *Nature Geoscience* 2: 681-686.

Syvitski, J.P.M., Y. Saito, 2007. Morphodynamics of deltas under the influence of humans. *Global Planetary Change* 57: 261–282.

Ta, T.K.O., V.L. Nguyen, M. Tateishi, I. Kobayashi, Y. Saito., 2005. Holocene delta evolution and depositional models of the Mekong River Delta, Southern Viet Nam. In: Giosan, L. and J. P. Bhattacharya. (eds.). River Deltas: Concepts, Models, and Examples. Society of Economic Paleontologists and Mineralogists, Special Publication 83: 453–466.

Ten Brinke, W.B.M., 2005. The Dutch Rhine, a restrained river. Veen Magazines, Diemen, the Netherlands. 228 pp.

Ten Brinke, W.B.M., M.M. Schoor, A.M. Sorber, H.J.A. Berendsen, 1998. Overbank deposition in relation to transport volumes during large-magnitude floods in the Dutch sand-bed Rhine river system. *Earth Surface Processes and Landforms* 23: 809-824.

Terry J.P., S. Garimella, R.A. Kostaschuk, 2002. Rates of floodplain accretion in a tropical island river system impacted by cyclones and large floods. *Geomorphology* 42: 171-182.

Thomsen K.J., A.S. Murray, L. Bøtter-Jensen L, Kinahan J. 2007. Determination of burial dose in incompletely bleached fluvial samples using single grains of quartz. *Radiation measurements* 42: 370-379.

Thonon, I., 2006. Deposition of sediment and associated heavy metals on floodplains. PhD thesis Utrecht University. Netherlands Geographical Studies 337, 174 pp.

Thonon, I., H. Middelkoop, M. van der Perk, 2007. The influence of floodplain morphology and river works on spatial patterns of overbank deposition. *Netherlands Journal of Geosciences* 86: 63–75.

Thorne, C.R., 1990. Effects of vegetation on riverbank erosion and stability, In Thornes JB (ed.), Vegetation and erosion: Processes and Environments, John Wiley & Sons: Chichester; 125-144.

Thorne, C.R., N.K. Tovey, 1981. Stability of composite river banks. *Earth Surface Processes and Landforms* 6: 469-484.

Toonen, W.H.J., 2013. A Holocene flood record of the Lower Rhine. Dissertation, Utrecht University. Utrecht Studies in Earth Sciences 041, 204 pp.

Törnqvist, T.E., 1993. Holocene alternation of meandering and anastomosing fluvial systems in the Rhine-Meuse delta (Central Netherlands) controlled by sea-level rise and subsoil erodibility. *Journal of sedimentary petrology* 63(4): 683-693.

Törnqvist, T.E., J.S. Bridge, 2002. Spatial variation of overbank aggradation rate and its influence on avulsion frequency. *Sedimentology* 49: 891–905.

Törnqvist, T.E., D.J. Wallace, J.E.A. Storms, J. Wallinga, R.L. van Dam, M. Blaauw, M.S. Derksen, C.J.W. Klerks, C. Meijneken, E.M.A. Snijders, 2008. Mississippi Delta subsidence primarily caused by compaction of Holocene strata. *Nature Geoscience* 2008(1): 173-176.

Törnqvist, T.E., T.R. Kidder, W.J. Autin, K. van der Borg, A.F.M. de Jong, C.J.W. Klerks, E.M.A. Snijders, J.E.A. Storms, R.L. van Dam, M.C. Wiemann, 1996. A revised chronology for Mississippi River subdeltas. *Science* 273: 1693–1696.

Truelsen J.L., J. Wallinga, 2003. Zeroing of the OSL signal as a function of grain size: investigating bleaching and thermal transfer for a young fluvial sample. *Geochronometria* 22: 1-8.

V&W, 2008. Waterbase; http://www.waterbase.nl. The Hague, Ministry of Transport, Public Works and Water Management.

Van de Ven, G.P., 1976. Aan de wieg van Rijkswaterstaat. Wordingsgeschiedenis van het Pannerdens Kanaal. Walburg Pers, Zutphen, 1976. Gelderse Historische Reeks VIII. 439 pp.

Van de Ven, G.P., 1993. Man-made lowlands – history of water management and land reclamation in The Netherlands. Matrijs, Utrecht, 432 pp.

Van de Ven G., 2007. Verdeel en beheers: 300 jaar Pannerdensch Kanaal. Veen Magazines, Diemen; 176 pp.

Van den Berg, G.A., M. van Wijngaarden M., 2000. Sedimentatie langs de Grensmaas (snelheid van sedimentatie en kwaliteitsontwikkeling op de uiterwaarden). RIZA-rapport 2000.046, RIZA, Dordrecht.

Van den Berg, J.H., 1995. Prediction of alluvial channel pattern of perennial rivers. *Geomorphology*, 12, 259-279.

Van der Meulen, M.J., A.P. Wiersma, M. van der Perk, H. Middelkoop, N. Hobo, 2009. Sediment management and the renewability of floodplain clay for structural ceramics. *Journal of Soils and Sediments* 9(6): 627-639.

Van der Meulen, M.J., A.J.F. Van der Spek, G. De Lange, S.H.L.L. Gruijters, S.F. Van Gessel, B.L. Nguyen, D. Maljers, J. Schokker, J.P.M. Mulder, R.A.A. Van der Krogt, 2007. Regional sediment deficits in the Dutch Lowlands: implications for long-term land-use options. *Journal of soils and sediments* 7: 9-16.

Van Dinter, M., 2013. The Roman Limes in the Netherlands: how a delta landscape determined the location of military structures. *Netherlands Journal of Geosciences* 92(01): 11–32.

Van Geelkercken N., 1634. Carte van bevaringe, gedaen door de Rekenkamer des vorstendoms Gelre ende graeffschap Zutphen, anno 1634 den 10 octobris, van de sanden, gelegen onder den weer ontrent de Snor [onder Dodewaard].

Van Heerd, R.M., E.A.C. Kuijlaars, M.P. Teeuw, R.J. Van 't Zand, 2000. Productspecificatie AHN 2000. Rapport MDTGM 2000.13, Rijkswaterstaat, Adviesdienst Geo-informatie en ICT, Delft, pp. 22.

Van Urk, G., H. Smith, 1989. The lower Rhine geomorphological changes. In Petts, G.E. (Ed.) Historical change of large alluvial rivers: western Europe. John Wiley and sons, Chichester, United Kingdom: 167-183.

Van Vuren, S., H. De Vriend, S. Ouwerkerk, M. Kok, 2005. Stochastic modelling of the impact of flood protection measures along the river Waal in the Netherlands. *Natural Hazards* 36: 81-102.

Vellinga, P., C.A. Katsman, A. Sterl, J.J. Beersma (eds), 2008. Exploring high-end climate change scenarios for flood protection of the Netherlands: an international scientific assessment. KNMI and Wageningen UR (Alterra, Earth System Science and Climate Change Group), Wageningen, the Netherlands.

Vos, P.C., 2015. Origin of the Dutch coastal landscape. Long-term landscape evolution of the Netherlands during the Holocene, described and visualized in national, regional and local palaeogeographical map series. PhD thesis Utrecht University. Deltares, Utrecht / Bakhuis, Groningen, 359 p.

Walling, D.E., S.B. Bradley, C.P. Lambert, 1986. Conveyance losses of suspended sediment within a flood plain system. In Drainage Basin Sediment Delivery, Hadley RF (ed.), IAHS Publication 159. IAHS, Wallingford, 119–132.

Walling D.E., S.B. Bradley, 1989. Rates and patterns of contemporary floodplain sedimentation: a case study of the river Culm, Devon, UK. *GeoJournal* 19: 53-62.

Walling D.E., Q. He, 1997. Use of fallout ^{137}Cs in investigations of overbank sediment deposition on river floodplains. *Catena* 29: 263-282.

Walling, D.E., Q. He, 1998. The spatial variability of overbank sedimentation on river floodplains. *Geomorphology* 24: 209–223.

Walling D.E, P.N. Owens, G.J.L. Leeks, 1998. The role of channel and floodplain storage in the suspended sediment budget of the River Ouse, Yorkshire, UK. *Geomorphology* 22: 225-242.

Walling, D.E., P.N. Owens, 2003. The role of overbank floodplain sedimentation in catchment contaminant budgets. *Hydrobiologica* 494: 83-91.

Walling, D.E., A.L. Collins, P.A. Jones, G.J.L. Leeks, G. Old, 2006. Establishing fine-grained sediment budgets for the Pang and Lambourn LOCAR catchments, UK. *Journal of hydrology* 330: 126-141.

Wallinga J, N. Hobo, A.C. Cunningham, A.J. Versendaal, B. Makaske, H. Middelkoop, 2010. Sedimentation rates on embanked floodplains determined through quartz optical dating. *Quaternary Geochronology* 5:170-175.

Wallinga J., 2002a. Optically stimulated luminescence dating of fluvial deposits: a review. *Boreas* 31(4): 303-322.

Wallinga J., 2002b. Detection of OSL age overestimation using single-aliquot techniques. *Geochronometria* 21: 17-26.

Wallinga, J., 2001. The Rhine-Meuse system in a new light: optically stimulated luminescence dating and its application to fluvial deposits. PhD thesis Utrecht University. Netherlands Geographical Studies 290, 180 pp.

Weerts, H.J.T., 1996. Complex confining layers. Architecture and hydraulic properties of Holocene and Late Weichselian deposits in the fluvial Rhine-Meuse delta. PhD thesis Utrecht University. Netherlands Geographical Studies 213, 189 pp.

Williams, G.P., 1986. River meanders and channel size. *Journal of Hydrology* 88: 147-164.

Wintle A.G., 2008. Luminescence dating: where it has been and where it is going. *Boreas* 37: 471–482.

Wintle, A.G., Murray, A.S. 2006. A review of quartz optically stimulated luminescence characteristics and their relevance in single-aliquot regeneration dating protocols. *Radiation Measurements* 41: 369-391.

Wolfert, H.P., 2001. Geomorphological change and river rehabilitation: case studies on lowland fluvial systems in the Netherlands. Alterra scientific contributions 6, Alterra, Wageningen. 200 pp.

Appendix A. List of symbols used in chapters 5 and 6

Sites (index s)	
HEN	Hennisdijk channel belt
SOO	Schoonrewoerd channel belt

Stages (index *i*)	
Av	Avulsion stage
S1	Stage 1
S2	Stage 2
Ab	Abandonment stage

Morphological units and associated lithostratigraphic units (index *u*)			
CH	Channel	*CH1*	Holocene channel deposits (fine sand, medium sand, coarse sand)
		CH2	Holocene channel deposits (silty clay, sandy clay)
NL	Natural levee	*NL(FB)*	Distal Holocene natural levee and overbank deposits (clay, silty clay, sandy clay)
		NL(CH)	Proximal Holocene natural levee and overbank deposits (clay, silty clay, sandy clay)
FB	Flood basin	*FB1*	Holocene floodbasin deposits (clay)
		FB2	Holocene floodbasin peat (peat)
		FB3	Pleistocene overbank deposits (clay, silty clay, sandy clay)
		FB4	Pleistocene channel deposits (sand, gravel)
RC	Residual channel	*RC1*	Holocene residual channel deposits (clay, silty clay, sandy clay)

Location within bend (index *b*)	
apx	Apex
ifl	Inflection point
max	Deepest point within cross-section
min	Undeepest point within cross-section
avg	Average depth within cross-section

Channel belt characteristics (for each site *s*)

T	Age [^{14}C a]
d_{50}	Grain size [μm]
Qp	Paleodischarge [m^3/s]
W_{CB}	Channel-belt width [m]
H_{CB}	Channel-belt thickness [m]
$A_{CB,i}$	Channel-belt cross-sectional area at stage *i* [m^2]
S_{CB}	Channel-belt slope [-]
L_{CB}	Channel-belt length [m]
$W_{C,i}$	Channel-width at stage *i* [m]
$H_{C,i}$	Channel depth at stage *i* [m]
$H_{L,i}$	Levee height at stage *i* [m]
$H_{B,i}$	Bank height at stage *i* [m]
$A_{C,i}$	Cross-sect. flow area at stage *i* [m^2]
$S_{C,i}$	Channel slope at stage *i* [-]
$L_{C,i}$	Channel length at stage *i* [m]
$P_{ind,i}$	Sinuosity index at stage *i* [-]
$L_{M,i}$	Meander wave length at stage *i* [m]
$A_{M,i}$	Meander amplitude at stage *i* [m]
$R_{,i}$	Bend radius at stage *i* [m]
$A_{NL(u),i}$	Cross-sectional area of overbank unit *NL(u)* at stage *i* [m^2]

Model parameters

j	Index for sensitivity analysis scenarios
Fs	Factor of safety [-]
$V_{,j}$	Series of sensitivity analysis scenarios for each input variable j
$V_{,0}$	0-scenario for sensitivity analysis
$Es_{,i}$	Erosion rate bank scour at stage *i* [m/a]
$Ef_{,i}$	Erosion rate by bank failure at stage *i* [m/a]
$Et_{,i}$	Total bank retreat rate at stage *i* [m/a]
$Et(l)_{,i}$	Lateral component of total bank retreat rate at stage *i* [m/a]
$Et(d)_{,i}$	Downstream component of total bank retreat rate at stage *i* [m/a]
$\alpha_{,i}$	Angle between $Et_{,i}$ and $Et(d)_{,i}$ [°]
$\beta_{,i}$	Angle between $Et_{,i}$ and $Et(l)_{,i}$ [°]
τ_c	Critical shear stress [kg m^{-1} s^{-2}]

Sediment budget parameters	
$E_{,i,u}$	Erosion volume in stage *i*, unit *u*, derived from reconstruction [m^3]
$D_{,i,u}$	Reconstruction volume in stage *i*, unit *u*, derived from reconstruction [m^3]
t	Index for time [a]
$C_{i,t}$	Lateral position of channel, as distance from channel axis, *t* years after onset stage *i* [m]
$X_{i,t}$	Downstream position of channel, as distance along the channel axis, *t* years after onset stage [m]
$H_{E,i}$	Spatially averaged erosion depth per scenario *i* [m]
$H_{D,i}$	Spatially averaged deposition depth per scenario *i* [m]
RWS_i	Reworked surface derived from modelling [m^2/a]
$RWV_{E,i}$	Reworked erosion volume derived from modelling [m^3/a]
$RWV_{D,i}$	derived Reworked deposition volume derived from modelling [m^3/a]

About the author

Noortje Hobo was born on the 25th of November 1980 in Ammerzoden, The Netherlands. She followed secondary school (VWO) at the Jeroen Bosch College in 's-Hertogenbosch and graduated in 2000. Later that year, Noortje started studying Applied Mathematics at TU Eindhoven. There, she realized that she was more interested in the natural processes on the earth surface, and decided to switch to Earth Sciences at Utrecht University in 2001. While growing up in the Bommelerwaard floodbasin, in the proximity of the rivers Maas and Waal, Noortjes interest in rivers must have been awakened, and she consequently specialised in Coastal Dynamics and River Systems. She wrote her BSc thesis on the impact of hurricanes on the development of beach ridges in the Mississippi delta, USA. For her MSc thesis she analysed rip-channel morphology on the intertidal beach of Egmond aan Zee, the Netherlands. In addition, she conducted a five-month internship at Alterra in Wageningen, where she modelled the hydraulic effects of different nature restoration scenarios along the Overijsselse Vecht, using SOBEK. Noortje obtained her MSc degree (*cum laude*) in November 2006, after which she started working at Alterra, on the geomorphological mapping of embanked floodplains along the river Rhine. In March 2007 she began working at Utrecht University, in cooperation with Alterra, as a Junior Researcher on the sedimentary dynamics in embanked floodplains. After two years, this research developed into a PhD study, which she temporarily paused another two years later when her son Mats was born. Noortje continued her PhD research in 2013, and the results are presented in this thesis.

List of publications

Peer-reviewed journal papers

Van der Meulen, M.J., A.P. Wiersma, M. van der Perk, H. Middelkoop, N. Hobo, 2009. Sediment management and the renewability of floodplain clay for structural ceramics. Journal of Soils and Sediments 9(6): 627-639, DOI 10.1007/s11368-009-0115-8.

Wallinga, J., N. Hobo, A.C. Cunningham, A.J. Versendaal, B. Makaske, H. Middelkoop, 2010. Sedimentation rates on embanked floodplains determined through quartz optical dating. *Quaternary Geochronology* 5: 170-175, DOI:10.10.16/j.quageo.2009.01.002.

Hobo, N., B. Makaske, H. Middelkoop, J. Wallinga, 2010. Reconstruction of floodplain sedimentation rates: a combination of methods to optimise estimates. *Earth Surface Processes and Landforms* 35: 1499-1515, DOI: 10.1002/esp.1986.

Hobo, N., B. Makaske, J. Wallinga, H. Middelkoop, 2014. Reconstruction of eroded and deposited sediment volumes of the embanked river Waal, the Netherlands, for the period 1631 AD – present. *Earth Surface Processes and Landforms* 39: 1301–1318, DOI 10.1002/esp.3525.

Cunningham A.C., J. Wallinga, N. Hobo, A.J. Versendaal, B. Makaske, H. Middelkoop, 2015. Re-evaluating burial doses and bleaching of fluvial deposits using Bayesian computational statistics. *Earth Surface Dynamics* 3: 55-65, DOI: 10.5194/esurf-3-55-2015.

Selected conference presentations

Hobo, N., K.A. Hebinck, H. Middelkoop, B. Makaske, 2007. The sedimentary dynamics of embanked floodplains. In: A.G. van Os (Ed.) 2007. Proceedings NCR-days 2007, a sustainable river system?! NCR-publication 32-2007, Netherlands Centre for River studies, Delft, pp. 22-23.

Hobo, N., J. Wallinga, B. Makaske, H. Middelkoop, 2008. Optically Stimulated Luminescence dating of young floodplain sediments. Abstracts NAC 9 - sedimentary systems (pdf-document), 9e Nederlands Aardwetenschappelijk Congres, Veldhoven, 18-19 maart 2008, abstract 218, pp. 5-6.

Hobo, N., B. Makaske, H. Middelkoop, J. Wallinga, 2008. Reconstruction of recent sedimentation rates in embanked floodplains, a comparison of four methods. In A.G. van Os, C.D. Erdbrink (Eds.) 2008. Proceedings NCR-days 2008, 10 years NCR. NCR-publication 33-2008, Netherlands Centre for River studies, Delft, pp. 80-81.

Hobo, N., B. Makaske, H. Middelkoop, J. Wallinga, 2009. Reconstruction of recent sedimentation rates in the river Rhine embanked floodplains (the Netherlands); a comparison of three methods, including OSL dating. In: Pascucci, V. and Andreucci, S. (eds.) IAS 2009 Book of Abstracts, pp.204.

Hobo, N., B. Makaske, H. Middelkoop, J. Wallinga, 2009. Reconstruction of recent sedimentation rates in the Rhine embanked floodplains, using OSL-dating. In J. Wallinga, J. Storms (Eds.) 2009. NCL Symposium Series, Volume 6, Netherlands Centre for Luminescence Dating, pp. 9-11.

Hobo, N., B. Makaske, H. Middelkoop, 2010. Reconstruction of eroded and deposited sediment volumes in the floodplains of the embanked River Waal, the Netherlands, for the period 1650 – 1850 AD. Abstracts NAC 10 - sedimentary systems (pdf-document), 10e Nederlands Aardwetenschappelijk Congres, Veldhoven, 22-23 april 2010, abstract 118, pp. 2-3.

Hobo, N., B. Makaske, H. Middelkoop, 2010. Reconstruction of eroded and deposited sediment volumes in the floodplains of the embanked River Waal, the Netherlands, for the period 1650 – 1850 AD. Geophysical Research Abstracts, Vol. 12, EGU2010-15067, EGU General Assembly 2010.

Hobo, N., B. Makaske, H. Middelkoop, J. Wallinga, 2010. Reconstruction of floodplain sediment dynamics of the embanked river Waal, the Netherlands, for the period 1650 – 1850 AD. In E. Stouthamer 2010 (Ed.). NCR-days 2010, Book of abstracts, pp. 13.

Hobo, N., H. Middelkoop, B. Makaske, M.G. Kleinhans, 2011. Decadal to century-scale sediment dynamics in the Rhine Delta. World's Large Rivers Conference 2011.

Hobo, N., B. Makaske, H. Middelkoop, 2015. Human impacts on sediment dynamics within the Rhine delta, the Netherlands. EGU General Assembly 2015.